MASTER COPY KEEP THIS COPY FOR REPRODUCTION PURPOSES

REPORT DOCUMENTATION PAGE

Form Approved
OMB No. 0704-0188

1. AGENCY USE ONLY (Leave blank)	2. REPORT DATE	3. REPORT TYPE AND DATES COVERED
		Final Report- 3 Sept. '92 - 31 Dec. '95

4. TITLE AND SUBTITLE
Adsorption and Catalytic Oxidation with Hydrogen Peroxide of Sulfide and Thioate Substrates

5. FUNDING NUMBERS
DAAL03-92-G-0395

6. AUTHOR(S)
Russell S. Drago

7. PERFORMING ORGANIZATION NAME(S) AND ADDRESS(ES)
Department of Chemistry
University of Florida
Gainesville, Florida 32611-7200

8. PERFORMING ORGANIZATION REPORT NUMBER

9. SPONSORING/MONITORING AGENCY NAME(S) AND ADDRESS(ES)
U. S. Army Research Office
P. O. Box 12211
Research Triangle Park, NC 27709-2211

10. SPONSORING/MONITORING AGENCY REPORT NUMBER
ARO 30464.13-CH

11. SUPPLEMENTARY NOTES
The view, opinions and/or findings contained in this report are those of the author(s) and should not be construed as an official Department of the Army position, policy, or decision, unless so designated by other documentation.

12a. DISTRIBUTION/AVAILABILITY STATEMENT
Approved for public release; distribution unlimited.

12b. DISTRIBUTION CODE

13. ABSTRACT (Maximum 200 words)

This report describes advances made in the catalytic oxidation of sulfides with transition metal complexes and H_2O_2. Also included is a discussion of a multiple equilibrium model for evaluating the adsorption properties of gases by solid adsorbents including porous carbon.

14. SUBJECT TERMS
Catalytic oxidation, metal complex catalyzed oxidations, multiple equilibrium model, adsorbents, porous carbon.

15. NUMBER OF PAGES

16. PRICE CODE

17. SECURITY CLASSIFICATION OF REPORT	18. SECURITY CLASSIFICATION OF THIS PAGE	19. SECURITY CLASSIFICATION OF ABSTRACT	20. LIMITATION OF ABSTRACT
UNCLASSIFIED	UNCLASSIFIED	UNCLASSIFIED	UL

Adsorption and Catalytic Oxidation with Hydrogen Peroxide

of Sulfide and Thioate Substrates

Final Technical Report

by

Russell S. Drago
University of Florida
Department of Chemistry
Gainesville, FL 32611

June 4, 1996

U.S. ARMY RESEARCH OFFICE

DAAL03-92-G-0395

UNIVERSITY OF FLORIDA

The following articles have been published with ARO support during this grant period.

Pore-Resolved NMR Porosimetry, Drago, R. S.; Ferris, D. C.; Burns, D. S. J. Am. Chem. Soc **1995**, 117, 6914-6920.

Redox Considerations for a Ruthenium Complex Catalysis of Substrate Oxidation by Hydrogen Peroxide in Aqueous Solution, Robbins, M. H.; Drago, R. S. J. Chem. Soc., Dalton Trans. **1996**, 105-110.

A New Absorption Model for Analyzing Gas-Solid Equilibria in Porous Materials, Drago, R. S.; Burns, D. S.; Lafrenz, T. J. J. Phys. Chem. **1996**, 100(5), 1718.

In addition to the above results, the rest of the research carried out during this grant period has been submitted for publication. The abstracts of these articles are presented below in lieu of a report and the details included in the preprints which are included as an appendix.

PHYSICAL STUDIES OF MoO_3 CATALYSTS ON SILICA

AND CARBON SUPPORTS

by

Russell S. Drago*, Vaneica Young*, David J. Singh and

Gerald C. Grunewald

ABSTRACT

The nature and characteristics of the catalytic surface of supported MoO_3 catalysts were studied. Changes that occurred on oxidizing alcohols in air over carbon and silica supported MoO_3 were examined. Structural data were combined with electron microscopy and photoelectron spectroscopy to demonstrate that the carbon support promotes segregation and fragmentation of MoO_3, whereas sintering occurs on silica. Results indicated that this may be correlated with a synergism between the carbonaceous material and metal oxide which provides a reoxidation pathway for reduced Mo, thus preventing formation of extended zones of MoO_2, which in inactive for the oxidation of alcohols.

GAS-SOLID EQUILIBRIA IN POROUS CARBONACEOUS MATERIALS

by

Russell S. Drago*, Douglas S. Burns[1], J. Michael McGilvray, Wm. Scott Kassel

Steven K. Showalter[2] and Todd J. Lafrenz[3]

ABSTRACT

Temperature dependent adsorption isotherms for a series of adsorptives on two microporous carbonaceous solids, are used to develop a method that characterizes the affinity of an adsorbent for gas molecules. A predominantly carbon adsorbent (A-572), and a nitrogen containing adsorbent, pyrolyzed poly-acrylonitrile (PPAN), are studied. A multiple process equilibrium interpretation of the data is used to calculate adsorption equilibrium constants for the distribution of the adsorptive between the gas and the solid. Equilibrium constants for three distinct processes ($K_{1,ad}$, $K_{2,ad}$, and $K_{3,ad}$) are found to describe most of the gas-solid adsorption isotherms on both solids. The analysis shows that the first process ($K_{1,ad}$), involves adsorption of the gas by the solid surface in micropores of molecular dimensions. The second process involves adsorption in slightly larger micropores. The third process involves adsorption by larger micropores that can accomodate bilayer adsorption, and for condensible gases multilayer adsorption. In order to define the n's and K's for the three processes, isotherms are measured at several temperatures. In this model, the n-values are temperature independent. Enthalpies for these processes result from the temperature dependent isotherms. The free energies of adsorption plot up linearly with the enthalpies.

For adsorptives which possess little or no dipole moment there is a direct relationship between their polarizability and both the ln K_{ad} values and the enthalpies of adsorption. Molecules with a dipole moment are adsorbed more

effectively by the solid than is expected on the basis of their polarizability (i.e., $K_{1,ad}$ is larger than expected). The free energies and enthalpies of adsorption of all adsorptives on A-572 correlate with the van der Waals constant of the adsorptive to afford predictions of the affinity of these solids for gases that have not been measured. The polar, acceptor adsorbate SO_2 is shown to undergo specific donor-acceptor interactions with PPAN by the van der Waals correlation. The utility of this information for catalytic, gas storage and separation applications is illustrated.

A quantity, referred to as effective pressure (P_{eff}), is introduced to compare the concentrating power of different microporous solids. Effective pressure is of utility in catalytic systems as it indicates the pressure that would have to be applied to an ideal gas to attain a comparable concentration of reactants. The magnitude of P_{eff} is related to adsorptive properties and is influenced by the surface area, pore size, pore distribution, polarity, dispersion, and reactivity of the support.

MOLYBDATE AND TUNGSTATE DOPED POROUS CARBONS AS HYDROGEN PEROXIDE ACTIVATION CATALYSTS FOR SULFIDE OXIDATIONS.

by

Russell S. Drago* and Douglas S. Burns[a]

ABSTRACT

Sodium molybdate, copper$^{(II)}$ molybdate, and sodium tungstate doped into the carbonaceous adsorbent Ambersorb® 572 produced very effective catalytic systems for the oxidation of the mustard simulant ethylphenyl sulfide and the ethylphenyl sulfide intermediate to ethylphenyl sulfone. Complete conversion to the corresponding sulfone occurs using H_2O_2 as the oxidant in a matter of minutes. The novel feature of these catalysts is that they function under basic conditions where base catalyzed hydrolysis reactions can be employed for agent destruction.

STOICHIOMETRIC AND CATALYTIC OXIDATION OF ORGANIC SUBSTRATES WITH IN-SITU GENERATED PERACIDS

by

Russell S. Drago, Alfredo L. M. L. Mateus and Douglas Patton

ABSTRACT

Thioethers are efficiently oxidized by peracids generated *in situ* from carboxylic acid anhydrides and H_2O_2 using 1-methyl-2-pyrrolidinone as the solvent. Sulfoxides or sulfones can be produced in high yields by varying the amount of hydrogen peroxide when an excess of carboxylic acid anhydride is used. Catalytic use of the carboxylic acid was demonstrated for the thioether oxidation by the total conversion of a 2:1 excess of the substrate. This behavior

could not be observed for epoxidation reactions due to the poor nucleophylicity of the olefins. Attempts to increase the concentration of peroxy acid in solution and the secondary reactions of the epoxide product are discussed.

OXIDATIONS OF ALKANES BY THE H_2O_2-VANADIUM-PYRAZINE -2-CARBOXYLIC ACID COMPLEX

by

Georgiy B. Shul'pin, Russell S. Drago, and Michael Gonzalez

ABSTRACT

Light alkanes (ethane, propane, *n*-butane, *n*-pentane) are readily oxidized in acetonitrile solvent by H_2O_2 with vanadium-pyrazine-2-carboxylic acid (PCA) as the catalyst at 75°C and pressures of ~3 atm to produce predominantly or exclusively ketones (aldehydes). Isobutane is transformed selectively into *t*-butanol. The oxidation of cyclohexane at 26°C in acetone or acetic acid is less efficient than that in acetonitrile. The reaction does not occur in *t*-butanol.

Activation Of Hydrogen Peroxide For Oxidations By Copper(II) Complexes

By

Michael H. Robbins[+] and Russell S. Drago*

ABSTRACT

Copper(II) complexes of the general formula $[LCu(H_2O)_4]^{n+}$ (where L is a bidentate ligand and n=1 or 2) activate hydrogen peroxide for the oxidation of quinaldine bule, an oxidation indicator. The copper(II) complexes of tri- and tetra-dentate ligands are shown to be inactive, as are the *bis*-complexes of bidentate ligands. The proposed mechanism for peroxide activation involves the formation of a copper(II)-hydroperoxide complex, which then rapidly oxidized the substrate. Comparison of reaction rates with different ligand systems, and different ligand to metal ratios, lead to the conclusion that two equatorial coordination positions must be occupied by easily displaced water to form the active complex. Rate studies are performed which give an experimental rate law which is first-order in copper(II) complex, zero-order in substrate, and variable order in peroxide. These kinetics are predicated by the rate law derived from our proposed mechanism. The variable order in peroxide can be explained in terms of Michaelis-Menten type kinetics, as linear Lineweaver-Burk plots of $(rate^{-1})$ vs. $([O_2H^-]^{-1})$ are obtained from our experimental data. This is consistent with our proposed mechanism, as the derived rate law can be rearranged into the Michaelis-Menton equation.

Project Dates: September 3, 1992 - December 31, 1995

List of all Participating Scientific Personnel Showing any Advanced Degrees Earned by Them While Employed on the Project

Douglas Patton	(Ph.D. - '93)
John Hage	(Ph.D. - '94)
Chris Chronister	(Ph.D. - '94)
Donald Ferris	(Ph.D. - '94)
Michael Robbins	(Ph.D. - '95)
Todd Lafrenz	(Ph.D. - '95)
Alfredo Mateus	(Grad student)
Kenneth Lo	(Grad student)

APPENDIX

Redox considerations for a ruthenium complex catalysis of substrate oxidation by hydrogen peroxide in aqueous solution

Michael H. Robbins and Russell S. Drago*

Department of Chemistry, University of Florida, Gainesville, FL 32611, USA

The pH dependence of the redox chemistry of $[Ru(dmphen)_2(H_2O)]^{2+}$ has been measured (dmphen = 2,9-dimethyl-1,10-phenanthroline). Comparison of the results with those for similar complexes illustrates the unique acidity of the co-ordinated waters and the large oxidizing strength of the ruthenium. The reaction of $[Ru(dmphen)_2(H_2O)_2]^{2+}$ with H_2O_2 has been studied as a function of pH and the results are used to provide a mechanism for the catalysis of alkane oxidation by this complex.

The metal-catalysed oxidation of organic substrates is a subject of intensive research. Che,[1] Meyer,[2] Takeuchi[3] and Groves[4] and co-workers have extensively examined the synthesis, reactivity and electrochemical properties of a large number of ruthenium complexes. They exist in a wide range of oxidation states and can form stable oxo and dioxo species in solution through proton-coupled electron-transfer reactions. These properties are attractive for oxidation catalysts.

Our research has focused on a unique sterically hindered ruthenium complex, $[Ru(dmphen)_2(H_2O)_2]^{2+}$, where dmphen is 2,9-dimethyl-1,10-phenanthroline. In acetonitrile, this complex is oxidized by hydrogen peroxide and dioxygen to form oxoruthenium(IV) and by hydrogen peroxide to form *cis*-dioxoruthenium(VI). It is a catalyst for oxidizing alkenes and alkanes with O_2 and H_2O_2. The sterically hindering ligands prevent the formation of both μ-oxo dimers and the *trans*-dioxo species. In other polypyridyl complexes the dimers are not very reactive and the *trans*-dioxo complex is a weaker oxidant than the *cis* complex.[1d,2a,d,g,5]

An earlier paper[6a] proposed a mechanism for ruthenium-catalysed oxidation of alkenes and alkanes with dioxygen and hydrogen peroxide. This paper focuses on the inorganic chemistry of the catalyst. The kinetics of formation and thermodynamic oxidization potentials of the various aqua- and oxo-complexes of Ru(dmphen) involved in the catalytic oxidation cycle are studied. The pH dependences of the ruthenium potentials in aqueous solution are reported and compared to the pH-dependent potentials required for the activation of dioxygen and hydrogen peroxide. The use of Pourbaix plots for the prediction of feasible metal complex intermediates is examined. A kinetic study of the reaction of the ruthenium(II) complex with hydrogen peroxide is also reported and the effect of pH examined. The implications of this chemistry on aqueous and non-aqueous catalytic oxidation mechanisms are discussed.

Experimental

Materials

Ruthenium(III) chloride, 2,9-dimethyl-1,10-phenanthroline, $LiClO_4$ and LiCl were all used as received from Aldrich. Potassium hydrogenphthalate (Fisher) was dried overnight at 100 °C under vacuum. 30% Hydrogen peroxide (Fisher) was diluted as appropriate for the kinetic studies and the peroxide concentrations were measured by iodometric titration. The KOH solution used in the pH measurements was prepared by dilution of a stock solution made from KOH pellets (Fisher), followed by standardization with potassium hydrogenphthalate.

Measurements

The UV/VIS measurements were performed on a Perkin-Elmer Lambda-6 spectrophotometer, pH measurements with a Fisher Accumet model 630 pH meter. Cyclic voltammetry was done with a PAR 173 potentiostat/galvanostat attached to a PAR 175 universal programmer, a PAR 179 digital coulometer and a Houston Instrument Omnigraphic 2000 XY-recorder. The reference was a Corning Ag–AgCl general-purpose electrode and the working electrode a Cypress Systems glassy carbon minielectrode. Cyclic voltammetry measurements were done in aqueous solution with 0.1 mol dm^{-3} $LiClO_4$ as the supporting electrolyte and 1.0×10^{-4} mol dm^{-3} ruthenium(II) complex. The pH was adjusted by adding small amounts of dilute KOH. Volume changes were negligible. Cyclic voltammograms were obtained at many different pH levels ranging from 2.42 to 9.90, with a scan rate of 200 mV s^{-1}.

Synthesis

The complex $[Ru(dmphen)_2Cl_2]$ was synthesized as previously described[5] (Found: C, 55.70; H, 3.95; N, 8.95. Calc: C, 55.45; H, 4.30; N, 9.25%).

The complex $[Ru(dmphen)_2(H_2O)_2][PF_6]_2$ was synthesized by a modification of the literature procedures:[5,6a] $[Ru(dmphen)_2Cl_2]$ (0.5 g) was suspended in distilled water (200 cm^3) and then heated to 70 °C. At the higher temperature water displaces the chloride ligand to give the orange diaqua complex. A saturated $NaPF_6$ solution (50 cm^3) in 0.1 mol dm^{-3} HPF_6 was added to the orange solution, which was then cooled in an ice-bath to precipitate the product. The resulting orange-red microcrystals were filtered off, rinsed with 0.1 mol dm^{-3} HPF_6 solution, and then with water. Rinsing was continued until the filtrate was free of chloride ($AgNO_3$ test).

Determination of the oxidation rate of $[Ru(dmphen)_2(H_2O)_2]^{2+}$

The rate of oxidation of $[Ru(dmphen)_2(H_2O)_2][PF_6]_2$ by H_2O_2 was measured by placing a solution (aqueous) (3 cm^3) containing a known concentration of the complex (pH 3.3 for the rate-law study) in a spectrophotometer cell, and then adding aqueous hydrogen peroxide solution (0.5 cm^3). The cell was capped, shaken thoroughly to ensure complete mixing and then placed in the spectrophotometer. The ruthenium(II) absorbance at 495 nm was determined as a function of time and the ionic strength was assumed to be constant. Experiments demonstrated that a ten-fold increase in ionic strength by addition of KCl does not significantly alter the rates and that addition of an excess of chloride to the reaction solution does not alter the reactant complex in the time frame of the experiments; pH changes in the reaction with H_2O_2 were negligible.

In order to determine the change in concentration of ruthenium(II) a correction accounting for the absorbance of oxidized ruthenium species was made. Ref. 6(*b*) shows that ruthenium(III) is first formed when peroxide is added to ruthenium(II). Ruthenium-(IV) and -(VI) are formed sequentially as the amount of added peroxide increases. Isosbestic points are observed for each step and molar absorption coefficient, ε, values for the ruthenium-(II) and -(IV) species can be obtained from analysis of the UV/VIS data. These are 6870 and 3540 $dm^3\ mol^{-1}\ cm^{-1}$, respectively. The concentration of ruthenium(II) and the approximate rate constants result from the measured absorbance, A, using equation (1), where

$$[Ru^{II}]_t = \frac{A - \varepsilon_{IV}[Ru^{II}]_i}{\varepsilon_{II} - \varepsilon_{IV}} \quad (1)$$

A_t = absorbance at time t, $[Ru^n]_t$ = concentration of ruthenium(n^+) at time t, $[Ru^{II}]_i$ = initial concentration of ruthenium(II) and ε_n = molar absorption coefficient of ruthenium(n^+). Since $A_t = [Ru^{II}]_t\varepsilon_{II} + [Ru^{IV}]_t\varepsilon_{IV}$ and $[Ru^{II}]_i = [Ru^{II}]_t + [Ru^{IV}]_t$, combining these equations gives $A_t = [Ru^{II}]_t(\varepsilon_{II} - \varepsilon_{IV}) + [Ru^{II}]_i\varepsilon_{IV}$ which rearranges to equation (1).

Results

Three separate experiments were performed to characterize the reactivity of the $[Ru(dmphen)_2(H_2O)_2]^{2+}$ complex. An electrochemical study was performed in aqueous solution to determine the change in reduction potentials as the pH was changed. Similar experiments have yielded useful insights about the reactivity of other ruthenium complexes.[1a,c,f,g,2l,3b] A pH titration of $[Ru(dmphen)_2(H_2O)_2]^{2+}$ with aqueous potassium hydroxide was carried out to determine the pK_a of the co-ordinated water. A pH titration was used because this complex does not exhibit large pH-dependent changes in the UV/VIS spectrum. The reaction of the ruthenium(II) *cis*-diaqua complex with hydrogen peroxide was also studied and an empirical rate law determined.

Electrochemistry

Fig. 1 shows a typical cyclic voltammogram for the complex at pH 9.9. While the separations between the cathodic and anodic peaks for both couples between 0 and 1 V are slightly greater than 60 mV, the equality of the cathodic and anodic peak currents suggests reversibility, as $i_{p,a}/i_{p,c} \approx 1$.[3b] Other reports of electrochemical studies with a glassy carbon electrode on similar complexes[1g] reveal quasi-reversible or irreversible couples. The Ru^{VI}–Ru^{IV} couple was irreversible.

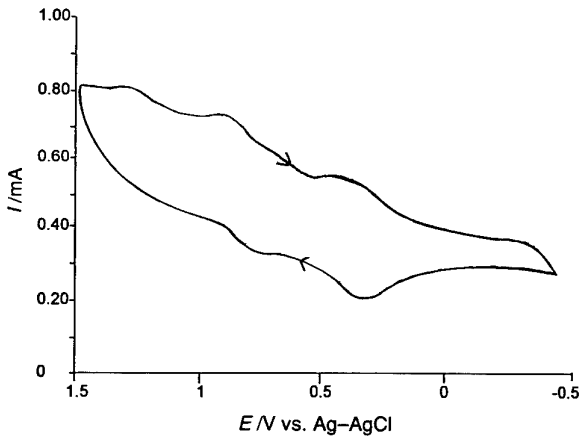

Fig. 1 A typical cyclic voltammogram for the $[Ru(dmphen)_2(H_2O)]^{2+}$ complex at pH 9.90. Reversible couples at 0.55 and 0.85 V and an irreversible reduction at 1.3 V are evident

The $E_{\frac{1}{2}}$ values for the ruthenium redox couples over a wide pH range are shown in Table 1. They have been adjusted to standard reduction potentials by adding 0.197 V to the values obtained with the Ag–AgCl reference.[7] These are reported as reduction potentials for a 1.0×10^{-4} mol dm^{-3} solution of the metal complex. At pH ≥ 5.8 oxidations attributed to the II–III, III–IV and IV–VI couples are observed. At lower pH values only two redox steps are distinguished. The II–III and IV–VI couples are sensitive to pH and the other couples are relatively insensitive. The column labelled IV–II in Table 1 refers to the $E_{\frac{1}{2}}$ value where the III–II and IV–III couples merge into one peak.

Electrochemical measurements of $[Ru(dmphen)_2(H_2O)_2]^{2+}$ in aqueous solution at pH < 3 have been previously reported.[5] We were not able to see the clear separation of the III–II and IV–III oxidations reported at low pH nor did we observe V–IV reduction. The reported $E_{\frac{1}{2}}$ values are in good agreement with ours and their change with pH will be discussed subsequently.

Titration

The solution pH changes for the $[Ru(dmphen)_2(H_2O)_2][PF_6]_2$ complex as it was titrated with standardized KOH(aq) solution, are shown in Fig. 2. The curve exhibits two inflection points, one at the addition of 1 mol of KOH(aq) per mol of ruthenium complex and the second after 2 mol. The measured pK_a values are 4 and 6 for the sequential deprotonation of two aqua ligands. The first conjugate base produced is $[Ru(dmphen)_2(H_2O)(OH)]^+$ and the species observed after removal of the second proton is proposed to be $[Ru(dmphen)_2(OH)_2]$. The small change in the UV/VIS spectrum with pH does not permit a correlation of the pK_a values to direct spectral changes.

The pK_a values for $[Ru(dmphen)_2(H_2O)_2]^{2+}$ are much lower than those reported by Meyer[2,8] and Che[1c,d,f,g] and co-workers for water co-ordinated to other ruthenium(II) centres and are closer to those reported by Che *et al.*[1g] for co-ordinated water in *trans*-diaquaruthenium(III) complexes. Steric problems cause the dmphen ligand to be more weakly bound, making the ruthenium centre more electrophilic and binding the water more strongly. The electrochemical results are consistent with more weakly bound dmphen ligands. The reduction potentials for high-valence *cis*-dioxoruthenium(VI) complexes are known to be higher (by over 200 mV)[1c,d] than those of the *trans* species. The dmphen complex of ruthenium shows an unusually high VI–IV reduction potential compared to the *cis*-bipyridine complexes of ruthenium.[1c] Less stabilization of the high oxidation state indicated by the electrochemical results is consistent with a weak interaction between the ruthenium centre and the dmphen ligand.

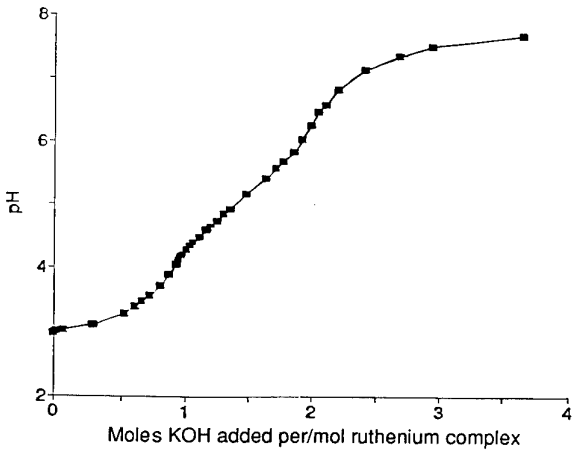

Fig. 2 Titration curve for $[Ru(dmphen)_2(H_2O)_2]^{2+}$ with KOH in water. Note the inflection points which give pK_a values for the co-ordinated water as 4 and 6

Table 1 The $E_{\frac{1}{2}}$ values for the different pH levels examined, adjusted to reflect voltages *vs.* normal hydrogen electrode

pH	Ru^{III}–Ru^{II}	Ru^{IV}–Ru^{II}	Ru^{IV}–Ru^{III}	Ru^{VI}–Ru^{IV}
9.90	0.747	—	1.05	1.52
8.24	0.747	—	1.05	1.52
7.12	0.772	—	1.05	1.52
6.49	0.847	—	1.05	1.52
5.78	0.872	—	1.05	1.52
5.19	—	1.02	—	1.52
4.60	—	1.02	—	1.52
3.74	—	1.05	—	1.52
3.09	—	1.06	—	1.60
2.42	—	1.06	—	1.70

Table 2 Results of initial rate measurements. All concentrations are in mol dm^{-3}, initial rates in mol $[Ru^{2+}]$ dm^{-3} s^{-1}. Initial rates were determined by a linear regression performed on the data from the first 10 s of the kinetic runs. In all cases the R^2 value was 0.99 or better, insuring linearity

Run	$[H_2O_2]$	10^4 $[Ru(dmphen)_2(H_2O)_2^{2+}]$	10^7 Initial rate
1	0.066 0	1.15	19.0
2	0.026 4	1.15	9.85
3	0.010 6	1.15	4.15
4	0.005 77	1.15	2.24
5	0.002 11	1.15	1.05
6	0.026 4	0.69	6.55
7	0.026 4	0.46	3.50
8	0.026 4	0.33	2.15

Oxidation of the ruthenium complex by hydrogen peroxide

The spectral changes that occur in the reaction between the $[Ru(dmphen)_2(H_2O)_2]^{2+}$ complex and hydrogen peroxide lead to a decrease in the strong absorbance at 495 nm for the ruthenium(II) complex in aqueous solution.[6b] The initial rates for different ruthenium and peroxide concentrations are given in Table 2. The initial rate is expressed as the decrease in concentration of the ruthenium(II) species over the first 10 s of the reaction. From these initial rates, the empirical rate law[9] is found to be first order in peroxide and ruthenium concentrations, equation (2), where $k = 0.32 \pm 0.04\ dm^3\ mol^{-1}\ s^{-1}$ at 23 °C.

$$-d[Ru^{II}]/dt = k[Ru^{II}][H_2O_2] \quad (2)$$

The reaction of $[Ru(dmphen)_2(H_2O)_2]^{2+}$ with hydrogen peroxide was observed over a range of pH values. As can be seen from the slopes of the lines in Fig. 3, the initial rate of oxidation changes only slightly as the pH changes. The equilibrium concentrations of aqua and hydroxo species apparently are compensated for by changes in the concentrations of H_2O_2 and HO_2^- leading to a small change in rate with pH. As can be seen in Fig. 3, when the pH is increased from 3.33 to 9.13, the net loss of absorbance at 495 nm decreases substantially. At pH $\leqslant$ 4 the Ru^{II} is almost completely oxidized to Ru^{VI}. However, as the pH increases the reaction seems to proceed to only the ruthenium(IV) species. The conclusion about the species formed is based upon the values for ε obtained from the data in ref. 6b. Since the molar absorption coefficient of Ru^{IV} is between those of Ru^{II} and Ru^{VI} a smaller decrease in absorbance is expected when Ru^{IV} is the product.

A more detailed kinetic analysis of the time dependence of the data in Fig. 3 would involve fitting these curves by rate constants for oxidation and reduction reactions of all the hydroxo- and oxo-ruthenium species present at each pH. The pK_a values for higher-oxidation-state complexes would also have to be solved. With so many unknown parameters, the added quantitative insights obtained from such an analysis about the species involved in catalytic reactions are limited so the data fit was not attempted.

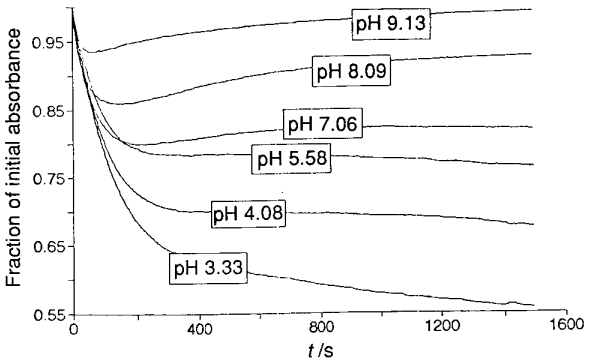

Fig. 3 Kinetic curves for ruthenium(II) oxidation by H_2O_2 at different pH. Note the similarity of initial rates, and the inability of the peroxide completely to oxidize the complex at higher pH values

Discussion

Metal complex activation of H_2O_2

The reactivity of H_2O_2 with $[Ru(dmphen)_2(H_2O)_2]^{2+}$ and the ability of the resulting system to catalyse substrate oxidation is governed by the dependence of the reduction potentials of the metal complex and hydrogen peroxide on the hydrogen-ion concentration. In peroxide activation the insights from electrochemical data become even more important because hydrogen peroxide can act as both a reductant and an oxidant, as shown in equations (3) and (4).

$$H_2O_2 + M^{(n+)} + 2H^+ \rightleftharpoons 2H_2O + M^{(n+2)} \quad (3)$$

$$H_2O_2 + M^{(n+2)} \rightleftharpoons O_2 + 2H^+ + M^{(n+)} \quad (4)$$

Peroxide reduction and metal oxidation, equation (3), is involved in substrate oxidation by Class III (metal oxide formed from peroxides) or Class V (high-valent metal-centred oxidants) mechanisms.[10] One-electron oxidation can be involved in some Class V mechanisms or in alkyl peroxide decomposition by a Class IVa (Fenton-type) mechanism. In a Class III reaction the metal undergoes the two-electron change shown in equation (3), but the product is an oxo metal complex. Catalysis (or peroxide activation) by the metal complex occurs when the oxidized metal complex, peroxo metal or oxo metal species is kinetically more reactive than peroxide in the oxidation of substrate. In addition, depending on the potentials, the oxidized complex may oxidize hydrogen peroxide as shown in equation (4). When the oxidized and reduced forms of a given metal complex catalyst lead to both peroxide reduction and oxidation the catalysed decomposition of hydrogen peroxide to water and dioxygen occurs.

The reduction potentials[11] in acidic (pH 0) aqueous solution for the half-reactions involving hydrogen peroxide are given in equations (5) and (6). The pH dependences of these potentials (a Pourbaix plot), as calculated by the Nernst equation, are shown in Fig. 4. The potential for peroxide being reduced (*i.e.* the peroxide half-reaction when it oxidizes the transition-metal complex) is given by line A. The reduction potential for the two-electron reduction of O_2 to H_2O_2 is given by line B in Fig. 4.

$$O_2 + 2H^+ + 2e^- \rightleftharpoons H_2O_2;\ 0.695\ V \quad (5)$$

$$H_2O_2 + 2H^+ + 2e^- \rightleftharpoons 2H_2O;\ 1.776\ V \quad (6)$$

The redox considerations presented above are not new.[1-3]

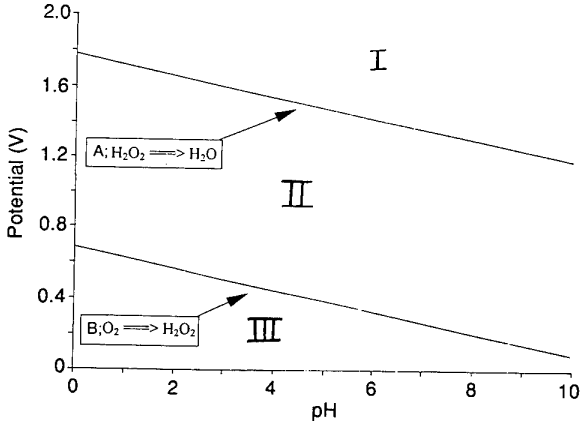

Fig. 4 The pH dependence of the half-reaction potentials for reduction (A) and oxidation (B) of hydrogen peroxide

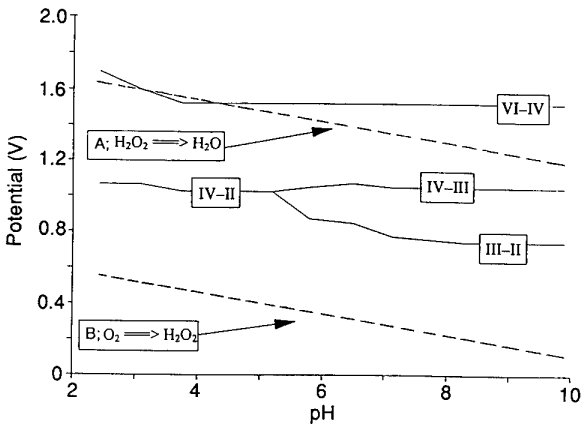

Fig. 5 Comparison of the ruthenium reduction potentials (solid lines) and the potentials for oxidation and reduction of hydrogen peroxide (dashed lines)

However, we do recommend a more consistent use of Fig. 4 as a template upon which metal redox potentials can be plotted to predict the reactivity of a prospective catalyst with hydrogen peroxide. In aqueous solution, metal complexes with two-electron reduction potentials falling in region I of Fig. 4 will act only as stoichiometric oxidants, because even hydrogen peroxide is not strong enough an oxidant to reoxidize the reduced form of the metal complex. Metal catalysts with two-electron reduction potentials falling in region II of Fig. 4 will activate hydrogen peroxide, but also have a thermodynamic tendency to decompose the peroxide. Those falling in region III will not decompose hydrogen peroxide, and will produce relatively mild oxidants that activate hydrogen peroxide with high utilization efficiency.

Based on the above thermodynamic considerations, any metal complex which utilizes hydrogen peroxide to produce a high-oxidation-state metal complex *cannot be*, on thermodynamic grounds, both as strong an oxidant as hydrogen peroxide and also efficiently use hydrogen peroxide in aqueous solution. Kinetic factors have to exist that slow peroxide reduction of the complex in order to obtain an efficient catalyst.

Fig. 4, while admittedly simplistic, also explains the behaviour of metal oxidases. Under standard conditions O_2 is not able to oxidize any metal complex having a reduction potential above line B in Fig. 4, and as a result these complexes cannot participate in metal-catalysed activation of O_2. If a sacrificial two-electron reducing agent can be used to convert O_2 into H_2O_2, any metal complex with a reduction potential below line A in Fig. 4 can be oxidized and can function as a catalyst for substrate oxidation. These thermodynamic considerations explain the role of the sacrificial reducing agent in monooxygenase-type systems. Without the sacrificial reducing agent to form peroxide, O_2 is not able to oxidize metal complexes having reduction potentials in region II of Fig. 4. These considerations have general applicability for eliminating metal species proposed as aqueous oxidizing agents in catalytic cycles. Unfortunately, the necessary redox potentials in non-aqueous solvents are not available to permit an analysis under these conditions.

pH Dependence of peroxide activation by $[Ru(dmphen)_2(H_2O)_2]^{2+}$

In this section the discussion presented above will be applied to the possibility of using $[Ru(dmphen)_2(H_2O)_2]^{2+}$ as a catalyst for substrate oxidation in aqueous solution. Fig. 5 shows the ruthenium reduction potentials (indicated by solid lines) superimposed on the peroxide potential template (dashed lines) of Fig. 5. The oxidation of ruthenium(II) to ruthenium(IV) by H_2O_2 is spontaneous at all pH values shown. The reduction potentials for the Ru^{IV}–Ru^{II} and Ru^{III}–Ru^{II} couples are both lower than that of hydrogen peroxide, but still high enough to be in region II, where hydrogen peroxide decomposition can occur. As we get to higher pH levels the reduction potential of H_2O_2 is too low (*i.e.* H_2O_2 is not a good enough oxidizing agent) to oxidize ruthenium(IV) to ruthenium(VI). The ruthenium(VI) complex is formed in diminishing amounts as the pH rises above 5. This chemistry accounts for the pH dependence of the oxidation of $[Ru(dmphen)_2(H_2O)_2]^{2+}$ by peroxide shown in Fig. 3. From pH 5.5 to 9 the absorbance decrease is attributed to the formation of Ru^{IV}. The increase in absorbance with time after 150–200 s above pH 5.6 results from the reduction of ruthenium(IV) to ruthenium(II) by H_2O_2. As the pH decreases below 5.6 the amount of Ru^{VI} formed increases, and a larger decrease in absorbance is observed.

In catalysed oxidations with this complex[6] efficient use of peroxide results from a slow kinetic pathway for peroxide oxidation/metal reduction. The nucleophilic oxygen of peroxide is more likely to displace water from the ruthenium(II) than to displace aqua or hydroxo ligands from the ruthenium(IV) complex and reduce it. The aqua and/or hydroxide ligands on the ruthenium(IV) are not likely to be removed when it is oxidized to Ru^{VI}. Rather, it is likely that a proton-coupled electron transfer occurs at this point. Proton-coupled electron transfer has been seen in similar complexes.[1e,2a,b] Thus, for kinetic reasons the ruthenium(II) complex is oxidized faster by peroxide than the ruthenium-(IV) or -(VI) complex is reduced.

Conclusions on the rates of competitive reactions cannot be based on thermodynamic considerations alone. For example, the potentials (Fig. 5) show that at pH 3 the reaction of hydrogen peroxide with ruthenium(IV) is spontaneous to form either ruthenium-(II) or -(VI). The reaction of the ruthenium(IV) complex and hydrogen peroxide to form the ruthenium(II) complex, and oxidize peroxide, is favoured thermodynamically over the reduction of the peroxide to form the ruthenium(VI) complex. However, the spectrophotometric studies in Fig. 3 show that the reaction to form the ruthenium(VI) species is favoured. Thus, kinetic factors must facilitate the reaction to produce ruthenium(VI).

Applications of the analysis presented above in catalytic oxidations can provide insights about the metal oxidants generated in catalytic cycles for peroxide and for dioxygen activation in aqueous solution. If the reduction potential for metal complex oxidation becomes significantly more positive than the peroxide or dioxygen reduction potential, substrate oxidations through Class III and V mechanisms are not possible. If substrate oxidation is found to occur a Class IV

mechanism involving nucleophilic attack on a co-ordinated peroxide is suggested. The metal complex must remain soluble for these considerations to be relevant and this is often a problem at higher pH, as transition-metal hydroxides and oxides often form under basic conditions.

Oxidation of alkenes by $[Ru(dmphen)_2(solv)_2]^{2+}$ and O_2 (solv = H_2O or MeCN)

The epoxidation of alkenes by O_2 occurs in acetonitrile solution.[6] In the absence of peroxides the reaction has a 24 h induction period. This induction period is eliminated when 3 equivalents of an alkyl hydroperoxide or hydrogen peroxide are added. Previously we had concluded that alkyl hydroperoxide is formed in the induction period, and this reacts to form ruthenium(IV). It was proposed that ruthenium(IV) is oxidized to ruthenium(VI) by dioxygen and ruthenium(VI) is the oxygen-atom-transfer agent. The addition of peroxides eliminated the induction period by oxidizing ruthenium(II) to ruthenium(IV).

The redox considerations presented above are not directly applicable to acetonitrile. Sauvage and Collins[5] report that the Ru^{III}–Ru^{II} reduction potential for $[Ru(dmphen)_2(solv)_2]^{2+}$ changes from 1.0 V in water to 1.7 V in MeCN. Unfortunately, the reduction potentials of O_2 in most non-aqueous solvents are not known. However, in view of the high reduction potential in aqueous solution, the generation of ruthenium(VI) by O_2 in non-aqueous solutions is suspect. The following scheme can be proposed as an alternative to the generation of a ruthenium(VI) species. Ruthenium(II) is oxidized to ruthenium(III) by alkyl hydroperoxide formed slowly in the induction period from alkene autoxidation. The formation, and subsequent decomposition, of the alkyl hydroperoxide is indicated by the small amounts of ketone and alcohol formed during the induction period when the alkene epoxidation is carried out with O_2.[6a] These products are not formed after the induction period. Radicals formed during the metal-catalysed peroxide decomposition which lead to ketone and alcohol have been identified[12] by spin-trapping experiments. During the induction period the ruthenium(III) concentration slowly increases. Once a significant concentration of ruthenium(III) forms (probably containing co-ordinated water) it can be oxidized to the oxoruthenium(IV) species by dioxygen in acetonitrile solvent. Nucleophilic attack on an alkene by $Ru^{IV}O$ results in oxygen-atom transfer to form epoxide and reduction of the metal to ruthenium(II). The ruthenium(II) complex can react with ruthenium(IV) to produce two ruthenium(III) complexes which then react with dioxygen to produce oxoruthenium(IV). The reaction becomes catalytic after the required steady-state concentration of ruthenium(III) forms. This mechanism is shown in Scheme 1.

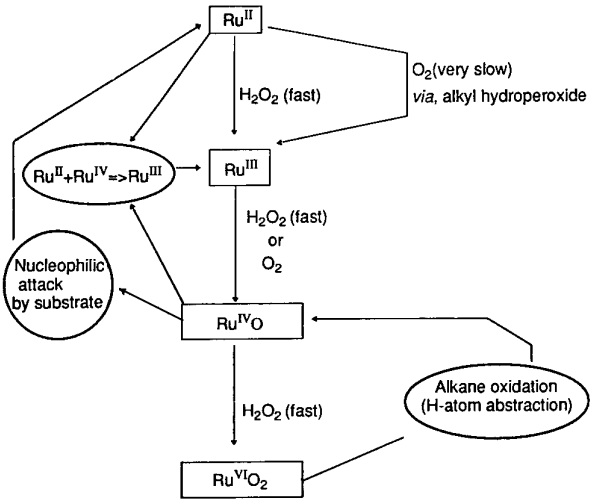

Scheme 1 An alternative mechanism for oxidation of alkanes and alkenes with the $[Ru(dmphen)_2(H_2O)_2]^{2+}$ complex in the presence of H_2O_2 and O_2

Conclusion

The complex $[Ru(dmphen)_2(H_2O)_2]^{2+}$ undergoes a reaction with hydrogen peroxide which is first order in both ruthenium and peroxide concentration. At pH > 4 the acidic protons of the aqua ligands are neutralized (pK_a 4 and 6). The electrochemical experiments confirm this transformation by showing breaks in the plot of $E_{\frac{1}{2}}$ *vs.* pH at the deprotonation pH values. The pK_a values illustrate the weak binding of the dmphen ligand and the high partial positive charge on the ruthenium centre in this complex. Kinetic studies of the reaction of the ruthenium complex with H_2O_2 show that significant amounts of the active *cis*-dioxoruthenium(IV) complex are not formed above pH 5.

Fig. 4 is proposed as a template upon which substrate and metal-ion potentials can be superimposed to predict and explain the reactivity of hydrogen peroxide with a transition-metal complex in aqueous solution. As with any thermodynamic argument, the only certain prediction about reactivity is that reactions with large positive free energies will not occur. The inability of $[Ru(dmphen)_2(H_2O)_2]^{2+}$ to form $[Ru(dmphen)_2O_2]^{2+}$ by reaction with hydrogen peroxide in aqueous solution at higher pH levels is described using this template. The procedures discussed can be used to screen transition-metal complexes as peroxide-activation catalysts in aqueous solutions of different pH. When free-energies are applied in aqueous solution under other than standard conditions or in non-aqueous solvents, qualitative estimates of the influence of these conditions on the relevant potentials must be made.

Acknowledgements

We acknowledge the support of this research by the US Army (Army Research Office and Edgewood Research Development and Engineering Centre) and Amoco.

References

1 (*a*) C. M. Che, T. F. Lai and C. W. Chan, *J Chem. Soc., Dalton Trans.*, 1994, 895; (*b*) C. M. Che, C. K. Li, W. F. Tong and T. F. Lai, *J. Chem. Soc., Dalton Trans.*, 1992, 816; (*c*) C. M. Che, W. H. Leung, C. K. Li and C. K. Poon, *J. Chem. Soc., Dalton Trans.*, 1991, 379; (*d*) C. M. Che, K. Y. Wong and W. O. Lee, *J. Electroanal. Chem. Interfacial Electrochem.*, 1991, **319**, 207; (*e*) C. M. Che, K. Lau, T. C. Lau and C. K. Poon, *J. Am. Chem. Soc.*, 1990, **112**, 5176; (*f*) C. M. Che, W. T. Tang, W. O. Lee, W. T. Wong and T. F. Lai, *J. Chem. Soc., Dalton Trans.*, 1989, 2011; (*g*) C. M. Che, W. T. Tang, W. T. Wong and T. F. Lai, *J. Am. Chem. Soc.*, 1989, **111**, 9048; (*h*) C. M. Che and W. O. Lee, *J. Chem. Soc., Chem. Commun.*, 1988, 881; (*i*) T. C. Lau, C. M. Che, W. O. Lee and C. K. Poon, *J. Chem. Soc., Chem. Commun.*, 1988, 1406; (*j*) C. M. Che and W. H. Leung, *J. Chem. Soc., Chem. Commun.*, 1987, 1376; (*k*) C. M. Che, W. H. Leung and C. K. Poon, *J. Chem. Soc., Chem. Commun.*, 1987, 173; (*l*) C. M. Che, T. F. Lai and K. Y. Wong, *Inorg. Chem.*, 1987, **26**, 2289; (*m*) C. M. Che, K. Y. Wong, W. H. Leung and C. K. Poon, *Inorg. Chem.*, 1986, **25**, 345.

2 (*a*) T. J. Meyer and A. Dovletoglou, *J. Am. Chem. Soc.*, 1994, **116**, 215; (*b*) T. J. Meyer, L. E. Roecker, W. K. Seok, A. Dovletoglou, M. E. McGuire and R. A. Binstead, *J. Am. Chem. Soc.*, 1992, **114**, 173; (*c*) T. J. Meyer and O. Geselowitz, *Inorg. Chem.*, 1990, **29**, 3894; (*d*) T. J. Meyer, A. Dovletoglou, S. A. Adeyemi, M. H. Lynn and D. J. Hodgson, *J. Am. Chem. Soc.*, 1990, **112**, 8989; (*e*) T. J. Meyer, A. Llobet and D. J. Hodgson, *Inorg. Chem.*, 1990, **29**, 3760; (*f*) T. J. Meyer, J. C. Dobson, J. H. Helms, P. Doppelt, B. P. Sullivan, and W. E. Hatfield, *Inorg. Chem.*, 1989, **28**, 2200; (*g*) T. J. Meyer and J. C. Dobson, *Inorg. Chem.*, 1988, **27**, 3283; (*h*) T. J. Meyer and L. Roecker, *J. Am. Chem. Soc.*, 1987, **109**, 746; (*i*) T. J. Meyer, L. Roecker, J. C. Dobson and W. J. Vining, *Inorg. Chem.*, 1987,

26, 779; (*j*) T. J. Meyer, J. Gilbert and L. Roecker, *Inorg. Chem.*, 1987, **26**, 1126; (*k*) T. J. Meyer, T. C. Dobson, and W. K. Seok, *Inorg. Chem.*, 1986, **25**, 1514; (*l*) T. J. Meyer, K. J. Takeuchi, M. S. Thompson and D. W. Pipes, *Inorg. Chem.*, 1984, **23**, 1845.
3 (*a*) K. J. Takeuchi, J. G. Muller and J. H. Acquaye, *Inorg. Chem.*, 1992, **31**, 4552; (*b*) K. J. Takeuchi and M. E. Marmion, *J. Am. Chem. Soc.*, 1988, **110**, 1472; (*c*) K. J. Takeuchi, R. A. Leising and J. S. Ohman, *Inorg. Chem.*, 1988, **27**, 3804; (*d*) K. J. Takeuchi and M. E. Marmion, *J. Chem. Soc., Chem. Commun.*, 1987, 1396; (*e*) K. J. Takeuchi and M. E. Marmion, *J. Am. Chem. Soc.*, 1986, **108**, 510.
4 J. T. Groves, K.-H. Ahn and R. Quinn, *J. Am. Chem. Soc.*, 1988, **110**, 4217; J. T. Groves and K.-H. Ahn, *Inorg. Chem.*, 1987, **26**, 3833; J. T. Groves and R. Quinn, *J. Am. Chem. Soc.*, 1985, **107**, 5790; *Inorg. Chem.*, 1984, **23**, 3844.
5 J. P. Sauvage and J. P. Collins, *Inorg. Chem.*, 1986, **25**, 135.
6 (*a*) R. S. Drago, R. H. Beer and A. S. Goldstein, *J. Am. Chem. Soc.*, 1994, **116**, 2424; (*b*) A. S. Goldstein and R. S. Drago, *J. Chem. Soc., Chem. Commun.*, 1991, 21; (*c*) C. L. Bailey and R. S. Drago, *J. Chem. Soc., Chem. Commun.*, 1987, 179.
7 A. J. Bard and L. R. Faulkener, in *Electrochemical Methods*, Wiley, New York, 1980.
8 T. J. Meyer and B. A. Moyer, *Inorg. Chem.*, 1981, **20**, 436; T. J. Meyer, K. J. Takeuchi, M. S. Thompson and D. W. Pipes, *Inorg. Chem.*, 1984, **23**, 1845.
9 K. Laidler, *Chemical Kinetics*, Harper and Row, New York, 1987.
10 R. S. Drago, *Coord. Chem. Rev.*, 1992, **117**, 185; R. S. Drago and R. H. Beer, *Inorg. Chim. Acta*, 1992, **198**, 359.
11 N. N. Greenwood and A. Earnshaw, in *Chemistry of the Elements*, Pergamon, New York, 1989.
12 S. Zhang and R. E. Shepherd, *Inorg. Chem.*, 1988, **27**, 4712.

Received 2*nd June* 1995; *Paper* 5/03547C

Pore-Resolved NMR Porosimetry

Russell S. Drago,* Donald C. Ferris, and Douglas S. Burns

Contribution from the Department of Chemistry, University of Florida, Gainesville, Florida 32611-7200

Received August 12, 1994[⊗]

Abstract: For the first time, high-field FT-NMR spectra of an adsorbate inside a porous solid exhibits multiple resonances corresponding to different sites. Frequency shift, T_1, and T_2 measurements as a function of adsorbate concentration support the assignment of these resonances to probe molecules in solution and in pores of various sizes within the solid. Resolution of the bands and combination of the NMR intensities with the adsorption isotherm lead to an unprecedented amount of detail about the distribution of the adsorbate in the solid pores as a function of probe concentration (see Figures 5 and 6). The detection of separate resonances by NMR is referred to as pore-resolved NMR porosimetry to distinguish this method from NMR analyses based on extracting information from a single resonance of an adsorbed probe molecule.

Introduction

The adsorptive properties of porous materials have been employed to separate and purify liquids and gases. Recent work from this laboratory has shown the advantage of porous solids when used as catalyst supports.[1] For these applications a fundamental understanding of gas−solid and liquid−solid equilibria is relevant. Investigations of gas−solid equilibria in porous carbonaceous adsorbents showed that the adsorption isotherms required different equilibrium processes involving surface adsorption and multilayer adsorption to fit the data.[2] This work was later extended to investigate the competitive adsorption of probe molecules from dilute solutions.[3]

In all of the above work, the process at low adsorbate concentrations is attributed to surface adsorption in the smaller pores. Pores in supports have been divided into three groups by IUPAC. Micropores are those pores that are <20 Å in diameter. Mesopores are those that are between 20 and 500 Å in size. Macropores are defined as pores with diameters larger than 500 Å.[4] Micropores adsorb molecules with significantly larger adsorption energies than do meso- or macropores due to superimposed interaction potentials from opposite surfaces within the pore.[5,6] Everett and Powl[7] calculated interaction energies as a function of pore size based on the Lennard-Jones potential model. In cylindrical pores of sizes that are five adsorbate diameters or less, the model predicts increasing adsorption energies with decreasing pore size. Preferential micropore adsorption occurs because of these higher adsorption energies.

The above studies employed the classical method for characterizing porous materials through the use of adsorption isotherms. This technique only provides information about the number of different processes required to describe the isotherm. In order to better understand the adsorptive properties of these solids, it would be useful to have a spectral measure of the distribution of the probe in the various micro-, meso-, and macropores at various probe concentrations. This work describes an NMR method that leads to a direct observation of the role of the various pores of carbonaceous adsorbents in the preferential adsorption of one component from a dilute binary solution.

Nuclear magnetic resonance (^{1}H-NMR) has been used extensively to investigate solid−solute interactions. In early work, two ^{1}H-NMR signals were reported for water in contact with Dowex 50W ion-exchange resin.[8] One peak was shown to be exterior water while the second peak was water inside the resin. ^{1}H-NMR has also been used[9] to study water in various hydrated aluminas. The NMR line widths of the protons were a function of surface area as measured by N_2 adsorption and the fraction of hydroxyl groups on the surface could be estimated from the width of the ^{1}H-NMR lines. A series of gels and macroreticular (highly ordered) ion-exchange resins[10,11] in water showed in all cases only a single broad peak for water in the resin and a second peak for external water. Broadened resonances corresponding to only a single interior site for probe molecules adsorbed by carbons have been reported.[12]

The last decade has seen the report of a large body of work using ^{129}Xe, ^{2}H, and proton NMR.[13] The xenon probe experiences large shifts that are very sensitive to the xenon environment.[14,15] The majority of the research in this area involves study of zeolites, silica gel, and porous glasses.[14] Recent reports describe extensions of xenon NMR to porous carbonaceous

[⊗] Abstract published in *Advance ACS Abstracts,* June 15, 1995.

(1) (a) Grunewald, G. C.; Drago, R. S. *J. Mol. Catal.* **1990**, *58*, 227. (b) Grunewald, G. C.; Drago, R. S.; Clark, J. L.; Livesey, A. B. *J. Mol. Catal.* **1990**, *60*, 239. (c) Grunewald, G. C.; Drago, R. S. *J. Am. Chem. Soc.* **1991**, *113*, 1636. (d) Petrosius, S. C.; Drago, R. S. *J. Chem. Soc., Chem. Commun.* **1992**, 334. (e) Petrosius, S. C.; Drago, R. S.; Young, V.; Grunewald, G. C. *J. Am. Chem. Soc.* **1993**, *115*, 6131.

(2) Drago, R. S.; Burns, D. S.; Lafrenz, T. J. *J. Phys. Chem.* Submitted for publication.

(3) Drago, R. S.; Burns, D. S.; Gregory, T. K. In preparation.

(4) (a) Sing, K. S. W.; Everett, D. H.; Haul, R. A. W.; Moscou, L.; Pierotti, R. A.; Rouquérol, J.; Siemieniewsky, T. *Pure Appl. Chem.* **1985**, *57* (4), 603. (b) Rouquérol, J.; Avnir, D.; Fairbridge, C. W.; Everett, D. H.; Haynes, J. H.; Pernicone, N.; Ramsay, J. D. F.; Sing, K. S. W.; Unger, K. K. *Pure Appl. Chem.* **1994**, *66* (8), 1739.

(5) Everett, D. H.; Whitton, W. I. *Proc. R. Soc. London* **1955**, *A230*, 91.

(6) Farrell, J.; Reinhard, M. *Environ. Sci. Technnol.* **1994**, *28*, 53.

(7) Everett, D. H.; Powl, J. C. *J. Chem. Soc., Faraday Trans. 1* **1976**, *72*, 619.

(8) Gordon, J. E. *J. Phys. Chem.* **1962**, *66*, 1150.

(9) (a)Pearson, R. M. *J. Catal.* **1971**, *23*, 388. (b) Baker, B. R.; Pearson, R. M. *J. Catal.* **1974**, *33*, 265.

(10) Frankel, L. S. *J. Phys. Chem.* **1971**, *75*, 1211 and references cited therein.

(11) (a) Creekmore, R. W.; Reilly, C. N. *Anal. Chem.* **1970**, *42*, 570. (b) Creekmore, R. W.; Reilly, C. N. *Anal. Chem.* **1970**, *42*, 725.

(12) Gradsztajn, S.; Conard, J.; Benoit, H. *J. Phys. Chem. Solids* **1970**, *31*, 1121.

(13) (a) Smith, D. M.; Davis, P. J. in *Characterization of Porous Solids II*; Rodriguez-Reinoso, F., Unker, K. K., Eds.; Elsevier Science Publishers B.V.: Amsterdam, 1991; p 301. For a good review see: (b) Klinowski *J. Chem. Rev.* **1991**, *91*, 1459. (c) Bahceli, S.; Al-Kaisi, A. R. S.; Strange, J. H. In ref 13a, p 293.

0002-7863/95/1517-6914$09.00/0

materials.[15] In all of these studies a single resonance is observed for the adsorbed probe molecule. Low-field FT-NMR and magnetic resonance imaging have also been employed[16] to give pore size information on silica gels and porous glasses.

In the work that will be described here, it will be shown that for the first time a conventional high-field FT-NMR procedure gives rise to multiple signals for an adsorbate inside different size pores of a solid adsorbent. Exchange of the adsorbate between the different pores, as well as between the solution and the solid pores, is shown to be slow on the NMR time scale. Integration of the signals provides quantitative information about the distribution of the probe in the pores of the solid.

Experimental Section

Materials. Probes and solvents were acetonitrile, dichloromethane, benzene, and carbon tetrachloride. All liquids were freshly distilled and stored over 4 Å sieves to prevent contamination from H_2O.

Ambersorb 572 (lot 2125) (A-572) was provided to us by Rohm and Haas Company (Philadelphia, PA) as 1 mm diameter beads. The beads were soxhlet extracted with methanol for 12−24 h, dried in a vacuum-oven overnight at higher than 110 °C, and stored in a capped vial. The same results were obtained when higher temperatures (200 °C) are used to dry the beads. When wet beads are used in an NMR experiment, water is displaced and appears as a separate resonance at low field. Addition of water increases the intensity of this peak. The solids were periodically placed in the vacuum-oven overnight to insure that water was not picked up during handling and standing.

NMR Measurements. Approximately 0.22 g of A-572 was precisely measured into a standard NMR tube. A 1.00-mL aliquot of a known concentration of probe in CCl_4 was then pipeted over the solid. The entire sample was shaken vigorously and allowed to settle and equilibrate for 1 day with occasional agitation unless otherwise noted. The tube was tapped until no trapped air was evident in and around the beads. The ^{1}H-NMR spectrum of the solution inside and surrounding the solid was then obtained using a Varian-300 MHz NMR instrument. The tube was filled so that the solid filled the probe coil. The sweep width was set to 12 000 Hz with the placement of 0 ppm set by an external lock. In all spectra, 256 transients were acquired and the sample tube was not spinning unless otherwise noted. All spectra were obtained at ambient pressure and unless otherwise noted at ambient temperature.

The spectra contain overlapping peaks and these were resolved into individual components to determine peak areas. The spectra were digitized using the program UN-PLOT-IT.[17] The spectra were deconvoluted using Lorentzian curves and a linear base line with the program PeakFit.[18] Various initial estimates of the amplitude, frequency shift, and peak widths converged to the same final spectra. Validity of the fitting procedure is provided by the constancy of the frequency components comprising a series of very different shaped spectra at different concentrations (see Figure 2).

The T_1 relaxation times were measured using the standard procedure.[19] These measurements were made on all samples studied. Measurements at several frequencies in a given resolved band produced the same T_1 within experimental error as those measured and reported at the resolved band maximum. This is not unexpected in view of the similarity of the T_1's for micro- and mesopores.

The T_2 relaxation times (s) were approximated by converting the half width at half height of the curve resolved peaks ($w_{1/2}$, ppm) to seconds using eq 1. Temperature dependent studies indicate the system is the fast exchange region where eq 1 is applicable.[20,21]

$$T_2 = \frac{1}{\pi w_{1/2}\,(300\ \text{MHz})} \tag{1}$$

Adsorption Measurements. The equilibrium acetonitrile solution concentrations were quantified using a Hewlett-Packard HP 5890 A-FID gas chromatograph outfitted with an RSL-160 30 m × 0.32 mm id capillary column from Alltech. The equilibrium concentrations of the benzene solutions were determined from UV/vis spectra ($\lambda = 260$ nm) in 0.1-cm quartz UV cells in a Perkin-Elmer Lambda 6 UV/VIS spectrophotometer.

The total number of moles of probe adsorbed per gram of A-572, n, was calculated using eq 2 where C_i is the initial probe concentration (mol/L), C_{eq} is the equilibrium probe concentration (mol/L), V is the volume of solution added (mL), and m is the mass of adsorbent (g).

$$n = \frac{(C_i - C_{eq})V(0.001\ \text{L/mL})}{m} \tag{2}$$

Total adsorption isotherms were obtained by plotting n vs C_{eq}. Best fit curves were drawn through the total adsorption isotherm. Contributions to the adsorption isotherms from the different pores were obtained by multiplying the curve resolved fractional peak area by the total moles of probe adsorbed, n_{total}, as shown in eq 3. The value of n_{total} was the n from the best fit line to eq 2.

$$n_{pore} = \frac{\text{Area}_{pore}}{\text{Area}_{total}}(n_{total}) \tag{3}$$

Results and Discussion

Adsorbents, Adsorbates, and Solvent. N_2 porosimetry was carried out on the carbonaceous adsorbent A-572 to afford a comparison to other materials. The results are summarized in Table 1. The plot of pore volume distribution was bimodal with very few pores in the 40−100 Å region. The large mesopore−macropore range encompassed a range of 100−900 Å with the maximum at ≈580 Å. These results should be considered in the context of recent reports discussing the inadequacy of the BET method for microporous solids.[15]

Table 1. N_2 Porosimetry of A-572[a]

surface area (m^2/g)	1160
pore volume (mL/g)	
micropore	0.43
mesopore	0.28
macropore	0.21

[a] The solids were characterized as follows: Surface area and pore volume data were obtained from the N_2 isotherm at 77 K using a Micromeritics ASAP 2000 instrument. Surface areas were determined using a five-point Brunauer−Emmett−Teller (BET) calculation. Micropore volumes were determined using the Harkens−Jura t-plot model with thickness parameters from 3.5 to 5 Å. The Barrett−Joyner−Halerda (BJH) adsorption curve was used for calculating meso- and macropore volumes. Macropore volumes are determined by difference. All calculations were carried out as described in the Micromeritics ASAP 2000 instrument manual.

(14) (a) Ito, T.; Fraissard, J. *J. Chem. Phys.* **1982**, *76*, 5225. (b) Ripmeester, J. A. *J. Am. Chem. Soc.* **1982**, *104*, 289. (c) Reisse, J. *Nouv. J. Chem.* **1986**, *10*, 665. (d) Scharpf, E. W.; Crecely, R. W.; Gates, B. C.; Dybowski, C. *J. Phys. Chem.* **1986**, *90*, 9. (e) Demarquay, J.; Fraissard, J. *Chem. Phys. Lett.* **1987**, *136*, 314. (f) Fraissard, J. *Z. Phys. Chem.*, **1988**, *269*, 657. (g) Ito, T.; Bonardet, J. L.; Fraissard, J.; Nagy, J. B.; Andre, C.; Gabelica, Z.; Derouane, E. G. *Appl. Catal.* **1988**, *43*, L5. (h) Heink, W.; Kärger, J.; Pfeifer, H.; Stallmach, F. *J. Am. Chem. Soc.* **1990**, *112*, 2175.

(15) (a) Foley, H. C.; Bansal, N.; Lafyatis, D. S.; Dybowski, C. *Prep. Am. Chem. Soc., Div. Pet. Chem.* **1991**, *36*, 502. (b) Bansal, N.; Foley, H. C.; Lafyatis, D. S.; Dybowski, C. *Catal. Today*, **1992**, *14*, 305. (c) Saito, A.; Foley, H. C. *AICHE J.* **1991**, *37*, 429.

(16) (a) Smith, D. M.; Davis, P. J. In ref 13a, p 301. (b) Ewing, B.; Davis, P. J.; Majors, P. D.; Drobbny, G. P.; Smith, D. M.; Earl, W. L. In ref 13a, p 709. (c) Glaves, C. L.; Brinker, J.; Smith, S. M.; Davis, P. J. *Chem. Mater.* **1989**, *1*, 34. (d) Gallegos, D. P.; Smith, D. M. *J. Colloid Interface Sci.* **1987**, *119*, 127.

(17) Silk Scientific Inc., P.O. Box 533, Orem, UT 94912.

(18) Jandel Scientific Inc., P.O. Box 7005, San Rafael, CA 84059.

(19) Varian VXR-300 User Manual.

(20) Drago, R. S. *Physical Methods in Chemistry*; W. B. Saunders Publishing: Philadelphia, PA. 1992.

(21) Drago, R. S.; Hirsch, M. S.; Ferris, D. C.; Chronister, C. W. *J. Chem. Soc. Perkin Trans. 2*, **1994**, 219.

Table 2. Summary of Solutes and CCl_4 and Physical Properties[a]

probe liquid	mw (g/mol)	polarizability[b] (Å^3)	dipole moment (D)	molar volume (mL/mol)	ΔH_v (kcal/mol)	S' [c]	T_1[d] (s)	δ[d] (ppm)
CH_3CN	40.05	4.40	3.92	52.2	7.3	3.00	4.25	2.15
C_6H_6	78.11	10.3	0	89.4	7.35	1.73	4.91	7.29
CH_2Cl_2	84.93	6.48	1.60	64.0	6.74	2.08	5.29	5.32
CCl_4	153.82	10.5	0	96.5	7.12	1.49		

[a] *Lange's Handbook of Chemistry*, 13th ed.; McGraw-Hill: New York, 1985. All data are from this source unless otherwise specified. [b] *Handbook of Chemistry and Physics*, 71st ed.; CRC Press: Boca Raton, FL, 1991. [c] See reference 21. [d] Obtained from this work. In CCl_4 solution relative to internal TMS.

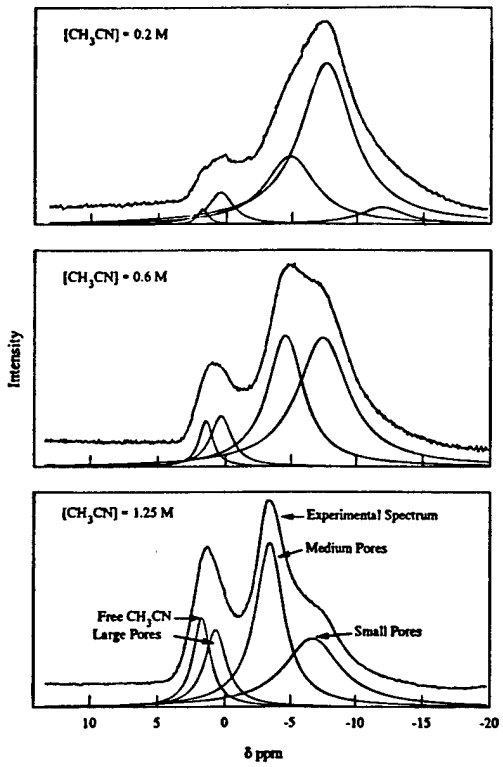

Figure 1. ^{1}H NMR spectra of CH_3CN in CCl_4 over A-572. Initial solution probe concentrations are shown. The intensity scale increases with increased probe concentration.

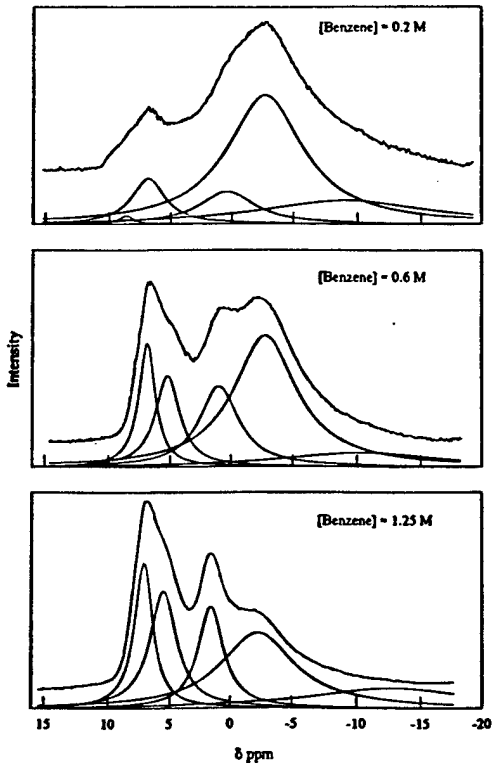

Figure 2. ^{1}H NMR spectra of benzene in CCl_4 over A-572. Initial solution probe concentrations are shown.

In this study, the distributions of three probe molecules between the carbonaceous adsorbent and solutions in carbon tetrachloride were studied by ^{1}H-NMR. Since CCl_4 is a nonpolar, poorly solvating solvent, solute–solvent interactions are minimized and the CCl_4–solid dispersion interactions remain constant when the probe is changed. Therefore, we are able to compare the donor, acceptor, dispersion, and polarity properties which influence the adsorption potential of the different probes. Using CCl_4 as the solvent has the added advantage that no protons interfere with the ^{1}H-NMR spectrum of the probe molecule. In addition, each probe only has equivalent protons producing a singlet in the solution ^{1}H-NMR spectrum. The relevant physical properties of the probes and solvent are summarized in Table 2.

Qualitative ^{1}H-NMR Analysis. The ^{1}H-NMR spectra for 0.2, 0.6, and 1.2 M solutions of acetonitrile, benzene, and dichloromethane in CCl_4 solutions inside and surrounding the carbonaceous adsorbent, A-572, are presented in Figure 1–3. The resolution of the spectra into the minimum number of components required to fit the observed spectra is also illustrated by the smooth solid lines. It should be emphasized that the intensities are relative and the absolute intensity increases with increasing concentration of each probe. For this reason, the small peak at highest field disappears at high concentration. Furthermore, CH_2Cl_2 has fewer protons per unit volume of solvent and gives a smaller signal-to-noise ratio than the other probes. This leads to difficulty in separating the large pore and solution resonances in the more concentrated solution. In the most dilute solution, the peak observed at lowest field is assigned to CH_2Cl_2 in the largest pores. A summary of the frequency shift, T_1, and T_2 values for the resolved signals of the three adsorbed probes is given in Table 3 along with the peak assignments (vide infra). It is significant to note that the difference in the frequency shift of the free and large pore resonances is 1.4 ± 0.4 ppm for all three probes. The free and the medium pore resonances differ by 5.9 ± 0.5 ppm for all three probes. The free and less shifted small pore resonances differ by 9.6 ± 0.3 ppm. Since acetonitrile and benzene are common donor molecules and CH_2Cl_2 is a common acceptor molecule,[22] these results suggest that the solid environment and not donor–acceptor interactions gives rise to the shifts. This conclusion is in agreement with literature[10,12] interpretation of the broadening mechanism.

The observation of separate resonances in the NMR indicates that the exchange of molecules between the sites corresponding to these resonances is slow on the NMR time scale. This is confirmed by the temperature independence of the spectra over 20 to 60 °C and the absence of off-diagonal peaks in a COSY spectrum accumulated for 8 h. Thus, the rate of exchange between pores is slowed by the probe access to the pores from

(22) Drago, R. S. *Applications of Electrostatic-Covalent Models in Chemistry*; Surfside Scientific Publishing: P.O. Box 13413, Gainesville, FL 32604, 1994.

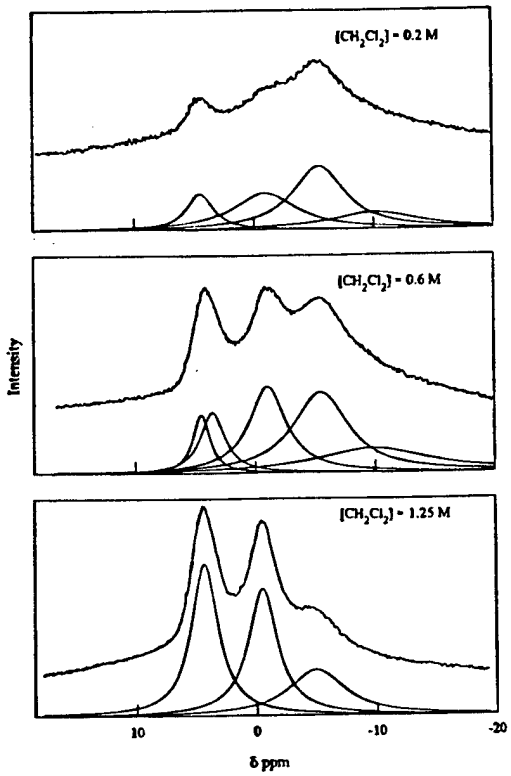

Figure 3. ^{1}H NMR spectra of CH_2Cl_2 in CCl_4 over A-572. Initial solution probe concentrations are shown.

Table 3. Peak Assignments for Adsorption of 0.6 M Probes from CCl_4 by A-572

probe	peak shift (ppm)	T_1 (s)	10^4 T_2[b] (s)	assignment
CH_3CN	1.9	1.5	18	"free"
	0.4	1.5	11	large pores
	−4.6	0.4	6.3	medium pores
	−7.5	0.3	4.4	small pores
	−11.9[a]	0.3		
benzene	6.9	2.1	13	"free"
	5.2	1.5	8.8	large pores
	1.0	0.6	5.6	medium pores
	−2.7	0.7	3.5	small pores
	−10.5	0.6	1.4	
CH_2Cl_2	4.4	1.0	12	"free"
	3.5	0.7	8.8	large pores
	−1.0	0.3	5.8	medium pores
	−5.5	0.1	3.9	small pores
	−10.0	0.1	1.9	

[a] From C_i = 0.2 M CH_3CN experiment. [b] The NMR spectra are temperature independent over the range 20−60 °C suggesting the system is in the fast motional narrowing limit.

solution. The different frequency shift, T_1, and T_2 values for the same probe molecule inside the porous solid arise from fast exchange of weakly bound surface molecules with those in the liquid-like multilayer of the different size probes. Acetonitrile in the micropores will have a larger shift and shorter T_1 and T_2 than acetonitrile in the macropores because the averaging in the micropores involves a greater fraction of surface-bound physisorbed molecules than the averaging in the macropores. As the pore becomes larger, the averaging involves fewer surface-bound molecules and the shifts, T_1, and T_2 approach those of the liquid. This interpretation leads to the assignment of the upfield peaks to probe in the smallest pores. The downfield peak arises from probe in the large pores and the middle peak from probe in the medium pores.

The quantitative interpretation of the magnitudes of the shifts, T_1, and T_2 is complicated by the inhomogeneity of surface and pore volumes which comprise the micropores, mesopores, or macropores. Surface sites of different binding strength would, under fast exchange conditions, average in different δ, T_1, and T_2 values. If there were any strong binding sites that do not exchange, they would not be detected in the NMR. The distribution of pore volumes contributing to the peak assigned to each small pore, medium pore, or large pore also influences δ, T_1, and T_2. Each peak is comprised of overlapping components with slightly different ratios of surface bound and multilayer probe molecules. The inhomogeneity of surface sites and pore volumes does not impact on the conclusions to be drawn, and is implied in our use of the terms micropore, mesopore, and macropore volumes. The novel aspect of the NMR spectra obtained in this study is the demonstration of gaps in the spectra which correspond to low concentrations or no pores of certain dimensions. This permits an easily measured, unambiguous view of the role of these pores in the adsorption process. The concentration dependence of the spectra for acetonitrile, benzene, and methylene chloride will be seen to provide further support for the spectral assignments.

Concentration Dependence of the Acetonitrile Spectra. The high-resolution ^{1}H-NMR spectrum of acetonitrile as the probe molecule in CCl_4 in contact with A-572 is shown in Figure 1. The observation of separate peaks for different pores indicates that the exchange of probe molecules from one type of pore to another must be slow on the NMR time scale. Temperature variation showed little change in the NMR spectrum over the range of 20 to 60 °C indicating that interpore exchange makes no contribution to the line width and that the width is dominated by intrapore exchange. The experimental spectrum consists of two very broad signals with shoulders which curve resolve into 4 or 5 smaller signals. Though significant changes in the spectra occur with probe concentration, it is gratifying that curve resolution gives, for all the spectra of a given probe, peaks with about the same frequency shifts that differ mainly in their relative intensities. The frequency shifts, T_2's, and relative areas of the resolved peaks as a function of probe concentration are given in Table 4 for the three probes. The peak assignments are borne out by the concentration-dependent studies shown in Figure 1. The downfield peak in the acetonitrile spectra is resolved into two components. The sharper component and more downfield peak in each resolved spectrum (1.9 ppm) appears where expected for acetonitrile in solution and is assigned to "free" acetonitrile in the bulk CCl_4 solution surrounding the solid. The slightly broader component, upfield by about 1.4 ppm from the solution CH_3CN resonance, is assigned to probe molecules in the large pores. These "large pores" probably include macropores and large mesopores of the adsorbent. Since these pores are quite large, most of the molecules in a given pore are in an environment similar to that in solution. As a result, this signal is shifted the least, T_2 is similar to that of the solution peak in the sample, and little change is observed in T_1. The concentration dependence of the intensity of this peak is consistent with this assignment. The relative intensity of this peak continues to increase with probe concentration at all concentrations employed.

The second large, broad up-field peak contains shoulders indicating that there are actually two or possibly three peaks under a common envelope. Curve resolution of the 0.2 M spectrum places the peaks at −4.8 and −7.6 ppm with a contribution from a peak at −11.9 ppm which is resolved only at low probe concentrations. At low concentration (Figure 1), this broad most upfield peak and a larger peak at −7 ppm develop first. As the CH_3CN concentration is increased over the A-572, the peak at −4 ppm becomes larger than the signal at −7 ppm. The peak at −11.9 ppm in the 0.2 M solution is masked by the peak at −7 ppm at higher probe concentrations.

Table 4. Summary of Frequency Shifts, T_2's, and Relative Areas from ^{1}H-NMR

probe	conc (M)	frequency shift (ppm)	10^4 T_2 (s)	relative area (%)
CH_3CN	0.2	1.9	24	1.2
		0.4	9.8	5.8
		−4.8	4.6	25.1
		−7.6	4.4	62.5
		−11.9	5.1	5.5
	0.6	1.9	18	4.9
		0.4	11	8.2
		−4.6	6.3	37.1
		−7.4	4.4	49.8
	1.25	1.8	14	13.1
		0.3	11	14.4
		−4.4	8.1	41.0
		−6.7	4.1	31.5
benzene	0.2	8.6	16	0.8
		6.9	6.8	9.9
		0.3	3.8	11.2
		−2.7	3.5	59.1
		−9[a]	1.2	19.0
	0.6	6.9	13	12.5
		5.2	8.8	13.5
		1.0	5.6	18.5
		−2.7	3.5	46.4
		−11[a]	1.4	9.1
	1.25	7.1	12	17.4
		5.5	8.0	20.7
		1.6	8.5	16.9
		−2.3	3.0	32.8
		−14[a]	1.4	12.1
CH_2Cl_2	0.2	4.4	7.9	12.9
		−1.0	3.4	28.8
		−5.5	4.1	41.7
		−10.3	2.5	16.6
	0.6	4.4	12	8.48
		3.5	8.8	12.2
		−1.0	5.8	26.3
		−5.5	3.9	34.8
		−10.0	1.9	18.3
	1.25	4.3	7.9	40.2
		−0.5	7.3	36.4
		−5.0	3.9	23.4

[a] These peaks are very broad and the frequency shifts are not accurately known.

T_1 measurements indicate that these up-field peaks relax ~4 times faster (≈0.4 s) than the signals assigned to the probe in the solvent and large pores (1.5 s).

The concentration dependence of the T_1 and T_2 values supports the peak assignments. The T_2 value (half width at half height) for the smallest pores (-7 ppm) is nearly the same at all concentrations (4.3×10^{-4} s). This suggests that the micropores are essentially filled at 0.2 M so the fraction of surface-bound molecules to multilayer molecules remains constant in 0.2–1.25 M solutions. Our previous analyses[2,3] also assigned highest adsorption equilibrium constants to surface adsorption within the smallest accessible pores of the solid. On the other hand, the T_2 values for the peak at −4.6 ppm assigned to the medium pores increases from 4.6×10^{-4} to 6.3×10^{-4} to 8.1×10^{-4} s as the concentration is increased from 0.2 to 0.6 to 1.25 M. This is expected behavior for incomplete filling of the mesopores at low concentration. Since the fraction of surface-bound molecules in the pore decreases as the amount of liquid-like CH_3CN in the multilayer is increased, the average T_2 increases and the half width at half height decreases.

The large-pore behavior leads to different spectral changes than adsorption in the medium pores. The T_2 values for the three probes are $10.7 \times 10^{-4} \pm 0.8 \times 10^{-4}$ sec and increase only slightly in going from 0.2–1.25 M CH_3CN. The surface area of the large pores is a very small fraction of the total solid surface area. Therefore, at all probe concentrations the number of surface-bound probe molecules in the large macropores is small compared to the number that are involved in multilayer adsorption. As such, the short T_2 associated with surface-bound CH_3CN has only a small effect on the mole fraction averaged, measured line width. Increasing the CH_3CN concentration up to 3 M shows that the intensities of the small pore and medium pore peaks reach a maximum while the solution and large pore resonances increase in intensity with increasing molarity.

The interpretation of the concentration dependence of the frequency shift parallels that of the T_2 values. Rapid exchange of surface-bound and multilayer molecules produces a mole fraction averaged frequency shift. This leads to the largest upfield shift for molecules in the micropores. There is a slight concentration dependence on the frequency shift for the various pores. The resonance for each pore type is shifted less with increasing concentration, and this is consistent with incomplete filling of the pores at low adsorbate concentration.

All three probes (CH_3CN, C_6H_6, and CH_2Cl_2) give rise to similar differences in the shifts of the solution resonances and that in the different small, medium, or large pores. This dependence on pore size suggests that the shift differences arise from the diamagnetic susceptibility contribution of the solid surface to surface-bound molecules. The mole fraction averaging of this shift and the more liquid-like multilayer shift gives rise to different frequency shifts for different size pores because of the differences in the ratios of multilayer and surface-bound molecules. The diamagnetic contribution is expected to be similar for donor (CH_3CN, C_6H_6) and acceptor (CH_2Cl_2) molecules.[22] The observation of similar shifts for all three probes indicates a minor, if any, donor–acceptor contribution to the shift. This absence could arise from weak donor–acceptor properties for the solid, or from such a small concentration of donor or acceptor sites that their average contribution to the observed shift is negligible. Thus, the principal mechanism leading to the observation of different resonances is the diamagnetic contribution to the surface-bound molecules from the walls of the pores.

The interpretation of the spectra obtained for CH_3CN in A-572 is consistent with the nitrogen porosimetry studies (Table 1) indicating a bimodal distribution of pore dimensions. Gaps exist in which there are few or no pores of intermediate size. The ^{1}H-NMR spectra show three distinct groups of pores. The gap separating the two broad signals corresponds to a group of pores of intermediate size in which few or no pores exist. If there were a continuous distribution in this range of pore dimensions, a single broad peak would result in the ^{1}H-NMR. The NMR explanation given above suggests that in each group of pores, minor changes in the size of the pores would contribute to the width of the observed peaks because the ratio of the surface-bound and multilayer molecules changes with size.

Concentration Dependence of the Benzene Spectra. Figure 2 shows the results for the concentration dependence of the adsorption of benzene by A-572 from CCl_4 solvent. Each spectrum contains two very broad signals similar to that observed for CH_3CN. These two broad signals are also curve resolved into five smaller signals. The sharpest and most downfield signal (7 ppm) has a frequency shift near that expected for benzene in solution and is attributed to benzene in the bulk CCl_4 solution surrounding the solid. The next peak upfield (5.2 ppm) is slightly more broad than the solution signal, and it is assigned to the signal of benzene in the macropores and large mesopores of the solid (large pores). Consistent with the data for CH_3CN, the signal is only slightly shifted with some

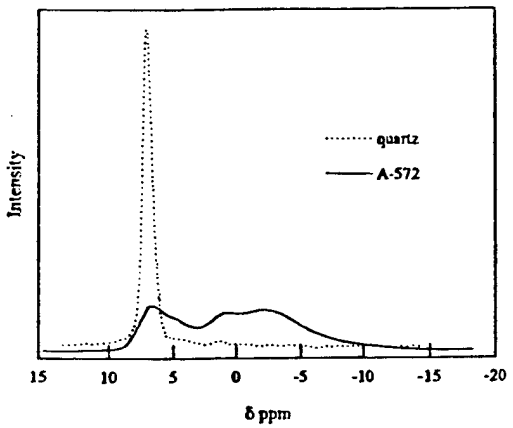

Figure 4. ^{1}H NMR of 0.6 M benzene in CCl_4 in contact with powdered glass.

broadening (T_2 decreases) and little change in T_1 (2.1 s for free; 1.5 s for large pore).

The large, broad upfield peak consists of three curve-resolved signals at 1.0, −2.7, and −10.5 ppm. The concentration dependence spectra for the 1.0 and −2.7 ppm peaks show the same behavior as observed for CH_3CN, and hence the interpretation of the frequency shifts T_1, and T_2 values indicates benzene being preferentially adsorbed by the micropores. The peak at −10.5 ppm is so broad that its maximum cannot be accurately determined.

In order to assess the influence of solid particles on the field homogeneity, a series of experiments were also carried out using quartz obtained from powdering an NMR tube. As shown in Figure 4, the spectrum of 0.6 M benzene in CCl_4 in the presence of the crushed quartz glass does not shift the signal. The signal is broadened from field inhomogeneity associated with not spinning the sample tube. In addition, the T_1 measurements of benzene around the crushed glass gave a value of 4.5 s whether the sample tube is spinning or not. This value is comparable to the solution T_1 value (4.9 s) and more than two times the largest T_1 measured for benzene/CCl_4 surrounding A-572. The observations of smaller T_1 values, increased line widths, and smaller T_2 values for benzene adsorbed by A-572 compared to crushed glass indicate the spectra for the former are not an artifact of the experimental procedure.

Concentration Dependence of the Dichloromethane Spectra. The ^{1}H-NMR spectra of dichloromethane, a hydrogen bonding probe molecule, are presented in Figure 3 and are similar to those of benzene and acetonitrile. The frequency shift, T_1, and T_2 values for the various signals are summarized in Tables 3 and 4. The peak assignments are consistent with those made for benzene and CH_3CN. The upfield peak again is two or three signals at −1.0, −5.5, and −10.0 ppm. The signal at −10.0 ppm is masked by the other peaks at higher concentration, and the peaks at −1.0 and −5.5 ppm grow relative to one another as observed for CH_3CN and benzene with increasing concentration. The downfield peak was curve resolved into two signals for 0.6 M CH_2Cl_2 in CCl_4 in contact with A-572. In the cases of 0.2 and 1.25 M CH_2Cl_2 solution, the free CH_2Cl_2 peak and the macropore peak are not separated. The frequency shift of the macropore resonance is the same as is the resonance for free CH_2Cl_2; however, the T_2 values suggest assignment of a component of the resonance to CH_2Cl_2 in the macropores.

Adsorption−^{1}H-NMR Experiments for Acetonitrile. In order to determine the number of moles of adsorbate in the various pore types, a total adsorption isotherm was measured for adsorption of the probe from CCl_4. In every case, the ratio of volume (1.00 mL) of probe solution to mass (0.220 ± 0.002 g) of A-572 was constant so that adsorption data from all samples could be directly compared. A best fit line was drawn through the total adsorption isotherm in which the total number of moles of probe adsorbed was calculated using eq 2. The curve-resolved areas from ^{1}H-NMR, Table 4, were then used with the best fit isotherm curve to calculate the fraction of probe molecules in each pore type as in eq 3. This procedure presents for the first time a direct measure of the components of the adsorption isotherm by the different pores.

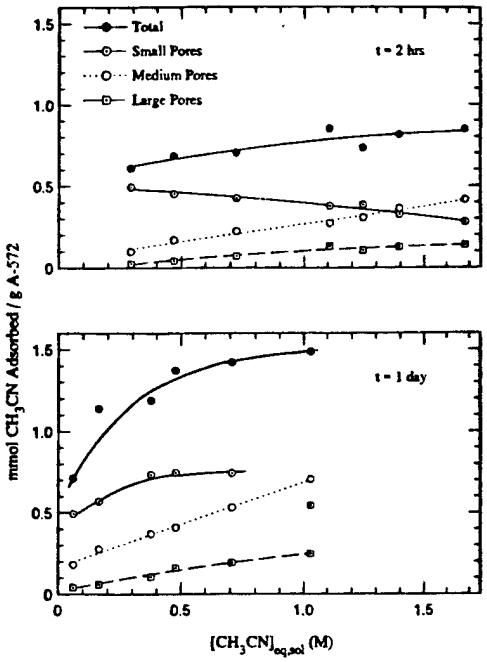

Figure 5. Adsorption of CH_3CN from CCl_4 by the different size pores in A572. Solution equilibrium probe concentrations are given on the abscissa.

Figure 5 shows the adsorption isotherms for adsorption of CH_3CN from CCl_4 by the pores of A-572. Results are presented for samples equilibrated for 2 h and 1 day. The total adsorption capacity is approached at longer time and higher concentrations. The number of moles of CH_3CN adsorbed by the large pores and medium pores increases with adsorbate concentration as expected from the NMR data shown in Figure 1 and with equilibration time. Furthermore, the number of moles of adsorbate in the medium and large pores, for a given equilibrium concentration, increases with time. For example, at $C_{eq} = 0.5$ M, the number of moles of CH_3CN adsorbed by the large pores increases from 0.05 to 0.15 mmol per gram of A-572 in changing the equilibration time from 2 h to 1 day. The number of moles of CH_3CN adsorbed by the medium pores increases from 0.17 mmol per gram of solid after 2 h to 0.4 mmol per gram of solid after 1 day. The adsorption process involves displacing CCl_4 from pores large enough to hold it.

The data in Figure 5 show that after 1 day of contact at $C_{eq,sol}$ = 0.06 M CH_3CN, 0.71 mmol of CH_3CN were adsorbed per gram of A-572. Of this total amount adsorbed, 0.49 mmol CH_3CN (68%) were adsorbed by the small pores, 0.18 mmol CH_3CN (25%) were adsorbed by the medium pores, and 0.04 mmol of CH_3CN (6%) were adsorbed by the large pores. At $C_{eq,sol}$ from 0.17 to 0.71 M, the number of moles CH_3CN adsorbed by the small pores (0.72 mmoles; 0.038 mL) is relatively constant, whereas the number of moles CH_3CN adsorbed by the medium and large pores increases with increasing equilibrium concentration. Consistent with the 2 h equilibration data, the fraction of CH_3CN molecules adsorbed in the medium pores increases more significantly than in the large pores over this concentration range. This is shown in Figure 5 and Table 4

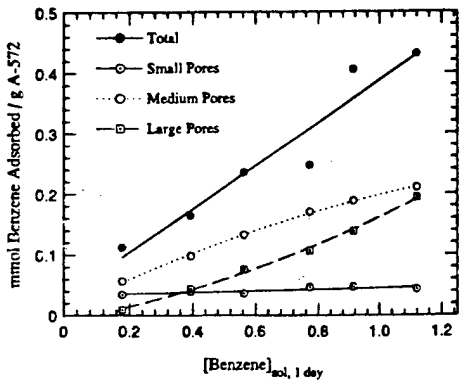

Figure 6. Adsorption of benzene from CCl_4 by the different size pores in A572. Solution equilibrium probe concentrations are given on the abscissa.

where the relative area of the large pore resonance increases from 5.8% to 14.4% ($\Delta\% = 8.6\%$). Over the same concentration range, the relative area of the medium pore resonance increases from 25.1% to 41.0% ($\Delta\% = 15.9\%$).

Although the ^{1}H-NMR spectrum of CH_3CN inside and surrounding A-572 is dependent on changes in bead packing in the NMR tube, these errors do not affect the adsorption studies. In cases where the beads are not packed as tightly, there is more "free solution" surrounding the beads and this signal becomes more intense in the measured spectrum. However, curve resolution of the spectra would give the same values for the relative peak areas for the resonances assigned to the small, medium, and large pores. Since the total amount of probe adsorbed is determined from the adsorption measurement, the amount of probe molecule adsorbed by the different pore types is only dependent on these relative areas.

Consider the adsorption after 2 h of contact time. The capacity of the small pores decreases with increasing concentration. This is not consistent with the NMR conclusion in which the small pores were considered essentially filled even at 0.2 M CH_3CN. At high adsorbate concentrations, in which a significant fraction of the molecules are adsorbed by the medium and large pores, errors associated with the curve-resolution technique of the most shifted resonances of the small pores increases. At low concentrations, a significant portion of the small pore peak area and the total peak area comes from the very broad resonance at -12 ppm. As shown in Figure 1, this signal is not resolved at higher concentration and since it is so broad, some of this peak area may be associated with the signal for the medium pores (-5 ppm). This leads to an underestimation of the small pore adsorption capacity and an overestimation of the medium pore capacity. It is likely that the isotherm for small pore adsorption is constant rather than decreasing with increasing concentration. At an equilibrated concentration of 0.2 M CH_3CN, the small pores are filled.

Adsorption–^{1}H-NMR Experiments for Benzene. Figure 6 presents the adsorption isotherm for benzene from CCl_4 by the pores of A-572. The samples were equilibrated for 1 day. Figure 6 shows the total adsorption isotherm, as well as the adsorption isotherms calculated for each pore type. The total adsorption isotherm indicates that the adsorbent has not reached its capacity for benzene even at the highest concentration studied. This isotherm has a shape similar to one obtained for adsorption of benzene from cyclohexane.[3] Interestingly, the number of moles of benzene adsorbed by the small pores is relatively constant and increases only slightly over the concentration range studied. This is in contrast to the data for CH_3CN in which the isotherm for the small pores decreases with increasing adsorbate concentration. For benzene, the small pore region of the spectrum was curve resolved into two components for all solution concentrations used. In this case, there is no underestimation of the adsorption by the small pores as in the case of CH_3CN. The capacity of the small pores is reached very quickly (0.04 mmol of C_6H_6 per gram of A-572; 0.004 mL). Hence, even at 0.2 M initial benzene concentration, most of the benzene is adsorbed by the medium pores (0.05 mmol of C_6H_6 per gram of A-572). The number of moles adsorbed by the medium pores and large pores increases at the same ratio with increasing benzene concentration up to about $C_{eq,sol} = 0.8$ M. At higher concentrations, the amount of benzene going into the medium pores relative to the large pores decreases as the medium pores become filled to capacity.

The preferential adsorption of benzene from CCl_4 is rationalized as follows. Both have the same polarizability. There are no dipole forces involved in either case. However, in addition to benzene having a larger ΔH_v, it also has a larger solvent polarity parameter, S^*.[21] Apparently, the smaller size and shape lead to larger nonspecific interactions.

Conclusions

Frequency shift, T_1, and T_2 data as a function of the amount of adsorbate are used to assign different resonances in the ^{1}H-NMR spectra of adsorbates in porous solids to different-size pores. A procedure is reported whereby an adsorption isotherm can be decomposed into components for different pores. These results (Figures 5 and 6) provide an unprecedented degree of detail about the distribution of adsorbates in the pores of the adsorbent. Preferential adsorption of a probe molecule from a dilute solution in CCl_4 solvent by the small pores occurs first. Upon increasing the probe concentration, the ^{1}H-NMR signals attributed to probe molecules in the small and medium pores reach a maximum, and the signals associated with the large pores and "free" probe increase.

There are several important applications of pore-resolved NMR porosimetry. Our N_2 porosimetry measurements were not able to resolve the pores below 40 Å into the bimodal distribution of pore sizes found by NMR porosimetry. More extensive and expensive software is required to gain this information. Another advantage of NMR porosimetry is that probe molecules of size comparable to those used in practical applications can be used to get a more relevant measure of the adsorptive capacity of the pores in a porous solid. Applications in which pore blockage leads to a bonded adsorbent or dead catalyst can also be studied by pore-resolved NMR porosimetry.

Acknowledgment. The authors acknowledge the support of this research by ARO and ERDEC.

JA9426913

A New Adsorption Model for Analyzing Gas−Solid Equilibria in Porous Materials

Russell S. Drago,* Douglas S. Burns,† and Todd J. Lafrenz

Department of Chemistry, University of Florida, Gainesville, Florida 32611-7200

Received: April 24, 1995; In Final Form: October 24, 1995®

Equilibria involving three probe gases adsorbed on two porous carbonaceous supports are measured at various temperatures. A novel analysis of the data is offered which uses multiple process equilibria to calculate adsorption equilibrium constants for the interaction of the gas with the solid. Equilibria involving three distinct processes are found. The equilibrium constants ($K_{1,ads}$, $K_{2,ads}$, and $K_{3,ads}$) are obtained as well as the capacity of the solid for each type of process (n_1, n_2, and n_3), in millimoles of adsorptive per gram of solid. The first process, $K_{1,ads}$, involves adsorption of the gas in the solid's micropores which are of molecular dimensions. The second process, $K_{2,ads}$, involves adsorption in the larger micropores. The third process, $K_{3,ads}$, involves adsorption by the remaining surface. Multilayer formation is likely involved in some processes. The temperature dependencies of the K_{ads}'s produce the enthalpy of adsorption for these processes. This analysis is important for, in contrast to BET analyses, it provides thermodynamic data for different adsorptives that can be interpreted in terms of those molecular properties that facilitate probe−solid interactions and can provide a quantitative definition of solid reactivity.

Introduction

Porous supports have been used in this laboratory to prepare a variety of catalysts.[1] This work has shown that in addition to surface area, the porosity and pore size distribution of the solid are important properties. The pores of the solid tend to concentrate reactants in the vicinity of the supported catalyst, and this increase in reactant concentration can increase the reactivity. Preferential adsorption of one of the reactants over another or preferential adsorption of the products over the reactants can inhibit the reaction by preventing access of the needed reactants to the catalytic site. For catalytic[2] and other applications of porous solids, an understanding of gas−solid equilibria and a quantitative measure of the solid's adsorption strength are essential for the rational selection of solid materials.

Gas−solid equilibria involve three types of interactions: absorption, chemisorption, and physisorption. We are concerned with the latter and will include in our use of the term physisorption the process referred to as reversible chemisorption. In the absence of specific interactions, the force of attraction for physisorption of nonpolar gases (e.g., N_2, Ar, and CH_4) involves mainly London dispersion interactions.[3-6] The dispersion energy is a function of r^{-6}, where r is the surface−molecule distance,[3] and is also dependent on the polarizability of the gas molecule and the support.[5] Polar gas molecules have contributions from these forces but are dominated by electrostatic interactions which are less sensitive to the distance from the surface[3] and are a function of r^{-3}. The electrostatic force is particularly important on electrically conducting supports such as graphite when the adsorptive molecule has an inherent dipole moment.[7] Dispersion and electrostatic forces between adsorptive molecules also govern the interactions in multilayer adsorption.[6]

In addition to the above interactions of gaseous molecules with flat surfaces, the porosity of the solid has a pronounced influence on gas−solid adsorption equilibria. There are three processes which may be present in a physisorption isotherm: micropore filling, monolayer−multilayer adsorption, or capillary condensation.[8] Pores in supports have been divided into three groups by IUPAC. Micropores are those pores that are less than 20 Å in diameter. Mesopores are those that are between 20 and 500 Å in size. Macropores are defined as pores with diameters larger than 500 Å. Micropores adsorb molecules with significantly larger adsorption energies than do mesopores or macropores, due to superimposed interaction potentials from opposite surfaces within the pore[9,10] as shown in Figure 1. Everett and Powl[11] calculated interaction energies as a function of pore size based on the Lennard-Jones potential model. In cylindrical pores of five adsorptive diameters or less, the model predicts increasing adsorption energies with decreasing pore size. Adsorption of molecules occurs preferentially in the micropores because of these higher adsorption energies. Furthermore, if the temperature is less than the critical temperature of the adsorptive, capillary condensation is possible in pores that are larger than four adsorptive diameters.

Adsorption measurements usually are interpreted with the BET equation:[12]

$$\frac{X}{n(1-X)} = \frac{1}{Cn_m} + \frac{(C-1)X}{Cn_m} \qquad (1)$$

where $X = P/P^o$ and P is the equilibrium pressure in Torr and P^o is the saturation pressure in Torr. The values of n_m and C are obtained from the linear best fit plot of $X/[n(1-X)]$ vs X where n is the number of moles adsorbed. The equation is typically applied over the relative pressure range, P/P^o, of 0.05−0.3. At lower pressures, the high adsorption potential from micropore filling causes this equation to predict too little adsorption. At higher pressures, multilayer adsorption is usually prevalent. The BET model predicts too much adsorption at these pressures. The BET constant C is a complex quantity related to the ratio of equilibrium constants for monolayer adsorption and multilayer adsorption, along with contributions from the enthalpy of adsorption of the monolayer and multilayer. Literature attempts to interpret C have led to different proposals.[12] This equation has become the standard for surface area determinations, usually with nitrogen at 77 K as the adsorptive.[8] The purpose of this article is to offer a complimentary method for the analysis of adsorption data. The goal of this analysis is

† Present address: ENSCO, Inc., 445 Pineda Ct, Melbourne, FL 32940.

® Abstract published in *Advance ACS Abstracts*, January 1, 1996.

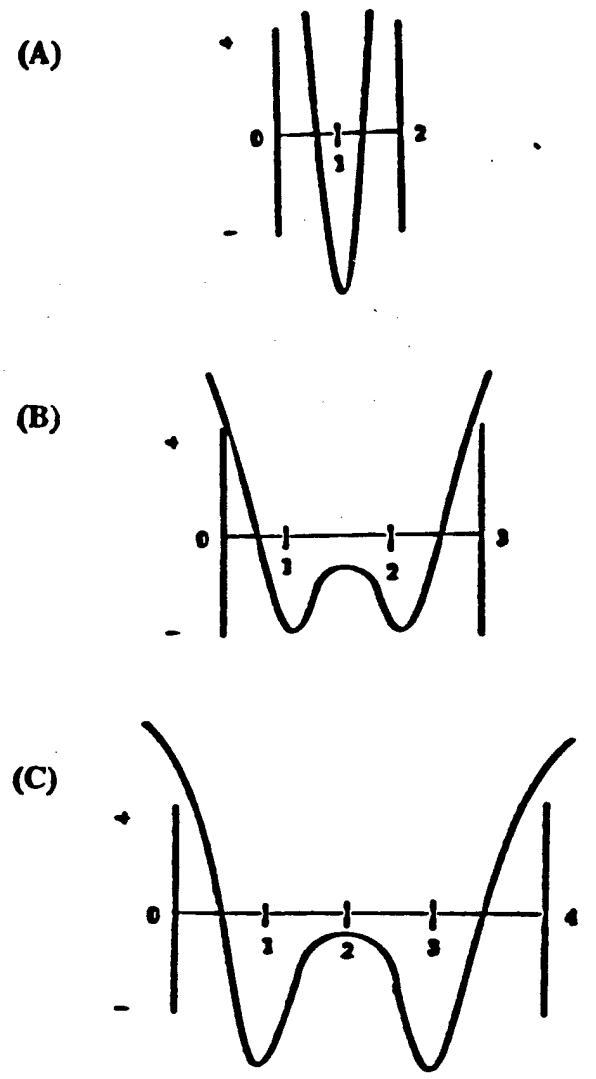

Figure 1. Adsorption Potential in micropores. (A) A pore that is 2 adsorbate diameters in width; (B) a pore that is 3 adsorbate diameters in width; (C) a pore that is 4 adsorbate diameters in width. Positive "Y" is a repulsive force, and negative "Y" is an attractive force.

to obtain thermodynamic data for the interaction of the adsorptive molecule with the stronger and more readily accessible binding sites in the porous carbonaceous solid. As a result, we are most interested in fitting data at low pressures and which equilibrate in minutes.

This study employs carbonaceous supports containing a distribution of micropores, mesopores, and macropores. Originally, carbonaceous adsorbents were prepared by pyrolysis of naturally occurring organic polymer sources including petroleum coke,[13] anthracite coal, wood char, pitch, coconut husks, compacted peat moss, etc.[14] Recently, materials have been synthesized by pyrolysis of functionalized macroreticular polymer resin beads leading to high pore volumes of specific dimensions within the final pyrolyzed solid.[15] Molecular sieving properties of these carbonaceous supports have been demonstrated and studied as a function of pore size distributions obtained using different pyrolysis temperatures and activation treatments.[16]

Experimental Section

Gases and Supports. The gases He and N_2 (99.99% purity) were procured from Liquid Air, Inc. The gases CO and CO_2 (99.99%) were purchased from Matheson Gas Co. All gases were used without further purification. Pyrolyzed poly(acrylonitrile), PPAN, and Ambersorb Adsorbent 572, A-572, were obtained from the Rohm and Haas Co. The supports were desorbed under a vacuum of $< 10^{-3}$ Torr at 200 °C for at least 8 h before adsorption data were obtained.

Characterization of Supports. Carbon, hydrogen, and nitrogen analyses (CHN) were performed by the University of Florida elemental analysis laboratory. Surface area and pore volume data were obtained from the N_2 isotherm at 77 *K* using a Micromeritics ASAP 2000 Instrument. Surface areas were determined using a five-point Brunauer–Emmett–Teller (BET) calculation.[17] Micropore volume was determined using the Harkins–Jura *t*-plot model with thickness parameters from 5.5–9.0 Å.[18] The Barrett–Joyner–Halenda (BJH) adsorption curve was used for calculating meso- and macropore volumes.[19] All calculations were carried out as described in the Micromeritics ASAP 2000 Instrument manual.[20,21]

Adsorption Measurements. The uptake of gases by the two solids was measured using the Micromeritics ASAP 2000 Chemi system. In a standard experiment, a sample was placed into a glass container sealed to the apparatus via Viton O-rings and degassed overnight at 200 °C under vacuum. Following a minimum of 8 h of desorption, adsorption measurements were taken. The free space was determined using helium. The assumption is made that helium is a nonadsorbing gas for our supports and, therefore, determines the volume above the sample as well as the dead volume within the sample. Free space, adsorbed gas volumes, and equilibration intervals were calculated as outlined in the Micromeritics ASAP 2000 Chemi reference manual.[21] The system was considered to be at equilibrium when the pressure change per unit time interval (10 s) was less than 0.01% of the average pressure during the interval. All adsorptions were reported at values between 0.1 and 760 Torr because we are interested in the applications of these materials at median-to-ambient relative pressures. Adsorption isotherms were obtained at temperatures ranging from 75 to −93 °C by immersing the sample tube into a Dewar filled with various liquid N_2/solvent mixes or ice water or by covering the sample tube with a heating mantle. The measured fluctuation in temperature was never greater than ±1 °C.

Two experiments were performed in which PPAN was desorbed at 110 and 200 °C, respectively, prior to measurement of the adsorption isotherm. Interestingly, the number of moles of N_2 adsorbed at P/P^o equals 1 by the 110 °C degassed sample (0.31 mmol/g of PPAN) was less than that adsorbed by the 200 °C sample (0.36 mmol/g of PPAN). Higher desorption temperatures or lower degassing pressures are required to empty the smaller micropores. However, use of too high a temperature can lead to changes in the nature of the adsorbent. Furthermore, any higher affinity small micropores not emptied at 200 °C are irrelevant for kinetic reasons in most catalytic and separation applications. For these reasons, we have selected a 200 °C pretreatment for the comparison of adsorptives and solids studied here.

Results and Discussion

Equilibrium Analysis. The measured isotherms were analyzed using an equilibrium model derived by analogy to a multiple-site Langmuir-type adsorption model.[12] The resulting equation (eq 2) is

$$n_{tot} = \sum_i \frac{n_i K_{i,ads} P_{atm}}{1 + K_{i,ads} P_{atm}} \qquad (2)$$

where n_{tot} is the total number of millimoles of gas adsorbed per gram of solid, n_i is the available capacity for process i in

millimoles per gram of solid, $K_{i,ads}$ is the adsorption equilibrium constant for process i, and P_{atm} is the equilibrium gas pressure in atmospheres. The n_i and $K_{i,ads}$ values were determined using a modified simplex routine designed to solve eq 2 for a series of equilibrium gas pressures. In using eq 2, the minimum number of processes, i, needed to obtain a good fit of the adsorption isotherm are used. As discussed in our earlier report[22] of the cal−ad method, a very shallow minimum results in the solution of the series of simultaneous equations that arise from even a two-process fit of adsorption data for $K_{1,ads}$, $K_{2,ads}$, n_1, and n_2. Uncertain values of the quantities result. In the cal−ad procedure, the definition of the minimum was improved by simultaneously measuring and solving enthalpy and adsorption data. However, the enthalpies of interaction of most carbon adsorbents are so small that this approach cannot be employed with these solids. Instead, a series of isotherms can be measured at various temperatures. Assuming the n_i values to be temperature independent, each temperature introduces only new K_{ads}'s as unknowns, leading to a better definition of the minimum in the solution of the combined data set because of the improved ratio of knowns to unknowns. It is to be emphasized that we are not assuming the same extent of micropore filling at all temperatures for P/P^o of one. The assumption is that the potential capacity is the same with K defining the conditions to saturate this capacity.

The reproducibility and precision in the adsorption measurements were determined from three successive experiments in which N_2 adsorption by A-572 at 25 °C was followed by evacuating and repeating the N_2 adsorption experiment on the same sample. The adsorption isotherms were very reproducible. At higher equilibrium pressures ($P_{atm} > 0.05$), the relative error (δ) in the average number of moles of N_2 adsorbed per gram A-572 was $\delta < 0.5\%$. At lower equilibrium pressures ($P_{atm} < 0.05$), the relative error was somewhat larger, with $\delta < 3\%$. This larger relative error arises because of the very small volumes of gas adsorbed. Two successive adsorption isotherms were also obtained for CO on A-572 at $T = -93$ °C. At this low temperature, CO leads to much higher volumes of gas adsorbed at the low pressures. As in the N_2 data, the greatest relative errors in successive runs were observed at lower pressures. For the two CO adsorption isotherms at $P_{atm} < 0.05$, a relative error of <4% was found. In the data analysis, it is essential to add processes only until the adsorption data are fit as accurately as it is known. We have used the relative errors discussed above as the criterion for the minimum number of processes needed to fit the adsorption data by the equilibrium analyses to within the precision of measurement. The procedure for obtaining n_i's and $K_{i,ads}$'s for the gases in this study is outlined as follows:

(1) The $T = -42$ °C isotherm is found to fit with two processes, leading to values for all four parameters (n_1, n_2, $K_{1,ads}$, $K_{2,ads}$). At this temperature, the value of n_1 is best defined because[23] the data points correspond to ranges from zero to near full capacity for process 1. Furthermore, $K_{1,ads}$ is different enough from the equilibrium constants of the other processes to distinguish the $K_{i,ads}$ values.

(2) The $T = -93$ °C isotherm requires three processes to fit the data to within the experimental error. The n_1 value is fixed to that obtained in step 1. These data provide a better definition of n_2, so it is not fixed to the value from step 1. The data fit of this isotherm provides $K_{1,ads}$, $K_{2,ads}$, $K_{3,ads}$, n_2, and n_3. Since processes 1 and 2 have data ranging from low to full capacity, the values of $K_{1,ads}$, $K_{2,ads}$, and n_2 are well defined, but $K_{3,ads}$ and n_3 are not as accurately known.

(3) Next, the above isotherms are reanalyzed and all other isotherms are analyzed with a three-process fit using fixed values of n_1, n_2, and n_3 from steps 1 and 2. This step produces the reported values of $K_{1,ads}$, $K_{2,ads}$, and $K_{3,ads}$ calculated for each adsorption isotherm at each temperature.

Step 3 constitutes a check to determine if meaningful parameters have been obtained. If good values result for n_1, n_2, and n_3 from steps 1 and 2, it will be possible to fit the isotherms obtained at all temperatures to within the precision of the experimental measurements with these n_i's fixed. A second check results by plotting ln $K_{i,ads}$ vs $1/T$ [K^{-1}]. Meaningful parameters will give a straight line with the slope related to the enthalpy of adsorption.

It is important to realize that the K_{ads} values calculated in these experiments correspond to an equilibrium that is established in minutes. On standing for hours, the adsorption capacity of the solid is found to increase. The equilibrium process that is rapidly established is of most interest for catalytic and separation applications. In these experiments, equilibrium is defined as the point at which the measured pressure changes by less than 0.01% of the average pressure during a 10-s time interval. In general, for these porous carbons, 3−5 min transpires between data points, although longer times are required at low pressures.

Supports and Adsorptives. Two chemically different porous carbonaceous supports and a series of different gases were studied to quantify the processes involved in gaseous adsorptive pickup. This research has focused on the carbonaceous adsorbents Ambersorb 572 (A-572) made from pyrolyzed, sulfonated, macroreticular polystyrene beads and a pyrolyzed poly(acrylonitrile) (PPAN) material.[24] Data for the physical characterization of these materials with elemental and BET analyses are listed in Table 1. Both solids have BET surface areas around 1000 m^2/g and a distribution of pores including micropores, mesopores, and macropores. The C constants are 1685 and 866 for PPAN and A572, respectively. Microporosity makes the calculated surface area suspect. The selection of these adsorbents enables us to compare properties of a predominantly carbon-containing solid material and one with nitrogen donor functionality.

The gases used in the adsorption measurements are summarized in Table 2 and were selected to provide a range of polarity, polarizability, and size. Helium is taken as a reference zero point to determine the dead volume of the support. The nonpolar N_2, slightly polar CO, and the quadrupolar CO_2 were chosen to investigate the influence of polarity on the application of this adsorption model and to provide an indication of the importance of these properties on adsorption by these solids. N_2 and CO are noncondensible gases in our studies because their critical temperatures are significantly less than the temperatures used in this work. These probes are subject to solid−probe and multilayer interactions but do not give rise to capillary condensation in the mesopores and large micropores. Condensible adsorptives are subject to both solid−probe and multilayer interactions, as well as capillary condensation.

TABLE 1: Physical Properties of the Adsorbents Used

	A-572	PPAN
surface area av [m^2/g] (C)[a]	1159 (865)	880 (1685)
pore vol [mL/g]		
micropore	0.428	0.334
mesopore	0.284	0.119
macropore	0.207	0.090
CHN anal.		
% C	91.1	70.2
% H	0.33	1.66
% N	0.00	5.31

[a] BET value of C constant.

TABLE 2: Summary of Gases and Physical Properties[a]

probe gas	MW, g/mol	polarizability,[b] Å^3	dipole moment D	molar vol,[c] mL/mol	T_c, °C	T_{bp}, °C	ΔH_v, kcal/mol	van der Waals const[a]
He	4.00	0.205	0	32	−268.0	−268.9	0.0194	0.03412
N_2	28.01	1.74	0	35.4	−146.9	−195.8	1.33	1.390
CO	28.01	1.95	0.112	34.9	−140.2	−191.5	1.44	1.485
CO_2	44.01	2.91	0	40.0[b] (−37 °C)	31.04	−78.44	6.03 (sub)	3.592

[a] *Lange's Handbook of Chemistry*, 13th ed.; McGraw-Hill: New York, 1985. All data is from this source unless otherwise specified. [b] *Handbook of Chemistry and Physics*, 71st ed.; CRC: Boca Raton, FL, 1991. [c] Molar Volume of the liquid at the normal boiling point. Hildebrand, J. H.; Prausnitz, J. M.; Scott, R. L. *Regular and Related Solutions*; Van Nostrand Reinhold: New York, 1970; p 217.

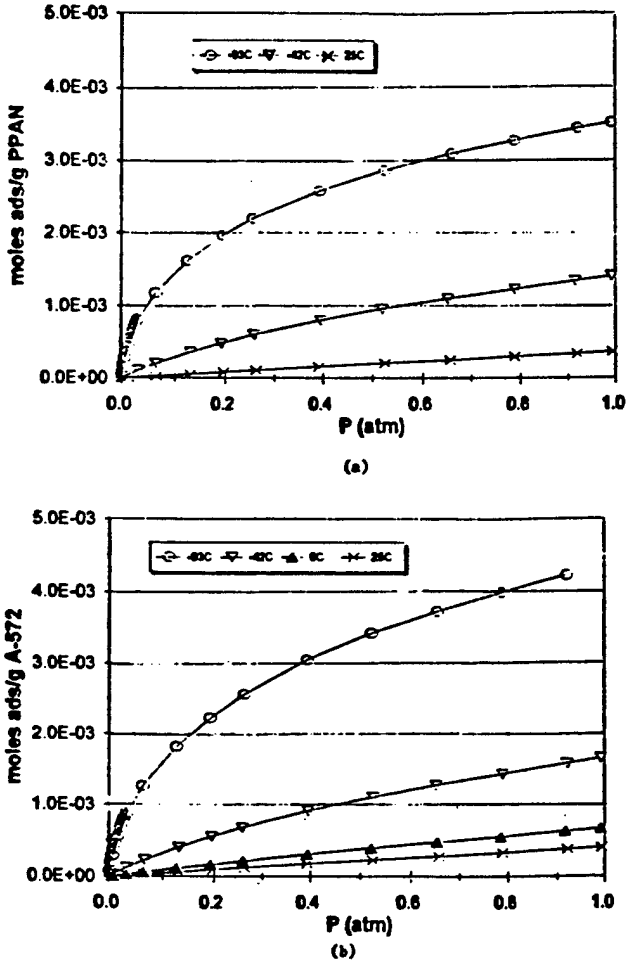

Figure 2. (a) Adsorption of nitrogen by PPAN; (b) adsorption of N_2 by A-572. T_c of N_2 is −146.9 °C.

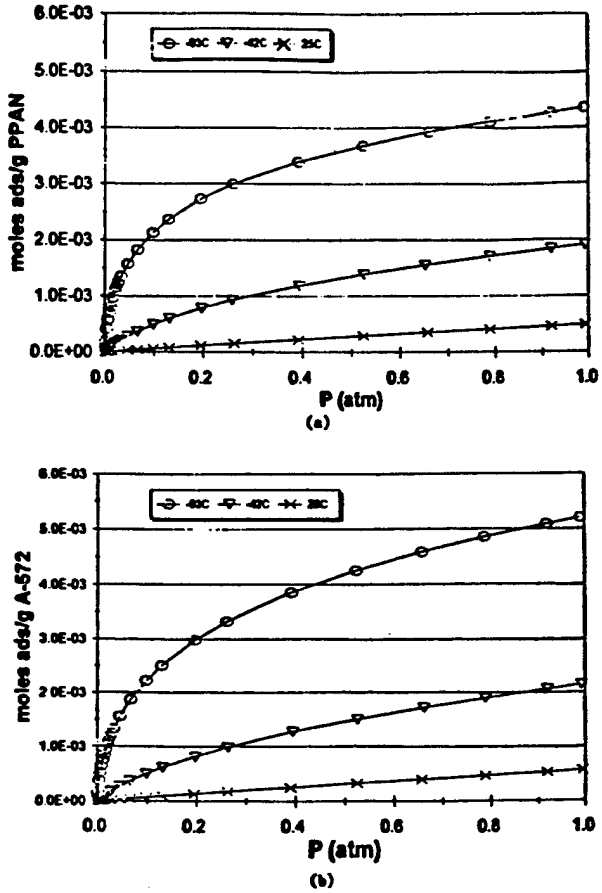

Figure 3. (a) Adsorption of CO by PPAN; (b) adsorption of CO by A-572. T_c of CO is −140.2 °C.

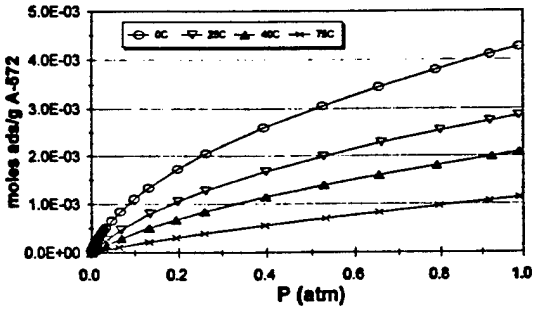

Figure 4. Adsorption of CO_2 by A-572. T_c of CO_2 is 31.04 °C.

Adsorption Isotherms. Figures 2–4 show the adsorption isotherms for N_2, CO, and CO_2 on A-572 and N_2 as well as CO on PPAN. The N_2 and CO isotherms at 25 °C are linear at the external pressures studied, whereas at lower temperatures, the isotherms are nonlinear and the solids have greater adsorption. The isotherms in Figures 2 and 3 were fit to eq 2 with n_1, n_2, and n_3 determined and fixed for each adsorptive as described in the calculational procedure. In the case of CO_2, the n_i values that were obtained from the isotherm at 0 °C by optimizing the n's and K's fit the data at all temperatures. The isotherms for all three adsorptives on both solids at all temperatures could be fit to the accuracy of the measurements using three different adsorption processes. The points shown in Figures 2–4 are the experimental data, and the curves are generated from the best fit analysis using eq 2. The excellent fit of the data for the noncondensible gases to the three-process model, using the same n_1, n_2, and n_3 values for isotherms at all temperatures studied, suggests that the n_1 and n_2 values obtained are accurate measures of the available capacity for these different processes.

It is important to note that in the case of CO on either solid, n_i and $K_{i,ads}$ values were within 10% of those reported when calculated solely from the $T = -93$ °C adsorption isotherm. The results for CO_2 at 0 °C and CO at −93 °C indicate that if one adsorbs enough adsorbate in the region of the isotherm in which processes 1 and 2 dominate and if enough measurements are taken at low pressures (approximately $P < 0.05$ atm), a

TABLE 3: Equilibrium Adsorption Parameters

solid	gas	process	n_i, mmol/g	$K_{i,ads}$ −93 °C	−42 °C	0 °C	25 °C	40 °C	75 °C
A-572	N_2	1	0.46	93	4.6	0.94	0.55		
		2	1.59	9.9	0.78	0.13	0.041[a]		
		3	5.32	0.86	0.13	0.05	0.041[a]		
	CO	1	0.53	180	8.26		0.66		
		2	1.82	16.7	1.1		0.06[a]		
		3	4.94	1.4	0.17		0.054[a]		
	CO_2	1	0.18			57.4	16.0	7.4	3.1
		2	1.38			6.39	2.8	1.6	0.52
		3	8.69			0.50	0.23	0.14	0.06[a]
PPAN	N_2	1	0.43	110	4.7		0.30		
		2	1.63	9.4	0.74		0.15[a]		
		3	3.62	0.81	0.11		0.015[a]		
	CO	1	0.56	250	8.9		0.72		
		2	1.79	19.3	1.1		0.05[a]		
		3	3.65	1.35	0.15		0.05[a]		

[a] There is very little filling of these sites at the temperature indicated. Therefore, these values have a greater uncertainty than the other processes.

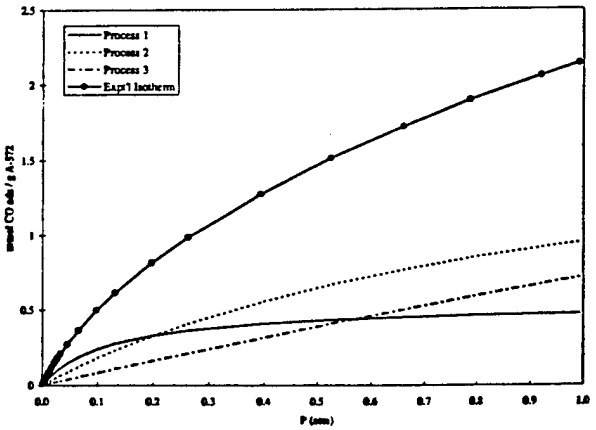

Figure 5. Contributions of three processes to the total isotherm of CO on A-572 at −42 °C.

reasonable estimate of n_1 and $K_{1,ads}$ is possible from measurements at one temperature. If it is not possible to get enough adsorption measurements in the low-pressure portion of the isotherm because of extensive filling of these high-affinity sites, then higher temperatures may be required to obtain a better value of n_1 and $K_{1,ads}$.

Table 3 summarizes the n_i and K_{ads} parameters for all of the N_2 ,CO, and CO_2 adsorption isotherms, where n_i is the capacity of the solid for the adsorption process in millimoles of gas adsorbed per gram of solid, and the equilibrium constants, K_{ads}, measure the affinity of the probe for that adsorption process. The K_{ads} values are such that the second and third types of processes begin before the first process, adsorption in the small micropores, has been completed. This simultaneous filling is illustrated in Figure 5 where the experimental isotherm for CO on A-572 at 42 °C is decomposed into the three-component processes using the determined $K_{i,ads}$ and n_i values.

It is important to emphasize that as in all heterogeneous equilibria, the K_{ads} is an average value of the adsorption process by different solid sites that have K_{ads} values close enough to be treated, within experimental error of the measurement, as a single process in the data workup. It is also important to emphasize that n_i for each type of process is a function of the pore distribution in the solid and the size of the probe molecule. The log $K_{i,ads}$ value is a quantitative measure of the free energy of probe-solid and probe−probe interactions for each different process. The log $K_{i,ads}$'s for a given adsorptive being adsorbed by different solids provide quantitative comparisons of the interactions of the adsorbate with the solid. For a given adsorbent, quantitative comparisons of the log $K_{i,ads}$'s for different adsorptives will give insight into the polarizability, polarity, and donor−acceptor properties of the solid surface.

TABLE 4: Summary of $-\Delta H_{ads}$ (kcal/mol) from ln K_{ads} versus 1/T Plots

process	A-572 N_2[a]	A-572 CO[b]	A-572 CO_2[c]	PPAN N_2[d]	PPAN CO[e]
1	4.7 ± 0.1	5.1 ± 0.04	7.4 ± 0.6	5.3 ± 0.2	5.3 ± 0.1
2	4.5 ± 0.3	5.1 ± 0.4	6.3 ± 0.3	3.8 ± 0.2	5.3 ± 0.5
3	3.0 ± 0.1	3.0 ± 0.3	5.4 ± 0.3	3.6 ± 0.2	3.0 ± 0.4

[a] Process 1: ln K = 2370 (±70)/T − 8.6 (±0.1). Process 2: ln K = 2270 (±160)/T − 10.2(±0.2); ln K_2 at 25 °C was omitted because it is poorly defined. Process 3: ln K = 1510 (±30)/T − 8.5 (±0.04); ln K_3 at 25 °C was omitted because it is poorly defined. [b] Process 1: ln K = 2560 (±0.1)1/T − 9.0 (±0.03). Process 2: ln K = 2550 (±220)1/T − 11.2(±0.3). Process 3: ln K = 1490 (±150)1/T − 8.0(±0.2). [c] Process 1: ln K = 3740 (±320)1/T - 9.7(±0.2). Process 2: ln K = 3200 (±160)1/T − 9.8(±0.1). Process 3: ln K = 2710 (±0.6)1/T − 10.6(±0.03). [d] Process 1: ln K = 2670 (±80)1/T − 10.1. Process 2: ln K = 1890 (±120)1/T − 8.3. Process 3: ln K = 1810 (±120)1/T − 10.2. [e] Process 1: ln K = 2670 (±40)1/T − 9.3. Process 2: ln K = 2690 (±240)1/T − 11.9. Process 3: ln K = 1510 (±190)1/T − 8.2.

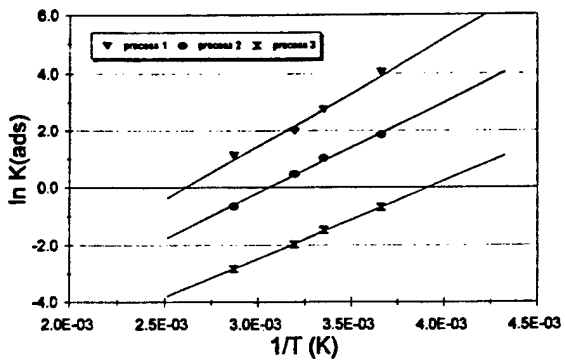

Figure 6. Van't Hoff plot of the three adsorption processes for CO_2 on A-572.

The enthalpies of adsorption, ΔH_{ads}, for the three adsorptives on the two solids have been determined using a Clapeyron-type relationship between ln $K_{i,ads}$ and inverse temperature. The results are summarized in Table 4, and plots are shown for CO_2 on A-572 in Figure 6. The least-squares fit of the plots for all of the systems are given in the footnote to Table 4. It should be noted that the third adsorption process is not defined as well as the first two since only a small fraction of these sites are occupied at the conditions studied.[23] Therefore, $K_{3,ads}$ and $\Delta H_{3,ads}$ are to be considered as rough estimates. The enthalpies

are consistent with those expected for weak physisorption processes.

Interpretation of the Processes Involved. The equilibrium, enthalpy, and BET surface area values can be utilized in conjunction with results[25] from NMR porosimetry (vide infra) on A-572 to provide an interpretation of the physical nature of the three processes. The interpretation of the processes involved is illustrated with A-572, which is more thoroughly characterized. PPAN was studied with N_2 and CO to afford a comparison of adsorbents. The different values of $K_{1,ads}$, $K_{2,ads}$, and $K_{3,ads}$ for A-572 are consistent with different interaction potentials for the different adsorption processes. At low pressures, adsorption of the gas into the small micropores of the solid should be the dominant process for these adsorptives. $K_{1,ads}$, the affinity of the adsorptive for the smallest pores, increases in the order N_2 < CO < CO_2 at any given temperature. The enthalpies increase in the same order and are directly proportional to the polarizability of the gas molecules. This result suggests that the predominant interaction of the adsorptive molecules studied with this solid surface involves dispersion forces.

The assignment of process 1 to adsorption in the smallest pores is supported by the literature[9-11] and by pore-resolved NMR porosimetry.[25] The NMR shows that the smallest pores fill first when CH_3CN is adsorbed from dilute CCl_4 solution by A-572. This is a direct observation that shows the equilibrium constant for this process is the largest. Decomposition of the total adsorption isotherm into three components using integrated intensities from the proton NMR experiment gives profiles similar to those in Figure 5. For all of the systems in Table 3, $K_{1,ads}$ is almost an order of magnitude larger than $K_{2,ads}$.

Process 2 is attributed to adsorption in the larger micropores of the solid. For N_2 and CO on A-572, the enthalpies for processes 1 and 2 are the same within experimental error. This indicates that the superimposed interaction potentials from the adsorbate on opposite walls (Figure 1) of the micropores has a small enthalpic and large entropic component. The predominant contribution to the enthalpy in process 1 is the solid–adsorptive dispersion interaction. With the larger molecule CO_2, the enthalpic contribution to process 1 is 1.1 kcal mol^{-1} larger than that for process 2. The small pores involved in the solids studied apparently have dimensions that lead to a larger, enthalpic, and entropic superimposed interaction potential for the larger CO_2 molecule. For smaller molecules, the enthalpic contribution is smaller.

The predominant contribution to the enthalpy of process 2 for CO, N_2, and CO_2 arises from the dispersion force interaction of these molecules with the carbon surface. The values of both n_1 and n_2 are about 12% larger for CO than for N_2. The quantities n_1 and n_2 will consist of varying combinations of micropores for different gases. Stronger interaction enables CO to bind more strongly than N_2 to some of the larger micropores, thus increasing n_1 and n_2.

Using an adsorbate area of 16.2 $Å^2$ for a nitrogen molecule,[26] the values of n_1 and n_2 for A-572 correspond to surface areas of 45 and 155 m^2/g, respectively. The value of n_3 corresponds to 519 m^2/g. A similar analysis for CO using an adsorbate area[26] of 15.0 $Å^2$ gives 48, 164, and 446 m^2/g for processes 1, 2, and 3, respectively. In both of these cases, process 3 is attributed to adsorption by the surface of the larger pores and remaining surface. The n's and K's for process 3 are not well-defined, and the calculated surface areas are not as well-known.

A polarized surface molecule could lead to multilayer adsorption even though we are above the critical temperature of the adsorbate. Whether the adsorbed molecules are all on the surface or on surface and bilayer sites is often of minor concern. Multilayer formation in the micropores is analogous to the accepted concept of micropore filling. Therefore, in all these processes, it is difficult to distinguish the contribution from multilayer adsorption and surface-bound interactions, for the two may proceed concurrently and with a comparable K_{ads}. However, for most applications, the concern is with the capacity and affinity of the various processes.

When similar calculations are done with the CO_2 data, using an adsorbate diameter[26] of 21.8 $Å^2$, the corresponding surface areas are 24 m^2/g for process 1 and 181 m^2/g for process 2. An area of 1140 m^2/g is found for process 3, which exceeds the reported BET total surface area. Thus, CO_2 must involve both adsorption by the solid surface and multilayer processes. In this case, it is clear that multilayer and surface adsorption have comparable equilibrium constants, for the data are fit to three processes.

The quantitative thermodynamic data for process 3 are poorly defined at the temperature and pressure regions studied due to only a fraction of n_3's capacity actually being occupied. These calculations show that condensation does not occur for N_2 or CO but does for CO_2.

This correlates with the critical temperatures of these gases. Both n_1 and n_2 are smaller for CO_2 than for either N_2 or CO, as expected from its larger size. However, n_3 is much larger and provides the only clear manifestation of a multilayer process in the systems in Table 3.

It is of interest to note that the enthalpies of process 3 are larger than the enthalpies of vaporization of the liquids. The polarization of a surface-bound molecule will increase the enthalpy of interaction of a second layer with the surface layer. In general, multilayer formation in each of the processes is expected to have comparable $K_{i,ads}$'s to those for surface adsorption of those processes. The interaction potentials that give rise to the different processes influence not only the surface interactions but also the multilayer interactions.

Comparison of Adsorbents. The solid adsorbent PPAN is very similar to A-572. At −93 °C, the n_1 and n_2 values for N_2 and CO are similar for these two solids. The −93 °C equilibrium constants and enthalpies for process 1 are slightly larger for PPAN than for A-572. The $K_{2,ads}$ and $K_{3,ads}$ values are similar for the two solids, as is the enthalpy for process 3. Thus, the nitrogen donor functionality of PPAN does little to change the interaction potential between the solid surface and the monolayer of N_2 or CO. Interestingly, the n_3 values obtained are larger for A-572 than for PPAN. This is consistent with porosimetry and BET experiments which indicate a larger pore volume and surface area for A-572.

It is also of interest to note that both adsorbents were cycled through adsorption experiments and degassing at 200 °C up to 15 times. We found no change in the surface area and pore size distribution between the original and final sample. This thermal stability is important for separation and catalytic applications.

Comparison of Adsorption Models. The BET model, which is the most often used standard adsorption model for porous materials, was developed to account for multilayer adsorption by assuming that the Langmuir equation, which involves only monolayer adsorption, applies to each layer. Following Adamson,[12] the C constant in the BET equation (eq 1) is related to the ratio of equilibrium constants for monolayer adsorption and multilayer adsorption. It is also related exponentially to the difference in the enthalpy of adsorption of the monolayer (Q_1) and the multilayer (Q_v). Therefore, C encompasses several processes and thus is difficult to relate to the affinity or strength of interaction of the probe with the solid.

In the multiple process equilibrium model presented here, the C constant of the BET equation is essentially being separated into components for surface adsorption in pores of different sizes and multilayer formation. A significant advantage of this model is that the thermodynamic quantities $K_{i,ads}$ are a true thermodynamic quantity and can be related to physical properties (e.g., polarizability, etc.) of the adsorptive. Thus, our method of analysis provides a thermodynamic measure of gas−solid equilibria and a thermodynamic basis for understanding the adsorption process.

Conclusions

The affinities of three gases for two porous carbonaceous solids have been compared using a multiple-process equilibrium analysis. For noncondensible adsorptives, N_2 and CO, a multiple-process adsorption model is able to separate the processes of small micropore adsorption, larger micropore adsorption, and adsorption by the remaining surface. The enthalpy of interaction for the condensible adsorptive, CO_2, indicates that multilayer condensation may accompany surface adsorption for each process and is clearly involved for CO_2 in the n_3 process. The $K_{i,ads}$ and n_i values for different adsorptives provide a quantitative characterization of the forces involved in porous solid-gas equilibria. Comparison of the ln $K_{i,ads}$ values and the enthalpies affords insight into the fundamental nature of the interaction of adsorbent and adsorptive molecules. The gas−solid interactions studied here are predominantly physisorption. K_{ads} or ΔH_{ads} can be used to provide a quantitative comparison of solids that affords a means of selecting solids which will facilitate adsorption of various adsorptives. Accordingly, the carbonaceous adsorbents studied here are expected to be effective in the separation of molecules that differ in polarizability. Comparison of the affinity of the solid for large and small probe molecules is complicated by the fact that a different distribution of pore sizes comprises processes 1 and 2 for different size probes. As a further note of caution, it should be mentioned that the systems treated all correspond to type 1 isotherms in the Brunauer classification.[27] Further research with solids that fall in the other classes is needed to ascertain the limitations of this approach.

Kinetic factors are also important in the practical applications of solids in separation and catalytic processes. This aspect of the problem is not addressed with these measurements.

Acknowledgment. This work was supported by Rohm and Haas and ERDEC. We thank Dr. Phil L. Rose for his donation of samples of the PPAN adsorbent.

References and Notes

(1) (a) Grunewald, G. C.; Drago, R. S. *J. Mol. Catal.* **1990**, *58*, 227. (b) Grunewald, G. C.; Drago, R. S.; Clark, J. L.; Livesey, A. B. *J. Mol. Catal.* **1990**, *60*, 239. (c) Grunewald, G. C.; Drago, R. S. *J. Am. Chem. Soc.* **1991**, *113*, 1636. (d) Petrosius, S. C.; Drago, R. S. *J. Chem. Soc., Chem. Commun.* **1992**, 334. (e) Petrosius, S. C.; Drago, R. S.; Young, V.; Grunewald, G. C. *J. Am. Chem. Soc.* **1993**, *115*, 6131.

(2) White, M. G. *Heterogeneous Catalysis*; Prentice-Hall: Englewood Cliffs, NJ, 1990; pp 3−13.

(3) Rigby, M.; Smith, E. B.; Wakeham, W. A.; Maitland, G. C. *The Forces Between Molecules*; Clarendon: Oxford, New York, 1986; pp 179−181.

(4) Neely, J. W. *Carbonaceous Adsorbents for the Treatment of Ground and Surface Waters*; Marcel Dekker: New York, 1982; p 80.

(5) Hildebrand, J. H.; Prausnitz, J. M.; Scott, R. L. *Regular and Related Solutions*; Von Nostrand Reinhold: New York, 1970; pp 44−61.

(6) Harkins, W. D.; Jura, G. *J. Am. Chem. Soc.* **1944**, *66*, 919.

(7) Gregg, S. J.; Sing, K. S. W. *Adsorption, Surface Area, and Porosity*; Academic: London, 1967.

(8) (a) Sing, K. S. W.; Everett, D. H.; Haul, R. A. W.; Moscou, L.; Pierotti, R. A.; Rouquerol, J.; Siemieniewsky, T. *Pure Appl. Chem.* **1985**, *57* (4), 603. (b) Rouquerol, J.; Avnir, D.; Fairbridge, C. W.; Everett, D. H.; Haynes, J. H.; Pernicone, N.; Ransey, J. D. F.; Sing, K. S. W.; Unger, K. K. *Pure Appl. Chem.* **1994**, *66* (8), 1739.

(9) Everett, D. H.; Whitton, W. I. *Proc. R. Soc. London, Ser. A* **1955**, A230, 91.

(10) Farrell, J.; Reinhard, M. *Environ. Sci. Technol.* **1994**, *28*, 53.

(11) Everett, D. H.; Powl, J. C. *J. Chem. Soc., Faraday Trans. 1* **1976**, *72*, 619.

(12) Adamson, A. W. *Physical Chemistry of Surfaces*, 5th ed.; John Wiley & Sons: New York, 1990.

(13) Connert, J.; D'Antonio, P. *Carbon* **1983**, *21*, 193.

(14) Jenkins, G. M.; Kawamura, K. *Polymeric Carbons−Carbon Fibre, Glass, and Chemistry*; Cambridge University: London, 1976.

(15) (a) Neely, J. W. Partially Pyrolyzed Macroporous Polymer Particles Having Multimodel Pore Distribution with Macropores Ranging from 50−100,000 Angstroms. U.S. Patent No. 4,040,990, 1977. (b) Amick, D. R. Sulfone-Crosslinked Polystyrene Ion Exchange Resins and Process of Manufacture. U.S. Patent No. 4,177,331, 1979. (c) Maroldo, S. G.; Betz, W. R.; Borenstein, N. Carbonaceous Adsorbents from Pyrolyzed Polysulfonated Polymers. U.S. Patent No. 4,839,331, 1989.

(16) Lafyatis, D. S.; Tung, J.; Foley, H. C. *Ind. Eng. Chem. Res.* **1991**, *30* (5), 865.

(17) Brunauer, S.; Emmett, P. H.; Teller, E. *J. Am. Chem. Soc.* **1938**, *60*, 309.

(18) Harkins, W. D.; Jura, G. *J. Phys. Chem.* **1943**, *11*, 431.

(19) Barrett, E. P.; Joyner, L. G.; Halenda, P. P. *J. Am. Chem. Soc.* **1951**, *73*, 373.

(20) Micromeritics ASAP 2000 System−Operators Manual V2.05, Appendix C; Micromeritics Instrument Corp.: Norcross, GA, 1992.

(21) Micromeritics ASAP 2000 Chemi System−Operators Manual V2.04, Appendix C; Micromeritics Instrument Corp.: Norcross, GA, 1992.

(22) Lim, Y. Y.; Drago, R. S.; Babich, M. W.; Wong, N.; Doan, P. E. *J. Am. Chem. Soc.* **1987**, *109*, 169.

(23) For the influence of the extent of complexation on the solution of simultaneous equations in data fits, see: Drago, R. S.; Rose, N. J. *J. Am. Chem. Soc.* **1959**, *81*, 6141.

(24) Ambersorb 572 is commercially available from the Rohm and Haas Company. PLR-0246 is a proprietary, high surface area, pyrolyzed poly(acrylonitrile) product supplied to us by Rohm and Haas Company.

(25) Drago, R. S.; Ferris, D. C.; Burns, D. S. *J. Am. Chem. Soc.* **1995**, *117*, 6914.

(26) McClellan, A. L.; Harnsberger, H. F. *J. Colloid Interface Sci.* **1967**, *23*, 577.

(27) Brunauer, S. *The Adsorption of Gases and Vapors*; Princeton University: Princeton, NJ, 1945; Vol. 1.

JP9511616

Oxidations of Alkanes by the H_2O_2-vanadium-pyrazine-2-carboxylic acid complex

5.*Oxidation of light alkanes to produce carbonyl compounds

Georgiy B.Shul'pin[a]*, Russell S.Drago[b], and Michael Gonzalez[b]

[a] N.N. Semenov Institute of Chemical Physics, Russian Academy of Sciences, 117977 Moscow, Russia. Fax (7095)-938-2156

[b] Department of Chemistry, University of Florida, Gainesville,Florida 32611-2046, USA. Fax (352)-392-4658

Summary: Light alkanes (ethane, propane, *n*-butane, *n*-pentane) are readily oxidized in acetonitrile solvent by H_2O_2 with vanadium-pyrazine-2-carboxylic acid (PCA) as the catalyst at 75°C and pressures of ~3 atm to produce predominantly or exclusively ketones (aldehydes). Isobutane is transformed selectively into *t*-butanol. The oxidation of cyclohexane at 26°C in acetone or acetic acid is less efficient than that in acetonitrile. The reaction does not occur in *t*-butanol.

The oxidation of organic compounds and especially hydrocarbons by molecular oxygen and hydrogen peroxide has been extensively investigated over the last few decades since these oxidizing reagents are inexpensive and produce only water as a by-product[2-5]. Reactions involving hydrogen peroxide are catalyzed by various transition metal complexes[6-13]. Vanadium complexes are known to play an important role in chemical as well as and biological oxidations,[14,15] and have been used as catalysts for the hydrogen peroxide oxygenation of hydrocarbons[16-24]. Earlier it was shown that a vanadium complex in the presence of pyrazine-2-carboxylic acid (PCA) catalyzes the rapid oxidation of hydrocarbons and other organic compounds (e.g. alcohols) with aqueous 50% solution of hydrogen peroxide in acetonitrile[1,25-28]. Since benzene, n-hexane, n-heptane,

2-methylhexane, 3-methylhexane, and cyclohexane were used as substrates, these oxidations were carried out in open vessels in air at 20-70°C. At low temperature the predominant product is the corresponding alkyl hydroperoxide. This hydroperoxide is then slowly decomposed to produce the respective ketone and alcohol. The study of the H_2O_2 oxidation of saturated hydrocarbons by the vanadium-PCA catalyst was extended to light alkanes as substrates to solvents other than acetonitrile.

Experimental:

The oxidations of light alkanes were carried out in thermostated, closed 250 ml Pyrex vessels with vigorous stirring. The volume of the reaction solution was 50 mL. Initially, 0.4 mL (6.7×10^{-3} mol) of a 50% aqueous solution of hydrogen peroxide (Fischer) was added to the solution of the catalyst (in all cases 5×10^{-6} mol of $(n\text{-}Bu)_4VO_3$ and 2×10^{-5} mol of PCA in 50 mL of MeCN). Then 5 mL of liquid pentane was added to the solution and the vessel sealed with a pressure head containing a pressure gauge. With gaseous alkanes, the reaction mixture comprised 50 mL of acetonitrile containing the amounts of H_2O_2 and the catalyst given above, and 12-40 psig of gaseous hydrocarbon (air was not remove from the reaction vessel prior to charging with the gaseous alkane). The temperature of the reaction was maintained at 75-77°C. After the reaction was complete, the vessel was cooled with ice and opened. The reaction of cyclohexane at 26°C in various solvents was carried out in a Pyrex vessel in air under vigorous stirring, the total volume of the reaction solution was 10 mL.

The reaction solutions were analyzed by means of GC (each sample was analyzed twice, i.e. before and after the addition of an access of solid triphenylphosphine). For the analysis, a Hewlett Packard Series II, 5890 chromatograph equipped with a FID detector and outfitted with the columns HP 50 (crosslinked 50% PhMe Silicone, 30 m x 0.53 mm x 1.0 μm film thickness) or a 30 m Altech RSL 160 column (5 μm thickness) was used. The carrier gas was helium. A Hewlett Packard 3396 Series II integrator was employed. Acetonitrile, used as the solvent, was distilled from CaH_2. Pentane and cyclohexane (Aldrich) were treated with H_2SO_4, washed with water and distilled. Gaseous alkanes were used as received.

Results and Discussion:

In the present paper we wish to report on the first results obtained in the H_2O_2 oxidation of lower alkanes at ~3 atm pressure by the vanadium-PCA catalyst at 75°C.

When heated in the acetonitrile solution, in a closed vessel, the catalyst system (for concentrations of the components, see Experimental) oxidized *n*-pentane exclusively to 2-pentanone and 3-pentanone. The solution of pentane (4.4×10^{-2} mol) heated at 77°C for 1 hour in a closed vessel containing H_2O_2 and 200 mL of air in the gas phase yielded 1.8×10^{-3} mol of 2-pentanone and 1.1×10^{-3} mol of 3-pentanone. The total turnover number was 580 for this reaction. Under analogous conditions, reaction at 75°C for 5 hours produced 2.2×10^{-3} mol of 2-pentanone and 1.3×10^{-3} mol of 3-pentanone. In this case, the total turnover number was 700 and the relative reactivities of hydrogen atoms at carbon atoms 2 and 3 of *n*-pentane was ca. C_2:C_3 = 1:1. The concentrations of the products arising from oxidation of methyl groups as well as subsequent oxidations of any

alcohols formed were much lower and have not been determined. No pentyl hydro-peroxide was present in the reaction solution since the chromatograms of the samples before and after the reduction with triphenylphosphine were similar[1]. It should be noted that reaction proceeds efficiently in respect to hydrogen peroxide: 2 molecules of H_2O_2 yield 1 molecule of pentanone. Molecular oxygen present in the gas phase in the reaction vessel may take part in the oxidation of the hydrocarbon.

n-Butane (12 psig, 5.7×10^{-3} mol) was oxidized (77°C; 1 hour) to produce exclusively methylethylketone (1.1×10^{-4} mol; turnover number 22). *i*-Butane under analogous conditions (20 psig, 9.0×10^{-4} mol; 75°C; 2.5 hours) afforded *t*-butanol (6.0×10^{-4} mol; turnover number 120). No acetone was detected by GC analysis. Propane (40 psig, 1.9×10^{-2} mol) was oxidized (75°C; 1 hour) to acetone (9.5×10^{-4} mol; turnover number 190) as the sole product detected by GC.

The following results have been obtained (amounts of products in the samples before the reduction with triphenylphosphine , $x10^4$ mol, and turnover numbers in parentheses are given) when ethane was oxidized by the reactants under discussion (40 psig, 1.9×10^{-2} mol; 75°C):

Product	***1 hour***	***2.5 hours***
Ethanol	0.8 (16)	1.3 (27)
Acetaldehyde	3.1 (62)	10.0 (200)
Acetic acid	4.0 (80)	7.5 (150)

Table 1: Products from Ethane Oxidation

The total turnover numbers were 158 and 377 after 1 and 2.5 hours, respectively. It is interesting that while the amounts of products obtained in 2.5 hours are not practically changed upon triphenylphosphine treating, the distribution of the products in the 1-hour

sample before the phosphine reduction (see Table above) differ from that in the sample after the reduction (ethanol, 1.5×10^{-4} mol, 30 turnovers; acetaldehyde, 2.3×10^{-4} mol, 46 turnovers; acetic acid, 4.0×10^{-4} mol, 80 turnovers). This indicates[1] that ethyl hydroperoxide is present in the reaction solution after one hour of the oxidation.

It may be concluded that lower alkanes are efficiently oxidized by H_2O_2 with the vanadium-PCA catalyst in acetonitrile at mild temperature and pressure, with the main product being ketones (aldehydes or carboxylic acids). These compounds probably are formed from alkyl hydroperoxides that are the primary products of the reaction. The mechanism of the last reaction is unclear. We assume that the high oxidation state vanadium complex abstracts a hydrogen atom from the hydrocarbon producing alkyl radicals. The latter reacts rapidly with an oxygen molecule to give alkylperoxy radicals. These radicals are capable of transforming into alkyl hydroperoxide which is decomposed to the carbonyl product (ketone or aldehyde). Apparently H_2O_2 oxidizes the vanadium complex which participates in these transformations. The accelerating role of PCA in the accumulation of alkyl hydroperoxide and involvement in its alkyl hydroperoxide decomposition is also to be elucidated. It should be noted that iron complexes with various chelating ligands have been shown to induce the ketonization of the CH_2 groups in alkanes under the action of hydrogen peroxide[4,5,9,10].

It was important to check the oxidation in other solvents. For this purpose cyclo-hexane was chosen as a substrate and the oxidation carried out at 26°C in open Pyrex vessels. If acetonitrile was used as a solvent the oxidation of cyclohexane (concentration 0.46 M) by the reactants under discussion (0.1 mM of $(n\text{-}Bu)_4NVO_3$, 0.4 mM of PCA and

0.15 M of H_2O_2 as 50% aqueous solution) gave cyclohexanone (11.3 mM) and cyclohexanol (30.0 mM) after 24 hours. Under the action of triphenylphosphine the composition of the product mixture is changed (2.3 mM of cyclohexanone and 43.0 mM of cyclohexanol) indicating that cyclohexyl hydroperoxide is the main product. Prolonged (72 hours) reaction of the stirred solution affords ketone (15.0 mM and 4.0 mM before and after the reduction with triphenylphosphine, respectively) and alcohol (60.0 mM and 75.0 mM).

The reaction proceeds more slowly and the yields of products are lower when acetone is used as a solvent. Indeed under the same conditions only 3.2 mM of cyclohexanone and 1.5 mM of cyclohexanol formed (0.8 mM and 3.6 mM respectively after the reduction withtriphenylphosphine). The concentrations of the products after 72 hours are also relatively low (5.2 mM of ketone and 4.9 mM of alcohol before the reduction; 2.0 mM and 9.0 mM after the reduction). Only trace amounts of products are detected in the absence of PCA in the reaction mixture.

The oxidation reaction is also less efficient if acetic acid is used instead of acetonitrile as the solvent. In this solvent the rate of the reaction is only 1.5 times higher if PCA is present in the reaction solution. Only traces of cyclohexanone and cyclohexanol have been detected by GC when *t*-butanol was employed as a solvent. Thus it may be concluded that acetonitrile seems to be the best solvent of those studied for the oxidation of alkanes by the catalyst system under consideration.

---

*For part 4, see Ref 1.

Acknowledgements:

This work was financially supported in part by the International Science Foundation (grants Nos. MMS000 and MMS300), INTAS (grant No. 93-1226) as well as the Russian Basic Reseach Foundation (grant No. 93-03-5226). One of us (G.B.Sh.) thanks University of Florida (Gainesville, USA) for the invitation for a sabbatical stay during which a part of this work was carried out. The authors are indebted to Mr. Kenneth Lo and Mr. Alfredo Luis Mateus for their help inexperiments.

References:

1. G.B.Shul'pin and G.Suss-Fink, J. Chem. Soc., Perkin Trans. 2, 1995, 1459.
2. A.E.Shilov and G.B.Shul'pin, Activation and Catalytic Reactions of Hydrocarbons, Nauka, Moscow, 1995 (in Russian).
3. R.S.Drago, Coord. Chem. Rev., 1992, 117, 185.
4. A.Sobkowiak, H.-C. Tung, and D.T.Sawyer, Progr. Inorg. Chem., 1992, 40, 291.
5. D.H.R.Barton and D.K.Taylor, Russ. Chem. Bull., 1995, 44, 575.
6. J.Muzart, A.N'Ait Ajjou, G.V.Nizova, and G.B.Shul'pin, Bull. Acad. Sci. USSR. Div. Chem. Sci., 1991, 40, 1294.
7. U.Schuchardt, C.E.Z.Krahembuhl, and W.A.Carvalho, New J. Chem.,1991, 15, 955.
8. D.H.R.Barton, S.D.Beviere, W.Chavasiri, E.Csuhai, D.Doller, and W.-G.Liu, J. Am. Chem. Soc., 1992, 114, 2147.
9. H.-C.Tung, C.Kang, and D.T.Sawyer, J. Am. Chem. Soc., 1992,114, 3445.
10. C.Kang, A.Sobkowiak, and D.T.Sawyer, Inorg. Chem., 1994, 33, 79.
11. A.S.Goldstein, R.H.Beer, and R.S.Drago, J. Am. Chem. Soc., 1994,116, 2424.
12. R.W.Murray, K.Iyanar, J.Chen, and J.T.Wearing, Tetrahedron Lett.,1995, 36, 6415.
13. D.R.H.Barton, B.M.Chabot, N.C.Delanghe, B.Hu., V.N.Le Gloahec, and R.U.R.Wahl, Tetrahedron Lett., 1995, 36, 7007.
14. A.Butler, M.J.Clague, and G.E.Meister, Chem. Rev., 1994, 94, 625.
15. M.J.Clague and A.Butler, J. Am. Chem. Soc., 1995, 117, 3475.
16. M.Bonchio, V.Conte, F.Di Furia, G.Modena, S.Moro, T.Carofiglio, F.Magno, and P.Pastore, Inorg. Chem., 1993, 32, 5797.
17. M.S.Rigutto and H. van Bekkum, J. Mol. Catal., 1993, 81, 77.
18. E.P.Talsi, V.D.Chinakov, V.P.Babenko, and K.I.Zamaraev, J. Mol. Catal., 1993, 81, 235.
19. R.Neumann, M.Chava, and M.Levin, J. Chem. Soc., Chem. Commun.,1993, 1685.
20. M.Bonchio, V.Conte, F.Di Furia, G.Modena, and S.Moro, J. Org. Chem., 1994, 59, 6262.
21. A.E.Gehman, N.I.Moiseeva, and I.I.Moiseev, Russ. Chem. Bull., 1995, 44, 584.
22. C.U.Dinesh, R.Kumar, B.Pandey, and P.Kumar, J. Chem. Soc., Chem. Commun., 1995, 611.
23. S.K.Das, A.Kumar, Jr., S.Nandrajog, and A.Kumar, Tetrahedron Lett., 1995, 36, 7909.
24. B.M.Choudary, P.N.Reddy, J. Mol. Catal., A: Chem., 1995, 103, L1.
25. G.B.Shul'pin, D.Attanasio, and L.Suber, Russ. Chem. Bull., 1993, 42, 64.
26. G.B.Shul'pin, D.Attanasio, and L.Suber, J.Catal., 1993, 142, 147.
27. G.B.Shul'pin, A.N.Druzhinina, and G.V.Nizova, Russ. Chem. Bull., 1993, 42, 1394.

28.G.V.Nizova and G.B.Shul'pin, Russ. Chem. Bull.,1994, 43, 1146.

Contribution from

Department of Chemistry

University of Florida

Gainesville, FL 32611-7200

Tel.: (352) 392-6043 Fax: (352) 392-4658

STOICHIOMETRIC AND CATALYTIC OXIDATION OF ORGANIC SUBSTRATES WITH IN-SITU GENERATED PERACIDS

by

Russell S. Drago, Alfredo L. M. L. Mateus and Douglas Patton

ww022896/peracids.am/dl

ABSTRACT

Thioethers are efficiently oxidized by peracids generated *in situ* from carboxylic acid anhydrides and H_2O_2 using 1-methyl-2-pyrrolidinone as the solvent. Sulfoxides or sulfones can be produced in high yields by varying the amount of hydrogen peroxide when an excess of carboxylic acid anhydride is used. Catalytic use of the carboxylic acid was demonstrated for the thioether oxidation by the total conversion of a 2:1 excess of the substrate. This behavior could not be observed for epoxidation reactions due to the poor nucleophylicity of the olefins. Attempts to increase the concentration of peroxy acid in solution and the secondary reactions of the epoxide product are discussed.

INTRODUCTION

The replacement of hypochlorite and alkyl hydroperoxides as oxidants by hydrogen peroxide is being driven by environmental and economic considerations, respectively. The byproduct when peroxide behaves as an oxidant is water. Though peroxide is a potent oxidant it is very slow reacting and needs to be activated.

One possible route to activation of H_2O_2 involves its conversion to peroxyacids. Organic peroxyacids are more effective oxidants than H_2O_2 and are reported to oxidize a variety of substrates under mild conditions.[1-5] Some of the peroxyacids used as oxidants include peroxyacetic acid, m-chloroperoxybenzoic, monoperoxyphthalic acid, peroxymaleic acid, and trifluoroperoxyacetic acid. As the electron withdrawing nature of the substituent increases, the peracid becomes more reactive. Peroxyacids have been used exclusively as stoichiometric oxidants.

Organic sulfides are important substrates to oxidize. One important application involves oxidation of bis(2-chloroethyl) sulfide, HD or mustard for decontamination and stock pile destruction.[6] Using less reactive organic peroxyacids, thioethers are converted to sulfoxides and the further oxidation of sulfoxides to the corresponding sulfones occurs at a slower rate.[7-9] Peroxymaleic acid, prepared by the reaction of maleic anhydride and 90% H_2O_2 in an inert solvent oxidized[10] diallyl sulfoxide to the corresponding sulfone in an 87% yield in methylene chloride at 0 °C.

The oxidation of p,p-dichlorobenzyl sulfide[11] and diphenyl sulfide[12] using a series of para-substituted peroxybenzoic acids[11] showed an increased oxidation rate when electron-withdrawing groups were used on the peracid, and a decreased oxidation rate with electron-donating groups. In both acidic and alkaline media, substitution of electron withdrawing groups on the oxidant led to an increase in the rates of oxidation of p-tolyl methyl sulfoxide.[13] These substituent variations and kinetic studies have led to a mechanism[5] involving nucleophilic attack on the peracid by the sulfide or sulfoxide with simultaneous proton transfer to the carbonyl as shown for alkene epoxidation in Scheme 1.

The oxidation of thioethers has been reported using a polymer-supported peroxyacid.[14] A 1:1 ratio of tetrahydrothiophene or L-methionine and oxidant yielded both the corresponding sulfoxides and sulfones. Higher yields of the sulfones were obtained using a 2:1 oxidant to substrate ratio.

Transition metal catalyzed oxidations by peroxyacids have received little attention. Thioethers are oxidized to the corresponding sulfones in the presence of a catalytic amount of $Mn(acac)_3$ using H_2O_2 in acetic acid.[15] The reactive oxidant was suggested to be peroxyacetic acid. In the presence of a catalytic amount of the catalyst, $[Fe(CH_3CN)_4[ClO_4]_2$, m-chloroperoxybenzoic acid oxidized diphenyl sulfide and diphenyl sulfoxide to the corresponding sulfoxide and sulfone, with 51-71% efficiencies in peroxyacid utilization.[16]

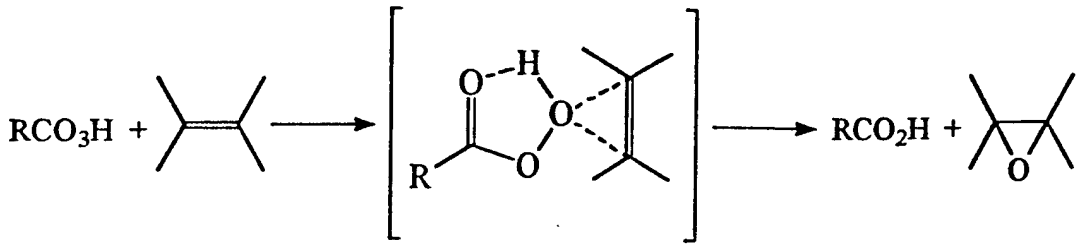

SCHEME 1

Reactions of peroxy acids with alkenes result in epoxidation and hydroxylation reactions.[17] The epoxide, formed by nucleophilic attack by the alkene (Scheme 1) may react with the carboxylic acid formed from the peroxyacid to yield the monocarboxylate of the diol (Scheme 2), which forms the diol upon hydrolysis. Acid catalyzed ring opening of epoxides also yield diols (Scheme 2).

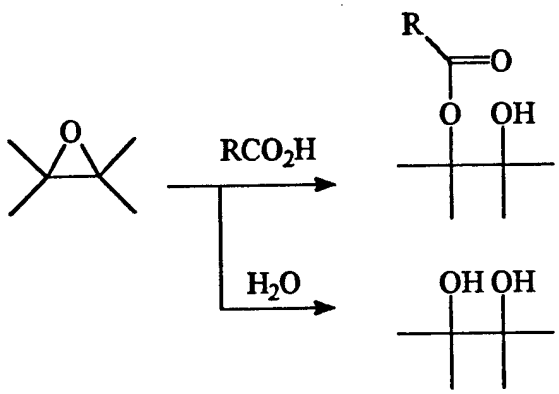

SCHEME 2

Perbenzoic acid gives good yields of epoxide with octenes and other high molecular weight olefins.[4] Monoperphthalic acid has also been used to

epoxidize alkenes but reactions are generally slower. The use of peracetic acid in epoxidation reactions generally is carried out in acetic acid and produces diols and their monoacetates. Good yields of epoxides are obtained [2,3] in inert solvents. Subsequently, it was shown that good yields of epoxides resulted if the reaction was carried out at 20-25 °C, short reaction times were employed, and strong acids were avoided.

This work is concerned with the in situ generation of organic peroxyacids from carboxylic acids and anhydrides with aqueous H_2O_2 in the solvent 1-methyl-2-pyrrolidinone. Conditions are examined to make peracid formation catalytic in the carboxylic acid. This oxidant system is studied for the oxidation of both sulfides and alkenes with and without transition metal co-catalysts.

RESULTS AND DISCUSSION

Sulfide Oxidations

When maleic anhydride (MAnh) (1.6×10^{-2} moles) and 30% aqueous H_2O_2 are added to 10 ml of N-methyl pyrrolidinone (NMP) a very efficient oxidant is produced for sulfide oxidation. A 0.2 M solution of n-butyl sulfide is completely oxidized in 1 hour at ambient temperature as shown in Table 1. By using a tenfold excess of maleic anhydride and varying the amount of H_2O_2, selective production of sulfoxide or sulfone can result. In the first reaction listed in Table 1, a 1:1 ratio of H_2O_2 to sulfide is used resulting in 100% conversion to sulfoxide and 100% efficiency in the utilization of peroxide. In an analogous reaction in

which maleic anhydride is omitted, only a 7% conversion to sulfoxide occurred. This result demonstrates the involvement of a much stronger oxidant than H_2O_2, i.e., the peroxyacid, in the previous reaction. The use of a 3:1 excess of H_2O_2 to sulfide results in the complete conversion of the sulfide to sulfone in one hour.

Using a 3:1 H_2O_2 to substrate ratio, the less nucleophilic thioether, diphenyl sulfide, also reacts with the maleic anhydride/H_2O_2 system leading to the complete oxidation of the substrate to sulfoxide (14%) and sulfone (84%) in one

TABLE 1

n-Butyl Sulfide Oxidations Using Maleic Anhydride and H_2O_2 [a]

Moles of Substrate	Moles of H_2O_2	Time (min.)	Products (%)
1.6×10^{-3} [b]	1.6×10^{-3}	5	R_2SO (12)
		30	R_2SO (21)
		60	R_2SO (29)
		240	R_2SO (62)
		360	R_2SO (79)
		600	R_2SO (94)
		720	R_2SO (97)
		840	R_2SO (100)
1.6×10^{-3} [b]	4.9×10^{-3}	5	R_2SO (62)
		30	R_2SO (38) R_2SO_2 (62)
		60	R_2SO_2 (100)
3.2×10^{-2} [b,d]	3.2×10^{-2} [+]	5	R_2SO (73) R_2SO_2 (27)
5.0×10^{-2} [b,d]	5.0×10^{-2}	5	R_2SO (67) R_2SO_2 (33)
3.2×10^{-2} [b]	3.2×10^{-2}	5	R_2SO (75) R_2SO_2 (11)

a. The amount of MAnh in all experiments was 1.6×10^{-2} moles. 30% aqueous H_2O_2 was used. The reactions were studied under N_2 at

25 °C unless otherwise indicated.

b. 10 mL of NMP was used
c. 4 ml of NMP was used
d. Run under air instead of N_2

hour. No oxidation products were observed in an analogous reaction containing no maleic anhydride.

It should be emphasized that conversion of the diphenyl sulfide to sulfone requires the peracid formed is to be a strong enough electrophile to oxidize the sulfur of the weak nucleophile diphenyl sulfoxide.

Catalytic Sulfide Oxidation

In order for the reaction to be catalytic in maleic anhydride, the maleic acid formed after oxygen atom transfer from the peracid would have to react with H_2O_2 to regenerate the peracid as illustrated in Scheme 3 and Equations (1)-(3). To evaluate this possibility, a twenty-fold increase in n-butyl sulfide

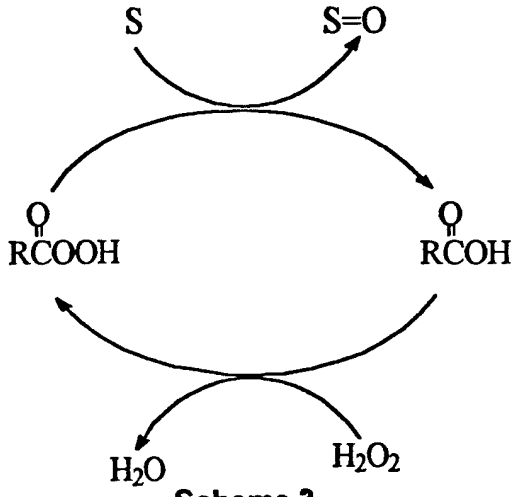

Scheme 3

$$(RCO)_2O + H_2O_2 \rightarrow RC(O)OH + RC(O)OOH \quad (1)$$

$$RC(O)OOH + S \rightarrow Products + RC(O)OH \quad (2)$$

$$RC(O)OH + H_2O_2 \rightarrow RC(O)OOH + H_2O \quad (3)$$

concentration over that in Table 1 was oxidized using a 1:1 H_2O_2 to substrate molar ratio at ambient conditions. This produces reactant molarities that are two times that of maleic anhydride. After 5 minutes of reaction, complete oxidation of the substrate had occurred. A similar result was obtained when a 3:1 reactant to maleic anhydride ratio was employed. The results obtained for these experiments show > 100% efficient use of H_2O_2. The addition of the H_2O_2 to these solutions, containing the acid anhydride and the substrate, results in a very exothermic reaction, with temperatures of >75 °C being observed. Since the reaction vessels were open to the atmosphere, it is most likely that the solvent, 1-methyl-2-pyrrolidinone, reacted with atmospheric oxygen to form the corresponding N-alkylamide hydroperoxide, which would result in the further oxidation of the sulfide and /or sulfoxide. Under an N_2 atmosphere, an analogous reaction showed a 97% efficient use of the H_2O_2 (Table 1). A blank run containing no maleic anhydride produced only 9% sulfoxide in 5 minutes and 16% in 30 minutes.

Effect of Transition Metal Catalysts

The activation of H_2O_2 in the solvent, 1-methyl-2-pyrrolidinone, was pursued using maleic anhydride, in the presence of transition metal co-catalysts. The addition of 5×10^{-3} moles of H_2O_2 and 1.6×10^{-2} moles of maleic anhydride to ten mL of 1-methyl-2-pyrrolidinone, led to ~90% oxidation of 1.6×10^{-3} moles of n-butyl sulfide to the sulfone in 30 minutes (Table 2). Several transition metal compounds increased the activity of this system. The addition of $Mo(O)_2(acac)_2$ to the above reaction led to complete oxidation of the sulfide to the sulfone in 5 minutes (Table 2). An analogous reaction containing $Mo(O)_2(acac)_2$ but no maleic anhydride required 48 hours to oxidize the sulfide to the sulfone.

Complete oxidation of the sulfide to the sulfone also occurred in 5 minutes when $NiCl_2 \cdot 6H_2O$ was added to the peroxyacid system. The use of H_2O_2 as the oxidant in an analogous reaction with $NiCl_2 \cdot 6H_2O$, but with no maleic anhydride led to only 10% substrate conversion to the sulfone in 48 hours. The reaction was accompanied by non-productive peroxide decomposition.

The catalysts, $RuCl_3 \cdot 3H_2O$ and $ReCl_3$ enhanced the activity but were less effective than the molybdenum(VI)- and nickel(II). No increase in activity was observed with, $V(O)(acac)_2$, $CoCl_2 \cdot 6H_2O$ and $FeCl_3 \cdot 6H_2O$ and metal-catalyzed peroxide decomposition becomes a factor.

TABLE 2		
Transition Metal-Catalyzed n-Butyl Sulfide Oxidations Using Peroxymaleic Acid [a]		
Co-catalyst	**Time (min.)**	**Products (%)**
none	5	R_2SO (35) R_2SO_2 (57)
	30	R_2SO (10) R_2SO_2 (88)
	60	R_2SO_2 (95)
$RuCl_3 \cdot 3H_2O$	5	R_2SO (2) R_2SO_2 (93)
	30	R_2SO (1) R_2SO_2 (98)
	60	R_2SO_2 (100)
$Mo(O)_2(acac)_2$	5	R_2SO_2 (100)
$ReCl_3$	5	R_2SO (2) R_2SO_2 (92)
	30	R_2SO (1) R_2SO (99)
	60	R_2SO_2 (100)
$NiCl_2 \cdot 6H_2O$	5	R_2SO_2 (100)

a. Reaction conditions:
substrate (1.6×10^{-3} moles), 1.6×10^{-4} moles of metal compounds, H_2O_2 (4.9×10^{-3} moles, 30% aqueous solution), MA (1.6×10^{-2} moles), NMP (10 mL), run under N_2 at ambient conditions.

Epoxidation of Alkenes

In view of the excellent reactivity observed for sulfide oxidations, the maleic anhydride/H_2O_2 system of Table 1 was used to attempt the epoxidation of olefins. The liquid olefin 1-octene was selected as the substrate because of its similarity to propene, but greater ease of handling. Terminal olefins tend to be

difficult to selectively epoxidize. When the same conditions used for the non-catalytic thioether oxidations (Table 1) are used for the 1-octene epoxidation, only a small consumption of olefin (9%) was observed after 16 hours. The epoxide peak could not be observed in this run because the maleic anhydride has similar retention times. Phthalic anhydride was used in the place of maleic anhydride under similar conditions and after three hours, no consumption of olefin or formation of epoxide was observed.

Phthalic anhydride was used for the epoxidation of 1-octene under the conditions used for the catalytic sulfide oxidations. A biphasic system resulted and no products could be observed in either of the phases after three hours of reaction. When reacting 5 mmoles of the olefin, 3 mmoles of 50% aqueous hydrogen peroxide and 1 mmole of phthalic anhydride at 65 °C only one phase was observed, run 4. After three hours very little olefin disappeared and no epoxide could be found by GC. Addition of $NiCl_2$ did not increase the rate of epoxidation to the extent required to react at the peracid concentrations in this system.

Commercial magnesium monoperphthalate (MgMMP, 2 mmoles), was employed as the oxidant for 1-octene (5 mmoles) with 3 mmoles of 50% H_2O_2 in 10 ml of NMP, run 5. In this reaction, 26% of the initial olefin was consumed and a 23% yield of epoxide was obtained after one hour of reaction. The olefin consumption corresponds to utilization of 65% of the MgMPP used. None of the

hydrogen peroxide reacts with the phthalate anion to regenerate the peracid at these conditions.

The poor reactivity of 1-octene in contrast to sulfide and sulfone is attributed to the poor nucleophilicity of 1-octene. Accordingly, the epoxidation of cis-cyclooctene was tried next at 65 °C, run 6. Cyclooctene (3 mmoles) was reacted with phthalic anhydride (2 mmoles) and 50% aqueous hydrogen peroxide (5 mmoles) in 10 ml of NMP. After one hour, 20% of the initial olefin was converted to the epoxide with a selectivity of 85%.

In order to increase reactivity, aqueous 50% hydrogen peroxide was substituted by the urea hydrogen peroxide adduct (UHP) in the same reaction, run 7, to increase the equilibrium concentration of peracid by decreasing the excess water in the system (Equation (3)). In this reaction, 2 mmoles of phthalic anhydride were added to a solution containing 5 mmoles of UHP and 3 mmole of cis-cyclooctene in 10 ml of NMP. After one hour at 65 °C, 37% of the initial olefin was converted to the epoxide with a selectivity of 93%.

Phthalic acid (2mmoles) was used instead of the anhydride in the oxidation of cyclooctene (3 mmoles) using UHP (5 mmoles) as the oxidant and 10 ml of NMP as solvent, run 8. After one hour at 65 °C, little consumption of the olefin (<5%) and no epoxide were observed. This result indicates that the epoxidation reaction would not be catalytic in anhydride.

A series of experiments were carried out in N-methylpyrrolidinone using benzoic acid, 3-chlorobenzoic acid and 3,5-dichlorobenzoic acid. The purpose

of these experiments was to study the regeneration step with increasingly electron withdrawing substituents. In all instances, the decrease in octene in 3 hours at 65 °C was 5% or less.

Since UHP provides a good source of anhydrous hydrogen peroxide (18) and increases the conversion of cyclooctene, attempts were made to oxidize 1-octene with this system. First, run 9, 40 mmoles of UHP were reacted with 10 mmoles of phthalic anhydride in 25 ml of NMP at 40 or 80 °C. After 30 minutes, 4 mmoles of 1-octene were added and the reaction mixture kept constant. The reaction at 40 °C gave an 18% decrease on the olefin and a similar amount of epoxide after three hours. The reaction at 80°C, run 10, gave a 38% decrease on the olefin, but only 13 percent epoxide after three hours. This difference is due to the reaction of phtahalic acid and epoxide to form the carboxylate of the diol.

The more facile reaction of sulfides than alkenes with the peracid generated in this system is readily understood in terms of their nucleophilicity. Much higher concentrations of peracid are needed for epoxidation than for sulfide oxidation. These concentrations are not produced at room temperature with phthalic anhydride and 50% aqueous H_2O_2 so little or no reaction occurs. Attempts to facilitate peracid formation by acid catalysis also catalyze ring opening hydrolysis.

TABLE 3						
Olefin Epoxidation Using *in situ* Generated Peracids[a]						
Run #	Olefin	Oxidant	Catalyst	Conversion	Yield	Selectivity
1[b]	1-octene 1.6 mmoles	H_2O_2 30% 1.6 mmoles	MAnh 16 mmole	9 %	---	---
2[b]	1-octene 1.6 mmoles	H_2O_2 30% 1.6 mmoles	PAnh 16 mmoles	---	---	---
3	1-octene 32 mmoles	H_2O_2 50% 32 mmoles	PAnh 16 mmoles	---	---	---
4	1-octene 5 mmoles	H_2O_2 50% 3 mmoles	PAnh 1 mmole	---	---	---
5	1-octene 5 mmoles	MgMPP 2 mmoles H_2O_2 50% 3 mmoles	---	26 %	23 %	88 %
6	cyclooctene 3 mmoles	H_2O_2 50% 5 mmoles	PAnh 2 mmole	20 %	17 %	85 %
7	cyclooctene 3 mmoles	UHP 5 mmoles	PAnh 2 mmole	37 %	34 %	92 %
8	cyclooctene 3 mmoles	UHP 5 mmoles	PAc 2 mmole	5 %	---	---
9[c]	1-octene 4 mmoles	UHP 40 mmoles	PAnh 10 mmoles	18 %	18 %	100 %
10[d]	1-octene 4 mmoles	UHP 40 mmoles	PAnh 10 mmoles	38 %	13 %	34 %

a - Reactions performed at 65 °C in 10 ml of NMP unless indicated.
b - Reaction run in 10 ml of NMP at 25 °C.
c - Reaction run in 25 ml of NMP at 40 °C.
d - Reaction run in 25 ml of NMP at 80 °C.

CONCLUSIONS

Thioethers, such as n-butyl sulfide, can be oxidized to the corresponding sulfoxides and sulfones in the solvent, 1-methyl-2pyrrolidinone, using maleic anhydride to activate H_2O_2 under ambient conditions. When compared with the

analogous thioether oxidations using H_2O_2, the addition of maleic anhydride to these reactions resulted in a very pronounced increase in activity. The use of a catalytic amount of the acid anhydride in reactions employing 1:1 molar ratios of H_2O_2 to substrate led to nearly complete oxidation of the sulfide in minutes, demonstrating the regeneration of the organic peroxyacid from the carboxylic acid formed from the reaction.

Catalytic amounts of transition metal complex catalysts showed an increase in the activity of the peroxyacid. These systems were considerably more active than the analogous metal-catalyzed reaction using the oxidant, H_2O_2.

The amount of peracid existing in solutions of H_2O_2 and carboxylic acid is low in the absence of strong acids. For the strong sulfide nucleophile this amount is enough for reaction and as the peracid is consumed this small amount is replenished via Equation (3). In the epoxidation reactions, this small concentration leads to a very slow reaction. Since the epoxide production is slow, secondary reactions of the epoxide can occur. If an acid is added to catalyze the peracid formation it also catalyzes the ring opening of the epoxide product. When a buffer is added to protect the epoxide from solvolysis, the concentration of the peracid in solution is decreased.

An increase in temperature to increase the rate and concentration of peracid in solution generated from the carboxylic acid also leads to an increase in rate of the competing epoxide reactions. Conditions can be found that lead to

good yields and selectivities for the stoichiometric reaction in which peracids are generated from anhydrides reacting with H_2O_2.

EXPERIMENTAL

Reagents and Equipment

The n-butyl sulfide, n-butyl sulfoxide, n-butyl sulfone, diphenyl sulfide, diphenyl sulfoxide, diphenyl sulfone, and 1-methyl-2-pyrrolidinone (HPLC Grade) were obtained from Aldrich Chemical Company and used as received. The metal complexes, $Mo(O)_2(acac)_2$, $C(O)(acac)_2$, $ReCl_3$, and $RuCl_3{\cdot}3H_2O$ were received from Aldrich Chemical Company as well. All other reagents and solvents were obtained from Fisher Scientific and used as received.

Product Analysis

A Varian 3700 GC with an FID and Hewlett Packard 3390A integrator was used to analyze the products of the sulfide reactions, using a 6 foot stainless steel column packed with Carbowax 20M (10%) on Chromosorb WHP (80/100 mesh) for the n-butyl sulfide oxidations and a 6 foot stainless steel column packed with SE-30 (3%) on Gas Chromosorb Q (80/100 mesh) for the diphenyl sulfide oxidations. All olefin reactions were carried out using o-dichlorobenzene as an internal standard. Reaction products were analyzed using an HP 5890 GC. The substrate(s) and product(s) were identified and quantified using known standards.

Peroxymaleic Acid Stability

Maleic anhydride, 30% aqueous H_2O_2 and the solvent 1-methyl-2-pyrrolidinone produces peroxymaleic acid, a potent oxygen atom transfer agent. This conversion is enhanced by the hydrogen bonding of the product water to the solvent. The solvent 1-methyl-2-pyrrolidinone is readily oxidized by O_2 at 75 °C so its oxidative stability to peroxy acids was investigated.

Maleic anhydride (1.6g, 1.6×10^{-2} moles) and 1-methyl-2-pyrrolidinone (10 mL) were placed in a 100 mL round bottom flask equipped with magnetic stirring. After 5 minutes of stirring, H_2O_2 (4.9×10^{-3} moles, 30% aqueous solution) was added dropwise to the acid anhydride solution. After 1 hour of stirring, the colorless solution was stored under ambient conditions. The peroxyacid solution was analyzed periodically. Under ambient conditions 1.6×10^{-2} moles of maleic anhydride and 4.9×10^{-3} moles of H_2O_2 showed less than 5% loss oxidation titer over a period of 168 hours. The peracid content in the solutions was determined as the difference of the total oxidant content and the hydrogen peroxide content. These were determined in separate titrations as follows. The total oxidant content was determined using an iodomeric titration. Samples were withdrawn and diluted in 2-propanol. A saturated solution of NaI in 2-propanol and acetic acid are added and the mixture is heated to reflux for 30 seconds. The iodine is titrated with a standard sodium thiosulfate solution. The H_2O_2 content was determined using a redox titration with Ce^{4+}, using ferroin

as an indicator. Samples were withdrawn and diluted in H_2SO_4 1M that was cooled to 0 °C. They were then titrated quickly with an standardized solution of $Ce^{IV}(NH_4)_4(SO_4)_4$ in 2.5M H_2SO_4.

Sulfide Oxidations

Maleic anhydride (1.6g, 1.6×10^{-2} moles) and 1-methyl-2-pyrrolidinone (5.0 mL) were placed in a 100 mL round bottom flask equipped with magnetic stirring and an N_2 atmosphere. After 5 minutes of stirring, the appropriate amount of H_2O_2 was added dropwise to the acid anhydride solution. The resulting colorless solution was stirred for 1 hour to ensure formation of the peroxyacid.

1-Methyl-2-pyrrolidinone (5.0 mL) and n-butyl sulfide (0.23 g, 1.6×10^{-3} moles) were placed in a 100 mL round bottom flask equipped with magnetic stirring and an N_2 atmosphere. After 30 minutes of stirring, the previously prepared peroxyacid solution was added dropwise to the reaction solution. Samples were analyzed periodically by GC.

Catalytic Maleic Anhydride

For the catalytic maleic anhydride experiment, maleic anhydride, n-butyl sulfide, and 1-methyl-2pyrrolidinone were placed in a 100 mL round bottom flask equipped with magnetic stirring and stirred for 5 minutes. Samples were analyzed periodically by GC.

Metal catalyzed sulfide oxidations were carried out by stirring maleic anhydride (1.6 g, 1.6×10^{-2} moles) and 1-methyl-2-pyrrolidinone (5.0 mL) in a 100 mL round bottom flask equipped with magnetic stirring and an N_2 atmosphere for 5 minutes. H_2O_2 (4.9×10^{-3} moles, 0.5 mL of a 30% aqueous solution) was added dropwise to the solution and stirred for 1 hour. 1-Methyl-2-pyrrolidinone (5.0 mL), n-butyl sulfide (0.23 g, 1.6×10^{-3} moles), and the appropriate catalyst (1.6×10^{-4} moles) were placed in a 100 mL round bottom flask equipped with magnetic stirring and an N_2 atmosphere. After 30 minutes of stirring, the previously prepared peroxyacid solution was added dropwise to the reaction solution. When 30% H_2O_2 was the oxidant, it was added dropwise to the sulfide-metal complex solution in NMP. Samples were analyzed periodically by GC.

Epoxidation of Olefins by Peracids

Epoxidation reactions were carried out either on a Parr pressure bottle or in a round bottom flask equipped with a cold water condenser. In general, anhydrides (1.0×10^{-3} moles) were allowed to react with hydrogen peroxide 50% (3.0×10^{-3} moles) in 10 mL of NMP for 0.5 hours at room temperature. Then 1-octene (5.0×10^{-3} moles) was added and the reaction flask placed in a silicon oil bath at 65 °C. The reaction was monitored by collecting samples periodically and analyzing by GC using an internal standard. Solutions of known

concentration were prepared and used to construct calibration curves to permit quantitative determination of octene and the corresponding epoxide.

ACKNOWLEDGMENT

The authors acknowledge financial support of this research by the US Army Research Office and ERDEC.

REFERENCES

1. Uemura, S. in "Comprehensive Organic Synthesis" Trost, B. M., Ed.; Pergamon Press: Oxford, 1991; Vol. 7, p.758.
2. Sawaki, Y. in "Organic Peroxides" Ando, W., Ed.; Wiley: New York, 1992, p. 426.
3. Swern, D. in "Organic Peroxides" Swern, D., Ed.; Wiley-Interscience, New York, 1971, p. 355-533.
4. Heaney, H. in "Topics in Current Chemistry", 1993; Vol. 164, p. 1-19.
5. "Syntheses of Sulphones, Sulphoxides and Cyclic Sulphydes" Patai, S.; Rapoport, Z. Eds.; Wiley: New York, 1994.
6. Yang, Y. C., Baker, J.A.; Ward, J. R., *Chem. Rev.* 1992, 92, 1729-1743.
7. Cerniani, A.; Modena, G.; Todesco, P. E. *Gazz. Chim.* **1959**, 89, 843.
8. Greco, A.; Modena, G.; Todesco, P. E. *Gazz. Chim.* **1960**, 90, 671.
9. Kresze, G.; Schramm, W.; Cerc, G. *Chem. Ber.* **1961**, 94, 2060.
10. White, R.W.; Emmons, W. D. *Tetrahedron* **1962**, 17, 31.
11. Overberger, C. G.; Cummins, R. W. *J. Am. Chem. Soc.* **1953**, 75, 4250.
12. Szmant, H. H.; Jarmberger, H. F.; Krahe, F. *J. Am. Chem. Soc.* **1954**, 76, 2185.
13. Curci, R.; Giovine, A.; Modena, G. *Tetrahedron* **1966**, 22, 1235.
14. Harrison, C. R.; Hodge, P. *J. Chem Soc., Perkin Trans. 1* **1976**, 21, 2252.
15. Doumaux, A. R.; McKeon, J. E.; Trecker, D. J. *J. Am. Chem. Soc.* **1969**, 91, 3992.

16. Sugimoto, H.; Sawyer, D. T. *J. Am. Chem. Soc.* **1985**, 107, 5712.

17. Swern, D. in "Organic Reactions", R. Adams, Ed.; Vol. 7, p. 378-401, Wiley: N New York, **1953**.

18. Cooper, M. S.; Heavey, H.; Newbold, A. J., Sowdersor, W. R.; *SYNLETT*, **1990**, 533.

PHYSICAL STUDIES OF MoO_3 CATALYSTS ON SILICA AND CARBON SUPPORTS

Contributions from Department of Chemistry
University of Florida, Catalysis Center
Gainesville, Florida 32611-7200

by

Russell S. Drago*, Vaneica Young*, David J. Singh and
Gerald C. Grunewald, Nicholas Kob

ABSTRACT

The nature and characteristics of the catalytic surface of supported MoO_3 catalysts were studied. Changes that occurred on oxidizing alcohols in air over carbon and silica supported MoO_3 were examined. Structural data were combined with electron microscopy and photoelectron spectroscopy to demonstrate that the carbon support promotes segregation and fragmentation of MoO_3, whereas sintering occurs on silica. Results indicated that this may be correlated with a synergism between the carbonaceous material and metal oxide which provides a reoxidation pathway for reduced Mo, thus preventing formation of extended zones of MoO_2, which in inactive for the oxidation of alcohols.

Keywords: A. oxides. C. electron microscopy. C. photoelectron spectroscopy. C. x-ray diffraction. D. microstructure.

INTRODUCTION

In an earlier report [1] the catalytic activity of MoO_3 doped carbon molecular sieves (CMS) was compared to unsupported and silica supported MoO_3. Catalysts were screened by studying the oxidation of various alcohols and aldehydes, as these reactions are reasonably well understood. Wide variations in activity and selectivity were found between the silica and CMS supported catalysts. A novel synergism was manifested in the MoO_3/CMS systems leading to an activity that greatly surpassed that of the separate components of the material. The synergism was attributed to the ability of the CMS to disperse and anchor the metal oxide during catalyst preparation, preventing migration to form larger clusters under reaction conditions. The higher activity obtained by a larger and more thermally stable dispersion was slightly offset by a decrease in selectivity. The high activity of MoO_3/CMS has also been observed in independent studies [2].

There have been several studies correlating the characteristics of the support with the activity and selectivity of the active phase [3-7]. It has been shown that the TOF (turn over frequency) of the surface molybdenum oxide species varies by a factor of 10 when different supports are used. The differences appear to be related to a property of the support-molybdenum oxide

overlayer interaction rather than the structure of the molybdenum oxide surface species [6]. It has been shown that the molecular structure of the surface molybdenum oxide is a distorted mono-oxo octahedral species [7] and is independent of the molybdenum oxide precursor and the support used. Research suggests that the oxide support acts as a very important ligand for the surface metal oxide and that its reducibility is a critical parameter in the redox activity of the supported metal oxide [6]. Sintering appears to occur in MoO_3/SiO_2 catalysts, leading to the growth of crystallite size and subsequent deactivation of the catalyst as the surface area of the active phase decreases. Sintering is believed to be due to poor interaction between MoO_3 and SiO_2 [5], which is unlike other support materials that interact strongly with the active phase [8-10]. This poor interaction does not preclude the formation of molybdenum silicate at the metal oxide/silica interface, but may be limited to that through interaction of Mo(IV) with the silica.

In contrast to the functionalities present on other common supports, CMS are characterized by a very high microporosity and the absence of oxide species to react with the active phase, i.e. MoO_3. Further, unlike silica CMS are known to undergo redox cycling [11]. Therefore, the use of CMS can provide a unique metal-support interaction resulting in enhanced activity [1] and

very different surface properties. Our previous work has demonstrated that the reaction conditions for oxidation of alcohols and aldehydes have little effect on the surface morphology of MoO_3/CMS. In this study, we will further demonstrate the unique features of MoO_3/CMS which makes it an excellent catalyst for these and similar reactions. MoO_3/CMS will be compared to bulk MoO_3 and MoO_3/SiO_2 before and after reaction. Catalytic activity of none of these materials will be presented as they have been already documented in the literature [1].

EXPERIMENTAL

Materials. The CMS support (AX21) was obtained from Anderson Development Co. (2800-3500 m^2/g), and was heated in vacuo for 8 hr at 100 °C. The material consisted (w/w) of 91% C; 6.2% O; less than 1% N, S, and H; and 1.8% K. Davison grade 62 silica was obtained from W.R. Grace and had a surface area of 340 m^2/g. MoO_3 was obtained from Aldrich. All materials were used without further purification.

Catalyst Preparation and Reaction Conditions. A 15% (w/w MoO_3) catalyst dopant level was prepared by refluxing a mixture of the support and the required mass of ammonium molybdate in water for 6 hr. The Davison silica gel was acid washed with 1M HCl prior

to use in order to remove alkali impurities present on the silica which are known to effect alcohol oxidation activity and the support-molybdenum oxide interaction [12, 13]. The H_2O was then removed by rotary evaporation to dryness followed by drying in vacuo at 100 °C for 8 hr to give the fresh catalyst (pre-catalyst). The catalysts were then used to catalyze the oxidation of methanol as follows: 0.5 g of catalyst was placed in a fixed bed flow reactor, N_2 at 5 ml/min was flowed through the reactor as it was heated to 250 °C, N_2 was switched to air at the same flow rate, methanol at a flow rate of 0.2 mL/hr was delivered via a syringe pump when N_2/O_2 reached 4, and the reaction was run for 10 hours. The used catalyst (post-catalyst) was recovered from the reactor and stored under normal atmospheric conditions prior to analysis. Notice that 15% (w/w MoO_3) on SiO_2 corresponds to an atom % Mo of 2.2%, while 15% (w/w MoO_3) on CMS corresponds to an atom% Mo of 1.4%.

Analysis and Characterization. Scanning Electron Microscopy (SEM) was performed with a Jeol JSM 35C electron microscope using an acceleration voltage of 25 kV. Studies were done at several magnifications, and micrographs at 6000X are reported here. X-ray powder Diffraction (XRD) analysis was done on a GE 3000 instrument using Cu-alpha radiation. X-ray Photoelectron Spectroscopic (XPS)

analysis was carried out on a Kratos XSAM 800 spectrometer, using unmonochromatized Al K_α radiation (15 kV and 12 mA). For the XPS experiments, each sample was prepared by first crushing, then pressing the powdered material onto the adhesive side of aluminum tape (Ted Pella, Inc.); the tape was then mounted on a quick insertion probe for introduction into the analysis chamber of the spectrometer. Spectra were collected in the fixed analyzer transmission mode using high magnification and medium resolution. A small area (0.25 mm x 0.25 mm) was used for analysis as several samples were insulators and quickly developed a surface charge after the start of photoemission. Typical methods for elimination of surface charging could not be used as they would have caused reduction of MoO_3. Bulk MoO_3 was etched with a rastered Ar^+ beam (5 keV, $\leq$ 5 $\mu A\ cm^{-2}$).

RESULTS AND DISCUSSION

SEM, XRD and XPS analyses were conducted on samples of bulk MoO_3, MoO_3/SiO_2 and MoO_3/CMS before and after they were employed in catalytic reactions. To ensure consistency these measurements were performed on samples from the same preparative and catalytic batch. Because the silica consists of fine particulates resembling finely crushed glass, molybdenum oxide is confined to the surfaces of the

particulates, where it may exist as particles or as thin films. The CMS substrate consists of small spheres, which have many pores. The walls of the pores constitute a so-called hidden" surface. Thus, in principle molybdenum oxide may exist as particles on the visible surface, as particles on the "hidden" surface, as thin films on the visible surface, as thin films on the "hidden" surface or as plugs completely filling the pores. SEM enables a visual observation of changes that occur at the visible surface of the various samples during the course of the reaction. XRD affords an analysis of bulk changes that occur as a result of composition and metal crystallite size. XPS provides a detailed examination of the surface oxidation states at the visible surface of the various components.

SEM Studies

In Figure 1, the SEMs (6000 X) of bulk MoO_3 are shown. Cigar-shaped crystallites are seen in the micrograph of the fresh catalyst. The used catalyst shows evidence of a large degree of sintering and crystal growth. Figures 2 and 3 display the micrographs of MoO_3/SiO_2 and MoO_3/CMS respectively before and after catalytic experiments. The areas under observation are the same for all four samples. These micrographs allow us to examine the particle morphology, the projected particle sizes and the particle

number density at the visible surface of the substrates. For the fresh MoO_3/SiO_2 catalyst, 100 particles are counted on that area, while for the used MoO_3/SiO_2 catalyst, only 36 particles are found.

The histograms for the projected particle size distributions of the two samples are shown in Figure 4. Each is bivariate, because most of the particles are ellipsoidal. From Figure 4a, it is evident that most of the particles have dimensions < 2500 Å, in fact the mean value for the longest dimension is 2042 Å, while the mean value for the shortest dimension is 1524 Å. By contrast, from Figure 4b, it is evident that the particles are much larger. The mean values for the dimensions are 8179 Å and 6066 Å, respectively. Both the particle number density and the particle size distribution changes show that on reaction, extensive agglomeration of the metal oxide occurs on the silica surfaces. These results are consistent with previous studies which show the aggregation on MoO_3 when supported on SiO_2 in methanol oxidation [12]. The extent of aggregation of MoO_3 on supports is linked to the strength of the MoO_3-support interaction and SiO_2 interacts weakly with MoO_3 [3].

For the fresh MoO_3/CMS catalyst, 30 particles are counted on the area, while for the used MoO_3/CMS catalyst, 148 particles are counted. The histograms for the particle size distributions of these two samples are shown in Figure 5. From these histograms, it is evident that the larger particles are found on the fresh

catalyst. The mean dimensions of the particles on the fresh catalyst are 10068 Å and 5760 Å, respectively. On the used catalyst, the mean particle dimensions are 4899 Å and 2636 Å. Both the particle number density and the particle size distribution changes show that on reaction, fragmentation of the metal oxide occurs on the CMS surfaces. We never encountered a continuous film of molybdenum oxide on any of the CMS spheres. Likewise, we never observed complete pore filling, although we have seen examples of metal oxide particles protruding from pore openings. Since the walls of the pores are expected to have a hydrophobicity which is equal to or greater than that of the visible surface, the metal oxide on the "hidden" surface should also be particulate. Overall, the observations for bulk MoO_3 and MoO_3/SiO_2 are substantially different from those for MoO_3/CMS.

XRD

X-ray Powder Diffraction studies were used to identify the crystalline nature and phase of the metal oxide particles. In Figure 6 is shown the diffraction patterns for fresh and used MoO_3/SiO_2. In both cases we see a set of relatively narrow lines superimposed upon a background of very broad maxima. The background is typical of the diffraction pattern expected for non-crystalline silica, since the broad band at $2\theta \sim 27°$ is the

characteristic d = 3.34 Å line for quartz. The narrow lines are due to a polycrystalline phase present in the sample. On the fresh catalyst, it is possible to identify a line due to MoO_2 [14], [011], and several lines ([021], [131], [060] and [150]) which belong to MoO_3 [15]. Since only the most intense line for MoO_2 is seen, MoO_3 is the predominant form of the metal oxide. For the used MoO_3/SiO_2 catalyst, it is evident that only MoO_2 is detectable.

A peak at $2\theta = 13.09°$ is seen on the fresh catalyst, but not on the used catalyst. Likewise, peaks at $2\theta \sim 44.5°$ are observed on both the fresh and the used catalysts. These peaks could not be assigned to any molybdenum oxides with known diffraction patterns.

Because the metal oxide lines for the used catalyst are more intense than those for the fresh catalyst, the metal oxide particles on the used catalyst have greater crystalline order than those on the fresh catalyst. In Figure 7, the diffraction patterns for fresh and used MoO_3/CMS are shown. Again we see sets of narrow lines superimposed upon a background of broad maxima. The background is typical of the diffraction pattern expected for non-crystalline carbon, since the broad band at $2\theta \sim 21°$ is characteristic of the (0002) line for graphite. With the exception of the starred peaks, all of the peaks for the fresh catalyst can be assigned to MoO_3 or to the defect MoO_3 oxides (Mo_4O_{11}, Mo_8O_{23} or

Mo_9O_{26}) [15]. For the used MoO_3/CMS catalyst, only one peak could be assigned - it corresponds to four overlapping lines of the defect oxide Mo_9O_{26}. At the 5% significance level, the other peaks can not be assigned to any of the molybdenum oxides for which diffraction data is available. We note that there is no diffraction data for defect oxides with stoichiometries less than $MoO_{2.75}$. One of the starred peaks occurs at $2\theta = 14.29°$; it is present only on the fresh CMS catalyst. The other starred peaks, one in the fresh catalyst diffractogram and the other in the used catalyst diffractogram, occur at $2\theta \sim 44.5°$. Low angle starred peaks occur only on the fresh silica or fresh CMS catalysts. Therefore, the component responsible for it is stable above 100° C, but not at 250° C. It is likely a hydrated species. The higher angle line must represent a component which is stable at 250° C. An example of such a component would be a hydroxide containing compound. The reactants contain only trace impurities, so impurities cannot be the source of these peaks. On comparing the silica and CMS results, we conclude that the particles on the used silica catalyst are more reduced than those on the used CMS catalyst.

XPS Studies

X-ray Photoelectron Spectroscopy was used to investigate the nature of molybdenum on the surface of the supports, and to compare its oxidation state with that in the bulk MoO_3. Five different samples were analyzed: bulk MoO_3, MoO_3/SiO_2 before and after reaction, and MoO_3/CMS before and after reaction. A doublet always appears for the Mo 3d orbital, because of spin orbit coupling to produce $3d_{5/2}$ and $3d_{3/2}$ electronic states. The energy separation between these two states is fairly constant and lies within the range of 3.0 to 3.2 eV, along with a relative intensity ratio of 1.5-1.9 ($3d_{5/2}$ to $3d_{3/2}$). These parameters were used to fix the boundary conditions on peaks constrained as doublets in the peak synthesis algorithm. The peak synthesis algorithm automatically subtracts the default background from the synthesis window. A Shirley background was used as the default, except for the spectra of MoO_3/SiO_2. Instead of increasing from low binding energy to high binding energy, the background in these spectra decrease from low binding energy to high binding energy. A linear background was used as the default, but the spectra are still distorted. The main result is that the highest binding energy peak is significantly truncated. In subsequent discussion, only the Mo $3d_{5/2}$ peak will be described as this information will be sufficient to fully describe

the particular oxidation state and coordination of the metal ion. Atom percentages have been calculated from the equation

$$\%j = \frac{\frac{A_j}{\sigma_j}}{\sum_i \frac{A_i}{\sigma_i}} \_100, \quad (1)$$

where A_i and A_j are time normalized peak areas and σ_i and σ_j are Scofield photoionization cross sections [16]. Atom ratios are calculated from the equation

$$\frac{\text{atoms}_j}{\text{atoms}_k} = \frac{\frac{A_j}{\sigma_j}}{\frac{A_k}{\sigma_k}}. \quad (2)$$

The Mo 3d level for bulk MoO_3 (Figure 8) may be resolved into two doublets. Assignments and binding energies associated with the two different $3d_{5/2}$ peaks are given in Table 1. The $3d_{5/2}$ peak at 232.5 eV matches exactly the value of 232.3±0.4 eV for charge compensated Mo(VI) [17-34]. No Mo 3d peaks with binding energies between 236 eV and 240 eV have been reported in the literature except for samples [5] with charged surfaces [17, 18]. The Mo $3d_{5/2}$ peak at 236.7 eV may therefore be attributed to Mo(VI) on charged sites, leading to a charging effect in the metal oxide of 4.2 eV. There is a strong correlation with the O 1s spectrum where two peaks are observed with a separation of 4.4 eV. The binding energy of charge compensated O 1s is given as 530.2±0.5 eV in the literature [25,30,34] and corresponds with one of the peaks observed in the experiment (530.4 eV). Charging and non-charging sites occur because x-ray irradiation of bulk MoO_3 (a narrow bandgap insulator with E_g = 2.8 eV [35]) produces a hidden layer of defect oxide [31], which is conducting. On bombardment of the surface of MoO_3 with Ar^+ particles, a large amount of MoO_2, a conducting oxide, is formed. However, MoO_3 is never completely lost from the surface. The peak synthesis of the Mo 3d level gives three sets of doublets, one set due to Mo(VI) and the other two sets due to reduced forms of MoO_3 (Figure 8b and Table 1a). In agreement with the literature, the doublet with $3d_{5/2}$ at 228.8 eV is

assigned to Mo(IV) in crystalline MoO_2. The doublet with $3d_{5/2}$ at 230.4 eV may be attributed to either nondiscrete Mo(IV) oxide [34] or a paired double-bonded Mo(IV) [36, 37]. These results are important in characterizing the metal oxide present in used MoO_3/SiO_2.

Because SiO_2 is a wide bandgap insulator, E_g = 11 eV [35], all sites on MoO_3/SiO_2 are charge shifted by a factor of -4.3 eV. The results are shown in Figure 9 and summarized in Table 1b. There are clearly two non-equivalent forms of molybdenum on the surface of the fresh catalyst. Applying a charge compensation of -4.3 eV, the peaks associated with Mo $3d_{5/2}$ match perfectly those assigned to Mo(VI) and nondiscrete Mo(IV) oxide or paired double-bonded Mo(IV).

There are also two chemically inequivalent substrate sites, one with Si 2s at 158.7 eV, O 1s at 537.8 eV and O/Si atom ratio = 2.7 and the other with Si 2s at 160.3 eV, O 1s at 539.0 eV and O/Si ratio = 2.0. These shall be referred to as substrate sites (I) and substrate sites (II), respectively. The two sites occur in almost equal amounts -- 46% sites (I) and 54% sites(II). Using equation 1, the atom% Mo is calculated to be 1.2%, a value which is smaller than that expected on the basis of the catalyst preparation (2.2%).

This result shows that the molybdenum oxide is not completely dispersed on the support, and is consistent with the presence of the ellipsoidal crystallites seen in the SEM studies. The used

catalyst has three sets of Mo 3d doublets (Figure 9b), the new doublet being Mo (IV) as crystalline MoO_2. The formation of crystalline MoO_2 is not due to reduction of MoO_3 by x-ray irradiation, else a peak attributable to it should have been seen for the fresh catalyst. It also is unlikely that it is due to radiation enhanced diffusion of crystalline MoO_2 to the surface, since that should also have been seen for the fresh catalyst. Therefore, crystalline MoO_2 must have been produced by reduction of MoO_3 or by crystallization of nondiscrete molybdenum (IV) oxide (or pair double-bonded Mo(IV)) during the course of the catalyzed reaction. The observation is consistent with the fact that XRD shows greater crystalline order for the used catalyst than for the fresh catalyst. About 34% of the Mo present at the surface exists as crystalline MoO_2. The relative amounts of substrate sites (I) and (II) also changes, to 33% and 67% respectively; as does the composition of the sites -- O/Si = 0.8 for sites(I) and O/Si = 2.7 for sites(II). The atom% Mo is 1.4%, which is not significantly different from 1.2%. Thus, the dispersion at the support surface does not change. This is not inconsistent with the SEM results, where large blocks of particles were formed by agglomeration. It merely means that two or more smaller particles form a single large particle by joining at their boundaries without changing their

morphology, e.g. flat particles do not join to form spherical particles.

In contrast to bulk MoO_3 and SiO_2, CMS is highly conducting, so peaks will not be charge shifted. Figure 10 shows the Mo 3d spectra for both fresh and used catalysts, where it is evident that a single doublet, due to Mo(VI) occurs. For the fresh catalyst, the atom% Mo is 1.5%, in good agreement with the value expected on the basis of the preparation (1.4%). For the used catalyst, the atom% Mo has increased to 2.6%. This indicates a segregation of molybdenum oxide to the surface.

CONCLUSIONS

Based on the atom% Mo at the surfaces of used MoO_3/SiO_2 and MoO_3/CMS, the latter catalyst would be expected to be almost twice as active as the former. The greater number of particles observed on the used CMS catalyst seems to be due to fragmentation and surface segregation. If oxidized sites on CMS act as "binding" regions for metal oxide particles, than perhaps air exposure at 250° C creates more such sites on CMS, which leads to fragmentation of large particles. By contrast, agglomeration occurs on silica due to loss of silanol groups under the same circumstances. Furthermore, the differences in particle sizes for the two used

catalysts shows that more of the oxide is particle surface oxide for the CMS catalyst than for the silica catalyst. This would also lead to greater activity for the CMS catalyst. Also, there could be significant numbers of metal oxide particles on the "hidden" surface of MoO_3/CMS, which XPS cannot see. Since gas molecules will have access to pores, another enhancement in activity would result. It appears that under the reaction conditions there is reduction of molybdenum, which is an important step in the catalytic cycle. The CMS support in MoO_3/CMS may provide a facile pathway for reoxidation [38] of molybdenum back to Mo(VI). Thus, the MoO_3/CMS is able to produce a sustained activity, whereas MoO_3/SiO_2 gradually deactivates as the crystallites of MoO_3 are gradually converted to relatively stable crystalline MoO_2, which is not catalytically active for the oxidation of alcohols. The carbons have been shown to undergo redox chemistry in the oxidative dehydrogenation of ethyl benzene [11]. Synergism between this support reactivity and the redox chemistry of MoO_3 provides a unique oxidation catalyst system.

Carbonaceous systems are particularly difficult to characterize. The combination of the analytical techniques presented here -- SEM, XRD, and XPS -- provide complementary information for characterizing heterogeneous catalytic materials. A view of the working catalyst results from these studies. The

experimental data clearly shows that there is a synergistic relationship between the MoO_3 dopant and the CMS support that does not exist on the silica supported material. The results from this study verify that the support-MoO_3 interaction varies from support to support and effects the methanol oxidation activity. Some of the results were unexpected. For example, the SEM results suggesting particle fragmentation was a surprise, because heat and pressure are well known as agents for inducing agglomeration of particles. The fact that carbon supports undergo redox cycling in the oxidative dehydrogenation of ethylbenzene [11] supports our conclusions concerning the activity of these molybdena catalysts. It is possible that CMS may catalyze radical reactions or the reoxidation of reduced molybdenum species in this system. The physical properties of CMS materials, i.e. surface area, metal oxide interaction and adsorption capability, are probably the most significant contributors to the unique properties of MoO_3/CMS.

ACKNOWLEDGEMENTS

SEM studies were performed by Mr. Richard Krockett at the Major Analytical and Instrumentation Center (MAIC), University of Florida. XRD studies were done in the laboratory of Dr. T. E. Mallouk, University of Texas at Austin. The authors wish to thank Mr. Michael Clay for acquiring the XPS data.

REFERENCES

1. Grunewald G. C., Drago, R. S., *J. Am. Chem. Soc.* 113 (1991) 1636.
2. Awe A. A., Milades G., and Vickerman J. C., *J. Catal.* 62 (1980) 202.
3. Carbucicchio M. and Trifiró F., *J. Catal.* 62 (1980) 13.
4. de Beer V. H. J., Duchet J. C. and Prins R., *J. Catal.* 72 (1981) 369. Duchet J. C., van Oers E. M., de Beers V. H. J. and Prins R., *J. Catal.* 80 (1983) 386.
5. Caceras C. V., Fierro J. L. G., Lázaro J., López Agudo A. and Soria J., *J. Catal.* 122 (1990) 113 and references therein.
6. Hu H. and Wachs I., *J. Phys. Chem.* 99 (1995) 10911.
7. Banares M., Hu, H. and Wachs, I., *J. Catal.* 150 (1994) 407.
8. Wang L. and Hall W. K., *J. Catal.* 66 (1980) 251.
9. Jeziorowski H., Knözinger H., Taglauer E. and Vogdt C., *J. Catal.* 80 (1983) 286.
10. Gil-Llambiàs, Escudey-Castro A. M., López Agudo A. and Fierro J. L. G., *J. Catal.* 84 (1984) 323.
11. Grunewald G. C. and Drago R. S., *J. Mol. Cat.* 58 (1990) 227.
12. Banares M. , Spencer N., Jones M. and Wachs I., *J. Catal.* 146 (1994) 204.

13. Williams, C. and Ekerdt J., *J. Catal.* 141 (1993) 430.

14. *Nat. Bur. Stand. (U.S.) Monogr. 25,* Sect. (1981) 18.

15. Magnéli A., Andersson G., Blomberg B. and Kihlberg L., *Anal. Chem.* 24 (1952) 1998.

16. Scofield, J. H., *J. Electron Spectrosc. Relat. Phenom.* 8 (1976) 129.

17. Zhou B., Ceckiewicz S. and Delmon B., *J. Am. Chem. Soc.* 91 (1987) 506.

18. Petterson T. A., Carver J. C., Leyden D. E. and Hercules D. M., *J. Phys. Chem.* 80 (1976) 1700.

19. Berry F. J., Hallett C. and Marbrow, R., *Inorg. Chim. Acta* 133 (1987) 57.

20. Furukawa H., Kanzaki T. and Katasura T., *J. Electron Spectrosc. Relat. Phenom.* 36 (1985) 1.

21. DeVries J. E., Yao H. C., Baird R. J. and Gandhi H. S., *J. Catal.* 84 (1983) 8.

22. Okamoto Y., Morikawa F., Degawa J., Imanaka T. and Teranishi S., *Chem. Lett.* (1983) 1853.

23. Okamoto Y., Morikawa F., Oh-Hiradi K., Imanaka T. and Teranishi S., *J. Chem. Soc. Chem. Commun.* (1981) 1018.

24. Okamoto Y., Imanaka T. and Teranishi S., *J. Catal.* 65 (1980) 448.

25. Cimino A. and DeAngelis B. A., *J. Catal.* 36 (1975) 11.

26. Matsuura I. and Wolfs M. W. J., *J. Catal.* 37 (1975) 174

27. Grim S. O. and Matienzo L. J., *Inorg. Chem.* 14 (1975) 1014.

28. Ratnasamy P., *J. Catal.* 40 (1975) 137.

29. DeClerck-Grimee R. I., Canesson P., Friedman R. M. and Fripiat J. J., *J. Phys. Chem.* 82 (1978) 889.

30. Nefedov V. I., Salyn Ya V., Leonhardt G. and Scheibe R., *J. Electron Spectrosc. Relat. Phenom.* 10 (1977) 121.

31. Kim K. S., Baitinger W. E., Amy J. W. and Winograd N., *J. Electron Spectrosc. Relat. Phenom.* 5 (1974) 351.

32. Brinen J. S., *J. Electron Spectrosc. Relat. Phenom.* 5 (1974) 377.

33. Holl Y., Touroude R., Maire G., Muller A., Engelhard P. A. and Grosmangin J., *J. Catal.* 104 (1987) 202.

34. Spevack P. A. and McIntyre N. S., *J. Phys. Chem.* 97 (1993) 11020.

35. Strehlow W. H.and Cook E. L., *J. Phys. Chem. Ref. Data* 2, (1973) 163.

36. Haber J., Marczewski W.,Stoch J. and Ungier, L., *Ber. Bunsen-Ges. Phys. Chem.* 79 (1975) 970.

37. Grünert W., Stakheev A. Yu., Feldhaus R., Anders K., Shapiro E. S. and Minachev K. M., *J. Phys. Chem.* 95 (1991) 1323.

38. Drago R. S., Jurczyk K., Singh D. J. and Young, V., *Appl. Catal. B: Environmental* 6 (1995) 155.

Table 1. XPS Binding Energies an Peak Assignments for Mo $3d_{5/2}$.

(a) Bulk MoO_3					(b) MoO_3/SiO_2					MoO_3/CMS				
	BE[1] (eV)	ON[2]	Site[3]	CE[4] (eV)		BE (eV)	ON	Site	CE		BE (eV)	ON	Site	CE
fresh	232.5	VI	NC		fresh	235.1	V/IV[5]	C	-4.5	fresh	232.3	VI	NC	
	236.7	VI	C	-4.6		236.6	VI	C	-4.5					
sputtered	228.8	IV	NC		used	233.1	IV	C	-4.5	used	232.3	VI	NC	
	230.4	V/IV[5]	NC			234.9	V/IV	C	-4.5					
	232.5	VI	NC			236.8	VI	C	-4.5					

1. Binding energy in eV (± 0.4eV).
2. Oxidation Number for molybdenum.
3. Type of site on which Mo is coordinated: C - charging; NC - non-charging.
4. Charging effect
5. Assigned either as nondiscrete Mo(IV) oxide or a paired doubly-bonded Mo(IV) (vida *infrared*).

FIGURE CAPTIONS

Figure 1 - SEM of bulk MoO3 (a) before and (b) after (used) reaction.

Figure 2 - SEM of MoO3/SiO2 (a) before (fresh) and (b) after (used) reaction.

Figure 3 - SEM of MoO3/CMS (a) before (fresh) and (b) after (used) reaction.

Figure 4 - Particle size distribution for MoO3/SiO2 (a) before (fresh) and (b) after (used) reaction.

Figure 5 - Particle size distribution for MoO3/CMS (a) before (fresh) and (b) after (used) reaction.

Figure 6 - XRD powder patterns for (a) fresh and (b) used MoO3/SiO2. The powder pattern for MoO2 is overlaid on the pattern in (b).

Figure 7 - XRD powder patterns for (a) fresh and (b) used MoO3/CMS.

Figure 8 - XPS ofthe Mo 3d orbitals of bulk MoO3 (a) fresh and (b) after 60 minutes sputter with Ar+. The lower figures are the curve fitted results. The doublets found for the 3d orbitals for each type of Mo are marked: 2-Mo (VI) on a non-charging site, 3-crystalline MoO2 on a non-charging site, and 4-nondiscrete Mo (IV) or paired double bonded Mo (IV) on a non-charging site. The curve fitted values for the 3d5/2 peaks are summarized in Table 1a.

Figure 9 - XPS of the Mo 3d orbitals of (a) fresh and (b) used MoO3/SiO2. The doublets found for the 3d orbitals for each Mo are marked: 1-Mo(VI) on a charging site, 2-nondiscrete Mo(IV) or paired double bonded Mo(IV) on a charging site, and 3-crystalline MoO2 on a charging site. The binding energies of the 3d5/2 peaks are summarized in Table 1b.

Figure 10 - XPS of the Mo 3d orbitals of (a) fresh, and (b) used MoO3/CMS. The doublet associated with the 3d orbital of Mo(VI) is marked. The binding energies of the 3d5/2 peaks are summarized in Table 1c.

(a) Fresh

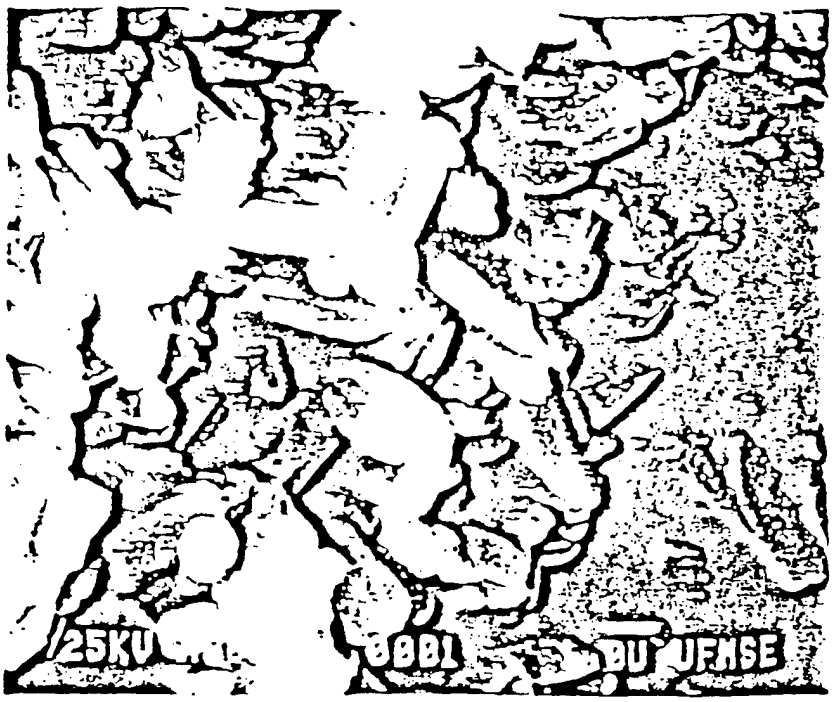

(b) Used

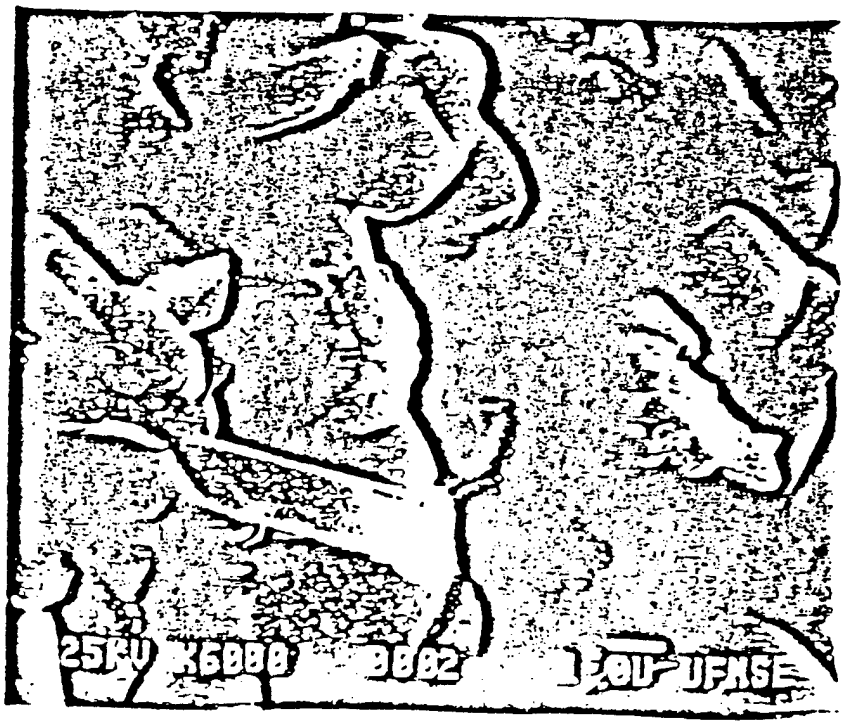

(a) Fresh

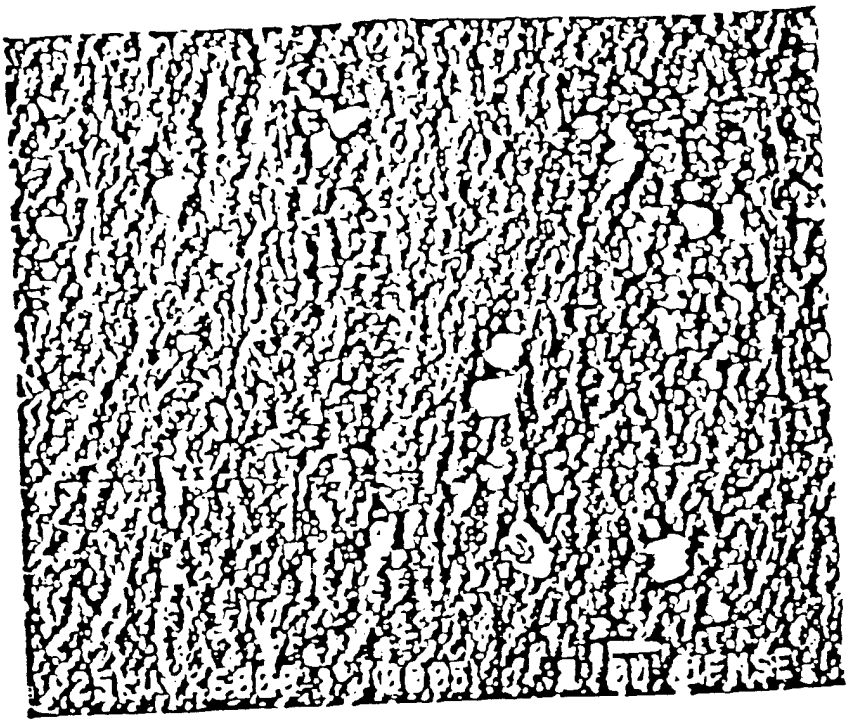

(b) Used

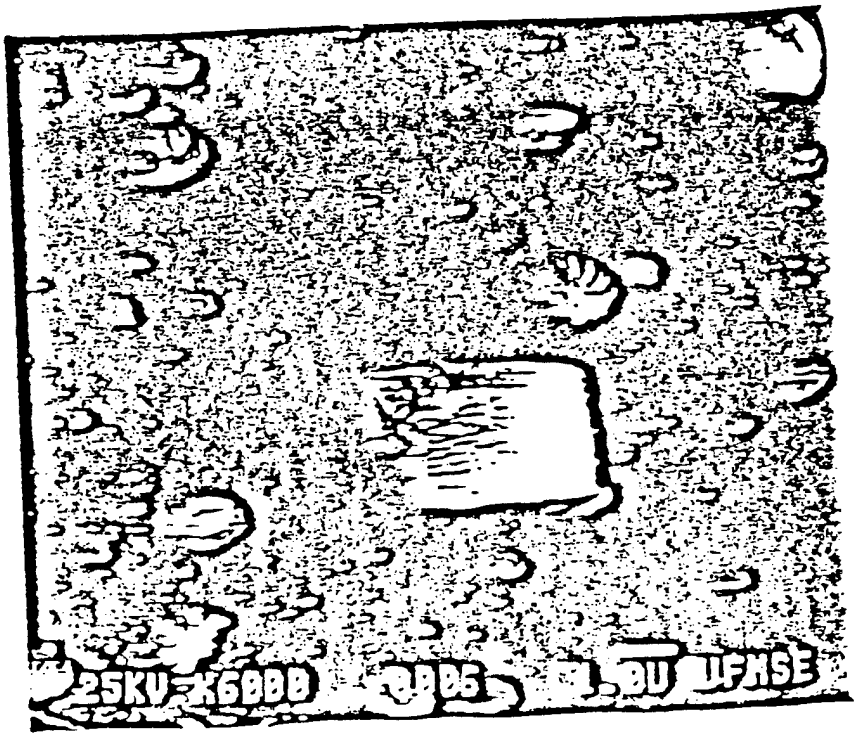

(a) Fresh

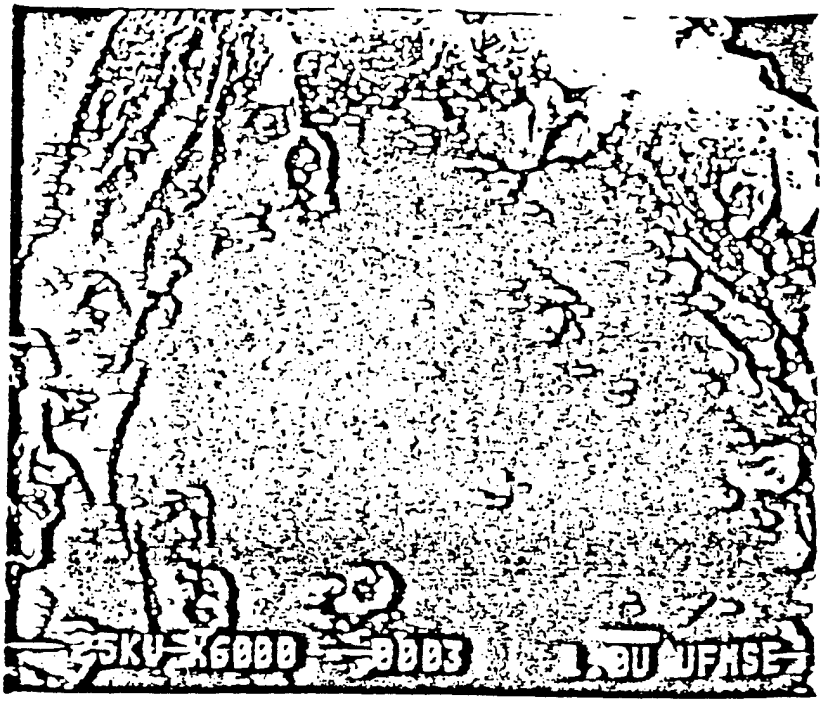

(b) Used

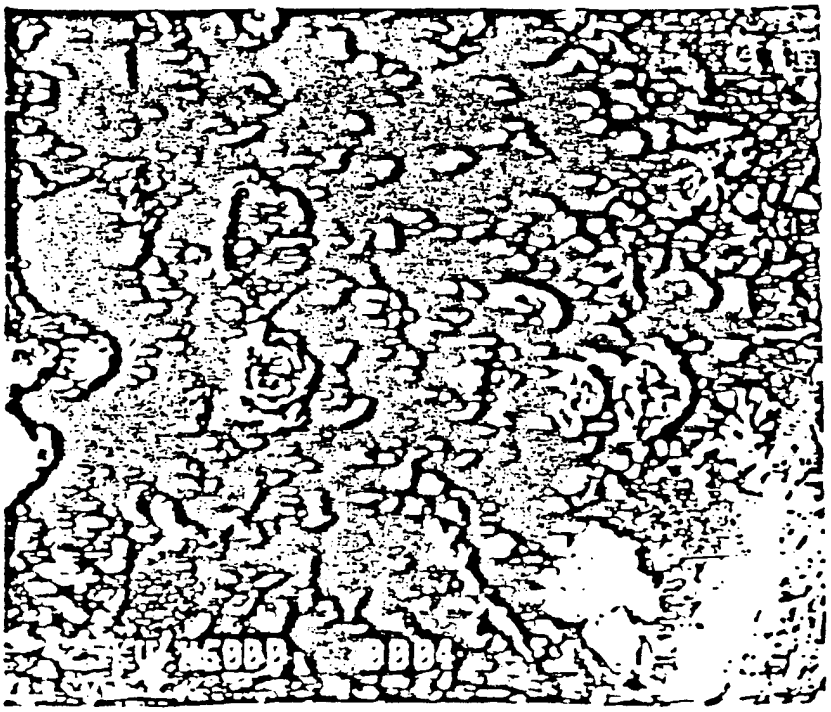

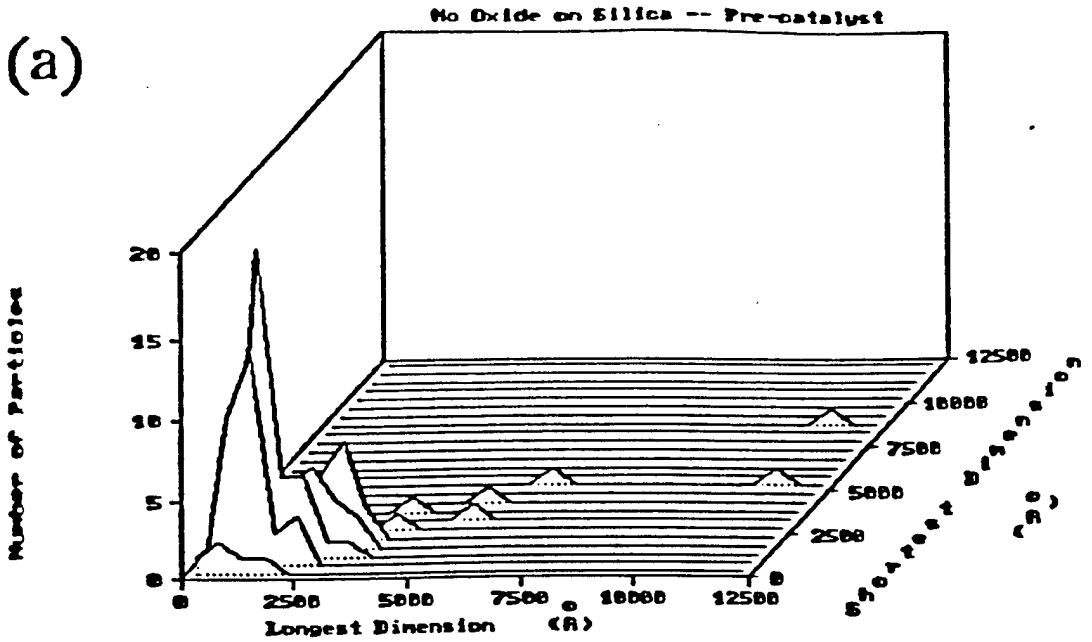
(a)
Mo Oxide on Silica -- Pre-catalyst
Number of Particles
20
15
10
5
0
0
2500
5000
7500
10000
12500
Longest Dimension (Å)
Shortest Dimension (Å)

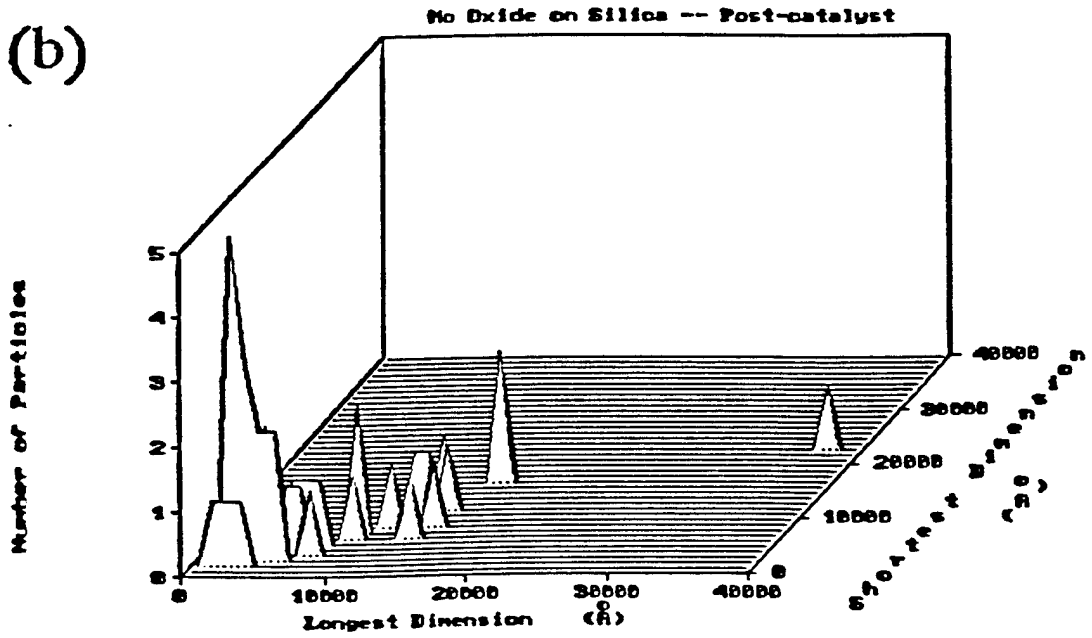
(b)
Mo Oxide on Silica -- Post-catalyst
Number of Particles
5
4
3
2
1
0
0
10000
20000
30000
40000
Longest Dimension (Å)
Shortest Dimension (Å)

(a)

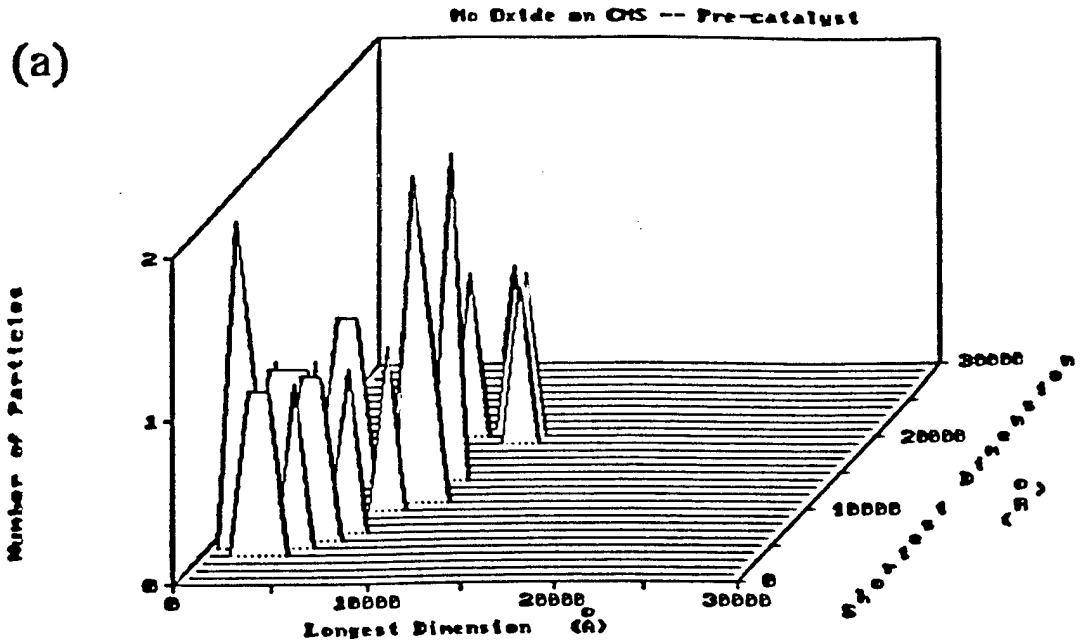
Mo Oxide on CMS -- Pre-catalyst
Number of Particles
0
1
2
0
10000
20000
30000
Longest Dimension (A)
Shortest Dimension (A)

(b)

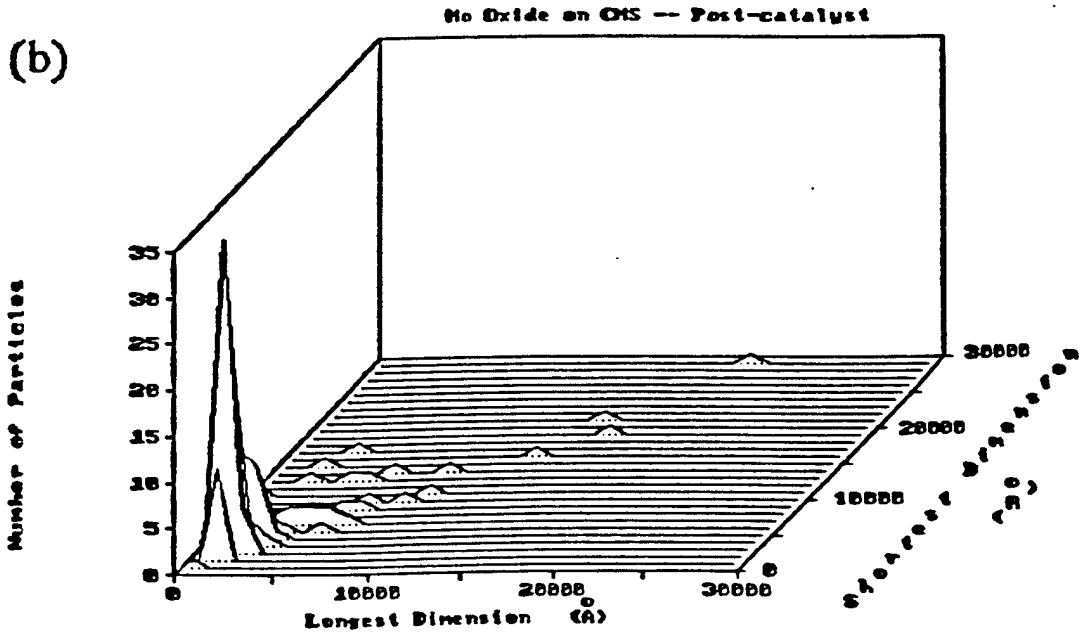
Mo Oxide on CMS -- Post-catalyst
Number of Particles
0
5
10
15
20
25
30
35
0
10000
20000
30000
Longest Dimension (A)
Shortest Dimension (A)

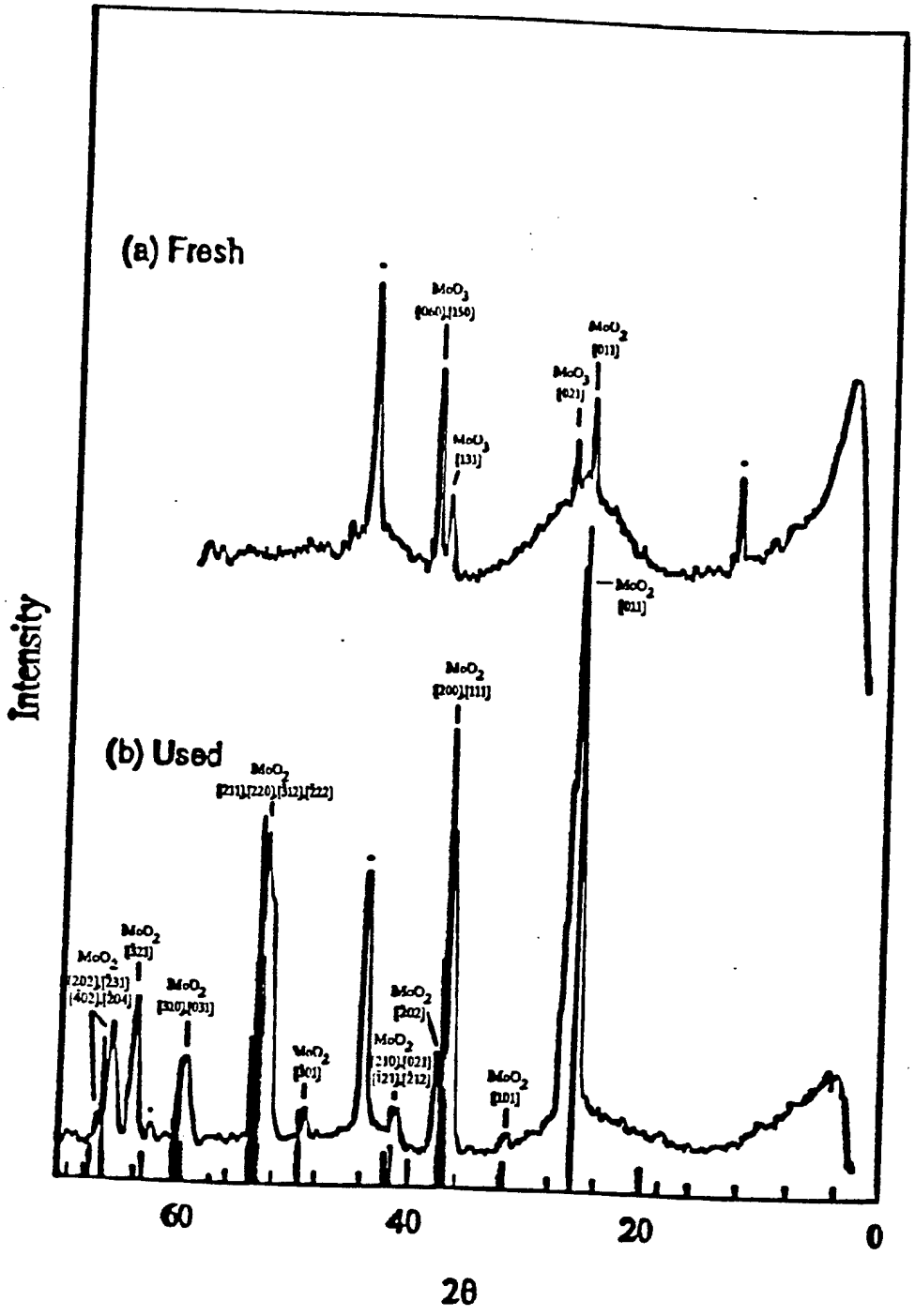
(a) Fresh
(b) Used
Intensity
2θ
60
40
20
0
MoO3 [060],[150]
MoO2 [011]
MoO3 [021]
MoO3 [131]
MoO2 [021]
MoO2 [200],[111]
MoO2 [201],[220],[312],[222]
MoO2 [202],[231] [402],[204]
MoO2 [121]
MoO2 [320],[031]
MoO2 [101]
MoO2 [202]
MoO2 [210],[021] [121],[212]
MoO2 [101]

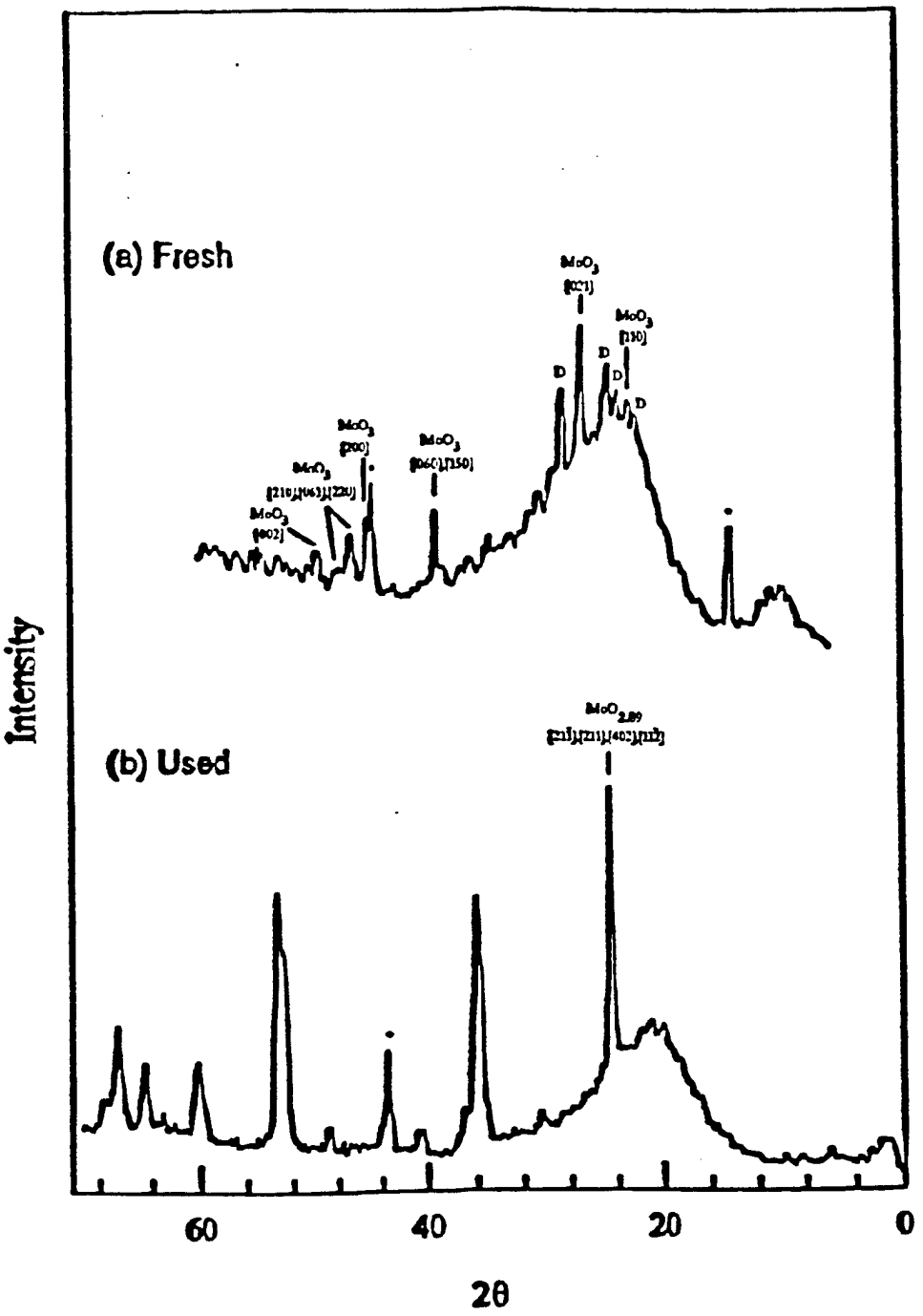
(a) Fresh
(b) Used
Intensity
60
40
20
0
2θ

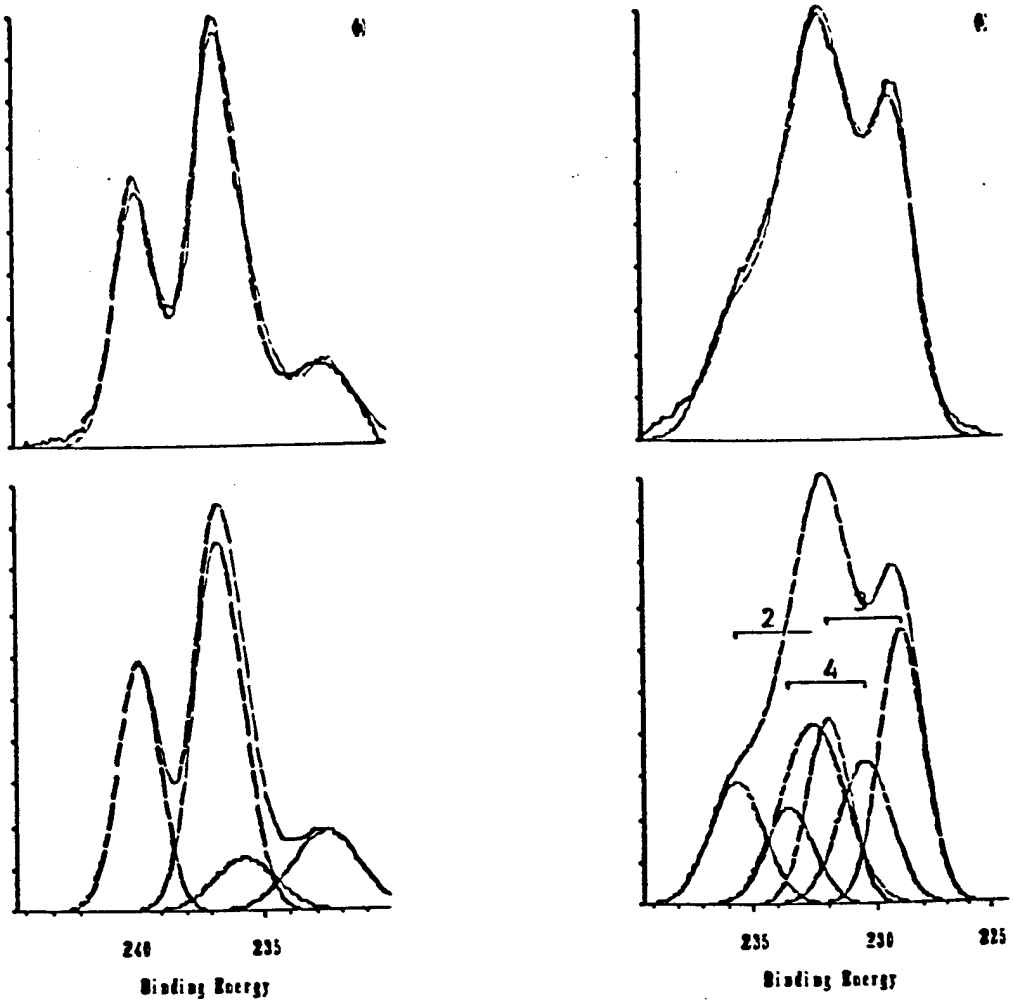
240
235
Binding Energy
2
3
4
235
230
225
Binding Energy

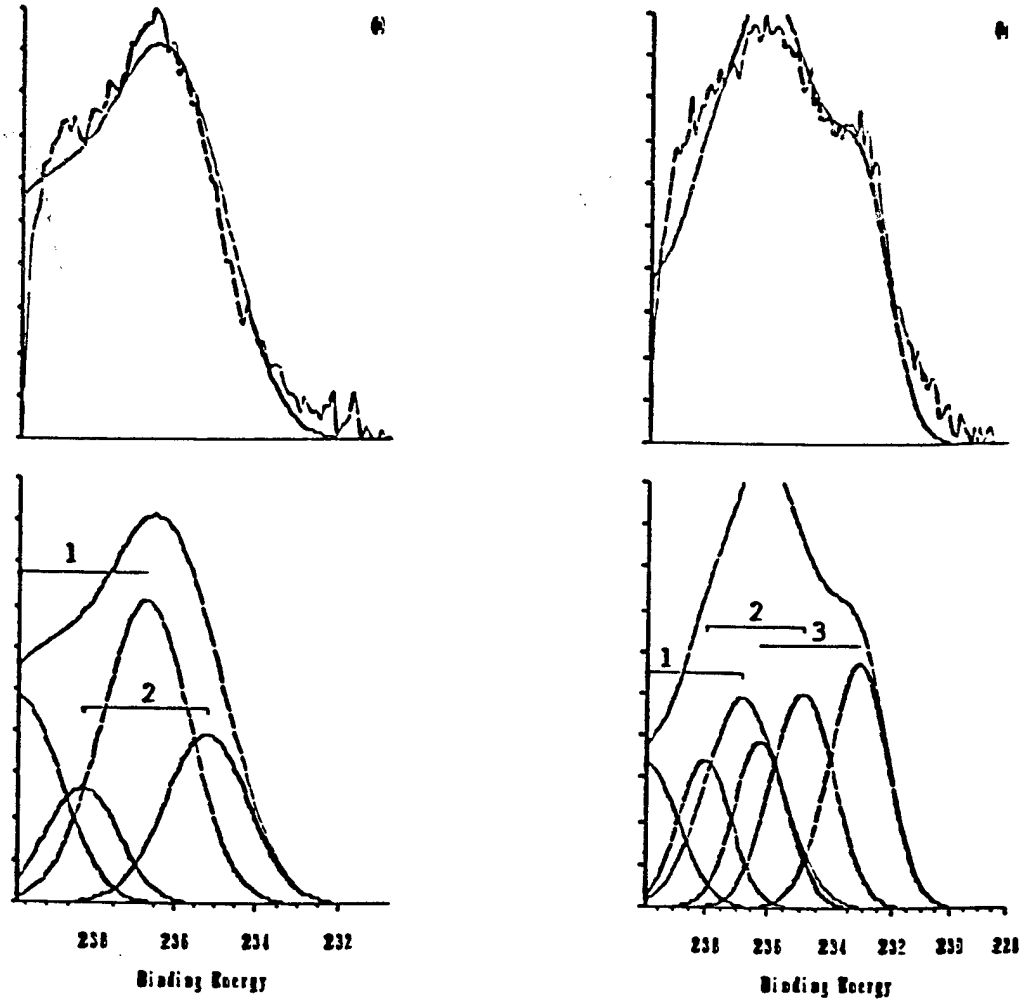
1
2
238
236
234
232
Binding Energy
2
3
1
238
236
234
232
230
228
Binding Energy

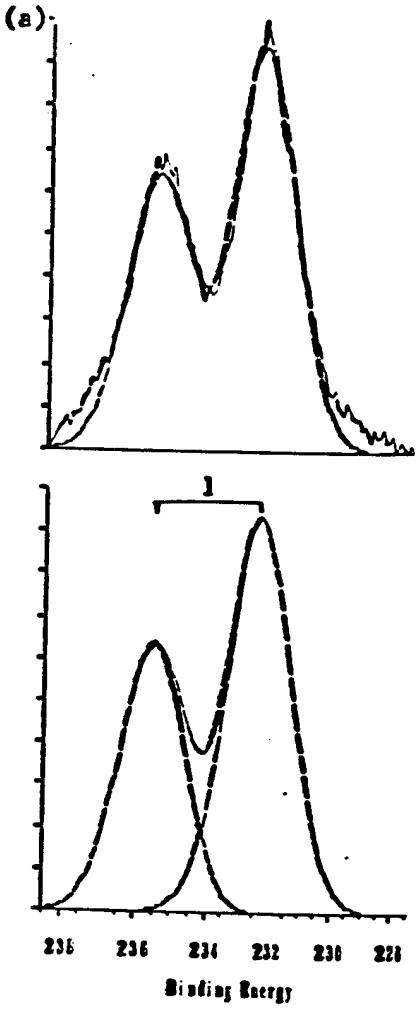
(a)
1
238
236
234
232
230
228
Binding Energy

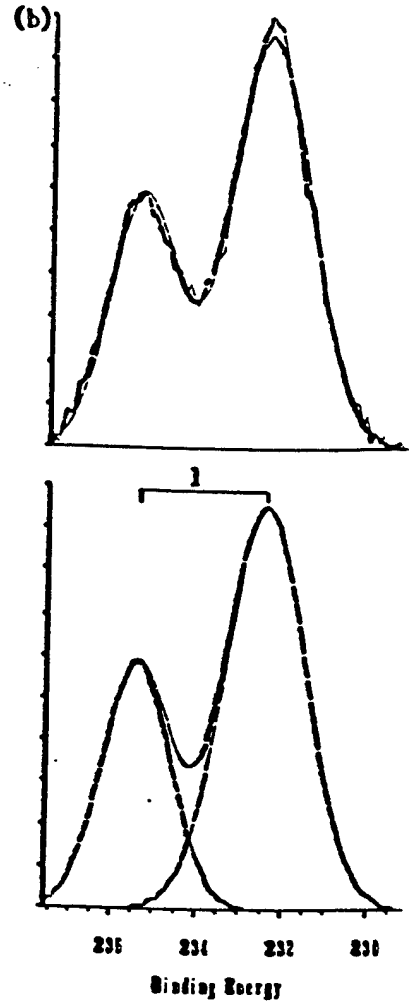
(b)
1
238
234
232
230
Binding Energy

Contribution from

Department of Chemistry

University of Florida

Gainesville, FL 32611

Tel.: (352) 392-6043 Fax: (352) 392-4658

MOLYBDATE AND TUNGSTATE DOPED POROUS CARBONS AS HYDROGEN PEROXIDE ACTIVATION CATALYSTS FOR SULFIDE OXIDATIONS.

by

Russell S. Drago* and Douglas S. Burns[a]

[a] Currently at ENSCO, Inc., 445 Pineda Court, Melbourne, FL 32940

ww/022296/Moly-T.dsb/dl/ml

ABSTRACT

Sodium molybdate, copper(II) molybdate, and sodium tungstate doped into the carbonaceous adsorbent Ambersorb® 572 produced very effective catalytic systems for the oxidation of the mustard simulant ethylphenyl sulfide and the ethylphenyl sulfide intermediate to ethylphenyl sulfone. Complete conversion to the corresponding sulfone occurs using H_2O_2 as the oxidant in a matter of minutes. The novel feature of these catalysts is that they function under basic conditions where base catalyzed hydrolysis reactions can be employed for agent destruction.

INTRODUCTION

The use of porous carbons as catalyst supports is an emerging area in catalysis (1-3). These carbons are themselves redox active catalysts (1a) and addition of metals and metal oxides lead to synergistic interactions which catalyze a variety of reactions, e.g., the low temperature oxidation of methanol (1c), the deep oxidation of chlorinated hydrocarbons (1d), the deep oxidation of hydrocarbons and the decomposition of NO (1h).

Recently, we have reported (4) that porous carbons, pore filled with solid NaOH retain nearly all the NaOH when stirred for 5-10 minutes in water. These materials are effective base catalysts for Michael reactions, the reaction of chalcone with nitromethane, and vapor phase aldol condensations. Recent reports also indicate that metal substituted polyoxometallates are effective catalysts for the oxidation of mustard analogs by t-butylhydroperoxide (5) and can be supported (5c) on porous carbons to produce heterogeneous catalysts.

Porous carbons have found applications in the adsorption of chemical warfare (cw) agents from personnel and small equipment (6). It would be desirable if the absorbed materials could be destroyed catalytically. A catalytic adsorbent could find widespread utility in decontamination as well as in cw agent stockpile reduction. The reaction chemistry of nerve agents is similar to that of insecticides, so catalytic adsorbents could also find applications in the remediation of these contaminants.

Mustard (HD; $(ClCH_2CH_2)_2S$) is destroyed by oxidation (6) and G-nerve agents are destroyed by hydrolysis which is base catalyzed by nucleophilic attack at phosphorus (6). For environmental concerns, H_2O_2 and O_2 constitute the most desirable

oxidants. Unfortunately, in most systems the basic conditions favorable for catalysis of hydrolysis reactions inhibit oxidations by peroxide.

Molybdenum and tungsten compounds activate hydrogen peroxide in homogeneous solution to oxidize a variety of substrates including organic sulfides (7). MoO_4^{2-} is also a remarkable nucleophile (8) with a second order rate constant 35 times that of phosphate for the hydrolysis of p-nitro-phenylacetate in spite of phosphate having a 1000-fold larger basicity. This research demonstrates that absorbent carbons, pore filled with molybdate and tungstate ions, are very effective catalysts for the oxidation of sulfides with 30% aqueous H_2O_2. The novel feature of these catalysts is that they carry out oxidations under basic conditions where G-agents would also undergo catalyzed hydrolysis.

RESULTS AND DISCUSSION

The oxidations were carried out by adding Ambersorb® 572 (A-572) (0.5 g) containing the catalyst (1% by mass in the support) to a solution of the sulfide (0.1 ml; 0.7 millimoles) in solvent (1.5 ml) containing 0.2 ml of 30% H_2O_2 (2.0 millimoles). The solution was stirred for six minutes at ambient conditions, filtered, and analyzed by G.C. In a random selection of experiments with active catalysts, the solid beads were crushed, extracted, and found to contain adsorbed sulfone, but no sulfide. Table 1 summarizes the results for catalyzed oxidation of the mustard simulant, $C_2H_5SC_6H_5$ (EtSPh).

The first three entries in Table 1 are blank runs. The effectiveness of the molybdate catalyst is seen in the homogenous oxidation where complete oxidation

occurs with 0.033 millimoles of catalyst in less than six minutes at ambient conditions. When $Na_2MoO_4 \bullet 2H_2O$ is added to A-572 by either reflux or pore filling techniques, a very effective catalyst results. The 0.02 millimoles of molybdate in the 0.5 g of catalyst oxidize 0.7 millimoles of sulfide to sulfone in six or less minutes giving at least 70 turnovers per minute for the heterogeneous reaction. In one experiment, complete conversion was observed in three minutes exceeding 140 turnovers per minute. The final solutions were not analyzed for residual H_2O_2, but a minimum value for the peroxide efficiency is 70% in those runs where 95-100% sulfone is obtained. The solution is filtered off the catalyst producing a clear filtrate. With a fresh 0.1 ml of sulfide and 0.2 ml of H_2O_2 added to this filtered solution, the traces of molybdate that have leached off the catalyst lead to 90% oxidation of the sulfide in six minutes. When the filtered solid carbon catalyst is reused, 100% oxidation of sulfide is again observed in six minutes at ambient temperatures. The catalyst prepared by pore filling is slightly more active than the catalyst prepared by reflux (see experimental). No apparent difference in leaching results with either method of preparation.

In an attempt to minimize leaching of the catalyst into solution, the $Na_2MoO_4 \bullet 2H_2O$/A-572 catalyst was pore filled with stoichiometric amounts of $Cu(NO_3)_2$ and a second batch with $Ni(NO_3)_2$ to prepare the less soluble $CuMoO_4$ and $NiMoO_4$ Complete oxidation of the substrate with H_2O_2 occurs in six minutes and the filtered solution resulted in 50% oxidation of a new charge of sulfide by peroxide. The solid $CuMoO_4$ and $NiMoO_4$ catalysts from the first oxidation were reused a second and third time. Complete oxidation of the new charges of sulfide resulted in all instances

TABLE 1

Catalyzed Oxidations of $C_2H_5SC_6H_5$

Catalyst[a]	Solvent[b]	% Conversion to Sulfone[c]
None, soln	CH_3CN	1-3% even after 30 minutes
None, soln	50/50	10%
None, soln	CH_3CN	3%
Na_2MoO_4, soln	CH_3CN	100%
Na_2MoO_4	CH_3CN	100%-90% lch-100%
Na_2MoO_4, R	CH_3CN	93%-90% lch
$CuMoO_4$	CH_3CN	100%-55% lch-99%-40% lch-99%
$NiMoO_4$	CH_3CN	100%-50% lch-99%-99%
Na_2WO_4, soln	CH_3CN	100%
Na_2WO_4, soln	buffer	95%
Na_2WO_4	CH_3CN	100%-90% lch-100%-98%-98%
Na_2WO_4	50/50	98%
Na_2WO_4	t-C_4H_9OH	100%-99%-99%
Na_2WO_4, SOX	CH_3CN	100%-70% lch
Na_2WO_4, 0.5% KOH	CH_3CN	100%-50% lch-98%
$H_3PO_4 \bullet 12WO_3$	CH_3CN	95-99%

a. Unless indicated, the catalyst (1% by mass) was supported on A-572 by pore filling; soln refers to a homogeneous reaction with no support. None refers to control reactions. R indicates the catalyst was prepared by refluxing in CH_3CN under N_2 for 24 hours and drying at 110 °C. SOX refers to a catalyst that was washed by soxhlet extraction with CH_3OH overnight.

b. Buffer refers to an aqueous solution of sodium tetraborate, pH = 9, and 50/50 refers to an equal mixture of this buffer and CH_3CN.

c. Reactions are typically carried out for six minutes. In all instances, the product of the reaction is ethylphenylsulfone, $EtSO_2Ph$. Dashes indicate repeat experiments with the same adsorbent catalyst after filtering off the product solution and washing with CH_3CN. Lch indicates that the product solution was separated from the catalyst and a homogeneous oxidation carried out with the filtrate.

establishing the point that oxidation is being catalyzed by molybdate in the solid carbon.

Results similar to $Na_2MoO_4 \bullet 2H_2O$ were obtained with $Na_2WO_4 \bullet 2H_2O$. The doped carbon gives over 95 turnovers per minute. This catalyst was also shown to be active in the solvent t-C_4H_9OH and in a 50/50 CH_3CN:buffer solvent. When pore filled $Na_2WO_4 \bullet 2H_2O$ is soxhlet extracted overnight with methanol, the amount of tungstate that leaches into solution during the first oxidation is decreased. In this case, only 70% sulfide oxidation occurred in the homogeneous oxidation using the filtrate. However, the reuse of the catalytic adsorbent leads to complete oxidation of sulfide to sulfone in six minutes at ambient conditions. This result indicates that the amount of leachate in the 1.5 ml of solvent used in an oxidation run is very small and the catalyst could be used many times before the dopant was lost by leaching. This result also demonstrates that a heterogeneous reaction is occurring.

The amount of leaching was also decreased by a second pore filling of the Na_2WO_4 catalyst with 0.5% KOH. Even with strong base present, efficient catalysis of the peroxide oxidation of EtSPh occurs at ambient conditions. A 1% loading of phosphotungstic acid ($H_3PO_4 \bullet 12WO_3$) in A-572 also produced an effective oxidation catalyst. Under reaction conditions, the phosphotungstic acid is probably a precursor for lower molecularity peroxometalates.[9]

$Na_2MO_4 \bullet 2H_2O$ (M=Mo or W) exists as aggregates in aqueous solution at a pH of 6 or lower. The species $MO(OH)_5^-$ forms first and as the pH is lowered, the next species detected in the case of molybdenum is $Mo_7O_{24} \bullet xH_2O^{2-}$. The species that exist on the surface of the carbon are unknown. With OOH^- able to replace OH^- in these species, it

is expected that coordination activates peroxide so that direct nucleophilic attack by sulfide and sulfoxide are the oxygen atom transfer mechanisms. In the reported[10] classification scheme for metal complex activation of O_2 and peroxides, this corresponds to the Class IVb mechanism. Alternatively, a one electron oxidation of the sulfide and reduction of the molybdenum or tungsten species can generate a sulfur cation radical[5a,11] that is subsequently converted to sulfoxide. One electron oxidation of the sulfoxide would then occur to give the sulfone. This reaction would be included in the Class V category[10].

CONCLUSIONS

Molybdate and tungstate doping of A-572 leads to catalytic absorbents for oxidative and base catalyzed reactions. Freshly prepared catalysts leach small amounts of dopant into solution. Reuse or extensive washing diminishes leaching while maintaining excellent catalytic activity. These results demonstrate that a heterogeneous reaction is occurring. With only 0.02 millimoles of $Na_2MoO_4 \bullet 2H_2O$ in 0.5 gram of carbon in the original catalyst, very little tungstate or molybdate is required for effective catalysis. The new and reused catalysts exhibit turnover numbers of 70-95 turnovers per minute and peroxide efficiencies of at least 70%.

EXPERIMENTAL

Reagents

$Na_2MoO_4 \bullet 2H_2O$, $Na_2WO_4 \bullet 2H_2O$, $Cu(NO_3)_2$ and $Ni(NO_3)_2$ were obtained from Fisher and used as received. Phosphotungstic acid was synthesized. All solvents and

reactants were obtained from Fisher. Ambersorb 572 (lot 2125), donated by Rohm and Haas was soaked in 6M HCl overnight, rinsed with water several times, soxhlet extracted with methanol for 6 hours, and dried in vacuum at 110 °C.

Catalyst Preparation.

Supported catalysts were prepared using two methods. Catalysts were prepared by refluxing the support, metal, and solvent (CCl_4, toluene, or acetonitrile) under nitrogen for 24 hours. Typically, the support:metal ratio was 100:1 by mass. Catalysts also were prepared by dissolving the metal compound into an appropriate solvent and pore filling the support (i.e., adding solution until the solid was barely moist). In both methods, the prepared catalysts were then dried in a vacuum oven at 105-110 °C for at least 16 hours. As summarized in Table 1, Na_2MoO_4 pore filled into A-572 resulted in complete conversion of EtSPh in six minutes compared to 90% conversion for the same composition catalytic adsorbent prepared by refluxing. Pore filling was the method used in all experiments unless indicated otherwise.

$CuMoO_4$/A-572 was prepared by pore filling A-572 with Na_2MoO_4 dissolved in water and drying the solid in a vacuum oven. This was followed by pore filling Na_2MoO_4/A-572 with $Cu(NO_3)_2$ dissolved in water. The catalyst was then washed with water several times to remove $NaNO_3$, and then dried in a vacuum-oven at 110 °C for 24 hours.

Oxidation Procedure.

Homogeneous Catalyzed Oxidations. Sodium tungstate and molybdate were used as catalysts in homogeneous oxidations of EtSPh. 1.5 ml of solvent, 0.1 ml EtSPh, and 0.2 ml H_2O_2 (30%), were added to about 0.008 g of the catalyst in a 6 inch test tube. The solution was stirred magnetically for six minutes at ambient temperature and pressure. The oxidation of EtSPh to the corresponding sulfoxide and sulfone was monitored using an SRI 8610-FID gas chromatograph outfitted with an AT-1000 15 m x 0.54 mm ID capillary column from Alltech.

Heterogeneous Catalyzed Oxidations. 0.5 g of supported catalyst (1% loading by mass unless otherwise specified), 1.5 ml solvent (e.g., CH_3CN), 0.1 ml EtSPh, and 0.2 ml H_2O_2 (30%), were added into a 6 inch test tube. The reaction mixture was stirred for six minutes at ambient temperature and pressure. The liquid above the support was filtered through a glass wool filter to remove any solid and the solution analyzed as described in the homogeneous oxidation procedure. The conditions used led to complete conversion to sulfone in all instances.

Test for Leaching and Repeat Catalyst Evaluation

The product from an oxidation reaction was filtered through glass wool. The solid was washed with CH_3CN and used in a subsequent oxidation reaction following the above procedure.

To test for leaching, 0.1 ml of EtSPh and 0.2 ml of H_2O_2 (30%) were added to the solution that had been analyzed and after six minutes of stirring, the solution was again analyzed by G.C for sulfoxide and sulfone.

ACKNOWLEDGMENT

The authors acknowledge support of this research by ERDEC and the Army Research Office.

REFERENCES

1. a. Grunewald, G. C., and Drago, R. S., *J. Mol. Catal.* **58**, 227 (1990).

   b. Grunewald, G. C., Drago, R. S., Clark, J. L., and Livesey, A. B., *J. Mol. Catal.* **60**, 239 (1990).

   c. Grunewald, G. C., and Drago, R. S., *J. Am. Chem. Soc.* **113**, 1636 (1991).

   d. Petrosius, S. C., and Drago, R. S. *J. Chem. Soc., Chem. Commun.* **344** (1992).

   e. Petrosius, S. C., Drago, R. S., Young, V., and Grunewald, G. C., *J. Am. Chem. Soc.* **115**, 6131 (1993).

   f. Drago, R. S., Petrosius, S. C., Grunewald, G. C., and Brendley, W. H., *ACS Symp. Ser.* **552**, 340 (1994).

   g. Brendley, W. H., Grunewald, G. C., Petrosius, S. C., and Drago, R. S., U.S. Patent #5,344,630 (1994).

   h. Vandersall, M. T., Maroldo, S. G., Brendley, Jr., W. H., Jurczyk, K., and Drago, R. S., *ACS Symp. Ser.* **552**, 331 (1994).

   i. Brendley, Jr., W. H., Drago, R. S., and Jurczyk, K., U.S. Patent #5,403,798 (1995).

   j. Drago, R. S., Jurczyk, K., Singh, D. J., and Young, V., *Applied Catalysis B: Environmental* **6,** 155 (1995).

   k. Drago, R. S., and Jurczyk, K., Submitted.

2. a. Foley, H. C., *ACS. Symp. Ser.* **368**, 335 (1988).

   b. Lafyatis, D. S., and Foley, H. C., *Chem. Eng. Sci.* **45**, 2567 (1990).

   c. Lafyatis, D. S., Mariwala, R. K., Lowenthal, E. E., and Foley, H. C., *in* "Synthesis of Microporous Materials" (M. Occelli and H. Dobson, Eds.), Vol. II. Van Nostrand, New York, 1992.

3. a. Gaffney, A. M., Nandi, M. K., Pitchai, R., and Han, Y.-Z., U.S. Patent #5,319,114 (1994).

b. Yamashita, H., and Tomita, A., *Energy and Fuels* **7**, 85 (1993) and references therein.

4. Drago, R. S., and Jurczyk., K., *J. Chem. Soc., Trans. 2* 0000 (1996).

5. a. Gall, R. D., Faraj, M., and Hill, C. L., *Inorg. Chem.* **33**, 5015 (1994).

b. Hill, C. L., and Prosser-McCartha, C. M., *Coord. Chem. Rev.* **143**, 407 (1995).

c. Gall, R. D., Hill, C. L., and Walker, J. E., *J. Catal.* 0000 (1996).

6. Yang, Y. C., Baker, J. A., and Ward, J. R., *Chem. Rev.* **92**, 1729 (1992).

7. a. Mimoun, H., *in* "Comprehensive Coordination Chemistry" (G. Wilkinson, R. D. Gilard, and J. A. McCleverty, Eds.), Vol. 6. Pergamon Press, Oxford, 1987.

b. Curci, R., Di Furia, F., Testi, R., and Modena, G., *J. Chem. Soc., Perkin Trans. 2* 752 (1974).

c. Arcoria, A., Ballistrerc, F. P., Tomaselli, G. A., DiFuria, F., and Modena, G., *J. Mol. Catal.* **18**, 177 (1983).

d. Arcoria, A., Ballistrerc, F. P., Tomaselli, G. A., DiFuria, F., and Modena, G., *J. Mol. Catal.* **24**, 189 (1984).

8. Wekjord, B., and Byers, L. D., *J. Am. Chem. Soc.* **114**, 5553 (1992).

9. Duncan, D. C., Chambers, R. C., Heckt, E., and Hill, C. L., *J. Am. Chem. Soc.* **117**, 681 (1994).

10. Drago, R. S., *Coord. Chem. Rev.* **117**, 185 (1992).

11. Riley, D. P., *Inorg. Chem.* **22**, 1965 (1983).

UNIVERSITY OF
FLORIDA

Fax (352) 392-4658

Department of Chemistry

PO Box 117200
Gainesville, FL 32611-7200

February 22, 1996

Prof. W. Nicholas Delgass
Dept. of Chemical Engineering
Purdue University
1283 CHNE
W. Lafayette, IN 47907

Dear Professor Delgass,

Thank you for your letter on our Molybdate manuscript. It does not matter to me whether this article is published as a Note or short Article. I have made the changes you requested and hopefully the article will now be suitable for publication. There is no doubt that a heterogeneous component accompanies a homogenous component from leaching from the reuse and soxhlet extraction experiments. It is also clear that the catalyst can be reused many times. Your suggestions are much appreciated for the manuscript now does a better job of showing what a remarkable catalyst this is. I have added a conclusion section to emphasize this point.

Thanks for your help.

Sincerely,

Russell S. Drago
Graduate Research Professor

RSD/dl

Enclosures

ww/022296/Moly-T.dsb/dl

Contribution from

Department of Chemistry

University of Florida

Gainesville, FL 32611

Tel.: (904) 392-6043 Fax: (904) 392-4658

Activation Of Hydrogen Peroxide For Oxidations By Copper(II) Complexes

By

Michael H. Robbins[+] and Russell S. Drago*

[+] The Clorox Co., 7200 Johnson Dr., Pleasanton, CA 94566

ww052296/Newcop6/dl

Abstract

Copper(II) complexes of the general formula $[LCu(H_2O)_4]^{n+}$ (where L is a bidentate ligand and n=1 or 2) activate hydrogen peroxide for the oxidation of quinaldine bule, an oxidation indicator. The copper(II) complexes of tri- and tetra-dentate ligands are shown to be inactive, as are the *bis*-complexes of bidentate ligands. The proposed mechanism for peroxide activation involves the formation of a copper(II)-hydroperoxide complex, which then rapidly oxidized the substrate. Comparison of reaction rates with different ligand systems, and different ligand to metal ratios, lead to the conclusion that two equatorial coordination positions must be occupied by easily displaced water to form the active complex. Rate studies are performed which give an experimental rate law which is first-order in copper(II) complex, zero-order in substrate, and variable order in peroxide. These kinetics are predicated by the rate law derived from our proposed mechanism. The variable order in peroxide can be explained in terms of Michaelis-Menten type kinetics, as linear Lineweaver-Burk plots of $(rate^{-1})$ vs. $([O_2H^-]^{-1})$ are obtained from our experimental data. This is consistent with our proposed mechanism, as the derived rate law can be rearranged into the Michaelis-Menton equation.

INTRODUCTION

Environmental concerns have motivated replacement of aqueous hypochlorite as an oxidant with peroxide, and use of water as a reaction medium. Activation of hydrogen peroxide by transition metal complexes for the oxidation of organic substrates has been studied extensively.[1-3] Few transition metal complexes catalyze oxidations by hydrogen peroxide in water, and fewer are active above pH 8. Precipitation of the catalytically active metal complex as the oxide or hydroxide at higher pH is a major limitation. Chelating ligands can stabilize metal ions in basic solution and prevent precipitation.[4] Thus, a manganese complex of 1,4,7-triazocyclononane (TACN)[5] is an effective peroxide activator in basic aqueous solution. This complex catalyzes the epoxidation of styrene and 4-vinylbenzoic acid with hydrogen peroxide and was commercialized as a bleaching agent for household applications. This discovery has heightened interest in aqueous transition metal catalyzed peroxide activation with a primary goal of finding complexes that react with hydrogen peroxide to produce active oxidants in basic aqueous solution.

Activation of hydrogen peroxide by metal redox mechanisms[6] almost invariably leads to catalysis of peroxide decomposition. This can be avoided by employing catalysts that function by a Class IVb mechanism[6] if the metal does not change its oxidation state when activating hydrogen peroxide, but coordinates HO_2^- to the metal center. Coordination can be viewed as replacing the proton of H_2O_2 with a Lewis acid (the metal complex) and, in the process, making MO_2H which is more electrophilic than HO_2^-. Accordingly, a series of experiments were carried out with complexes that might function as peroxide activators through hydroperoxide coordination.

Bis(ethylenediamine)[7] and bis(bipyridine)[8] copper complexes are reported to be active for peroxide activation, though not in aqueous base. Many copper complexes containing a bound peroxo species are known, although most are

dimeric species.[9-12] Complexes with cumylhydroperoxide and *tert*-butylhydroperoxide as ligands to a copper(II) monomer have been isolated.[13]

This paper examines the activation of hydrogen peroxide by a series of copper(II) complexes. The initial experiments were done with picolinic acid ligand, which is effective in promoting peroxide activation with iron in a pyridine-acetic acid solvent mixture.[2,3] Finding activity in aqueous base with the copper(II)-picolinic acid complex, the study was expanded to other ligands.

Applications of catalysts for oxidation in basic aqueous solutions require broad base oxidants. This requirement is in contrast to selective oxidations whose objective is to produce a single desired product. Accordingly, a redox indicator, quinaldine blue, was chosen as the substrate for oxidation. Though the oxidation products are unknown, this substrate has several advantageous properties for a study whose primary focus is to ascertain desirable metal complex properties for activation. Initial rates of oxidation of quinaldine blue (I) can be measured conveniently as a function of pH, peroxide concentration, ligand to metal ratio, and complex concentration. A mechanism for peroxide activation with complexes of this type is proposed.

EXPERIMENTAL

Materials

Copper(II) chloride and sodium tetraborate were used as received from Fisher. 30% Hydrogen peroxide was used after iodometric titration to verify its concentration. Quinaldine blue, 2-pyridinecarboxylic acid (picolinic acid, PA), 2,4-pentanedione (acetylacetone, AcAc), 1-aminoacetic acid (glycine, GLY), 2-aminopropanoic acid (alanine, ALA), 4-amino-2-methylbutonic acid (leucine, LEU), 2,6-pyridinedicarboxylic acid (dipicolinic acid, DPA), (iminodiacetic acid, IDA), 1,2-diaminoethane (ethylenediamine, EN), N,N,N',N'-

tetramethylethylenediamine (TMED), 2,9,-dimethyl-1,10-phenanthroline (DMP), 2.2′-dipyridylamine (bipyridylamine, BPA), tris(2-aminoethyl)amine (TREN), bis(1-aminopropyl)amine (IBPA), and 2,2′:6′,2″-dipyrdylpyridine (terpyridine, TERPY) were all used as received from Aldrich. Water used for the peroxide solutions was purified by a Barnstead NANOpure unit to eliminate metal-ion contaminants that might cause peroxide decomposition. Its final resistance was 18 megaohm·cm^{-1}.

Measurements

UV-Vis measurements were performed on a Perkin-Elmer Lambda-6 spectrophotometer at room temperature. Rate data was obtained by monitoring the decrease in quinaldine blue concentration at 600 nm over time. pH measurements were made with a Fisher Accumet model 630 pH meter.

Preparation Of Reaction Mixtures For Kinetic Measurements

1) Preparation of the substrate

Quinaldine blue, I, 0.0060g, was dissolved in a 0.01 M aqueous sodium tetraborate buffer solution. This gives a deep purple solution with an absorbance between 1.0 and 1.1 at 600nm. The initial absorbance was checked before the solution was used to ensure that it was in the above range. The substrate oxidation was performed at pH 9.1 in a 0.1 M borax buffer unless otherwise indicated.

2) Preparation of the catalysts

The catalyst solution used was prepared from 2.5 x 10^{-3} M aqueous copper(II) chloride and 2.5 x 10^{-3} M aqueous solutions of the appropriate ligands, as previously described[2,8] for *in situ* generation of active catalysts. Use of copper(II) nitrate, rather than the copper(II) chloride, as the

copper(II) source did not significantly affect the rates, nor did addition of excess chloride to the system. At these concentrations, precipitation was not observed, and the catalyst solutions did not loose activity upon standing.

3) Preparation of the peroxide solution

A 0.200 M stock solution of hydrogen peroxide was made by adding 10 mL of 30% hydrogen peroxide (whose concentration was checked by iodometric titration) to a 500 mL volumetric flask and diluting with purified water to 500mL. Subsequent dilutions were made to give the peroxide solutions used. All the rate data were obtained with peroxide solutions that were no more than 48 hours old.

4) Procedure

In each experiment, 2 mL of the buffered substrate (I) solution, 1 mL of catalyst solution (in blank runs, water), and 0.5 mL of peroxide solution were added, in that order, to a UV-Vis cell. This combination of buffer/substrate solution, copper complex, and hydrogen peroxide has a pH of 9.1. The cell was capped and shaken for 5 seconds and then placed in the cell holder in the UV-Vis, at which point data collection was initiated. Decreasing absorbance at 600nm was monitored as a function of time. The initial rates of reaction were determined from data collected during the first 10 to 20 seconds of reaction. These initial rates are given in the results section.

RESULTS AND DISCUSSION

Substrate Selection

Oxidations in basic solution generally require a catalyst that is effective for a wide range of substrate functional groups. Redox

indicators[15-19] have been used to measure peroxide activation because the reaction can be monitored continuously and conveniently. This permits screening of a large number of systems and simpler evaluation of the inorganic chemistry of peroxide activation.

Quinaldine blue [I] (pinacyanol chloride) is a redox indicator that has convenient spectral properties to monitor peroxide activation.

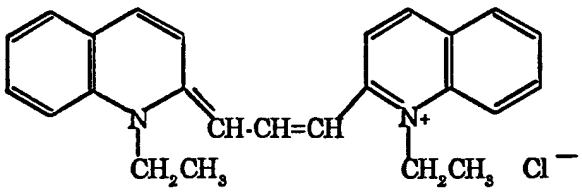

I

Its absorbance maximum at 600nm is insensitive to pH's above pH 4. (I) is not oxidized by H_2O_2 at the concentrations used in this work. Stronger oxidants such as oxone (monosodium peroxysulfate) or hypochlorite produce a colorless product with negligible absorbance at 600nm. Reactions of (I) are readily monitored with UV/Vis spectroscopy.

Copper(II) complexes have been shown to oxidize amine containing buffers in aqueous solution without peroxide.[19,20] To rule out the possibility of this occurring here, the absorbance of a solution containing equimolar concentrations of copper(II) and copper (II) with picolinic acid and (I) showed no change in absorbance over a 2-hour period. We therefore conclude that copper(II) does not oxidize I on the timescale of our experiments.

Several products can result from the oxidation of I.[14] For elucidating the essential properties of the complex to activate H_2O_2 in basic solution this information is not essential. Catalyst specificity is expected and these conclusions are expected to be substrate dependent.[6]

Activation of Peroxide by Copper(II) Chloride and Picolinic Acid

The first set of copper(II) complexes examined as catalysts uses picolinic acid as the ligand. A solution containing 1.0×10^{-4} M picolinic acid and copper(II) chloride (a 1:1 mole ratio) was found to effectively activate peroxide for the oxidation of I. The absorbance at 600nm versus time for this reaction is shown in Figure 1. Picolinic acid itself does not catalyze the oxidation of I by hydrogen peroxide. In the absence of a strong-binding ligand, copper(II) forms the insoluble hydroxide which decomposes H_2O_2 on the surface of the solid particles. Only a small amount of quinaldine blue oxidation occurs in the absence of ligand.

Figure 1

The activity of the copper(II)-picolinic acid system as a function of the ligand: copper(II) mole ratio at constant [copper(II)] is shown in Figure 2. The decrease noted at a ratio of 1.5 to 1 is larger than expected for 1:1 mixture of 1:1 and 2:1 complexes and could be due to a 3:2 aggregate.

Figure 2

The most active species is formed at a 1:1 ratio of copper to ligand. Stability constants predict that $Cu(PA)^+$ is the dominant species under these conditions[21].

Oxidations were studied with different concentrations of $Cu(PA)^+$, peroxide, and I (Table I). Runs 1-8 in Table 1 give the initial rates of quinaldine blue oxidation with a [Cu(II)] of 2.9×10^{-5} M and $[H_2O_2]$ between 5.7×10^{-4} M and 2.9×10^{-2} M.

Table 1

The reaction is zero order in $[H_2O_2]$. Repeated rate measurements were reproducible to 5%. Next, the peroxide concentration was held constant (0.029 M) while the $Cu(PA)^+$ concentration was varied. These results are shown in Table 1 as runs 9-14. Consistent with our discussion of Figure 2 the ln(initial concentration) versus ln(rate) plot is non-linear. This is in contrast to the systems in Table 3 where the reaction is first order in [Cu(II)]. The order with respect to substrate is zero, as determined from runs 13, 15, and 16. A mechanism consistent with these observations will be presented in the discussion section of this paper.

Effect of pH on Quinaldine Blue Oxidation Rate

The rate of quinaldine blue oxidation catalyzed by the copper(II)-picolinic acid system was measured at different pH's. The copper complex concentration was held constant at 2.9×10^{-5} M, and the peroxide concentration was 2.9×10^{-3} M. The pH was adjusted by addition of small amounts of concentrated KOH solution to a solution of the catalyst and sodium tetraborate. Figure 3 shows the rate dependence on pH.

Figure 3

The rate of quinaldine blue oxidation is negligible below pH 8.0. The rate of reaction increases up to pH 10.0, where it becomes independent of pH. The pH did not change during the reaction.

Peroxide Activation by Copper(II) Complexes of Anionic Bidentate Ligands

Experiments were performed with acetylacetone (AcAc), glycine (GLY), alanine (ALA), and leucine (LEU) as ligands, with $[Cu(II)] = 2.8 \times 10^{-5}$ M and $[H_2O_2] = 2.8 \times 10^{-2}$ M. The oxidation rate was studied with 1:1 and 2:1 ratios

of ligand to copper(II). Initial rates of oxidation are shown as runs 1-10 in Table 2.

Table 2

All these amino acid complexes catalyze the oxidation of quinaldine blue by hydrogen peroxide, with glycine being the least active and leucine being the most active at a 1:1 ratio of ligand to metal. The copper(II) complex of acetylacetone showed the highest activity, with an oxidation rate 15-20% greater than for the copper(II) leucine complex. As with picolinic acid, all of the complexes exhibited a sharp decrease in activity when the ligand to metal ratio was greater than 1.

Peroxide Activation by Copper(II) Complexes of Tridentate Anionic Ligands

Two tridentate anionic ligands, dipicolinic acid (DPA) and iminodiacetic acid (IDA) were examined. The results are shown as runs 11-14 in Table 2. At a 1:1 mole ratio, tridentate anionic ligands lead to much poorer catalysts for peroxide activation than bidentate anionic ligands. Complexes with tridentate anionic ligands show little activity for peroxide activation at a 2:1 ligand to copper ratios. Lower activity for complexes of anionic tridentate ligands shows that a positively charged complex is needed or that two adjacent equatorial coordination sites must be occupied by water to generate an effective copper(II) catalyst for peroxide activation.

Peroxide Activation by Copper(II) Complexes of Neutral Bidentate Ligands

Copper(II) complexes of the bidentate neutral ligands ethylenediamine (EN), N,N,N',N'-tetramethylethylenediamine (TMED), 2,9-dimethyl-1,10-phenanthroline (DMP), and 2,2'-bipyridylamine (BPA) were evaluated as possible catalysts. Table 2, runs 15-24, demonstrates that the copper(II) complexes of

bidentate neutral ligands are very effective as catalysts for hydrogen peroxide activation. The copper(II) complex of 2,2′-bipyridylamine has exceptional activity.

Rate variations with the copper(II) complexes of ethylenediamine (EN) and N,N,N′,N′-tetramethylethylenediamine (TMED) in the presence of excess ligand are interesting. The activity of the EN complex is reduced by a factor of 50 at a 2:1 ratio of ligand to metal. However, the activity of the TMED complex decreased only slightly in the presence of a four-fold excess of ligand. Sterically hindering ligands that decrease the equilibrium constant for binding a second bidentate ligand give copper catalysts that function in the presence of excess ligand. Formation constants for the 1:1 and 2:1 complexes of both EN and TMED show that the formation of the 2:1 complex is much less favorable with TMED.[21]

Peroxide Activation With Copper(II) Complexes of Neutral Multidentate Ligands

To complete this study, several copper(II) complexes with neutral tri- and tetradentate ligands were evaluated as possible catalysts. Table 2, runs 25-30, shows the results with copper(II) complexes of tris(2-aminoethyl)amine (TREN), 3,3′-iminobis(propylamine) (IBPA), and 2,2′:6,6″-terpyridine (TERPY). The conditions and peroxide concentrations were the same as in previous runs. Since the copper(II) complexes of tri- and tetradentate neutral ligands result in poor or inactive catalysts, we can conclude that having two adjacent coordination positions occupied with easily displaced solvent, and not the complex charge, is the necessary condition for active copper (II) catalysts.

Rate Studies

The following four complexes were selected for further kinetic examination. The copper(II)/leucine catalyst was selected because it gave the best performance for peroxide activation of the amino acid ligands. The

copper(II)/acetylacetone complex gave the best performance with anionic ligands. The bipyridylamine copper complex gave the best overall peroxide activation. The copper(II)/ N,N,N',N'-tetramethylethylenediamine complex was selected to determine the influence of steric effects on the reaction rates.

Rates with all these ligands are first-order in [Cu(II)] (Table 3). The copper(II)-leucine complex obeys Equation (1). However, rates with the copper(II) complexes of the other three ligands depended on [peroxide], Table 4. The catalyst concentration is kept constant at 2.8×10^{-5} M for the copper(II)-AcAc and copper(II)-TMED complexes and, because of its higher activity, at 2.8×10^{-6} M for the copper(II)- BPA complex.

Table 3

Table 4

The Rate Law and Proposed Mechanism

A wide variety of copper(II) complexes activate hydrogen peroxide. Activities decrease dramatically when the ligand to metal ratio is greater than 1:1. Tri- and tetradentate ligand complexes are much less active than those with bidentate ligands. These results suggest that a significant concentration of copper(II) complexes with two adjacent coordinated aquo ligands is required for efficient hydrogen peroxide activation.

The mechanism of hydrogen peroxide activation by copper(II) must account for the following observations:

1) The order with respect to [quinaldine blue] is zero.

2) All the reactions are first order in [Cu(II)].

3) Addition of ligand above a 1:1 mole ratio decreases activity. Tri- or tetradentate ligands tend to give inactive complexes.

4) The reaction rate is pH dependent.

5) The reaction rate is independent of $[H_2O_2]$ with PA and LEU ligands, but increases with $[H_2O_2]$ in a non-linear manner with AcAc, TMED, and BPA ligands.

A mechanism consistent with these observations is shown in Figure 4.

Figure 4

The first step is the reversible dissociation of a water molecule from a distorted octahedral, copper(II) complex. This process is reported to be reasonably facile.[22] The next step is coordination of the hydroperoxide anion (O_2H^-) to produce the peroxo or hydroperoxo complex. Once formed, this copper-hydroperoxide species reacts extremely rapidly with the substrate. As a result, the rate of oxidation is determined by the rate of formation of the copper-hydroperoxide complex, giving the zero order substrate dependence.

Assuming that the rate of formation of the copper-hydroperoxide complex is rate limiting, and is followed by rapid oxidation of quinaldine blue, the rate of oxidation catalyzed by the copper(II) complex is given by:

$$V_{ox} = d\,[LCu^{II}(H_2O)(O_2H)] \,/\, dt = k_3\,[LCu^{II}(H_2O)]\,[O_2H^-] \qquad (1)$$

A steady-state approximation for the $[LCu^{II}(H_2O)]$ concentration leads to the following expression:

$$[LCu^{II}(H_2O)] = \frac{k_1[LCu^{II}(H_2O)_2]}{k_{-1} + k_3[O_2H^-]} \qquad (2)$$

The concentration of the hydroperoxide anion is directly proportional to peroxide concentration and pH; $[O_2H^-] = K_a\ [H^+]\ [H_2O_2]$. Substituting Equation (2) into Equation (1) gives the rate of oxidation as:

$$\text{Reaction Rate} = \frac{k_1 k_3 [LCu^{II}(H_2O)_2]\ [O_2H^-]}{k_{-1} + k_3[O_2H^-]} \qquad (3)$$

Equation (3) can be rearranged to:

$$\text{Reaction Rate} = \frac{k_1 [LCu^{II}(H_2O)_2]\ [O_2H^-]}{(k_{-1} / k_3) + [O_2H^-]} \qquad (4)$$

In addition, if we derived the rate law by using two consecutive steady-state approximations for both $[LCu^{II}(H_2O)]^{2+}$ and $[LCu^{II}(O_2H)]^{+}$, we obtain the same rate law as in Equation (4). The only requirement for this to be valid is the rate of substrate oxidation needs to be greater than the rate of copper(II) hydroperoxide complex formation.

Experimental observations support the above mechanism and suggest that other possibilities are less reasonable. The active species is not a dissociated hydroxyl radical produced by peroxide decomposition. While this pathway exists, as shown in the mechanism (the k_2 pathway), this reaction does not account for the dramatic decrease in catalytic reactivity for complexes of tri- and tetradentate ligands.

Another possible mechanism involves a high oxidation state of copper as the active oxidant. While copper(II) complexes have been shown to oxidize amine-containing buffers,[19,20] no oxidation of quinaldine blue by Cu(II) occurs in the absence of hydrogen peroxide. Copper(III) species are known in aqueous solutions.[23-26] However, a Class V reaction mechanism[6] involving copper(III) redox cycling cannot explain the need for two available equatorial binding sites. A mechanism involving a coordinated peroxide explains the trends in

reactivity of the mono- and di-positively charged copper(II) complexes and reduction in reactivity in the presence of excess ligand.

Dissociation of water occurs from the axial positions. Once the five coordinate copper complex is formed, the attack by O_2H^- occurs to coordinate the O_2H^- in the strong binding equatorial position (Figure 5). The strongest binding of hydroperoxide anion occurs when it is bound to the same d_{x2-y2} orbital that is involved in ligand coordination. Coordination of O_2H^- to the equatorial position is important because the use of this orbital leads to a stronger acceptor than the axial position. Strong Lewis acidity activates hydrogen peroxide in Class IVb mechanisms. When the 2:1 ligand to copper(II) complex is formed, the reactivity decreases because there are no strong-binding equatorial positions available to bind the hydroperoxide anion.

Our experiments show that it is necessary to have two equatorial coordination sites occupied by easily displaced solvent. This is demonstrated by the large decrease in reactivity seen with complexes of tri- and tetradentate ligands, as compared to the bidentate ligands. The most straightforward explanation requires two coordination sites to bind the peroxide, Figure 5a. Complexes of copper(II) dimers have been shown to bind O_2^{2-} in a similar manner.[9c,11b-e,12b,13a] Peroxo complexes of other metals are known[1b] and several are useful oxidants and oxidation catalysts.[1c]

Another possibility is that the metal-peroxo complex is stabilized by a hydrogen bonding interaction between bound hydroperoxide and an equatorial water. A similar interaction has been used to explain the stability of a vanadium-peroxo complex in aqueous solution.[27] This interaction can only occur when one bidentate ligand is coordinated to the copper center, as shown in Figure 5b. When a tri- or tetradentate ligand is coordinated to the copper(II) complex, or a 2:1 complex of the bidentate ligand is formed, stabilization of the hydroperoxide anion through hydrogen bonding does not occur.

Figure 5a,b

Our proposed mechanism leads to a rate law, Equation (5), that explains our kinetic data. The requirement that our mechanism gives zero order kinetics for quinaldine blue oxidation is satisfied with the assumption that the copper(II) hydroperoxide species will react very rapidly with quinaldine blue. This is reasonable, as oxone® and sodium hypochlorite oxidize quinaldine blue too rapidly to study with the procedures used here.

The rate of oxidation is predicted, by the derived rate law, to be first order in copper(II) complex. This was experimentally observed. A zero order dependence of the rate on peroxide concentration was observed for copper(II) complexes of picolinic acid (PA) and leucine (LEU). However, the copper(II) complexes of acetylacetone (AcAc), N,N,N′,N′-tetramethylethylenediamine (TMED), and bipyridylamine (BPA) all showed significant deviations from zero order kinetics.

While these results differ from the zero-order dependence seen for copper(II) complexes of picolinic acid or leucine, the rate law derived from the proposed mechanism (Equation (4)) can be used to explain these differing orders. If we define V_{max} as $k_1[LCu^{II}(H_2O)_2]$ and K_m as k_{-1} / k_3 we obtain the following expression:

$$\text{Reaction Rate} = \frac{V_{max}[O_2H^-]}{K_m + [O_2H^-]} \qquad (5)$$

Equation (5) is now in the same form as the Michaelis-Menten equation.[28] Systems having kinetic behavior described by equation (5) give linear plots of $(\text{rate})^{-1}$ versus $[HO_2^-]^{-1}$. Figure 7 shows this plot for the Cu-AcAc system. The plots for Cu-TMED and Cu-BPA are also linear.

Figures 7

Thus, these systems follow the kinetics predicted by the derived rate law, Equation (5). From these plots we can determine K_m/V_{max}, and $(V_{max})^{-1}$ whose values are given on Table 5. For the copper(II) complexes of picolinic acid and leucine, V_{max} is the observed rate of reaction, because peroxide concentrations low enough to cause deviation from zero order kinetics were not examined. K_m must clearly be lower than $[HO_2^-]$ to give zero-order kinetics in peroxide (see Equation (5)). Thus K_m values for the picolinic acid and leucine complexes are estimated based on the lowest hydroperoxide anion concentration studied.

Table 5

Interestingly, di-positively charged copper(II) complexes (neutral ligands) have significantly higher values of K_m for peroxide activation. K_m is equal to k_{-1} / k_3 in the derived rate law, which implies that coordination of water to the dissociated copper(II) complex ($[LCu(H_2O)]$), rather than coordination of the hydroperoxide anion, is more favorable for the more positively charged copper complexes. However, in view of the complex enthalpic and entropic contributions to the coordination of these species, we cannot provide a more detailed explanation of the trends observed in K_m or V_{max}.

Since the rates of oxidation are dependent upon the concentration of the hydroperoxide anion, rather than hydrogen peroxide, changes in pH affect reaction rates. For the copper(II) - picolic acid complex, at high pH the concentration of hydroperoxide anion will be high enough to give zero-order kinetics, where the observed rate is equal to V_{max}. As the pH drops below 9, the concentration of hydroperoxide anion decreases enough to see deviation

from zero-order kinetics similar to that seen for the copper(II) complexes of AcAc, TMED, and BPA. This gives rise to a dependence of rate on hydroperoxide anion concentration. If the concentration of $[HO_2^-]$ is calculated for the data in figure 3 (in the range from pH 9.7 to 7.3) and a $(rate)^{-1}$ versus $[HO_2^-]$ plot constructed, linear behavior is observed supporting the above conclusion.

CONCLUSIONS

We have found a series of copper(II) complexes that activate hydrogen peroxide for oxidation in basic aqueous solution. In all cases, increasing the amount of ligand above a 1:1 ratio to copper(II) decreases the rate of peroxide activation, and in some cases this occurred dramatically. Complexes of tri- and tetradentate ligands are generally inactive. A mechanism (Figure 4) is proposed which involves the dissociation of coordinated water from an axial position followed by nucleophilic attack by a hydroperoxide anion, to form an equatorially bound copper(II)-hydroperoxide complex. The more strongly coordinating equatorial position provides the needed Lewis acidity to activate bound hydroperoxide for oxidations. Several theories are examined on why two equatorial coordination sites containing easily displaced solvent are necessary for peroxide activation with these complexes. One possibility is that the peroxide occupies two coordination sites, as shown in Figure 5a. Another possibility is that the coordinated hydroperoxide is stabilized by hydrogen-bonding interaction with a coordinated water, also shown in Figure 5a. A first order dependence of rate on catalyst concentration is observed, which is shown to agree with the rate law derived from our mechanism (Equation (4)). The observed zero order dependence of oxidation rate on substrate concentration is also explained within the context of the proposed mechanism.

The observation of zero-order dependence of rate on hydrogen peroxide concentration for PA and LEU and the nonzero-order rate dependence for AcAc,

TMED, and BPA are also explained. This is done by re-writing Equation (4), the derived rate law, in the form of the Menten-Michaelis expression. This expression predicts under which conditions the rate of reaction is equal to V_{max}, where the zero-order rate dependence on peroxide concentration occurs. This also explains the observed dependence of reaction rate upon pH for oxidations catalyzed by the copper(II)-picolinic acid complex. As the pH decreases the concentration of hydroperoxide anion also is decreased. When the pH drops below that needed for sufficient concentration of hydroperoxide anion to give the observed rate as V_{max}, a decreased rate is observed.

The mechanism offered for these systems can be generalized. In order to activate hydrogen peroxide by coordination of the peroxide to a metal center, the complex used must be capable of binding O_2H^- to a strongly acidic coordination position. The stability constants for successive ligand binding can be employed to select metal complexes that have the potential to bind and activate O_2H^-. The sequence of formation constants must allow the existence of aquo complexes with which O_2H^- can react by displacing water from strong binding metal orbitals. For copper(II), the 2:1 ($Cu(L)_2$) formation constant (when L is bidentate) must be low enough relative to 1:1 (Cu(L)) to permit substantial quantities of the 1:1 complex to exist in solution. For metal ions with fewer d-electrons, strong axial coordination positions exist. Bidentate ligand complexes, ML, strongly bind O_2H^- and activate peroxide.

REFERENCES

1) a) R. A. Sheldon and J. K. Kochi, *Metal-Catalyzed Oxidations of Organic Compounds*, Academic Press, New York, 1981.

b) F. Di Furia and V. Conte in *Catalystic Oxidations with Hydrogen Peroxide as Oxidant*, Strukul, G. Ed., Kluwer Academic Publishers, Netherlands, 1992; F. Di Furia, V. Conte and G. Modena in *Organic Peroxides*, ed. W. Ando, Wiley, New York, 1992.

c) H. Mimoun in *Comprehensive Coordination Chemistry*, G. Wilkinson, ed. Pergamon Press, New York, 1987, vol. 6.

2) a) D. T. Sawyer, V. Cepak, C. Redman and C. Kang, *Bioorg. & Med. Chem.* 1993, **1**, 125. b) D. T. Sawyer, C. Kang and H. C.Tung, *J. Am. Chem. Soc.* 1992, **114**, 3445. c) D. T. Sawyer, J. R. Kanofsky, A. Sobkowiak, B. Ross, P. Cofré, S. A. Richert and C. Shew, *J. Am. Chem. Soc.*, 1990, **112**, 1936.

3) a) D. H. R. Barton, G. Balavoine, J. Boivin and A. Gref, *Tetrahedron Lett.*, 1990, **31**, 659. b) D. H. R. Barton, G. Balavoine, J. Boivin, A. Gref, P. L. Coupanec, N. Ozbalik, J. A. X. Pestana, and H. Riviere, *Tetrahedron*, 1990, **44**, 1091. c) D. H. R. Barton, G. Balavoine, J. Boivin, A. Gref, N. Ozbalik and H. Riviere, *Tetrahedron Lett.*, 1986, **27**, 2849. d) D. H. R. Barton, J. Boivin, N. Ozbalik, K. M. Schwartzentruber and K. Jankowski, *Tetrahedron Lett.*, 1985, **26**, 447.

4) a) S. R. Ellis, U.S. Patent #5041142, Aug. 20, 1991. b) R. Hage, T. L. F. Favre, K. Helm-Rademaker, H. Koek, R. J. Martens, T. Swarthoff and M. R. P. Vliet, European Patent 0458398A2, May 15, 1991. d) S. M. Harriot, U.S. Patent #5021187, Jun. 4, 1991. e) C. D. Bragg and P. A.Hardy, U.S. Patent #5002682, Mar. 26, 1991. f) D. H. Dolphin,

T. Nakano, T. K. Kirk, T. P. Wijesekera, R. L. Farrell and T. E. Maione, U.S. Patent #5041142, Aug. 20, 1991. g) J. Okes, U.S. Patent 4481129, Nov. 6, 1984.

5) a) A. E. Comyns, *Nature*, 1994, **369**, 609. b) R. Hage, et al., *Nature*, 1994, **369**, 637.

6) R. S.Drago, *Coord. Chem. Rev.*, 1992, **117**, 185. b) R. S. Drago and R. H. Beer, *Inorg. Chim. Acta*, 1992, **198**, 359.

7) K.Kushioka, I. Tanimoto, K. Maruyama, *Bull Chem. Soc. Jpn.*, 1989, **62**, 1147.

8) a) D. T. Sawyer, A. Llober, X. Lui, A. Qui and A. Sobkowiak, *J. Am. Chem. Soc.*, 1993, **115**, 609. b) D. T. Sawyer, A. Qui, X. Lui, *J. Am. Chem. Soc.*, 1993, **115**, 3239.

9) a. N.Kitajima, K. Fujisawa, C. Fujimoto, Y. Moro-oka, S. Hashimoto, T. Kitagawa, K. Torimumi, K. Tatsumi and A. Nakamura, *J. Am. Chem. Soc.*, 1992, **114**, 1277. b) N. Kitajima, T. Koda, S. Hashimoto, T. Kitagawa and Y. Moro-oka, *J. Am. Chem. Soc.*, 1991, **113**, 5664. c) N.Kitajima, K. Fujisawa and Y. Moro-oka, *J. Am. Chem. Soc.*, 1989, **111**, 8975.

10) T. N.Sorrell and M. L. Garrity, *Inorg. Chem.*, 1991, **30**, 210.

11) a) K. D. Karlin, J. Zubieta, Q. Chen, N. N. Murthy and N. Wei, *Inorg. Chem.*, 1994, **33**, 1953. b) K. D. Karlin, Z. Tyeklár, N. N. Murthy and N. W. Wei, *Inorg. Chem.*, 1994, **33**, 1177. c) K. D. Karlin, B. I. Cohen and M. S. Nasir, *J. Am. Chem. Soc.*, 1992, **114**, 2482. d) K. D. Karlin, E. I. Solomon, Z. Tyeklár, J. E. Pate, P. K. Ross and M. J. Baldwin, *J. Am. Chem. Soc.*, 1991, **113**, 8671. e) K. D. Karlin, E. I. Solomon, R. W. Cruse and J. E. Pate, *J. Am. Chem. Soc.*, 1987, **109**, 2624.

12) a) E. I. Solomon, N. Kitajima, K. Fujisawa, J. E. Pate, D. E. Root and M. J. Baldwin, *J. Am. Chem. Soc.*, 1992, **114**, 10421. b) E. I. Solomon, D. P. Ballou and J. L. Cole, *J. Am. Chem. Soc.*, 1991, **113**, 8544.

13) a) N. Kitajima, Y. Moro-oka, T. Katayama, K. Fujisawa and Y. Iwata, *J. Am. Chem. Soc.*, 1993, **115**, 7872. b) N. Kitajima, K. Fujisawa and Y. Moro-oka, *Inorg. Chem.*, 1990, **29**, 357.

14) G. W.Byers, S. Gross P. M., Henrichs, *Photochem. Photobiol.*, 1976, **23** 37.

15) a) J. H. Espenson, A. Bakac and J. Janni, *J. Am. Chem. Soc.*, 1994, **116**, 3436. b) J. H. Espenson, A. Bakac, W. J. Chen and S. L. Scott, *J. Phys. Chem.*, 1993, **97**, 6710.

16) a) T. C. Bruice, J. R. L. Smith and P. N. Balasubramanian, *J. Am. Chem. Soc.*, 1988, **110**, 7411. b) T. C. Bruice, E. S. Schmidt and P. Balasubramanian, *J. Am. Chem. Soc.*, 1987, **109**, 7865. c) T. C. Bruice, M. F. Zipplies and W. A. Lee, *J. Am. Chem. Soc.*, 1986, **108**, 4433.

17) W. Werner, H. Wielinger, K. Gawehn, *Z. Anal. Chem.*, 1970, **252**, 222.

18) W. G.Bardsley and R. E. Childs, *Biochem. J.*, 1975, **145**, 93.

19) L. M. Sayre and F. Wang, *Inorg. Chem.*, 1989, **28**, 169.

20) P. Saltman and K. Hegetschweiler, *Inorg. Chem.*, 1986, **25** 107.

21) R. M. Smith and A. E. Martell, *Critical Stability Constants*, Plenum Press, New York, 1975, Vol. 1-3.

22) N. N.Greenwood and A. Earnshaw, *Chemistry of the Elements*, Pergamon Press, New York, 1989.

23) R. van Eldik, D. Meyerstein, H. Cohen, G. Czapski, S. Goldstein, *Inorg. Chem.*, 1994, **33**, 3255.

24) D. W. Margerum, W. M. Scheper, M. R. McDonald, F. C. Fredericks, L. Wang and H. D. Lee in *Bioinorganic Chemistry of Copper*, eds. K. D. Karlin and Z. Tyeklár, Chapman and Hall, New York, 1993.

25) D. Meyerstein, *Inorg. Chem.*, 1971, **10**, 2244.

26) J. Lati, D. Meyerstein, *J. Chem. Soc. Dalton*, 1978, 1105.

27) H. Mimoun, L. Saussin, E. Daire, M. Postel, J. Fischer, R. Weiss, *J. Am. Chem. Soc.*, 1983, **105**, 3101.

28) F. B. Armstrong, *Biochemistry*, Oxford University Press, New York, 1989.

DATA TABLES

TABLE 1

Dependence of Quinaldine Blue Oxidation rate on Peroxide, $Cu(PA)^+$ and Substrate Concentrations[a]

Run	$[H_2O_2]$[a]	[Quin. Blue]	$[Cu(PA)^+]$	Rate[b]
1	5.70×10^{-4}	3.0×10^{-5}	2.9×10^{-5}	8.4×10^{-7}
2	5.70×10^{-4}	"	"	8.3×10^{-7}
3	2.86×10^{-3}	"	"	7.9×10^{-7}
4	2.86×10^{-3}	"	"	7.8×10^{-7}
5	8.59×10^{-3}	"	"	7.9×10^{-7}
6	8.59×10^{-3}	"	"	7.6×10^{-7}
7	1.72×10^{-2}	"	"	7.1×10^{-7}
8	2.86×10^{-2}	"	"	7.3×10^{-7}
9	2.86×10^{-2}	"	1.4×10^{-6}	9.2×10^{-9}
10	"	"	1.8×10^{-6}	2.0×10^{-8}
11	"	"	2.3×10^{-6}	5.4×10^{-8}
12	"	"	1.1×10^{-5}	3.2×10^{-7}
13	"	"	2.9×10^{-5}	$7.3 \times 10^{-7+}$
14	"	"	8.6×10^{-5}	9.3×10^{-7}
15	"	2.0×10^{-5}	2.9×10^{-5}	7.6×10^{-7}
16	"	1.0×10^{-5}	"	7.5×10^{-7}

a. All concentrations are M.
b. Rates are expressed as M sec^{-1}.

TABLE 2

Rates of Quinaldine Blue Oxidation with Copper(II) Complexes of Anionic Bidentate (runs 1-10), Anionic Tridentate (runs 11-14), Neutral Bidentate (runs 15-24), and Neutral Multidentate (runs 25-30) Ligands

Run No.	Catalyst[a]	Rate ($\times 10^{-7}$)[b]
1	Cu^{II} / 1 PA	7.9
2	Cu^{II} / 2 PA	0.21
3	Cu^{II} / 1 AcAc	11.1
4	Cu^{II} / 2 AcAc	1.8
5	Cu^{II} / 1 GLY	4.7
6	Cu^{II} / 2 GLY	1.9
7	Cu^{II} / 1 ALA	5.9
8	Cu^{II} / 2 ALA	3.2
9	Cu^{II} / 1 LEU	8.8
10	Cu^{II} / 2 LEU	2.6
11	Cu^{II} / 1 DPA	1.5
12	Cu^{II} / 2 DPA	0.014
13	Cu^{II} / 1 IDA	2.9
14	Cu^{II} / 2 IDA	0.17
15	Cu^{II} / 1 EN	5.2
16	Cu^{II} / 2 EN	0.10
17	Cu^{II} / 1 TMED	6.4
18	Cu^{II} / 2 TMED	5.9
19	Cu^{II} / 4 TMED	3.9
20	Cu^{II} / 1 DMP	10.2
21	Cu^{II} / 2 DMP	0.0
22	Cu^{II} / 1 BPA	35.1
23	Cu^{II} / 2 BPA	23.4
24	Cu^{II} / 5 BPA	12.6
25	Cu^{II} / 1 TREN	0.0
26	Cu^{II} / 2 TREN	0.0
27	Cu^{II} / 1 IBPA	0.0
28	Cu^{II} / 2 IBPA	0.0
29	Cu^{II} / 1 TERPY	0.06
30	Cu^{II} / 2 TERPY	0.05

a. [Copper(II)] = 2.8×10^{-5} M; [hydrogen peroxide] = 2.8×10^{-3} M. All reaction solutions were buffered at pH = 9.1.

b. Rates are M^{-1} sec^{-1}.

TABLE 3

Rates of Quinaldine Blue Oxidation with Various Concentrations of Copper(II) Complexes of LEU and AcAc. [Peroxide] = 2.8×10^{-2} M.

Run No.	Ligand	Complex Concentration[a]	Rate ($\times 10^{-7}$)[b]
1	LEU	2.9×10^{-5}	8.8
2	LEU	2.3×10^{-5}	6.8
4	LEU	1.1×10^{-5}	4.4
5	LEU	5.7×10^{-6}	1.7
6	LEU	2.3×10^{-6}	0.67
7	AcAc	2.9×10^{-5}	11.1
8	AcAc	1.7×10^{-5}	8.5
9	AcAc	1.1×10^{-5}	5.9
10	AcAc	5.7×10^{-6}	2.2
11	AcAc	2.3×10^{-6}	0.65

a. Concentrations are in moles per liter.
b. Rates are in units of (moles) $(\text{liter})^{-1}$ $(\text{second})^{-1}$.

TABLE 4

Rates of Quinaldine Blue Oxidation at Various Peroxide Concentrations. [Cu(II)] =

Run No.	Ligand	[Peroxide][a]	Rate ($\times 10^{-7}$)[b]
1	BPA	2.86×10^{-2}	3.66
2	BPA	9.16×10^{-3}	2.29
3	BPA	4.66×10^{-3}	1.55
4	BPA	5.73×10^{-4}	0.226
5	AcAc	2.86×10^{-2}	11.2
6	AcAc	9.16×10^{-3}	11.1
7	AcAc	4.66×10^{-3}	9.8
8	AcAc	1.15×10^{-3}	8.9
9	AcAc	5.73×10^{-4}	5.7
10	AcAc	2.86×10^{-4}	4.6
11	TMED	2.86×10^{-2}	5.8
12	TMED	2.86×10^{-2}	5.0
13	TMED	9.16×10^{-3}	4.5
14	TMED	9.16×10^{-3}	4.4
15	TMED	4.66×10^{-3}	3.0
16	TMED	4.66×10^{-3}	3.2
17	TMED	1.15×10^{-3}	1.6
18	TMED	5.73×10^{-4}	1.0
19	TMED	5.73×10^{-4}	0.97
20	TMED	2.86×10^{-4}	0.40
21	TMED	2.86×10^{-4}	0.383

a. Concentrations are M;.
b. Rates units are M^{-1} sec^{-1}.

TABLE 5		
Values for V_{max} and K_m as Determined for the Copper (II) Complexes of Various Ligands		
Ligand	V_{max}[a]	K_m
PA	7.9×10^{-7}	$< 8 \times 10^{-7}$
LEU	8.8×10^{-7}	$< 8 \times 10^{-7}$
AcAc	1.1×10^{-6}	9.4×10^{-7}
TMED	9.1×10^{-7}	1.4×10^{-5}
BPA	8.1×10^{-6}	4.8×10^{-5}

a. V_{max} is expressed for [Cu(II)] = 2.8×10^{-5} M.

FIGURE CAPTIONS

Figure 1: Oxidation of quinaldine blue with hydrogen peroxide catalyzed by copper(II) chloride + picolinic acid. $[H_2O_2] = 2.9 \times 10^{-3}$ M, [Cu(II)] = 2.9×10^{-5} M.

Figure 2: Effect of ligand:metal ratio on the rate of quinaldine blue oxidation. [Cu(II)] = 2.9×10^{-5} M, $[H_2O_2] = 5.7 \times 10^{-3}$ M. All rates are expressed $Msec^{-1}$.

Figure 3: Effect of pH on the rate of quinaldine blue oxidation. [Cu(II) = 5.7×10^{-3} M. Rates are expressed in $Msec^{-1}$.

Figure 4: The Proposed Mechanism.

Figure 5a and 5b: Proposed structures for: a) a μ^2 bound peroxide and b) a hydrogen-bond stabilized copper-hydroperoxide complex.

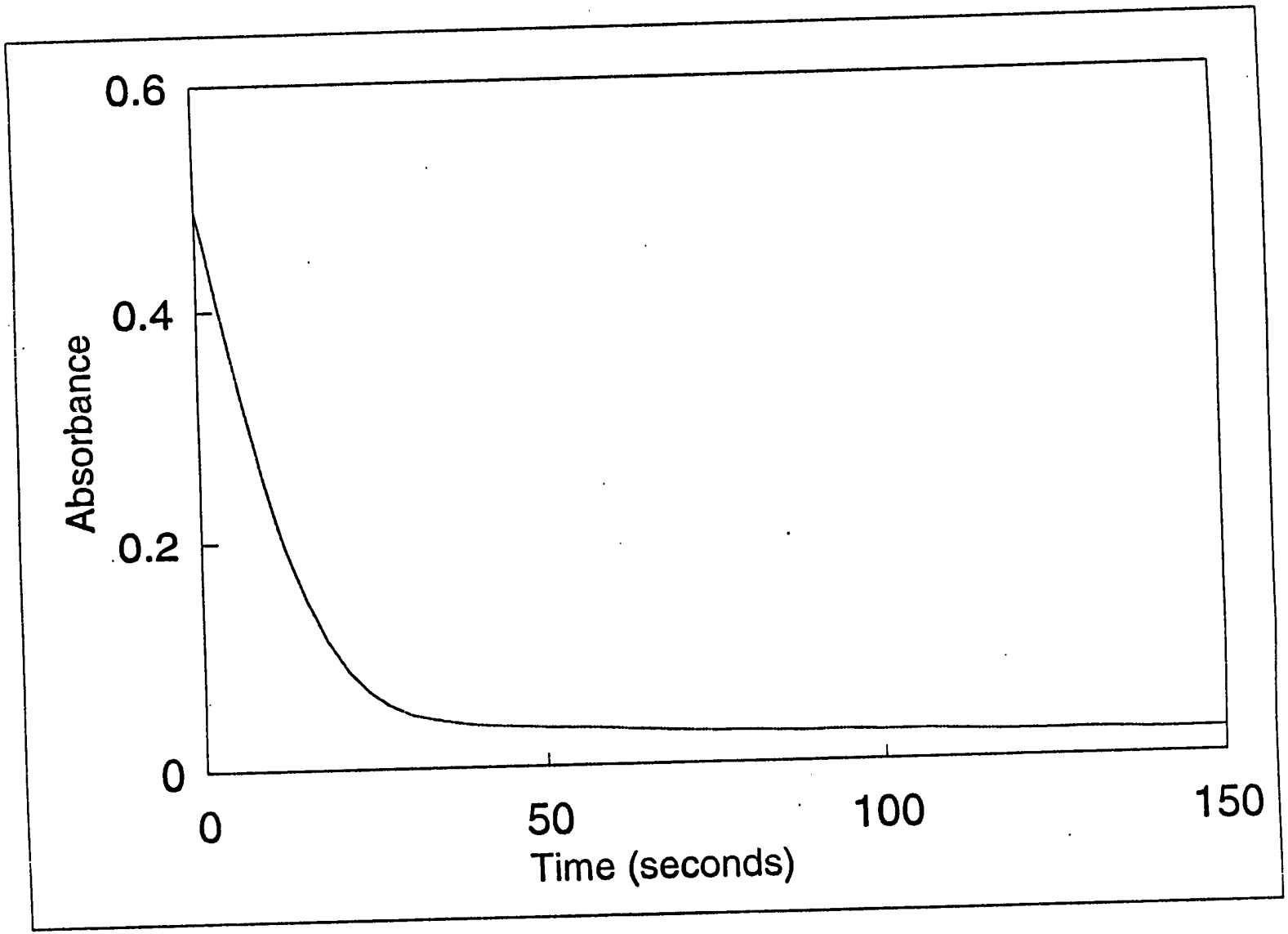
0.6
0.4
0.2
0
Absorbance
0
50
100
150
Time (seconds)

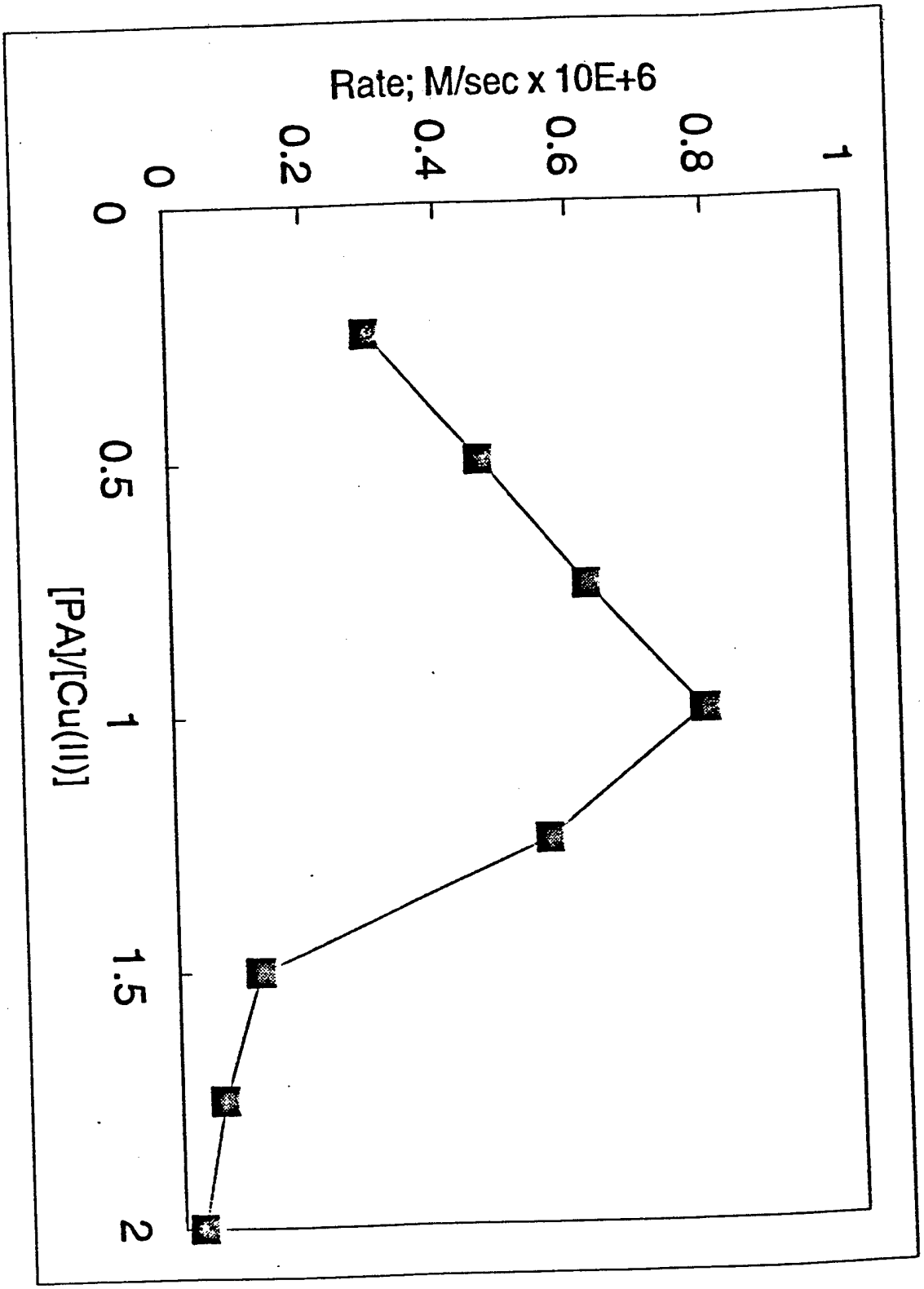
Rate; M/sec x 10E+6
0
0.2
0.4
0.6
0.8
1
0
0.5
1
1.5
2
[PA]/[Cu(II)]

Rate; M/sec x 10E+6
0
0.2
0.4
0.6
0.8
1
1.2
pH
6
7
8
9
10

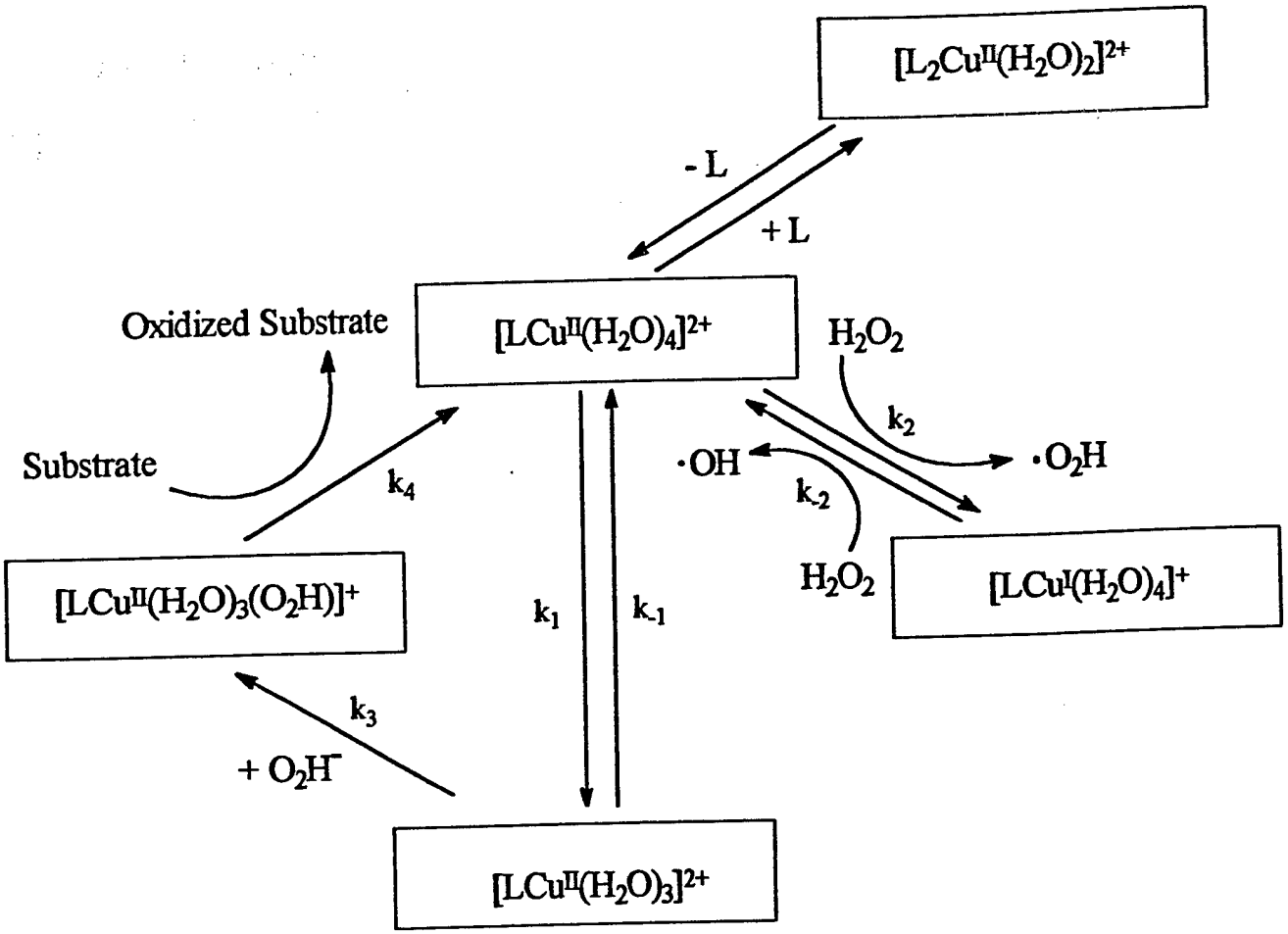
$[L_2Cu^{II}(H_2O)_2]^{2+}$
- L
+ L
Oxidized Substrate
$[LCu^{II}(H_2O)_4]^{2+}$
H_2O_2
k_2
Substrate
k_4
·OH
k_{-2}
$\cdot O_2H$
H_2O_2
$[LCu^{II}(H_2O)_3(O_2H)]^+$
k_1
k_{-1}
$[LCu^{I}(H_2O)_4]^+$
k_3
$+ O_2H^-$
$[LCu^{II}(H_2O)_3]^{2+}$

A

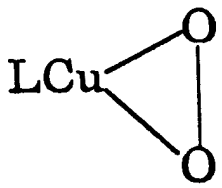

B

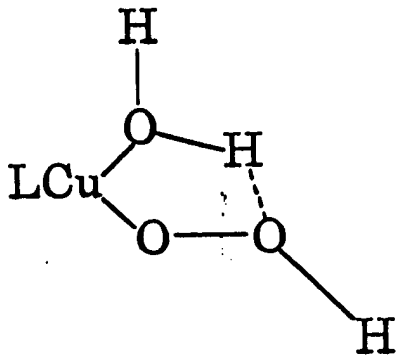

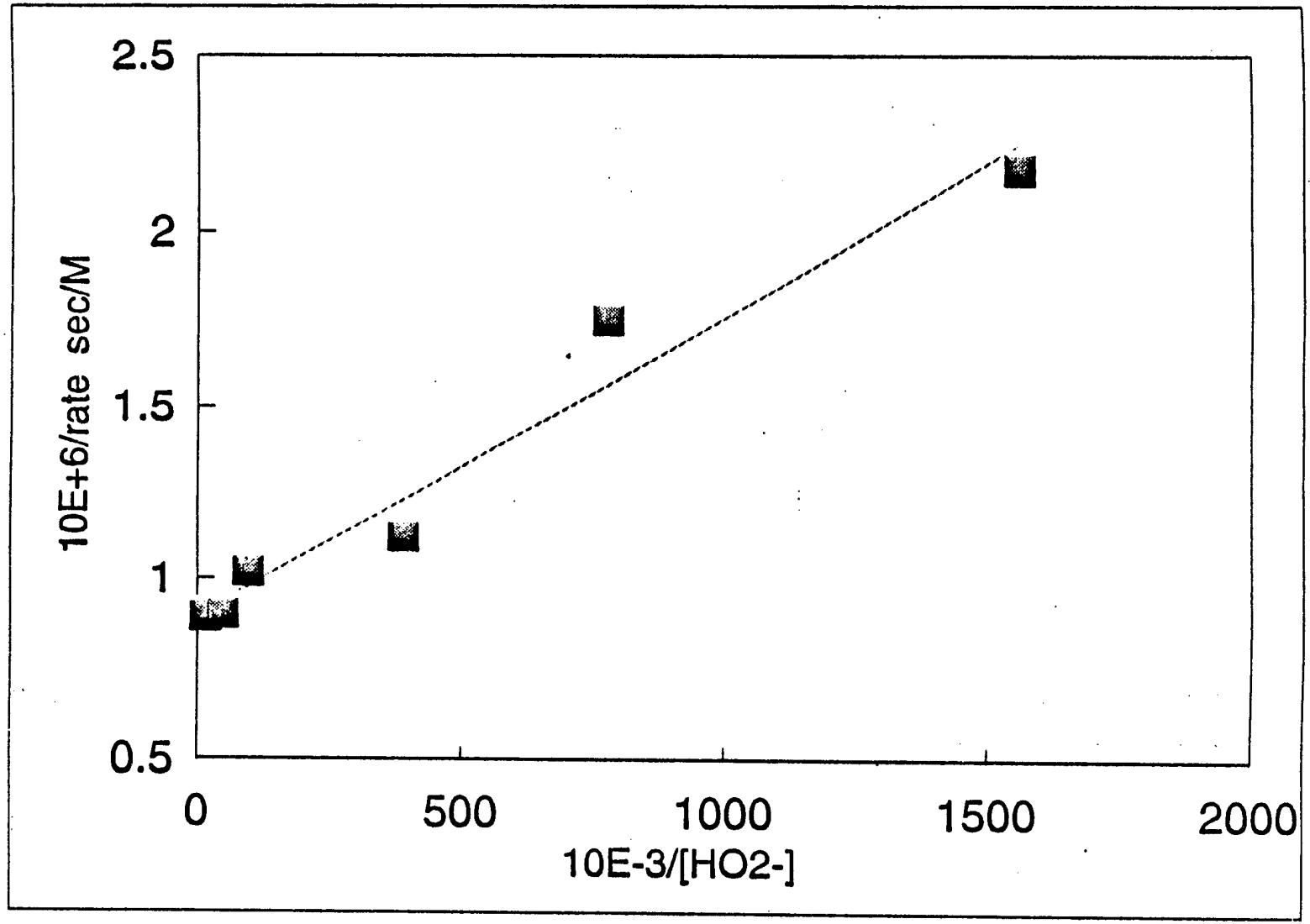
2.5
2
1.5
1
0.5
10E+6/rate sec/M
0
500
1000
1500
2000
10E-3/[HO2-]

Contribution from

Department of Chemistry

University of Florida

Gainesville, FL 32611

Tel.: (352) 392-6043 Fax: (352) 392-4658

GAS-SOLID EQUILIBRIA IN POROUS CARBONACEOUS MATERIALS

by

Russell S. Drago*, Douglas S. Burns[1], J. Michael McGilvray, Wm. Scott Kassel

Steven K. Showalter[2] and Todd J. Lafrenz[3]

[1] Present Address: ENSCO, Inc., 445 Pineda Court, Melbourne, FL 32940

[2] Present Address: Sandia National Laboratories, Org. 6211, Albuquerque, NM 87185

[3] Present Address: CINC, 3535-B Arrowhead Dr., Carson City, NV 89706

031996/g-s2.doc/#4dl/ml

ABSTRACT

Temperature dependent adsorption isotherms for a series of adsorptives on two microporous carbonaceous solids, are used to develop a method that characterizes the affinity of an adsorbent for gas molecules. A predominantly carbon adsorbent (A-572), and a nitrogen containing adsorbent, pyrolyzed poly-acrylonitrile (PPAN), are studied. A multiple process equilibrium interpretation of the data is used to calculate adsorption equilibrium constants for the distribution of the adsorptive between the gas and the solid. Equilibrium constants for three distinct processes ($K_{1,ad}$, $K_{2,ad}$, and $K_{3,ad}$) are found to describe most of the gas-solid adsorption isotherms on both solids. The analysis shows that the first process ($K_{1,ad}$), involves adsorption of the gas by the solid surface in micropores of molecular dimensions. The second process involves adsorption in slightly larger micropores. The third process involves adsorption by larger micropores that can accomodate bilayer adsorption, and for condensible gases multilayer adsorption. In order to define the n's and K's for the three processes, isotherms are measured at several temperatures. In this model, the n-values are temperature independent. Enthalpies for these processes result from the temperature dependent isotherms. The free energies of adsorption plot up linearly with the enthalpies.

For adsorptives which possess little or no dipole moment there is a direct relationship between their polarizability and both the ln K_{ad} values and the enthalpies of adsorption. Molecules with a dipole moment are adsorbed more effectively by the solid than is expected on the basis of their polarizability (i.e., $K_{1,ad}$ is larger than expected). The free energies and enthalpies of adsorption of all adsorptives on A-572 correlate

with the van der Waals constant of the adsorptive to afford predictions of the affinity of these solids for gases that have not been measured. The polar, acceptor adsorbate SO_2 is shown to undergo specific donor-acceptor interactions with PPAN by the van der Waals correlation. The utility of this information for catalytic, gas storage and separation applications is illustrated.

A quantity, referred to as effective pressure (P_{eff}), is introduced to compare the concentrating power of different microporous solids. Effective pressure is of utility in catalytic systems as it indicates the pressure that would have to be applied to an ideal gas to attain a comparable concentration of reactants. The magnitude of P_{eff} is related to adsorptive properties and is influenced by the surface area, pore size, pore distribution, polarity, dispersion, and reactivity of the support.

INTRODUCTION

The desirable properties of porous carbonaceous adsorbents for separation processes[1] and as novel supports for catalytic reactions[2] have motivated fundamental studies of gas-solid equilibria. In the first article in this series,[3] adsorption isotherms were analyzed through a series of equilibria of the form shown in Equation (1).

$$S_{(s)} + A_{(g)} \leftrightarrow SA_{(s)} \qquad (1)$$

To afford generality for the model and encompass physisorption, Equation (1) describes a process and not necessarily a chemical reaction. In the case of a single adsorption process, the equilibrium constant for this process is rearranged to produce the equilibrium expression of Equation (2),

$$[SA]_s = \frac{n_1 K_{1,ad}[A]_g}{1+K_{1,ad}[A]_g} \quad (2)$$

where $K_{1,ad}$ is the adsorption equilibrium constant, n_1, is the capacity of the solid for the adsorption process, $[SA]_s$ is the amount of adsorbate on the solid, and $[A]_g$ is the concentration (in atm) of the gaseous adsorptive in equilibrium with the solid.

In porous solids, adsorption processes of different affinities are expected to occur giving rise to a series of equilibria. Each of the i equilibria is described by an equation similar to Equation (1) and each corresponds to a different adsorption process, $S_i A_{(s)}$, in Equation (1), with a corresponding equilibrium constant, $K_{i,ad}$,and capacity n_i . The equilibria involving multiple processes are related to the total amount of adsorbate on the solid, $[SA]_s$, by Equation (3).

$$[SA]_s = \sum_i \frac{n_i K_{i,ad}[A]_g}{1+K_{i,ad}[A]_g} \quad (3)$$

It is important to emphasize that these processes may involve either a reversible chemical reaction, in which case n_i refers to a site, or a physical adsorption process, in which case n_i refers to a process capacity. The number of processes, i, employed are the minimum needed to fit all the points of the adsorption isotherm as accurately as they are known. A given $K_{i,ad}$ value may include groups of processes whose individual $K_{i,ad}$ values are so similar that experimental precision does not allow this analysis to distinguish them. Fortunately, for most applications each of these groups can be treated as an average process.

Even in the case of a two process system, solving for the points of a single adsorption isotherm with four unknowns (n_1, $K_{1,ad}$, n_2 and $K_{2,ad}$) leads to a very shallow

minimum in the data fit and uncertain parameters.[3,4] Collecting isotherms at a series of different temperatures has been shown to circumvent this problem.[3] Since the n_i values of the model are expected to be temperature independent, each new temperature introduces only new K_{ad}'s as unknowns. For a three process fit, the 6:1 ratio of unknowns to isotherms at one temperature becomes 9:2 at two temperatures, 12:3 at three, 15:4 at four, etc. The resulting higher ratio of knowns to unknowns leads to a better definition of the minimum in the fit of the combined data set. As an added benefit, the temperature dependence of the $K_{i,ad}$'s provides the enthalpies of the adsorbate interactions for each of the i-processes involved.

This procedure is complimentary to the BET[5,6,7] method and the advantages of the multiple process analysis are the quantitative thermodynamic measures of the interactions obtained. In the first article in this series,[3] data were presented for N_2, CO, and CO_2 interacting with a porous carbon, Ambersorb® 572(A-572), and a porous pyrolyzed polyacrylonitrile adsorbent, PPAN.[1,8,9] The data at several different temperatures are fit very well to three processes when each n_i is required to be the same at every temperature.[3] The three processes were interpreted to correspond to gas adsorption on the surface of the very small micropores (i=1), gas adsorption on the surface of larger micropores (i=2), and gas and multilayer adsorption to the rest of the micropores and solid surface (i=3). In this article, the number of different gases employed in the original study is expanded to include larger adsorptives and an acceptor molecule in order to advance our understanding of the fundamental interactions involved in gas-solid equilibria and in order to quantify the adsorption

processes for different solids. An improvement in the methodology of the earlier analysis[3] is the simultaneous fitting of adsorption isotherms at all temperatures studied. This new procedure leads to an improvement in the K's, n's, and ΔH's reported earlier.

In interpreting each of the isotherms, the process capacities n_1, n_2, n_3 and adsorbate molar volumes will be compared to pore volumes from conventional N_2 porosimetry methods. In addition, the n-values and the literature reported cross sectional areas of the adsorptive are used to calculate an area[10] that can be compared to surface areas from conventional N_2 BET analyses.[7] Finally, $-\Delta G$ and $-\Delta H$ values are correlated to molecular properties of the adsorbate leading to a definition of the dispersion and polarity characteristics of the adsorbent. These comparisons and correlations are very important for they indicate that the parameters from the data fit have meaning in the context of the model employed.

EXPERIMENTAL

Gases and Supports.

The gases He and N_2 (99.99% purity) were obtained from Liquid Air, Inc. The gases CH_4, CO, CO_2, C_2H_6 and C_3H_8 (99.99% purity) were purchased from Matheson Gas Company. The gas SO_2 was obtained in a lecture bottle from Aldrich. The adsorbents were desorbed under a vacuum of $<10^{-3}$ torr at 200 °C for at least 8 hours before adsorption data was collected.

Characterization of Supports.

Carbon, hydrogen, and nitrogen analyses (C, H, N) were performed by the University of Florida elemental analysis laboratory: A-572, %C = 91, %H = 0.3, %N = 0; PPAN, %C = 70, %H = 1.5, %N = 5.0. Surface area and pore volume data were obtained from the N_2 isotherm at 77 K using a Micromeritics® ASAP 2000 Instrument. Surface areas were determined using a five point Brunauer-Emmett-Teller (BET) calculation.[6,7] Micropore volume was determined using the Harkins-Jura t-plot model with thickness parameters from 5.5 - 9.0 A.[11] The Barrett-Joyner-Halenda (BJH) adsorption curve was used for calculating meso- and macropore volumes.[12] All calculations were carried out using the Micromeritics® ASAP 2000 Instrument software.[13] A-572 has a surface area of 1160 m^2/g and PPAN 880 m^2/g. The micropore volumes are 0.43 and 0.33 mL/g respectively; mesopore volumes are 0.28 and 0.13 mL/g and macropore volumes 0.21 and 0.09 mL/g.

Adsorption Measurements.

The uptake of gases by the solids was measured using the Micromeritics® ASAP 2000 Chemi system. All adsorptions were reported at values between 0.5 and 760 torr which is the limit of our instrumentation and which reflects our interest in the catalytic behavior and adsorptive applications of these materials at ambient pressures.

Adsorption measurements were obtained on the Micromeritics® instrument after the samples were degassed at 200 °C for a minimum of 8 hours under vacuum. The

procedure was previously described.[3] The adsorption isotherms are available as supplementary material.

Experience in the multiple equilibrium analysis of adsorption isotherms enables us to describe optimal conditions for data collection. An accurate characterization of a process requires collecting 10-20 data points that cover a range from zero to at least 70% of the process capacity. This is best accomplished by measuring an isotherm ten degrees above the critical temperature and carrying out a preliminary analysis. Subsequent experiments should use temperatures and pressure increments that permit roughly 10-20 data points to be collected as the capacity of n_1 is filled and a similar number at a temperature region at which n_2 is filled to 70% capacity. The pressure increments will vary with temperature. A good definition of the K's and n's for processes 1 and 2 will result.

To define process 3, experiments should be carried out at or below the critical temperature where 70% of the n_3 capacity can be filled by 1 atm external pressure. At these temperatures it will be very difficult to collect many data points before process 1 is completed so K_1 will be poorly defined. However, n_1 is known from studies at higher temperatures and a more accurate K_1 can be calculated from the van't Hoff plot.

The experimental adsorption isotherms were analyzed using Equation (4) where $[SA]_s$ is the experimentally measured total number of millimoles of gas adsorbed per gram of solid, P_{atm} is the equilibrium gas pressure in atmospheres, n_i the available capacity for process i in millimoles per gram of solid and, $K_{i,ad}$ is the adsorption equilibrium constant for process i in atm^{-1}. The best fit n_i and $K_{i,ad}$ values were

determined using a modified simplex routine designed to solve Equation (4) for a series of isotherms at a series of temperatures.

$$[SA]_s = \sum \frac{n_i K_{i,ad} P_{atm}}{1 + K_{i,ad} P_{atm}} \qquad (4)$$

In our previous work, adsorption isotherms were obtained at various temperatures and the data set for each individual temperature was fit to three processes. The n_i values were determined by a series of iterations between the individual temperature data sets. In this article the determination of the n's and K's was carried out by analyzing the data sets at all temperatures simultaneously. In order to prevent the minimization routine from settling into a false minimum, (i.e., one where the minimum value for the sum of the residual is not obtained), the initial guesses of the parameters have to be close to the actual values. This is accomplish as outlined below.

The measured adsorption pressure data is converted to relative pressure and the amount of gas adsorbed is converted from cc/g to mols/g. Langmuir isotherms, i.e., pressure divided by mols ads [(P/Po)/n] vs. pressure (P/Po), are prepared for each temperature. This plot is divided into three linear regions. A Langmuir analysis of the slopes and intercepts from a least square determination provide initial values for the n's and K's in the non-linear simplex minimization of the multiple temperature data fits. It should be noted that the initial n_1 and n_2 values from the Langmuir analysis are in close agreement at all temperatures. In the combined data fit, the n's are allowed to vary with the constraint that they be the same at all temperatures. The first iterative set of best fit n's and K's result. These values are used as initial guesses for a second

minimization leading to new n's and K's. The process is repeated until the initial guesses and final n's and K's are the same.

For data sets involving adsorbates that have only been studied well above the critical temperature, the process described above is employed, but more iterations are required to achieve minimization.

RESULTS AND DISCUSSION

Supports and Adsorbates.

Two chemically different porous carbonaceous supports were studied with a series of different gases. This research has focused on the carbonaceous adsorbents Ambersorb® 572 (A-572) which is made by pyrolyzing sulfonated, macroreticular polystyrene beads and a pyrolyzed polyacrylonitrile (PPAN) material.[1] Both solids have BET surface areas around 1000 m^2/g and a distribution of pores including micropores, mesopores, and macropores. Measurements using these adsorbents enable us to compare properties of a predominantly carbon containing solid material and one with extensive nitrogen donor functionality.

The gases used in the adsorption measurements, Table 1, were selected to encompass a range of polarity, polarizability, and acceptor properties. Helium is taken as a reference zero point to determine the dead volume of the support and its properties, as well as those for other gases studied, are listed in Table 1. The non-polar adsorptives N_2 and CH_4 as well as the slightly polar CO, are noncondensible gases since the critical temperatures of these probes are below the temperature of the

measurements. These probes are subject to solid-probe and bilayer interactions, but do not give rise to capillary condensation in the mesopores and large micropores. Condensible adsorptives are, in principle, subject to both solid-probe and multilayer interactions, as well as capillary condensation. These adsorptives were also selected to provide a range of properties.[14,15] Propane and ethane are non-polar, CO_2 is quadrupolar, and SO_2 is a polar adsorptive with acceptor tendencies.[16] This range of properties enables one to characterize the dispersion, polarity, and donor properties of different adsorbents.

Figure 1 shows adsorption isotherms for a noncondensible gas (CO) at -93 °C and a condensible adsorptive (SO_2) on A-572 at 25 °C. The points in Figure 1 correspond to experimental data, and the lines are generated from the best fit analysis using Equation (4). All of the adsorptives studied with PPAN and A-572 produce the Type I isotherms shown in Figure 1 at pressures of 1 atm or less.

Analyses of Noncondensible Gases.

Table 2 summarizes the results of data fits for the adsorptives where n_i is the capacity of the solid for the i^{th} adsorption process in millimoles per gram of solid and $K_{i,ad}$, the adsorption equilibrium constant in atm^{-1}, is a measure of the affinity of the probe for the solid surface. For the noncondensible probe molecules, capillary condensation does not occur, but formation of a second layer of adsorbate could be included in n_3 if K for the bilayer interaction is comparable to that for the solid-gas interaction, vide infra. It is also important to emphasize that as in all heterogeneous

equilibria, the $K_{i,ad}$ is an average value of adsorption by different solid pores that have K_{ad} values close enough to be treated, within experimental error of the measurement, as a single process in the data workup.

The more accurate parameters in Table 2 for N_2 and CO differ slightly from earlier values that were calculated by fitting each temperature separately. The K_{ad} values for all the gases studied are such that adsorption by the second and third processes begins before the first process has been completed. The set of $K_{i,ad}$ and n_i values make it possible to calculate the individual isotherms for the three processes, thus indicating the contribution of each process to the total isotherm. This information is presented for the adsorbate CH_4 on A-572 at -43 °C in Figure 2. Note that even at low pressures, all three processes contribute simultaneously to the adsorption isotherm. At the highest pressures studied, process 1 is completed, there is 50% capacity remaining for process 2 and 90% capacity remaining for process 3. When experimental data are solved for two unknowns, in this case, K_i and n_i, a process has to be at least 50% completed to obtain accurate parameters.[17] Thus, the parameters for processes 1 and 2 are most accurately known and those for process 3 are least accurately known for the non-condensible gases. Studies at higher pressures or lower temperatures are needed for a more accurate determination of process 3.

Analyses of Condensible Gases.

The isotherms for the condensible gases (C_3H_8, C_2H_6, CO_2, SO_2) show that there is more adsorption than is the case for the non-condensible gases, see Figure 1.

Condensible adsorptives clearly require three processes for the data fit and support the adding of a third process for the fit of the noncondensible gases. The resulting values of K_i, n_i and ΔH_i for condensible adsorptives are also given in Table 2.

For those condensables which have large errors in the values of $K_{3,ad}$ and n_3, the third process at the respective temperatures is far from being completed at the pressures studied. For those condensables that have large K_1 values with large errors, process 1 is essentially complete at very low pressures after the first three data points are measured. This leads to large errors in the actual numbers for K_1, but a good definition of n_1. If there is need to know K_1 more accurately, ten or more measurements could be made at lower pressures than used in this study or the K's from the higher temperatures can be used to calculate K at lower temperatures from the enthalpy and entropy.

Insights from the Equilibrium Capacities.

The main advantages of the multiple equilibrium model are the detailed insights that result concerning adsorption. The n_1, n_2, and n_3 values (in moles/g) can be multiplied by the molar volume of the adsorbate as a liquid to produce the volumes available for processes 1, 2, and 3. This assumes that adsorbed gas molecules pack as effectively on the solid as they do in the liquid. The results are given in Table 3. The sum of the capacities for the three processes for N_2 adsorptions on A-572 is 0.261 mL/g. The capacity for CO is similar at 0.271 mL/g. These quantities are less than the micropore volume of 0.43 mL/g obtained from N_2 porosimetry and suggest that the

entire adsorption isotherms for these gases correspond to processes occurring in ~60% of the micropore volume. This is an exciting result for it indicates that the micropore volume can be resolved into different components by these equilibrium measurements.

The capacities of processes 1 and 2 are probe dependent for N_2 and CO on A-572. CO has a smaller molar volume than N_2 and could be accessing ~0.006 mL of smaller pores not available to N_2. However, more CO capacity than N_2 capacity is also available for process 2 where small pore dimensions would not exclude adsorbate. This suggests that by virtue of its slight polarity, slightly larger pores can be used by CO for both processes 1 and 2 than by N_2. The values of n_3 are not known accurately enough to interpret the 2% difference for these two adsorbates.

The data in Table 3 for N_2 and CO on PPAN show a similar pattern to A-572 with 0.201 (N_2) and 0.210 (CO) mL/g total capacities using ~60% of the available 0.33 mL/g of micropore volume. Even though the total micropore volume is less, the capacity of PPAN for process 1 is larger than that for A-572 and only a slight difference exists in the capacities for N_2 and CO. PPAN uses 5.4% of the micropore volume for process 1 for N_2 and A-572 uses 4.4%. The other main difference in the two solids is the capacity for process 3.

The methane, ethane, and propane capacities of A-572 dramatically illustrate the probe dependence of the capacities. At least 62% of the pores available to CO for process 1 on A-572 are not accessed by the larger adsorbate CH_4. Since methane may use some of the CO process 2 pores for process 1, as suggested by a lower n_2 value for CH_4 than CO, none of the process 1 pores for CO may be accessed. The

process 3 capacity is better defined for CH_4 and is the same as N_2 and CO within experimental error of their n_3 values. It is interesting to note that process 1 and 2 capacities for CO_2 are similar to CH_4. The capacity for process 3 is considerably larger suggesting that the larger micropores can be used by CO_2 but not CH_4 for process 3.

The ethane and propane capacities indicate that 77 and 95% of the micropores are used for the three processes, respectively. The 5% not used for propane are the smaller process 1 pores of CO. For these adsorbates, some of the pores used in process 2 for CO are now used for process 1 for ethane and propane, while process 2 for ethane and propane, utilize process 3 pores for CO. The process 3 pores for propane are not used for any of the three processes for CO at the temperatures studied. The total volume of A-572 for processes 1 to 3 for SO_2 is 0.52 mL which exceeds the micropore volume. Thus, SO_2 utilizes the accessible micropore volume and some of the small mesopores. The probe dependence of the various adsorption capacities emphasizes the incomplete characterization of a solid that is provided by only nitrogen porosimetry pore volume considerations.

The greatly reduced capacity of PPAN for propane (0.28 ml) is consistent with its smaller micropore volume (0.33 ml) with the small process 1 pores of CO being inaccessible.

The probe molecules studied suggest that the 0.43 ml micropore volume of A-572 consists of a group of smallest pores, component (I), with ~0.01 mL/g capacity, a second group of slightly larger pores, component (II), with a capacity of 0.07 mL/g, the

next larger group, component (III), with a capacity of 0.20 mL/g, and a group of largest micropores, component (IV), with a volume of 0.15 mL/g.

PPAN has a group of smallest pores (I) with ~0.02 mL/g capacity, a second group (II) with ~0.06 mL/g, the third group (III) at 0.13 mL/g, and a fourth group at 0.14 mL/g. PPAN has twice the capacity of smallest pores but a 65% lower volume for component (III) pores than A-572.

The smallest probes (N_2 and CO) utilize components (I) to (III). Methane uses only a few percent of the component (I) pores and the remaining adsorption is in components (II) and (III). Larger molecules (C_2H_6, CO_2, C_3H_8, SO_2) adsorb in components (II), (III) and (IV). Using the molar volume of liquid CH_4 to provide an upper limit estimate of the van der Waals molecular volume and thus the diameter of the sphere produces 4.93 Å. Thus the component 1 pores of A-572 not accessed by CH_4 are less than 4.9 Å in diameter.

The surface areas corresponding to the above groupings of pores can be estimated by multiplying the millimoles of gas adsorbed by the cross sectional area per millimole. In view of multilayer formation this quantity provides an upper limit for the solid surface area involved in the process. Table 3, contains the surface areas that would correspond to a monomolecular film of the adsorbate on the solid for each of the three processes. Comparing the areas occupied by CO, N_2, and CH_4 with the micropore surface area suggests that processes 1 and 2 for these adsorptives involve monolayer adsorption of the gas on the solid. On the other hand, multilayer formation is definitely involved in the larger micropores with the condensible gases propane and

SO_2. This coverage suggests that process 1 involves gas molecules interacting with both walls of a slit shaped pore; in process 2 a gas molecule interacts with one wall strongly and the second wall weakly or two molecules are adjacent to each other on separate walls interacting with the walls and each other; and in process 3, adjacent gas molecules interact with separated opposite walls and have a third or fourth molecule in between.

Comparison of Adsorptive Affinities

The affinities of the adsorbates for the solids have been quantified with the equilibrium constants for adsorption by the three processes ($K_{i,ad}$). The temperature dependence of K gives the enthalpies for the three processes which are summarized in Table 2. The ln K vs. 1/T plots are shown for different adsorptives on A-572 in Figure 3. The magnitudes of the enthalpies of adsorption on these solids are indicative of a physisorption process and are dependent on the adsorbate polarizability and polarity. The least squares lines for the three non-polar (N_2, CH_4, C_2H_6) and two slightly polar (CO, C_3H_8) adsorptives are given by:

A-572	$-\Delta H_1 = 1.19(\pm 0.7)\alpha + 3.00(\pm 0.6)$	$R^2 = 0.942$	(5)
	$-\Delta H_2 = 1.07(\pm 0.9)\alpha + 2.58(\pm 0.3)$	$R^2 = 0.981$	(6)
	$-\Delta H_3 = 1.25(\pm 0.07)\alpha + 0.90(\pm 0.3)$	$R^2 = 0.989$	(7)
PPAN	$-\Delta H_1 = 1.30(\pm 0.12)\alpha + 2.71(\pm 0.4)$	$R^2 = 0.982$	(8)
	$-\Delta H_2 = 1.15(\pm 0.24)\alpha + 2.02(\pm 0.9)$	$R^2 = 0.921$	(9)

Plots of $-\Delta H$ vs. polarizability (α) show the expected deviation of more adsorption for quadrupolar CO_2 and the polar adsorptive SO_2.

It is significant that the enthalpies for N_2, CO, CH_4, C_2H_6,and C_3H_8 fall on a straight line for process 1 even though our analysis of the capacities indicated that a different distribution of micropores is utilized for the different gases. Thus, process 1 utilizes pore widths of molecular dimensions. Process 2 involves dimensions up to two molecules at their van der Waals separation interacting with the walls and each other. Process 3 involves larger pores in which molecules on opposite walls weakly interact with the walls and bilayer of multilayer absorptive molecules. In this manner, a given process, i, is fundamentally the same for all the probes studied, but different dimension micropores are utilized for the i'th process of each probe.

The coefficients on α characterize the solid's effective surface polarizability for each process. Within experimental error, the α-values of the two solids are the same. These equations can be used along with the polarizabilities of other non-polar molecules to predict their enthalpies of interaction with A-572 and PPAN. The deviations of polar gas molecules from the polarizability plot can be used to further measure solid properties. As more data become available, the magnitude of the miss can be correlated to the dipole moment or other measures of adsorbate polarity if these deviations arise from non-specific interactions. The slope of the line of the deviations versus adsorbate polarity gives a constant that characterizes the solid polarity. If the deviations arise because of specific donor-acceptor interactions, attempts can be made to characterize the surface donor or acceptor strength by fitting the deviations to the E

and C model.[16] The limited data available at present do not permit this further characterization of the surface properties of A-572 and PPAN and the above discussion is presented to show the potential of this model.

With the data on hand, it is possible to distinguish between non-specific and specific interactions as the cause of the deviation of polar adsorbates from Equations (5) - (9). The van der Waals constant, a, measures the interaction of a gas molecule with itself. As a increases, the intermolecular attractive forces increase. For gases that do not undergo specific intermolecular interactions e.g., hydrogen bonding, a measures the relative non-specific dipolar and dispersion intermolecular interactions of gases. The square root of a should measure trends in these properties toward a given molecule. As shown in Figure 4, there is a linear relationship between the square root of the van der Waals constant, a, and the enthalpy of interaction of the adsorptive with A-572 for process 1. Thus, non-specific interactions of the gas with A-572 and PPAN provide the driving force for adsorption. With the exception of SO_2 on PPAN, all of the adsorbates investigated with A-572 and PPAN fall on or near a best fit line whose Equations are given as (10 - 14).

A-572	$-\Delta H_1 = 3.02(\pm 0.26)a^{1/2} + 1.54(\pm 0.53)$	$R^2 = 0.96$	(10)
	$-\Delta H_2 = 2.66(\pm 0.14)a^{1/2} + 1.31(\pm 0.29)$	$R^2 = 0.98$	(11)
	$-\Delta H_3 = 3.24(\pm 0.15)a^{1/2} - 0.75(\pm 0.31)$	$R^2 = 0.988$	(12)
PPAN	$-\Delta H_1 = 3.32(\pm 0.33)a^{1/2} + 1.16(\pm 0.61)$	$R^2 = 0.98$	(13)
	$-\Delta H_2 = 2.96(\pm 0.57)a^{1/2} + .58(\pm 1.10)$	$R^2 = 0.93$	(14)

For many applications of porous solids, the equilibrium constants for the various processes are of prime concern. Figure 5 shows the linear relationship between $-\Delta G$ and $-\Delta H$ for processes 1 and 2 on PPAN and A-572. Thus, free energies will correlate to polarizability and the square root of the van der Waals $\underline{a}$ parameter in the same manner as $-\Delta H$. The plot of $-\Delta G$ for A-572 vs. $\underline{a}^{1/2}$ is shown in Figure 6 for processes 1 and 2. This plot has practical utility for the prediction of $-\Delta G$ and thus equilibrium constants for binding gas molecules to these solids via processes 1 and 2.

In the correlations of ΔH to polarizability and $\underline{a}^{1/2}$, the slopes of the lines are within experimental error for a given process on PPAN and A-572. The chemical compositions of these two solids differ and the presence of nitrogen in the aromatic rings of PPAN has little influence on the polarizability and polarity of the π-system comprising the solid surface.

Specific donor-acceptor interactions of adsorbate molecules with a solid surface are expected to give rise to deviations in the van der Waals plots if these interactions are stronger than those in the gaseous adsorbate. We conclude that the solid-adsorbate interactions for the systems correlated by Equations 10-14, involve non-specific interactions. The possibility exists that there may be a small concentration of catalytically active donor sites. The fact that the adsorption data for the lowest measured pressures at the higher temperatures are fit by $K_{1,ad}$ suggests that if any strong donor-acceptor sites are present they must be at concentrations per gram of solid less than 10^{-5} moles per gram.

In contrast to the behavior of SO_2 on A-572 (3-process fit, correlations of log K and ΔH to $\underline{a}^{1/2}$), this absorptive on PPAN requires a four process fit with process 1 producing a large K and ΔH that leads to deviations in the plot vs. $\underline{a}^{1/2}$. This result indicates a specific donor-acceptor interaction of SO_2 with donor sites on PPAN. The amount of this donor functionality is 0.66 millimoles/g. The enthalpy of 17.1 kcalmole^{-1} contains both a dispersion and donor-acceptor component. Consistent with this interpretation, the log K and $-\Delta H$ for process 2 would correspond to that of process 1 on A-572, process 3 would correspond to process 2 and process 4 to process 3. The corresponding values of K and $-\Delta H$ for processes 2-4 are reasonable in the context of Equations 13 and 14 as well as in the log K counterparts.

Practical Utility of the Data in Table 2

The multiple equilibrium model leads to important practical as well as fundamental information for characterizing porous solids. The thermodynamic parameters permit comparison of the affinity of a solid for different adsorptives. The relationship shown in Figure 6 permit the estimation of $K_{1,ad}$ for any small molecule whose van der Waals parameter is known. This information is important for selection of a solid material as a support for a catalytic reaction or for separation applications. Porosity is expected to produce desirable results in a catalytic reaction when the products have a lower affinity for the solid, i.e. a smaller $K_{1,ad}$, than the reactants. In using these carbonaceous adsorbents to separate mixtures of these gases, the best separation will be achieved for materials with a large difference in intermolecular

attraction. For the comparison of different solids as adsorbents, consider CH_4 as the adsorptive. It is a nonpolar, nonreactive, and noncondensible gas. A-572 has a capacity of 0.25 mL/g whereas PPAN's is 0.21 mL/g. Process 1 has a larger capacity, but a smaller K is found for PPAN than for A-572. Thus, if CH_4 needed to be removed from a dilute gas, A-572 would be a more effective material, but would have a lower capacity if only the process 1 pores were utilized.

The use of carbon for storage and transport of CH_4 is an active research area. This study would suggest that, based on capacity, A-572 is a better storage solid than PPAN at one atmosphere external pressure. However, the smallest 4% of the micropore volume of A-572 is not utilized nor is the larger 45% of the micropores, the mesopores, or the macropores. These results indicate how to modify the design of the solids pore distribution to produce a more desirable material for this application. Using the diameter of 4.93 Å for CH_4, calculated from the molar volume of liquid CH_4, an optimal storage material, involves synthesis of a solid with a large pore volume whose pore diameters range from 4.9 to 10 Å.

Effective Pressure.

The adsorption equilibrium constants ($K_{i,ad}$) provide a quantitative description of the amount of adsorption of an adsorptive. For heterogeneous catalytic processes, the ability of the porous support to concentrate reactants around the catalytic center can lead to increased reaction rates. For a homogeneous gas phase reaction, the concentration is increased by increasing the pressure of the gas. It is enlightening to

compare the concentration effect of porosity by calculating an effective pressure, P_{eff}, that would have to be applied to an ideal gas to obtain a concentration in the gas phase equal to the moles of gas adsorbed per ml of pore volume within the support. The number of moles of gas adsorbed varies with the pressure of gas over the solid, the temperature, and the type of adsorbent. For any given adsorptive, P_{eff} provides a facile comparison of the concentrating power of solid supports. For illustrative comparisons of solids and adsorptives, P_{eff} is calculated at an external pressure of 1.0 atm and room temperature. Other temperatures and pressures can be used depending upon the desired application of the solid. Using the ideal gas law, the number of moles adsorbed, and the total micropore volume of the solid, Equation (10) is used to calculate P_{eff}.

$$P_{eff} = \frac{n_{ad,\,1\,atm} RT}{V_{micropores}} \qquad (10)$$

This quantity represents the pressure that would have to be exerted on an ideal gas in a container whose volume corresponds to the volume of the micropores in order to obtain a comparable concentration of gas. By using the total micropore volume, we are in effect assuming that processes 1, 2, and 3 provide a reactant reservoir for catalysis in all the micropores.

For many reasons, P_{eff}, is a semi-quantitative concept. A gas under these conditions would not be ideal, the adsorbate is distributed over all the adsorption processes, and condensables are involved in multilayer interactions. The utility of this quantity is to provide a dramatic comparison of the influence of porosity on reactivity by expressing the influence of porosity in terms of the more widely appreciated influence

of pressure on the reactivity of a homogeneous gas phase reaction. The influence would be even greater than P_{eff} indicates for reactions involving only process 1 or only processes 1 and 2 pores.

Table 4 summarizes the number of moles of various gases adsorbed at an equilibrium pressure of 1.0 atm, and the calculated P_{eff}, for all of the isotherms measured for PPAN and A-572. Again, the adsorptives can be separated into two categories: noncondensable and condensable. The first group of gases cannot be liquefied at any effective pressure. The second group of gases can be condensed if P_{eff} is large and the temperature is below the critical temperature. The P_{eff} for condensible gases is unreasonably large consistent with these materials condensing as liquids through multilayer adsorption within the micropores and small mesopores at the internal pressures inside the support. Reactions of these materials approach concentrations corresponding to reactions of the liquid. Under these conditions, the pressure generated by the solid porosity can be assumed to be the partial pressure of the liquid adsorptive and P_{eff} is simply a measure of the moles of adsorbate per unit volume of solid.

The data in Table 4 indicates that although A-572 has a greater capacity for the various adsorptives, the concentrating power of PPAN is greater. For example, more CO is adsorbed by A-572 (0.56 mmols/g solid) than by PPAN (0.50 mmols/g solid). Since PPAN has a much smaller total micropore volume than A-572, the effective pressure of CO in the pores of PPAN (37.2 atm) is larger than in A-572 (32.0 atm). The same comparison can be made for all of the adsorptives.

The utilization of the data in Table 4 to illustrate the importance of porosity for catalytic reactions can be illustrated. Consider a reaction of CH_4 that requires an external pressure of 70 atm in order to occur at room temperature. If PPAN is the catalyst, with active sites in the micropores, the reaction can be carried out at one atm external pressure and a higher CH_4 concentration attained in the PPAN catalyst than with the gas at 70 atm. It should be pointed out that if PPAN or A-572 were used as a support to which a catalyst is added, the process capacities and moles of gas adsorbed by the supported catalyst would have to be redetermined to calculate the effective pressure.

If the P_{eff} indicates that one of the reactants is present as a liquid in the pores, and the other a gas, the reaction in the porous solid is comparable to carrying out a liquid-gas reaction. Condensation of the liquid reactant could slow transport of the gaseous reactant to the catalyst, and the reaction will be slowed. If the reaction product is adsorbed more effectively than the reactants, product inhibition will occur. For these reactions, microporosity would be detrimental. These considerations suggest that high surface area which often parallels high porosity, does not provide a complete picture of catalytic reactivity. The information from equilibrium analyses has the potential to lead to a major advance in the understanding of and a rational basis for support selection for heterogeneous catalysis and adsorption.

CONCLUSIONS

Adsorption isotherms as a function of pressure for non-acceptor adsorptives at multiple temperatures support a three process equilibrium model for the two carbonaceous adsorbents A-572 and PPAN. Comparison of the volume of gas adsorbed with the pore volume from H-J t-plots and BJH analyses indicates that the three processes are occurring in the micropores. The surface areas of non-condensible adsorbate molecules are comparable to the solid micropore surface areas suggesting a monomolecular coverage. Process 1 is occurring in slit shaped micropores whose walls are separated by van der Waals molecular dimensions, process 2 occurs in micropores of dimensions slightly larger than the molecular dimensions and process 3 utilizes the remaining micropores with monolayer and bilayer coverage. Condensible gases undergo multilayer interactions in the larger pores.

The model provides free energies and enthalpies for different probe molecules participating in the three processes. These results correlate with the polarizabilities of non-polar molecules and provide a measure of the solid surface polarizability showing that A-572 and PPAN are similar. Deviations of CO_2 and SO_2 on A-572 from the polarizability plot and their correlation to a van der Waals plot suggest these interactions involve non-specific van der Waals forces. The magnitude of the deviations of SO_2 from the polarizability plots suggest PPAN is a more polar surface than A-572. These conclusions about surface polarity and polarizability are supported by comparison of the ΔG values of non-polar and polar adsorbates on the two solids.

The correlation of $-\Delta G$ and $\underline{a}^{1/2}$ enable one to predict the relative affinities of adsorbates whose van der Waals constants are known.

In addition to the adsorption equilibrium constant, the effective pressure is proposed to indicate the ability of solid supports to concentrate gases in catalytic systems. In the area of catalysis, high surface area is normally desired in order to get high reactivity per gram of catalyst. The concentrating effects of highly porous supports add a second factor to surface areas to consider in the interpretation of results and selection of solid materials as catalyst supports.

ACKNOWLEDGMENTS

This work was supported by Rohm and Haas and ERDEC/ARO. The authors thank Dr. Phil L. Rose for his donation of samples of PPAN and Dr. William Brendley for samples of A-572 carbonaceous adsorbents. Helpful comments from Dr. William Brendley and Dr. Stephen Maroldo are also acknowledged.

TABLE 1 Summary of Gases and Physical Properties[a]									
Probe Gas	MW g/mol	Polariz-ability[b] $Å^3$	Dipole Moment Debye[c]	Molar Volume[d] mL/mol	Critical Temp T_c °C	Normal Boiling Temp. T_{bps} °C	ΔH_v kcal/mol	van der Waals Const. [a]	Cross Sectional Area [$Å^2$]
He	4.00	0.205	0	32	-268.0	-268.9	.0194	0.03412	
N_2	28.01	1.74	0	35.4	-146.9	-195.8	1.33	1.390	16.2
CO	28.01	1.95	0.13	34.9	-140.2	-191.5	1.44	1.485	15.0
CO_2	44.01	2.91	0.18	40.0[b] (-37 °C)	31.04	-78.44	6.03 (sub)	3.592	21.8
CH_4	16.04	2.59	0	37.8	-82.60	-161.5	1.95	2.253	17.8
C_2H_6	30.07	4.47	0	52.6	32.3	-88.65	3.52	5.489	23.0
C_3H_8	44.10	6.29	0.084	75.0	96.7	-42.1	4.49	8.664	36.1
SO_2	64.06	4.28	1.61	43.8[b]	157.5	-10.0	5.96	6.714	27.1

a. Lange's Handbook of Chemistry, 13th Edition; McGraw-Hill: NY, **1985**. All data is from this source unless otherwise specified.

b. Handbook of Chemistry and Physics, 71st Edition; CRC Press: Florida, **1991**.

c. McClellan, A. L. Tables of Experimental Dipole Moments; W. H. Freeman and Company, San Francisco, **1963**, p. 123.

d. Molar Volume of the liquid at the normal boiling point. Hildebrand, J. H.; Prausnitz, J. M.; Scott, R. L. Regular and Related Solutions; Van Nostrand Reinhold Company: NY, **1970**, p. 217.

TABLE 2

Equilibrium Constants,[a] Enthalpies[b], Free Energies[c] and n-values[d]

N_2/A-572

$n_1 = 0.322 \pm 0.001$; $n_2 = 1.688 \pm 0.001$; $n_3 = 5.388 \pm 0.001$

$-\Delta H_1 = 4.5 \pm 0.2$; $-\Delta H_2 = 4.1 \pm 0.1$; $-\Delta H_3 = 3.1 \pm 0.1$

T °C	K_1	$-\Delta G_1$	K_2	$-\Delta G_2$	K_3	$-\Delta G_3$
-93	125 ± 46	1.7	11.5 ± 0.1	0.872	0.859 ± 0.008	-0.0545
-42	5.74 ± 0.09	0.802	0.92 ± 0.02	-0.038	0.121 ± 0.005	-0.969
0	1.1 ± 0.4	0.036	0.21 ± 0.08	-0.86	0.04 ± 0.03	-1.7
25	0.7 ± 0.1	-0.2	0.05 ± 0.02	-1.8	0.045 ± 0.007	-1.83

N_2/PPAN

$n_1 = 0.5006 \pm 0.0001$; $n_2 = 1.589 \pm 0.001$; $n_3 = 3.584 \pm 0.001$

$-\Delta H_1 = 4.6 \pm 0.1$; $-\Delta H_2 = 4.4 \pm 0.3$; $-\Delta H_3 = 2.7 \pm 0.1$

T °C	K_1	$-\Delta G_1$	K_2	$-\Delta G_2$	K_3	$-\Delta G_3$
-93	84 ± 5.0	1.59	8.70 ± 0.03	0.774	0.812 ± 0.003	-0.0746
-42	4.21 ± 0.9	0.659	0.66 ± 0.02	-0.189	0.12 ± 0.01	-0.99
25	0.46 ± 0.01	-0.46	0.043 ± 0.004	-1.87	0.043 ± 0.002	-1.87

CO/A-572

$n_1 = 0.5147 \pm 0.0001$; $n_2 = 1.934 \pm 0.001$; $n_3 = 5.324 \pm 0.003$

$-\Delta H_1 = 5.2 \pm 0.1$; $-\Delta H_2 = 4.7 \pm 0.3$; $-\Delta H_3 = 3.0 \pm 0.2$

T °C	K_1	$-\Delta G_1$	K_2	$-\Delta G_2$	K_3	$-\Delta G_3$
-93	204 ± 111	1.9	16.5 ± 0.5	1.003	1.2 ± 0.1	0.056
-42	8.4 ± 0.3	0.98	1.11 ± 0.06	0.0479	0.15 ± 0.02	-0.89
25	0.68 ± 0.02	-0.23	0.077 ± 0.005	-1.52	0.042 ± 0.002	-1.87

CO/PPAN

$n_1 = 0.5697 \pm 0.0001$; $n_2 = 1.802 \pm 0.003$; $n_3 = 3.642 \pm 0.03$

$-\Delta H_1 = 5.2 \pm 0.1$; $-\Delta H_2 = 3.3 \pm 0.4$; $-\Delta H_3 = 2.9 \pm 0.2$

T °C	K_1	$-\Delta G_1$	K_2	$-\Delta G_2$	K_3	$-\Delta G_3$
-93	243 ± 127	2.0	18.7 ± 0.5	1.048	1.3 ± 0.2	0.1
-42	8.8 ± 0.3	1.00	1.10 ± 0.08	0.0456	0.15 ± 0.04	-0.88
25	0.70 ± 0.03	-0.21	0.50 ± 0.01	-0.41	0.050 ± 0.005	-1.78

CH_4/A-572

$n_1 = 0.1775 \pm 0.0001$; $n_2 = 1.427 \pm 0.001$; $n_3 = 5.037 \pm 0.008$

$-\Delta H_1 = 6.6 \pm 0.5$; $-\Delta H_2 = 5.6 \pm 0.1$; $-\Delta H_3 = 4.4 \pm 0.1$

T °C	K_1	$-\Delta G_1$	K_2	$-\Delta G_2$	K_3	$-\Delta G_3$
-42	153 ± 100	2.30	13.7 ± 0.2	1.202	1.00 ± 0.03	-0.00140
0	15.9 ± 0.8	1.500	2.08 ± 0.03	0.397	0.238 ± 0.009	-0.779
25	4.9 ± 0.2	0.94	0.88 ± 0.02	-0.076	0.111 ± 0.007	-1.300
40	3.3 ± 0.2	0.73	0.56 ± 0.02	-0.36	0.081 ± 0.005	-1.57

TABLE 2 (Cont.)

CH_4/PPAN

$n_1 = 0.3778 \pm 0.0001$; $n_2 = 1.488 \pm 0.001$; $n_3 = 3.56 \pm 0.02$

$-\Delta H_1 = 6.6 \pm 0.2$; $-\Delta H_2 = 5.7 \pm 0.1$; $-\Delta H_3 = 4.7 \pm 0.1$

T °C	K_1	$-\Delta G_1$	K_2	$-\Delta G_2$	K_3	$-\Delta G_3$
-42	71 ± 2	1.95	8.0 ± 0.2	0.96	0.83 ± 0.07	-0.088
0	7.2 ± 0.2	0.16	1.20 ± 0.03	0.101	0.17 ± 0.01	-0.97
25	2.6 ± 0.1	0.56	0.49 ± 0.03	-0.42	0.08 ± 0.01	-1.5
40	1.69 ± 0.06	0.328	0.31 ± 0.02	-0.72	0.059 ± 0.006	-1.76

C_3H_8/A-572

$n_1 = 0.971 \pm 0.002$; $n_2 = 2.5 \pm 0.5$; $n_3 = 2.0 \pm 240$

$-\Delta H_1 = 10.0 \pm 0.2$; $-\Delta H_2 = 9.1 \pm 0.1$; $-\Delta H_3 = 8.6 \pm 0.8$

T °C	K_1	$-\Delta G_1$	K_2	$-\Delta G_2$	K_3	$-\Delta G_3$
25	$3200 \pm 7.3 \times 10^4$	4.8	67 ± 1	2.49	4 ± 2	0.7
40	1100 ± 3000	4.3	31 ± 2	2.14	2 ± 1	0.4
55	440 ± 390	4.0	16 ± 7	1.82	1 ± 8	-0.01
75	173 ± 42	3.56	8 ± 8	1.4	0.5 ± 9	-0.5
125	26 ± 3	2.58	2 ± 1	0.33	0.04 ± 1	-2.5
150	11 ± 1	2.05	0.8 ± 0.4	-0.1	0.04 ± 05	-2.7
175	6.6 ± 0.6	1.68	0.4 ± 0.2	-0.8	0.05 ± 0.2	-2.7

C_3H_8/PPAN

$n_1 = 0.819 \pm 0.001$; $n_2 = 1.7 \pm 0.2$; $n_3 = 1.2 \pm 230$

$-\Delta H_1 = 10.8 \pm 0.2$; $-\Delta H_2 = 9.2 \pm 0.1$; $-\Delta H_3 = 9.8 \pm 0.5$

T °C	K_1	$-\Delta G_1$	K_2	$-\Delta G_2$	K_3	$-\Delta G_3$
25	$3000 \pm 5.8 \times 10^4$	4.7	86 ± 24	2.6	4 ± 2	0.9
40	1000 ± 7100	4.3	39 ± 5	2.28	2 ± 1	0.4
55	490 ± 920	4.0	20 ± 1	1.96	1.1 ± 0.9	0.037
75	180 ± 50	3.59	9 ± 2	1.5	0.5 ± 3	-0.5
125	23 ± 4	2.47	2 ± 2	0.3	0.04 ± 2	-2.5
150	11.4 ± 0.9	2.048	0.9 ± 0.4	-0.08	0.04 ± 0.5	-2.8
175	5.4 ± 0.5	1.49	0.4 ± 0.2	-0.8	0.02 ± 0.3	-3.7

SO_2/A-572

$n_1 = 0.9322 \pm 0.0005$; $n_2 = 4.7 \pm 0.1$; $n_3 = 6 \pm 2$

$-\Delta H_1 = 9.4 \pm 0.2$; $-\Delta H_2 = 8.1 \pm 0.1$; $-\Delta H_3 = 8.0 \pm 0.1$

T °C	K_1	$-\Delta G_1$	K_2	$-\Delta G_2$	K_3	$-\Delta G_3$
25	360 ± 560	3.5	11.8 ± 0.3	1.463	2.8 ± 0.2	0.61
40	140 ± 35	3.06	6.1 ± 0.9	1.13	1.4 ± 0.9	0.22
55	66 ± 15	2.7	3.4 ± 0.8	0.80	0.8 ± 0.6	-0.1
75	30 ± 4	2.35	1.6 ± 0.5	0.32	0.4 ± 0.4	-0.6

TABLE 2 (Cont.)

SO_2/PPAN

$n_1 = .658 \pm 2E^{-5}$ $n_2 = .69 \pm .002$ $n_3 = 4.01 \pm 0.2$ $n_4 = 4 \pm 81$
$-\Delta H_1 = 7.1 \pm 2.4$ $-\Delta H_2 = 1.1 \pm 0.1$ $-\Delta H_3 = 4.8 \pm 0.4$ $\Delta H_4 = 4.8 \pm 0.4$

T °C	K_1	$-\Delta G_1$	K_2	$-\Delta G_2$	K_3	$-\Delta G_3$	$-K_4$	$-\Delta G_4$
25	$2E^4 \pm 1E^6$	5.9	209 ± 60	3.2	$14.2 \pm .3$	1.6	$.24 \pm .2$	-0.85
40	$2E^3 \pm 4E^4$	4.8	82.6 ± 20	2.7	$6.7 \pm .4$	1.2	$.2 \pm .3$	-1.2
55	900 ± 8600	4.4	36.2 ± 5.5	2.3	$3.4 \pm .1$	0.8	$.1 \pm .1$	-1.5
75	300 ± 800	3.9	14.0 ± 2.3	1.8	$1.5 \pm .9$	0.3	$.1 \pm .7$	-1.8

CO_2/A-572

$n_1 = 0.18 \pm 0.01$; $n_2 = 1.38 \pm 0.01$; $n_3 = 8.69 \pm 0.02$;
$-\Delta H_1 = 7.3 \pm 0.2$; $-\Delta H_2 = 6.2 \pm 0.3$; $-\Delta H_3 = 5.2 \pm 0.1$

T °C	K_1	$-\Delta G_1$	K_2	$-\Delta G_2$	K_3	$-\Delta G_3$
0	58 ± 4	2.21	6.46 ± 0.08	1.012	0.50 ± 0.01	-0.37
25	16 ± 12	1.7	3.2 ± 0.2	0.70	0.24 ± 0.02	-0.86
45	7.4 ± 0.9	1.26	1.64 ± 0.09	0.314	0.14 ± 0.01	-1.24
75	3.1 ± 0.1	0.79	0.52 ± 0.01	-0.45	0.06 ± 0.002	-1.90

C_2H_6/A-572

$n_1 = 0.4063 \pm 0.0003$; $n_2 = 1.95 \pm 0.07$; $n_3 = 3.7 \pm 7.6$
$-\Delta H_1 = 9.0 \pm 0.2$; $-\Delta H_2 = 7.7 \pm 0.1$; $-\Delta H_3 = 6.7 \pm 0.1$

25	220 ± 220	3.2	14 ± 8	1.57	1 ± 4	0.2
40	150 ± 200	3.1	9.4 ± 0.4	1.40	0.8 ± 0.2	-0.2
55	64 ± 16	2.7	4.9 ± 0.7	1.04	0.4 ± 0.4	-0.5
100	11.9 ± 0.6	1.836	1.23 ± 0.07	0.186	0.14 ± 0.04	-1.47

a. Gas-Solid Equilibrium Constant in atm^{-1}.
b. Gas-Solid Enthalpies of Interaction in kcal $mole^{-1}$.
c. Free Energies in kcal $mole^{-1}$.
d. Process capacity in millimoles/gram

TABLE 3

Volumes and Surface Areas for Processes 1-3

A-572[a]

	N_2 (MV = 35.4)[c]			CO (MV = 34.9)[c]			CH_4 (MV = 37.8)[c]		
process	mmols ads	ml ads	area[d]	mmols ads	ml ads	area[d]	mmols ads	ml ads	area[d]
n_1	0.32	0.0114	31	0.515	0.0178	46	0.178	0.00673	19
n_2	1.68	0.0595	164	1.93	0.0674	174	1.43	0.0541	153
n_3	5.38	0.1905	525	5.32	0.1860	481	5.04	0.1905	540
TOTAL	7.38	0.2614	720	7.76	0.2712	702	6.65	0.2513	712

PPAN[b]

	N_2 (MV = 35.4)[c]			CO (MV = 34.9)[c]			CH_4 (MV = 37.8)[c]		
process	mmols ads	ml ads	area	mmols ads	ml ads	area	mmols ads	ml ads	area
n_1	0.501	0.0177	49	0.57	0.0199	51	0.378	0.0143	41
n_2	1.59	0.0563	155	1.80	0.0628	163	1.49	0.0563	160
n_3	3.58	0.1267	349	3.64	0.1270	329	3.56	0.1346	381
TOTAL	5.67	0.2007	553	6.01	0.2097	543	5.43	0.2052	582

A-572[a]

	C_3H_8 (MV = 75.0)[c]			SO_2 (MV = 43.8)[c]			CO_2 (40)		
process	mmols ads	ml ads	area	mmols ads	ml ads	area	mmols ads	ml ads	area
n_1	0.97	0.0728	211	0.93	0.0408	152	0.18	0.0072	24
n_2	2.50	0.1875	543	4.75	0.2081	775	1.38	0.0552	181
n_3	2.00	0.1500	435	6.21	0.2720	1013	8.69	0.3476	1140
TOTAL	5.47	0.4103	1189	11.89	0.5209	1940	10.25	0.4100	1345

	PPAN[b]						**A-572**		
	C_3H_8 (MV = 75.0)[c]			SO_2 (MV = 43.8)[c]			C_2H_6 (MV = 52.6)		
process	mmols ads	ml ads	area	mmols ads	ml ads	area	mmols ads	ml ads	area
n_1	0.82	0.0614	178	0.66	0.0288	107	0.41	0.0214	56
n_2	1.70	0.1275	369	0.69	0.0302	113	1.95	0.1026	270
n_3	1.20	0.0900	261	4.01	0.1756	654	4.00	0.2104	554
TOTAL	3.72	0.2789	808	e	e	e	6.36	0.3344	880

a. A-572 pore volumes (ml): micro -0.43; meso -0.28; macro -0.21.
b. PPAN pore volumes (ml): micro -0.33; meso -0.13; macro -0.09.
c. Molar volumes of adsorptives. CO_2 value is at -37 °C.
d. Areas in m^2/g.
e. Values for process 4 are 4, 0.1752 and 653 and the totals are: 9.36, 0.41 and 1526.

TABLE 4

Summary of Calculated P_{eff} Values[a]

Solid	Gas	mmols gas adsorbed @ 1 atm	P_{eff}
PPAN	N_2	0.372	27.58
	CO	0.502	37.22
	CH_4	1.02	75.62
	C_3H_8	3.50	259.5
	SO_2	6.96	516.0
572	N_2	0.438	24.92
	CO	0.562	31.98
	CH_4	1.32	75.11
	C_2H_6	4.36	248.1
	CO_2	2.87	163.3
	C_3H_8	5.01	285.1
	SO_2	9.90	563.3

a. P_{eff} values in parentheses correspond to probes which are likely condensed in the pores.

REFERENCES

1. a) Neely, J. W. "Carbonaceous Adsorbents for the Treatment of Ground and Surface Waters," **1982**, Marcell Dekker, Inc.: New York, p. 80.

   b) (1) Neely, J. W. "Partially Pyrolyzed Macroporous Polymer Particles Having Multimodal Pore Distribution with Macropores Ranging from 50-100,000 Angstroms" *U.S. Pat. #4,040,990*, **1977**.

   (2) Amick, D. R. "Sulfone-Crosslinked Polystyrene Ion Exchange Resins and Process of Manufacture," U.S. Pat. #4,177,331, **1979**.

   (3) Maroldo, S. G.; Betz, W. R.; Borenstein, N. "Carbonaceous Adsorbents from Pyrolyzed Polysulfonated Polymers," U.S. Pat. #4,839,331, **1989**.

   c) Ambersorb® 572 is commercially available from the Rohm and Haas Company. PPAN is a proprietary, high surface area, pyrolyzed polyacrylonitrile product supplied to us by Rohm and Haas.

2. a) Grunewald, G. C.; Drago, R. S. *J. Mol. Cat.* **1990**, *58*, 227.

   b) Grunewald, G. C.; Drago, R. S.; Clark, J. L.; Livesey, A. B. *J. Mol. Cat.* **1990**, *60*, 239.

   c) Grunewald, G. C.; Drago, R. S. *J. Am. Chem. Soc.* **1991**, *113*, 1636.

   d) Petrosius, S. C.; Drago, R. S. *J. Chem. Soc., Chem. Commun.* **1992**, 334.

   e) Petrosius, S. C.; Drago, R. S.; Young, V.; Grunewald, G. C. *J. Am. Chem. Soc.* **1993**, *115*, 6131.

3. Drago, R. S.; Burns, D. S.; Lafrenz, T. J. *J. Phys. Chem.* **1996**.

4. Lim, Y. Y.; Drago, R. S.; Babich, M. W.; Wong, N.; Doan, P. E. *J. Am. Chem. Soc.* **1987**, *109*, 169.

5. Gregg, S. J.; Sing, K. S. W. "Adsorption Surface Area, and Porosity," **1967**, Academic Press: London.

6. Adamson, A. W. "Physical Chemistry of Surfaces," 5th Ed., **1990**, John Wiley & Sons, Inc.: New York.

7. Brunauer, S.; Emmett, P. H.; Teller, E. *J. Am. Chem. Soc.* **1938**, *60*, 309.

8. Jenkins, G. M.; Kawamura, K. "Polymeric Carbons-Carbon Fibre, Glass, and Chemistry" **1976**, Cambridge University Press: London.

9. Lafyatis, D. S.; Tung, J.; Foley, H. C. *Ind. Eng. Chem. Res.* **1991**, *30(5)*, 865.

10. McClellan, A. L.; Harnsberger, H. F. *J. Colloid and Interface Science* **1967**, *23*, 577.

11. Harkins, W. D.; Jura, G. *J. Am. Chem. Soc.* **1944**, *66*, 1366.

12. Barrett, E. P.; Joyner, L. G.; Halencia, P. P. *J. Am. Chem. Soc.* **1951**, *73*, 373.

13. a) Micromeritics ASAP 2000 System - Operators Manual V2.05, Appendix C, Micromeritics Instrument Corp., 1992; Norcross, GA.

    b) Micromeritics ASAP 2000 Chemi System - Operators Manual V2.04, Appendix C, Micromeritics Instrument Corp, 1992; Norcross, GA.

14. Hildebrand, J. H.; Prausnitz, J. M.; Scott, R. L. "Regular and Related Solutions," **1970**, Van Nostrand Reinhold: New York, pp. 44-61.

15. Rigby, M.; Smith, E. B.; Wakeham, W. A.; Maitland, G. C. "The Forces Between Molecules," **1986**, Clarendon Press-Oxford: New York, pp. 179-181.

16. Drago, R. S. "Applications of Electrostatic Covalent Models" Surfside Scientific Publishing, Gainesville, Florida 32604.

17. Person, W. B. *J. Am. Chem. Soc.* **1965**, *87*, 167.

FIGURE CAPTIONS

Figure 1: Adsorption Isotherms for CO and SO_2 on A-572 at -93 °C and 25 °C, respectively. Points ⊙ represent experimental values for CO and △ those for SO_2. The dashed and solid lines represent the calculated isotherm for SO_2 and CO respectively using the K and n values in Table 2.

Figure 2: Contributions of the Processes 1(- · - ·), 2 (- - -) and 3 (· · · · · ·) to the Total Adsorption Isotherm for CH_4 adsorption on A-572 at -43 °C. Component isotherms are calculated with the K's and n's in Table 2.

Figure 3: Log K vs. 1/T Plots for Various Adsorptives by A-572.

Figure 4: Correlation of Enthalpies of Adsorption with the Square Root of the van der Waals constant of the Adsorptive. The enthalpy for process one is illustrated.

Figure 5: Correlation of the Enthalpy of Adsorption with the Free Energy of Adsorption at 25 °C. The probe gases of Table 2 are shown for A-572 and PPAN for process 1.

Figure 6: The Free Energy of Adsorption at 25 °C vs. the Square Root of the van der Waals Constant. Data is shown for adsorption processes 1 (—) and 2 (- · - ·) on A-572 with the adsorptives in Table 2.

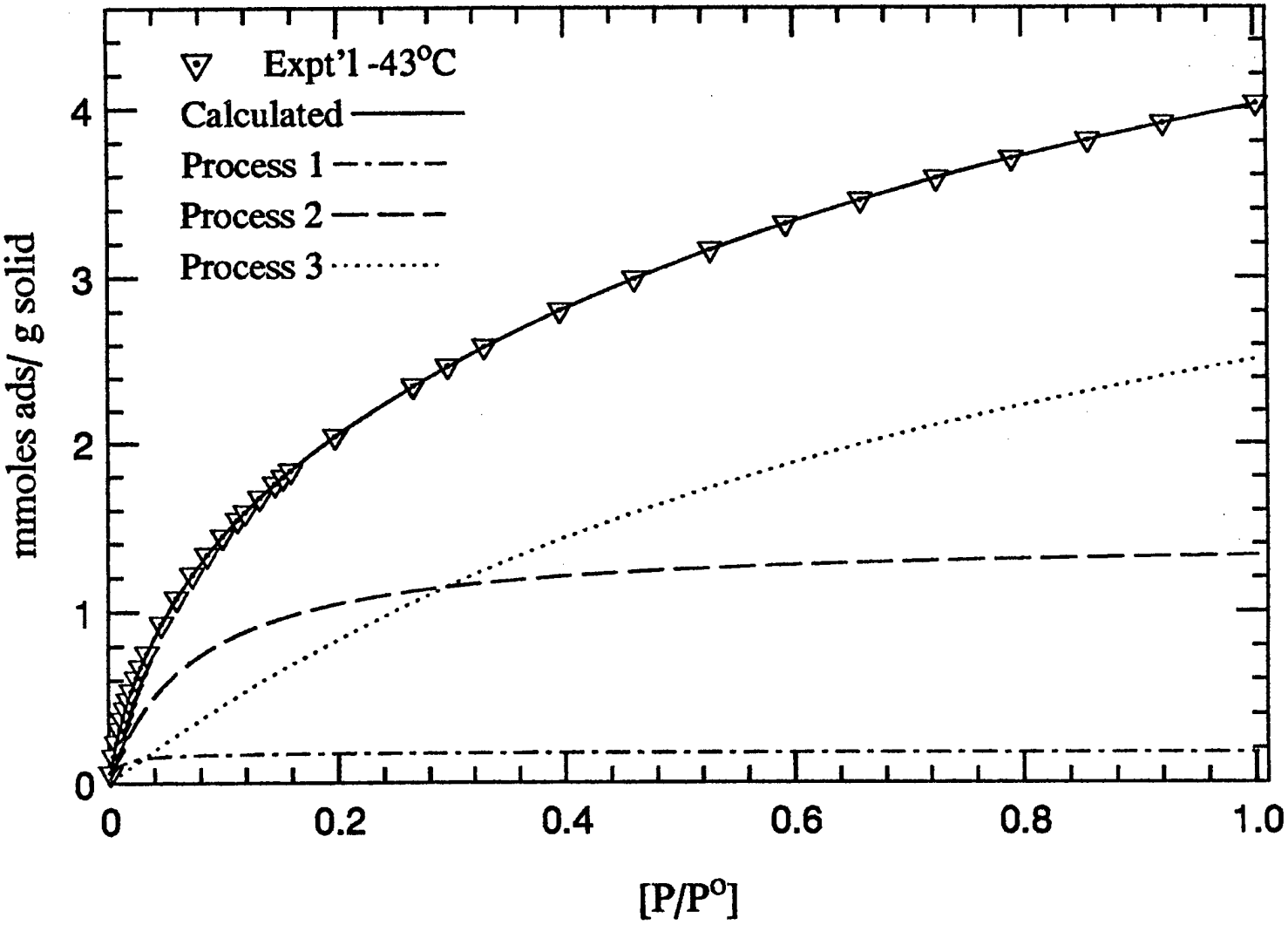
Expt'l -43°C
Calculated
Process 1
Process 2
Process 3
mmoles ads/ g solid
0
1
2
3
4
0
0.2
0.4
0.6
0.8
1.0
[P/P°]

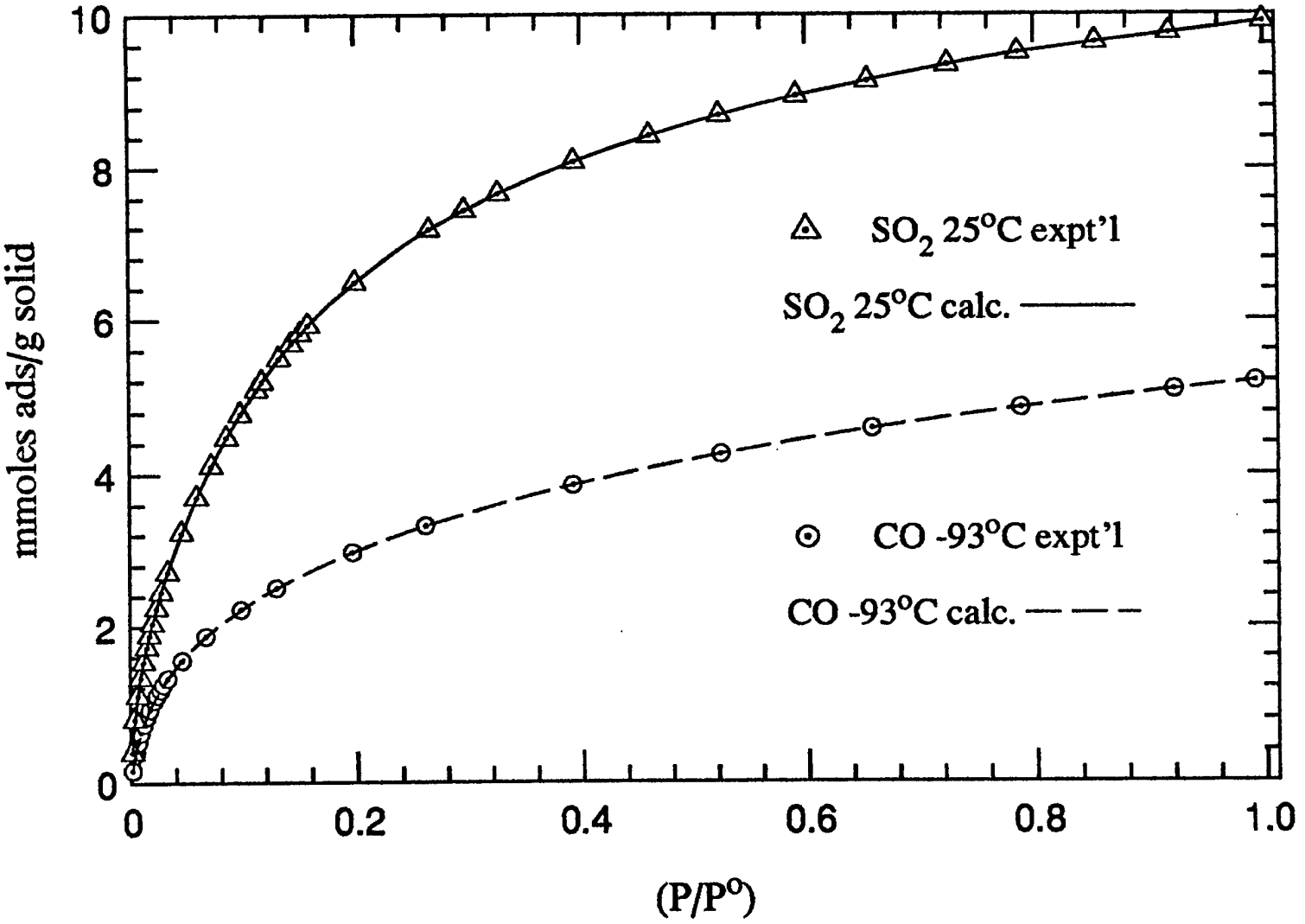
10
8
6
4
2
0
0
0.2
0.4
0.6
0.8
1.0
mmoles ads/g solid
(P/P°)
SO2 25°C expt'l
SO2 25°C calc.
CO -93°C expt'l
CO -93°C calc.

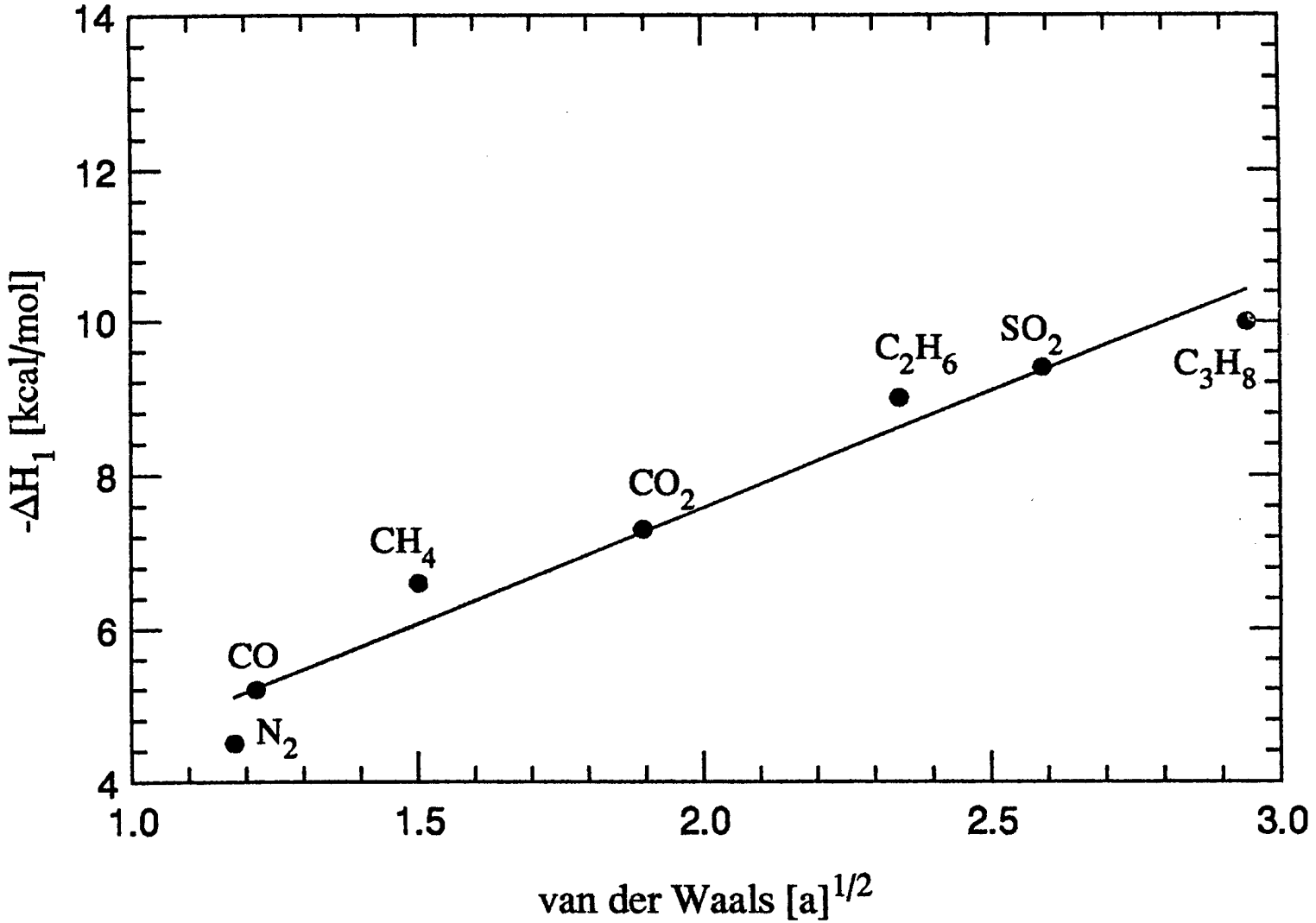
14
12
10
8
6
4
1.0
1.5
2.0
2.5
3.0
$-\Delta H_1$ [kcal/mol]
van der Waals [a]$^{1/2}$
N_2
CO
CH_4
CO_2
C_2H_6
SO_2
C_3H_8

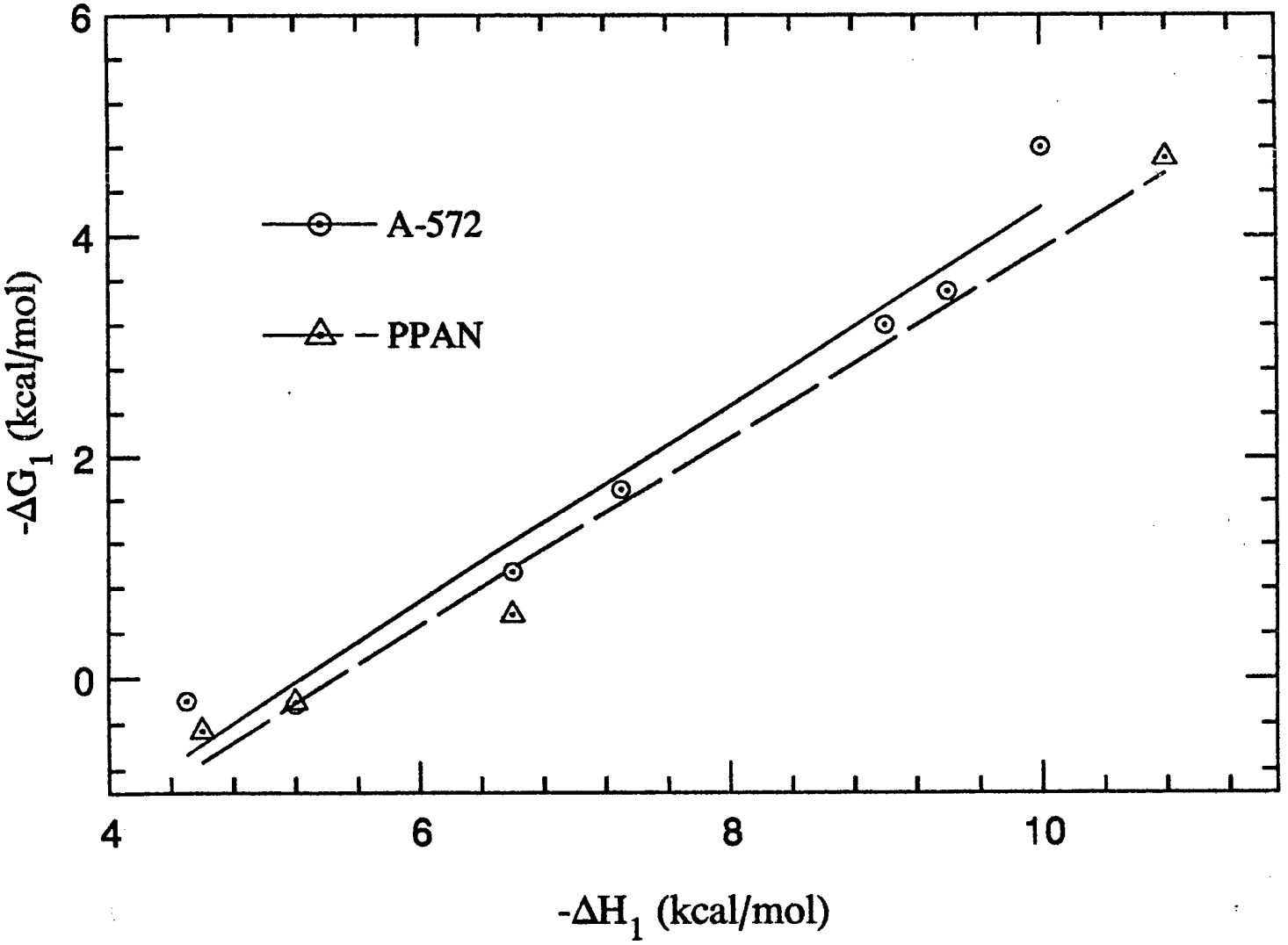
6
4
2
0
4
6
8
10
A-572
PPAN
-ΔG1 (kcal/mol)
-ΔH1 (kcal/mol)

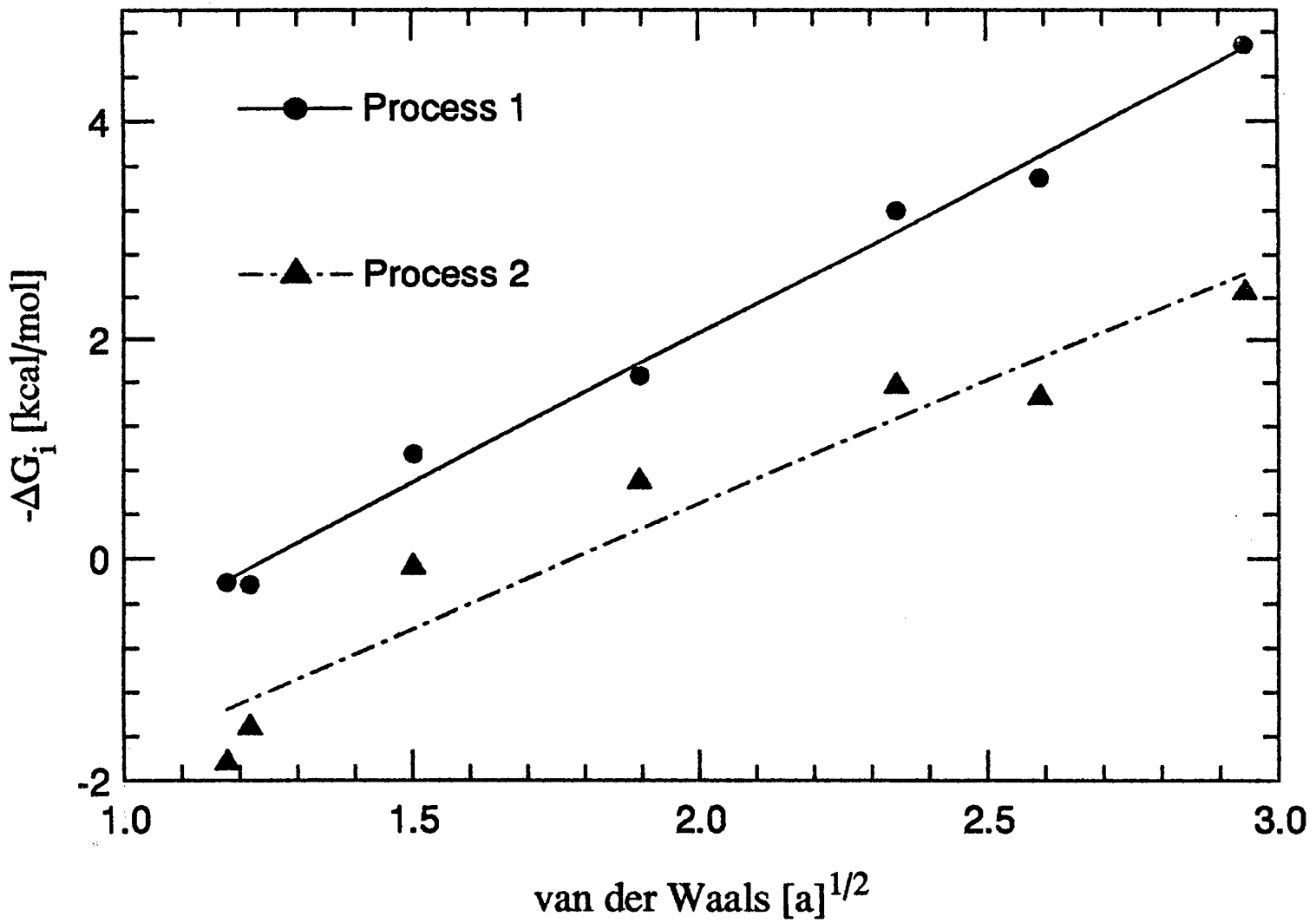
Process 1
Process 2
4
2
0
-2
1.0
1.5
2.0
2.5
3.0
-ΔG_i [kcal/mol]
van der Waals [a]^1/2

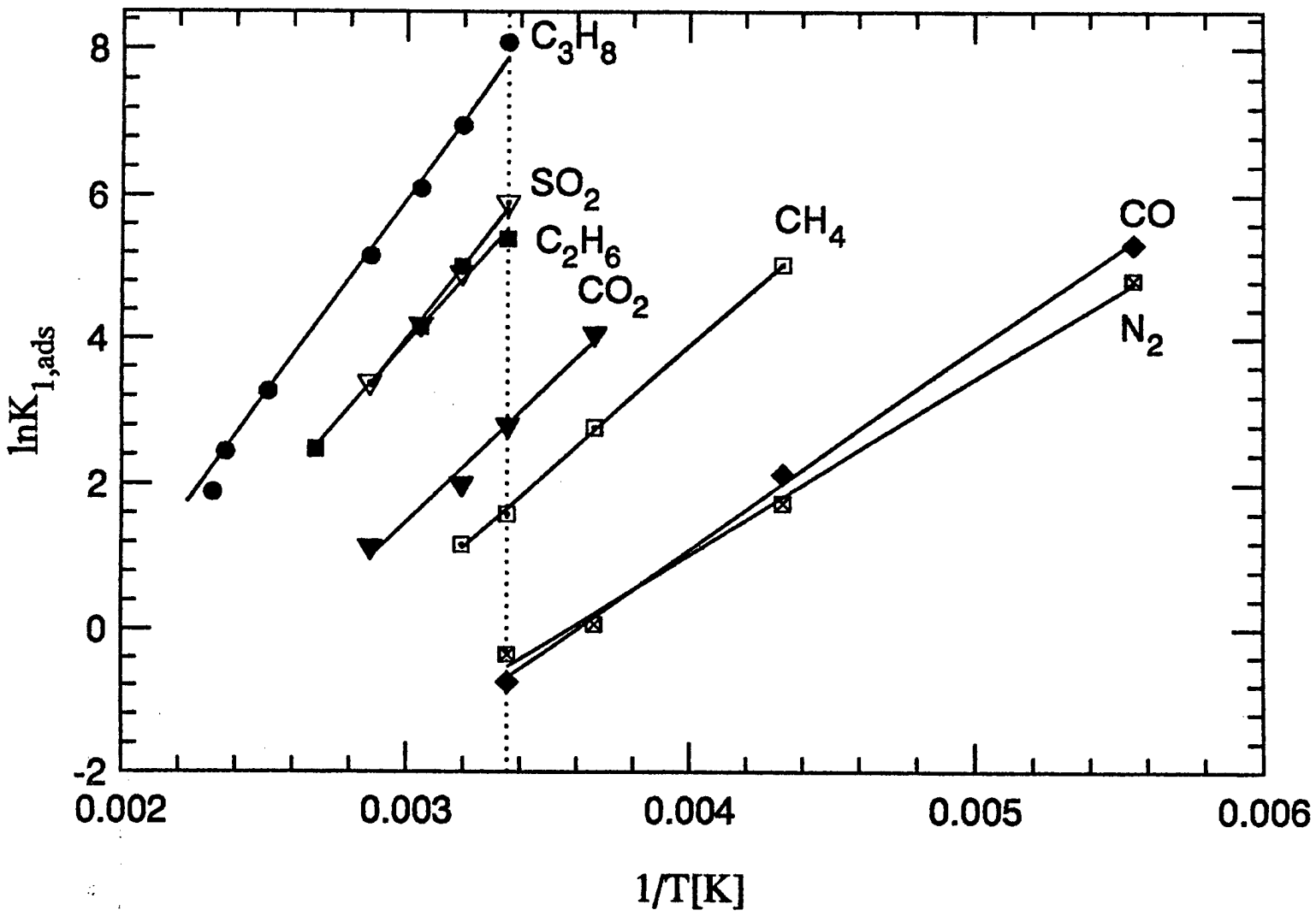
8
6
4
2
0
-2
0.002
0.003
0.004
0.005
0.006
lnK1,ads
1/T[K]
C3H8
SO2
C2H6
CO2
CH4
CO
N2